UNI
BASEL

PHARMACEUTICAL TABLETS AND NEAR-INFRARED SPECTRAL INFORMATION

Investigation of sampled tablet sections and press effect on predictions

Inauguraldissertation

zur

Erlangung der Würde eines Doktors der Philosophie

vorgelegt der

Philosophisch – Naturwissenschaftlichen Fakultät

der Universität Basel

von

Muhanned Saeed
aus Grossbritannien

Basel, 2011

Genehmigt von der Philosophisch – Naturwissenschaftlichen Fakultät auf Antrag von

Professor Dr. Beat Ernst

und

Dr. Gabriele Betz

und

Dr. Lorenz Liesum

Basel, den 27. April 2010

Professor Dr. Eberhard Parlow
Dekan

Table of Contents

List of abbreviations

AOTF	Acousto-optic tunable filter
API	Active pharmaceutical ingredient
ASTM	American society of testing and materials
BP	British pharmacopoeia
CCD	Charge-coupled device
CFR	Code of federal regulations
cGMP	Current good manufacturing practice
cGLP	Current good laboratory practice
CPCA	Classical principle component analysis
Db1	First derivative 4 points
DC	Direct current
DR	Diffuse reflectance (reflection)
DT	Diffuse transmittance (transmission)
ECT	Effective contact time
EDT	Effective dwell time
EMEA	European medicines agency
EP	European pharmacopoeia
FDA	Food and drug administration
FFT	Fast Fourier transform
FT	Fourier transform
HPLC	High performance liquid chromatography
HPMC	Hydroxypropyl methylcellulose
ICH	International conference on harmonisation
InGaAs	Indium Gallium Arsenide semi-conductor
IPC	In-process control
IR	Infra-red
LED	Light-emitting diode
MCC	Microcrystalline cellulose
MIR	Midrange infra-red
MLR	Multiple linear regression
MMPS	Mass median particle size
MPS	Mean particle size
MSC	Multiplicative signal correction
Nil	Normalisation by closure
NIPALS	Non-linear iterative partial least squares
NIR	Near infra-red
NIRS	Near infra-red spectroscopy
Nile	Normalisation to unit length
NLM	Non-linear mapping
nsd	Normalisation by standard deviation
PASG	Pharmaceutical analytical science group
PAT	Process analytical technology
PBZ	Phenylbutazone
PC (PCs)	Principle component(s)
PCA	Principle component analysis
PCD	Pitch circle diameter
PCR	Principle component regression

PLS	Partial least squares
PLSR	Partial least squares regression
PRESS	Predicted residual error sum-of-squares
PSD	Particle size distribution
RF	Radio frequency
RPM	Revolution per minute
SD	Standard deviation
SE	Standard error
SEC	Standard error of calibration
SECV	Standard error of cross-validation
SEE	Standard error of estimation
SEM	Scanning electron microscope
SEP	Standard error of prediction
SNR	Signal-to-noise ratio
SNV	Standard normal variate
SST	System suitability test
SVD	Singular value decomposition
TPH	Tablets per hour
USDA	United States Department of Agriculture
USP	United States pharmacopoeia
UV	Ultra-violet
VBA	Visual basic for applications
VIS	Visual

List of figures

List of tables

Abstract

Near-infrared (NIR) spectroscopy offers tremendous advantages for pharmaceutical manufacturing as a fast and non-destructive method of quantitative and qualitative analysis. Content uniformity (end-product analytics) and process analytics are two important applications of the method.

Both modes of analysis, diffuse transmission (DT) and diffuse reflection (DR) are sensitive to changes in sample physical parameters. Scaling as well as baseline shifts due to tableting variations would be a potential cause of many outliers and prediction errors, and therefore these effects need to be more clearly understood. Moreover, there is currently no clear literature information about the sampling span in both modes (horizontal or radial in DT, and vertical or information depth in DR). This information is vital in content prediction using NIR in cases where inhomogeneities in the sample are detrimental (e.g. low-dose API in large samples).

The press effect was investigated using placebo tablets of different thickness and porosity ranges, which showed an exponential relationship with the diffuse transmission (DT) signal. The drug content of 2.5% m/m folic acid tablets produced under different compaction conditions was predicted and found to be in statistical agreement with UV assay results after inclusion of physical outliers to the training sets.

To determine the sampling span in DT, placebo tablets of 10 mm diameter were covered by different paper filters with incremental central block and the DT maximum at 8880 cm^{-1} was used to assess the degree of block. 90% of the signal was detected from a diameter of up to 7 mm.

For DR information depth assessment, three experiment approaches were pursued: I. 0.5–10 mm incremental thickness placebo tablets with constant porosity, II. MCC/Phenylbutazone (PBZ) double layered (DL) tablets (PBZ layer 0-100% in 0.5 mm steps) and III. Comparison of placebo and 30% caffeine tablet cores with incremental film coating (film thickness of 0 – 0.35 mm). Incremental thickness and cluster analysis of DL tablets showed that DR information depth was < 0.5 mm, while the data fitting from incremental coating showed that signal drop reached 50% at 0.05 – 0.07 mm depending on the wavenumber and 90% signal drop (10% information content) can be seen between 0.2 – 0.25 mm without extrapolation.

1. Introduction

Near-infrared spectroscopy (NIRS) is the measurement of the wavelength and intensity of absorption of near-infrared (NIR) light by a sample. The NIR spectral region spans the range from 700 to 2,500 nm (14,285 – 4,000 cm^{-1}) with absorptions representing overtone and combinations from the fundamental molecular vibrations found in the mid-infrared (MIR) region. These overtones and combinations mainly are associated with C–H, N–H, O–H and S–H functional groups. NIRS uses chemometrics to analyze the functional groups present in a sample mixture. As a quality and process control technique NIRS analysis methods are applied to raw material, intermediates and finished products. NIRS historically was developed as a quantitative analysis technique, but during the past 10 years chemometrics methods have led to qualitative applications.

As NIRS continues to grow in importance as a useful analytical technique, it offers unique potential as a rapid, non-destructive method of quantitative and qualitative evaluation. NIRS has been used extensively in the food and agricultural industries for many years to determine moisture, protein, and starch content in grains. The pharmaceutical industry has been cautiously slow to accept NIRS as a commonly used technique, probably because of the absence of primary absorption bands. In recent years, an increasing amount of academic research is being carried out on the theory behind NIR. The use of NIRS for pharmaceutical applications has grown owing, in part, to technological advances in instrumentation and software.

1.1 Historical overview

In his famous work, "Experiments on the Refrangibility of the Invisible Rays of the Sun," presented to the Royal Society (Hershel 1800), Sir William F. Herschel first demonstrated the existence of optical radiation beyond the limits of the visible spectrum. In a series of experiments probing the relationship between colour and heat, Herschel observed an increase in temperature from violet to red. In a serendipitous moment, however, he discovered that the hottest temperature was actually beyond the red limit of visible light. This invisible radiation, which he initially termed as "calorific rays," is actually what has come to be known as short-wave near-infrared.

The NIR spectral region was largely ignored as an analytical asset for nearly 150 years following Herschel's discovery (Burns and Ciurczak 2001) until Karl Norris, an agricultural engineer working for the U.S. Department of Agriculture (USDA), saw its potential for rapid, quantitative analysis of complex biological samples. Norris's work eventually initiated the development of an NIR industry that produced analyzers capable of rapidly determining the concentration of constituents in whole foodstuffs with very little sample preparation. From the mid-1960s until 1986 the rate of publications on NIR spectroscopy increased dramatically, with most articles concerned primarily with the analysis of food and agricultural products and in 1987 Phil Williams and Karl Norris edited a comprehensive text with nearly 1000 references on the subject of NIR technologies (Williams and Norris 2001).

NIR technology has generally advanced by following technology developments in seemingly unrelated industries. The interest in the NIR region of the electromagnetic spectrum lagged behind the UV, VIS and MIR regions for most of the twentieth century. Unlike the sharp absorbance bands of the MIR fingerprint region utilized for qualitative analyses in synthetic organic chemistry, the absorbance bands in the NIR are weak, broad, overlapping, and of great complexity to interpret. Moreover, early chemists had difficulty specifying baseline effects in the NIR region, and they viewed NIR spectroscopy as being less reliable for quantitative assays relative to UV/VIS spectrophotometry.

As enabling technologies began to appear in the mid of the 20th century, Karl Norris's early work was revolutionary in that it utilized grating/prism monochromators, new broad-band detectors and powerful digital computing capabilities (Norris and Williams 1984). After that, the popularity of NIR spectroscopy accelerated during the 1970s and 1980s with the development of low-cost personal computers.

After the 1990s, NIRS grew more with the introduction of InGaAs diode array detectors, tunable NIR lasers and fibre-optics and the method started to earn its reputation as a powerful analytical technology in its own right. It was not until then that the negative aspects of the technology were turned into positive features and NIRS was ultimately found to be useful because the relatively weak absorbance bands in the region allow for interrogation of sample matrices to greater depth than is possible in the IR and UV/VIS regions.

The complex nature of NIR absorbance bands and baseline effects initially posed a dilemma. The study of chemometrics has yielded the ability to resolve NIR spectra for simultaneous multi-component analyses. The scope of data treatment display and interpretation was enhanced to include MLR, PLS, PCA, and cluster analysis and third-party software suppliers started to offer a wide choice of chemometrics software freeing users from the constraints of instrument suppliers.

Today, NIRS have gained wide acceptance from many industries, including pharmaceutical, and is being tested and used in many areas of production starting from identification of raw materials, process control and end product analysis.

1.2 Theoretical aspects

An important point to be realized is that the NIRS has unique features among other regions of the electromagnetic spectrum. Therefore, treating the NIR region as an extension of IR or UV/VIS during method development or application will only lead to failure because of the unique aspect of the interaction between solid materials and NIR radiation at the molecular and particle scales set NIR spectroscopy apart from other methods.

1.2.1   Molecular vibrations

Atoms in a molecule are in a continuous movement even close to the absolute zero temperature. The physical scale of the vibrational movement of atoms in molecules is rather small. This movement is confined within this narrow range by a potential energy well, formed between the binding potential of the bonding electrons, and the repulsive (mainly electrostatic) force between the atomic nuclei a quantum distribution of energy levels is expected (Figure 1A) with a set of discrete allowed energy levels of equal intervals of energy between them and a non-zero potential energy within the well.

However, real molecules show non-conformity to the potential energy well in with the simple harmonic model. In the simple harmonic model, the potential well is entirely symmetrical and the potential energy rises equally with displacement in both positive and negative directions from the equilibrium position. This is counter-intuitive because the forces responsible for the rise in potential energy are different in the two cases. In the bond-stretching case the dominant factor is the shifting of the molecular orbital away from its minimum energy configuration. In the bond-compression case, there is the additional factor of electrostatic repulsive energy as the positively charged atomic nuclei approach each other. Thus one would expect the potential energy curve to rise more steeply on the compaction cycle, and (due to the weakening of the bond with displacement) to flatten off at large displacements on the decompression cycle (Figure 1B).

There are two effects of the anharmonicity of the quantised energy levels described above, which have significance for NIRS. First, the gap between adjacent energy levels is no longer constant, as it was in the simple harmonic case. The energy levels converge as n increases. Secondly, weak absorptions can occur with $\Delta n = \pm 2$ (first overtone band), or ± 3 (second overtone band), etc.
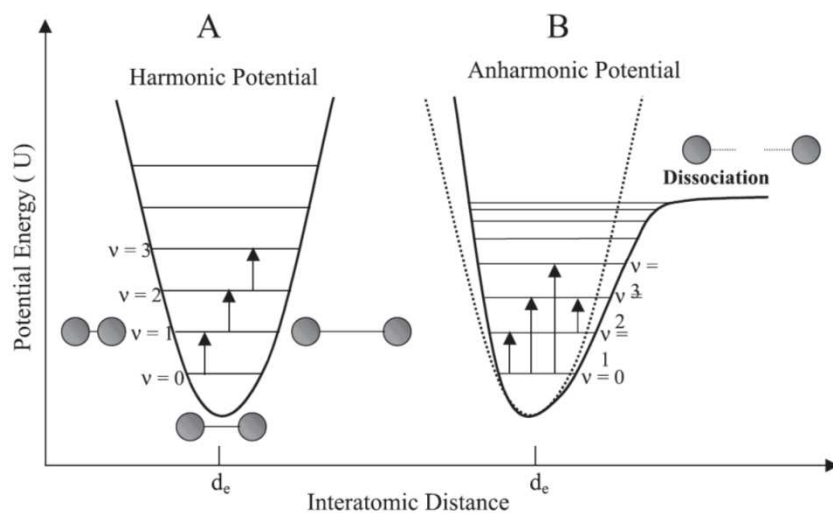
Figure 1: Schematic representation of the harmonic (A) and anharmonic (B) models for the potential energy of a diatomic molecule.

de = equilibrium distance (U = minimum) (Pasquini 2003)

1.2.2 The origin of absorption bands in the NIR region

The match of radiation energy with the energy difference between two vibrational levels causes a selective response of the molecular system to the incident radiation. It means that in a given wavelength range, some frequencies will be absorbed; others (that do not match any of the energy differences possible for that molecule) will not be absorbed while some will be partially absorbed. This complex figure of the intensity of absorption versus wavelength constitutes the absorption spectra of a substance or sample. For a vibration to be active, it is necessary that the electrical oscillating field of the electromagnetic wave can interact with the molecule. This can only occur if the displacement of the atoms in a vibrational mode can produce a change in the dipole moment of the molecule or in the local group of vibrating atoms.

In polyatomic molecules, transitions to excited states involving two vibrational modes at once (combination bands) are also weakly allowed, and are also affected by the anharmonicity of the potential. The role of combination bands in the NIR can be significant. The only functional groups likely to impact the NIR spectrum directly as overtone absorptions are those containing C-H, N-H, O-H or similar functionalities. However, in combination with these hydride-bond overtone vibrations, contributions from other, lower-frequency fundamental bands such as C=O and C-C can be involved as overtone-combination bands. The effect may not be dramatic in the rather broad and overcrowded NIR absorption spectrum, but it can still be evident and useful in quantitative analysis. For combination bands to occur, it would be necessary that only

one of the combining vibrations be active (causing dipole change). This feature may cause some vibrations, which cannot be observed in the middle infrared, to be displayed by a NIR spectrum.

The intensity of a given absorption band is associated with the magnitude of the dipole change during the displacement of atoms in a vibration and with its degree of anharmonicity. Both phenomena are present in great intensity associated with bonds involving the hydrogen atom and some other heavier element such as carbon, nitrogen and sulphur. The O-H, C-H, N-H and S-H bonds tend to present high anharmonicity and high bond energy with fundamental vibrational transitions in the region of 3000 – 4000 nm. Intensities are in between 10, for combinations, up to 1000, for successive overtones, times lower than the absorption resulting from fundamental vibrations. The spectral occurrences in the NIR region are dominated by overtones and combination absorption bands. Coupling or resonance between different vibrations of the same functional group and Fermi resonance between a fundamental and an overtone when their difference in energy is very low also occur resulting in a greater separation between the position of the two bands and in the intensification of the overtone band. The complexity of the combination spectral region in the NIR spectrum of hydrocarbons is partly due the possibility of resonance between the combination bands and high order overtone for C-H bonds. The primary practical consequence of both types of resonance on a NIR spectrum is the possibility of the appearance of two instead of one band in the combination region (1600 – 2500 nm).

1.3 NIR diffuse transmission for solids

One of the most important aspects of the interaction between NIR radiation and particulate solids is the unique combination of relatively weak absorbance intensity with high scattering efficiency. This combination allows the NIR radiation to probe the interior of many solid samples with little or no sample preparation. The spectroscopic analyses of solids in the NIR region are performed using two primary modes of sampling geometry: transmittance and diffuse reflectance (DR). The transmittance measurement through particulate solids is a distinctive capability of spectroscopy in the NIR relative to UV/VIS and IR.

In general, sample transmittance, T, is estimated as the ratio of intensities for light transmitted through an empty path (e.g., cuvette), I_0, and light transmitted through an equal distance of a particulate sample, I_s. Transmittance data are most often reported in terms of Beer-Lambert absorbance:

$$A = \log\left(\frac{1}{T}\right) = \log\left(\frac{I_s}{I_0}\right) = abc \qquad (0.1)$$

where, for a single wavelength, γ:
   A = Beer-Lambert optical absorbance
   T = transmittance ratio
   a = absorption coefficient, cm^{-1}
   b = pathlength (or sample thickness), cm
   c = concentration of absorbing species.

In contrast to UV/VIS (transmission) absorption spectrophotometry, which is typically performed in dilute solution, the transmittance of NIR radiation through a sample matrix comprised of tightly packed solid particles is expected to deviate nonlinearly from the Beer-Lambert law of absorption. The source of these deviations becomes apparent when the derivation and simplifying assumptions of the Beer-Lambert law, or simply Beer's law, are considered. The most notable deviations from Beer's law for NIR transmittance through clear liquids are due to changes in absorption coefficients across wide ranges of concentration. Beer's law assumes that the response between optical absorption, A, and concentration c, is expected to be linear. The transmittance through particulate solids is less accurately described by the Beer-Lambert law, however, because it also assumes that all radiation encountering an absorbing particle will either be transmitted or absorbed. There is, however, a finite probability that incident photons will be scattered or reflected either forward or backward relative to the direction of

propagation of the incident beam, I_0 (Figure 2). Thus, the incident photons are not transmitted directly through particulate samples; rather, they take a tortuous path through the material with multiple opportunities for scattering and backward reflection (Figure 3).
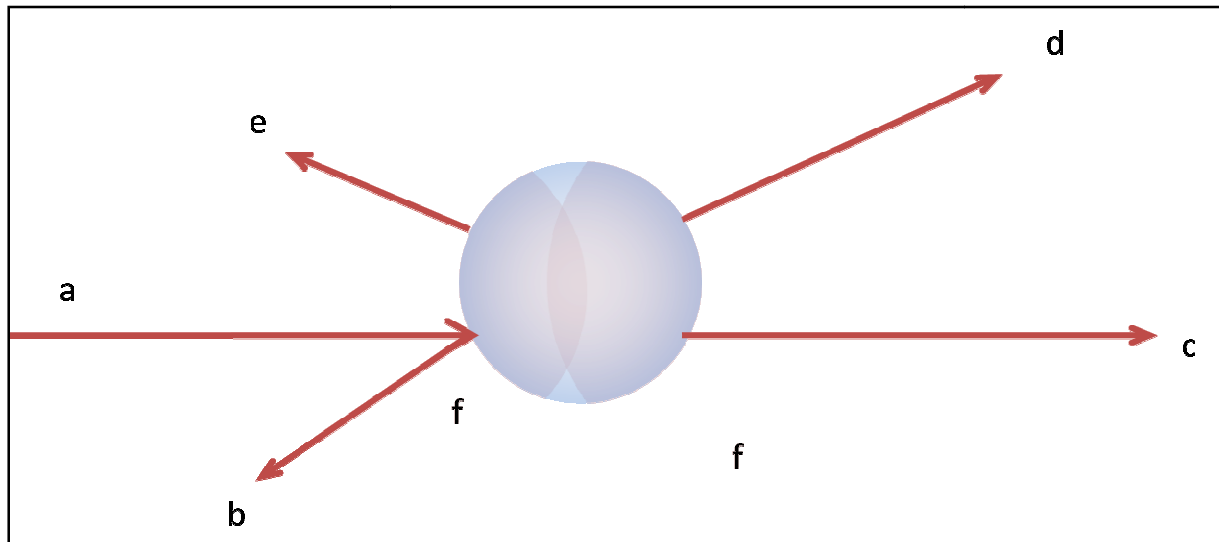
Figure 2: The optical interactions, of which the three fluxes are comprised of: (a) incident beam absorption, (b) specular reflectance, (c) transmittance, (d) forward scatter, (e) back scatter, (f) anisotropic scattering intensity fields

Because the intensity of scattered radiation decreases along with absorptivity, the transmittance through a solid sample will become less diffuse as the absorptivity decreases. These effects tend to increase the path a photon will travel before being emitted from the sample. Thus, the effective pathlength for transmittance through a plane of compressed particulates of thickness b will be a normally distributed amount greater than b. Furthermore, as b increases, the transmitted radiation will become more diffuse until the diffuse thickness is achieved (Birth and Hecht 1987), at which point the maximum amount of incident radiation reflected back toward the source occurs. Hence, solid-state transmittance in the NIR region might more aptly be termed diffuse transmittance spectroscopy.

DT NIRS is usually performed in the third overtone region, between 780-1100 nm. Although scatter coefficients increase in the NIR with increasing frequency, the scattering efficiency in the third overtone region is low because the amount of radiation loss to backward reflection is reduced along due to the decreasing absorption coefficient (Dahm and Dahm 2001).

The absorptivity, reflectance, and scattering characteristics for a particular sample are dependent on multiple material qualities, such as particle size and morphology, packing density, and index of refraction. Hence, the effective pathlength and the level of nonlinearity relative to Beer's law are difficult to predict in practical situations.
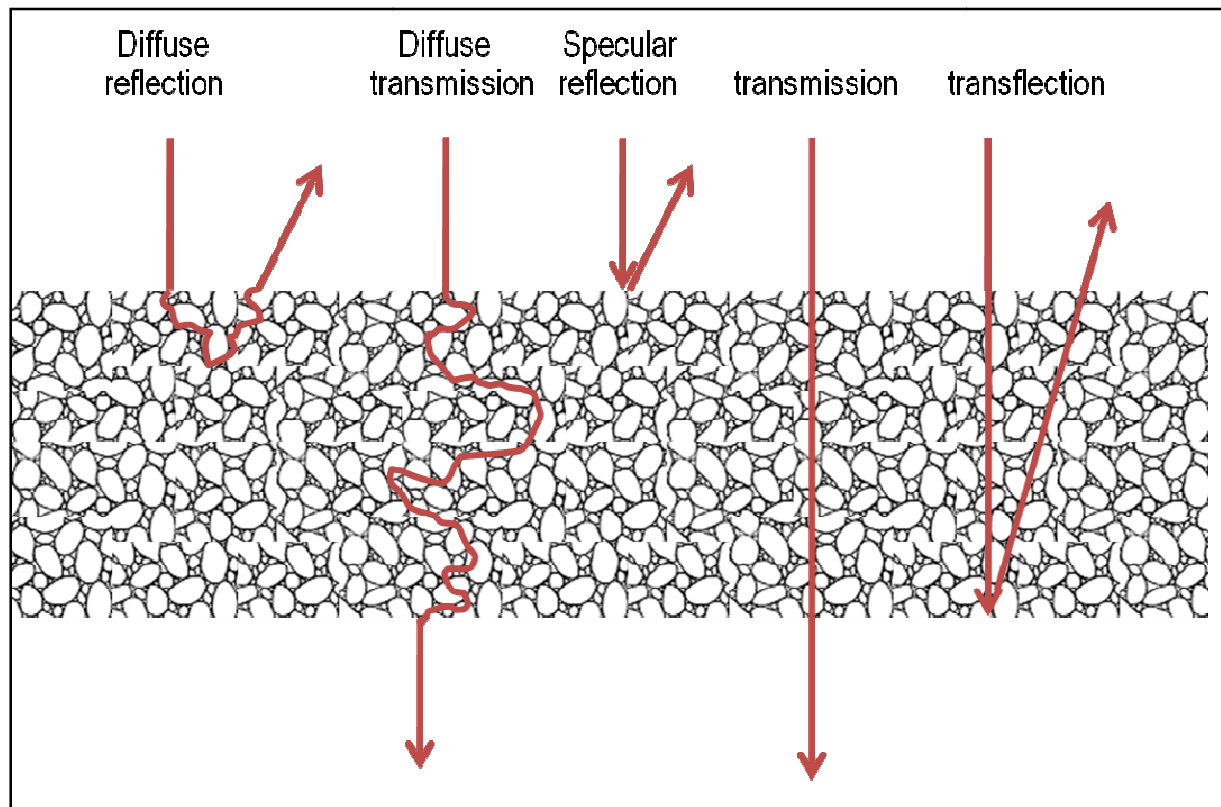
Figure 3: Diagram showing the types of light interaction in the NIR region with particulate solids. In practice, only diffuse reflection and transmission are observed

1.4 NIR diffuse reflection for solids and its theories

1.4.1 Early theories

NIR DR analysis is a defining quality of the method which permits quantitative analysis of material qualities for granular or particulate samples in fluidized beds, mixing vessels, or on moving belts.

The sample reflectance, R, is most often estimated as the ratio of intensities for light reflected from a non-absorbing, diffusely reflecting surface (e.g., white ceramic or inner surface of an integrating sphere), I_0, and light reflected from the sample, I_S. Reflectance is most often reported in terms of absorbance units, log (1/R), regardless of the derivation of Beer's law mentioned earlier. These *apparent* absorbance spectra collected in reflectance are also treated as being linearly correlated with the concentration according to Beer's law with nonlinearities being either ignored over a narrow concentration range or are approximated by additional empirical model factors or nonlinear terms.

The earliest attempts to describe DR treated it strictly as a surface phenomenon. Bouguer (1760) suggested it as mirror-type reflections from microcrystalline faces statistically distributed over all possible angles.

Lambert cosine law (Lambert 1760) went a step further by describing a mathematical relationship between the intensity of an incident beam of light, angle of incidence and angle of observation. The problem was that an ideal diffuse reflector postulated by the theory has never been found, and this was the reason why the theory fails in practice.

Seeliger (1888) was the first to consider DR as penetrating the surface of materials, where it is either absorbed or returned to the surface via reflection, refraction, or diffraction from the surfaces of the internal microstructure (summation of surface reflection and elastic scatter).

Mie Theory (Mie 1908) was one of the major works describing elastic scattering phenomenon and its relationship with the frequency of radiation. The theory's central assumption is that scattering is associated with isolated, spherical particles. According to this theory, scattering is not distributed isotropically (uniform optical properties in all

directions); rather, a complex pattern is produced; with forward scatter preferred over reverse scatter.

$$\frac{I_{\theta scat}}{I_0} = \frac{\lambda^2}{8\pi^2 R^2} = \left(i_1 + i_2\right)$$ (0.2)

where
λ = single wavelength under consideration
$I_{\theta scat}$ = intensity of scattered radiation at distance R and angle π from the centre of the scattering particle
i_1, i_2 = Complex functions of the angle of the scattered radiation, the spherical harmonics, or their derivatives with respect to the cosine of the angle of scattered radiation, the refractive index of both the sphere and surrounding medium, and the ratio of the particle circumference to wavelength

Equation (0.2) shows that as the wavelength increases, the intensity of scattered radiation will increase, one of the factors contributing to the shape of the upward-sloping baseline observed in the NIR absorbance of solids (downward sloping if reflectance is reported).

However, particles in real solid systems are not isolated but in intimate contact with one another. Additionally, the theory did not consider multiple forward- or back-scattering events. Theissing (Theissing 1950) showed that as the number of times a photon is scattered increases the distribution of scattered radiation will deviate further from Mie's theory, becoming more isotropic and with greater proportion of the radiation being scattered in the reverse direction.

1.4.2   Later works and Kubelka-Monk's theory

Most other theories have evolved from energy transfer treatments, which describe the change in intensity of a beam of radiation of a given wavelength in a sample of a given density and pathlength due to total radiation loss from scattering and absorption that corresponds an attenuation coefficient (Truelove 1988) and (Craig and Incropera 1984).

Schuster (1905) reported a simplified solution of the radiation transfer equation for the case of reflectance by assuming the total radiation flux is comprised of two components, one flux travelling in the forward direction and a second flux travelling in the reverse direction.

Kubelka and Munk (1931) made more assumptions in their derivation of a simplified solution to the radiation transfer equation. The final derivation is shown in equation (0.3) and shows that the measured DR (R_∞) is dependent on the ratio of K and S (absorption and scattering coefficients respectively).

$$f\left(R_\infty\right) = \frac{K}{S} = \frac{1 - 2R_\infty + R_\infty^2}{2R_\infty} = \frac{\left(1 - R_\infty\right)^2}{2R_\infty} \tag{0.3}$$

Kubelka and Munk's solution is the most widely accepted DR explanation since it is a two-constant equation and therefore experimentally testable. Moreover, many other derivations by other workers like Smith (1931), Amy (1937) and Bruce (1926) have been shown to be derivable from Kubelka and Munk's work.

1.5   Instrumentation and analyzer technologies

1.5.1   Light sources

The tungsten-halogen source is almost universally used for NIRS. It has a broadband, pseudo-blackbody emission spectrum with no significant structure. It is inexpensive and remarkably long-lived if operated at appropriate filament temperature and lamp wattage. The peak spectral radiance of a tungsten lamp is located at approximately 10,000 cm^{-1} (1000 nm) with a lifetime of around 10,000 hours.

1.5.2   Photon detectors

The most frequently employed detectors for the NIR spectral region are based on silicon, PbS and InGaAs photoconductive materials. The latter possess a very high photo-detectivity and response speed. Together with high powered radiation sources (a tungsten coil or a halogen lamp, *see above*) these detectors can impart a very high signal-to-noise ratio for NIR measurements. This fact partially compensates for the lower intensities of NIR absorption bands.

1.5.3   Wavelength section methods

1.5.3.1   Filter-based instruments

Filter instruments often employ a set of 10–20 interference filters mounted on a high-speed rotating filter wheel positioned between collection optics and a single detector. High-speed measurement is possible (approximately as fast as a diode array spectrometer) by spinning the filter wheel at a very high rate (10,000 rpm). Fast Fourier

transform (FFT) of the detected signal can be used to isolate the spectral intensity data from instrumental noise effects, which, along with the simple, efficient design, make filter instruments very robust devices for single-material measurement. Filter instruments have been significantly deployed as in-line moisture gauges, though some have been successfully calibrated for multi-constituent content predictions. However, they provide limited spectral information and are more expensive compared with low-cost diode array systems. (Scott 1995)

1.5.3.2 *LED-based instruments*

To reduce the price and size of the instruments, Light Emitting Diodes (LED) technology is used in some applications. These devices can produce NIR radiation with a band width of about 30 - 50 nm, centred in any wavelength of the spectral region. The instruments can employ a set of LEDs as sources of narrow bands of near infrared radiation[28-30] or use them to produce a polychromatic, highly stable source whose radiation is dispersed by using common monochromator devices such as those based on gratings or filter optics. However, LEDs operating at wavelengths higher than 1100 nm are still expensive. (Wilson, Barnes et al. 1995)

1.5.3.3 *AOTF instruments*

Acousto-Optical Tunable Filter (AOTFs) technology allows constructing instruments with no moving parts, capable of reaching very high scan speeds over a broad range of the NIR spectral region. Any number of wavelengths necessary to perform a given analytical determination can be easily implemented with scan speeds of up to 2000 wavelengths per second, which is only limited by the detector response time.

An AOTF is a device made of a birefringent crystal of TeO_2, cut in a special angle and a piezoelectric material (usually $LiNiO_4$) is attached to one end of the crystal which, under excitation from an external RF signal, producing an acoustic wave which propagates through the crystal and produces a periodic variation of the refractive index of the crystal in a frequency determined by the RF signal, in the range of 50 to 120 MHz. The interaction of the electromagnetic wave and the acoustic wave causes the crystal to refract selectively a narrow wavelength band. The birefringence of the TeO_2 crystal leads to the production of two monochromatic beams and both or only one diffracted beam can be used by NIR instruments (Figure 4).

This non-moving parts concept of the AOTF-based NIR spectrophotometers impart to them some unbeatable qualifying characteristics for use in the field or on the factory floor, aiming at in-line monitoring. The wavelength precision is about ±0.05 nm and the

resolution is dependent on the wavelength, with typical values in the range 5 to 15 nm for the wavelength in the range 1000 to 2500 nm. (Tran 1992)
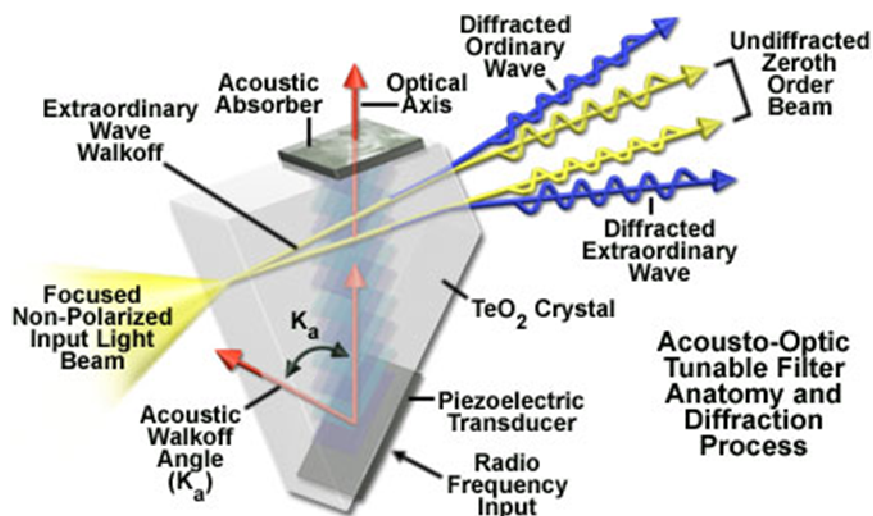
Figure 4: Schematic representation of AOTF (Davidson, Spring et al. 2006)

1.5.3.4 *Dispersive optics-based instruments*

Diffraction gratings dispersive instruments were among the earliest technologies employed in NIR (Figure 5). These instruments have the advantage of a relatively low cost when compared with other scanning instruments employing modern technologies. The main disadvantages, however, is the slow scan speed and low wavelength precision, which deteriorates with time due to mechanically driven mechanism fatigue, which limits the use of dispersive instruments in production environments.

Figure 5: Diffraction grating NIRS. The incident light is first collimated by a concave mirror and guided on to the diffraction grating, where it is spatially split into its different spectral components. A second concave mirror focuses the various spectral components of the light onto different columns of the CCD detector, thus capturing the light's spectrum in a single acquisition.

Nevertheless, recent evolution in sensor production technology gave dispersive optics a longer life by constructing linear arrays of PbS and InGaAs sensors containing up to 256 independent elements. This allowed scanning an entire spectrum in a few milliseconds and eliminated the moving parts.

1.5.3.5   *Fourier transform (FT) instruments*

FT-NIR spectrometers are most advantageous when high-resolution capabilities are important or if the spectrometer needs to have many options for sample interaction. The spectral resolution of an FT-NIR analyzer is constant across the spectral range detected and is adjusted by varying the length of the interferogram. In a Michelson interferometer, this corresponds to the range of displacement for the moving mirror and will require longer scan times for equivalent performance in terms of signal-to-noise ratio (SNR).

The FT spectrometers have a combination of three theoretical advantages, which make the technology attractive:

> All frequencies (wavelengths) are detected simultaneously (Fellgett's advantage)
> Wavelength accuracy is constantly maintained by an internal laser line (Connes advantage)
> The interferometer has much higher optical throughput than other (dispersive) technologies (Jacquinot's advantage)

In contrast to the analyses of gases or liquids, the resolution needs for most applications of NIR for the analysis of pharmaceutical solids could be met with relatively low resolution (8–64 cm^{-1} or 6–12 nm). This is due to the extensive coupling of molecular bond vibrations in pharmaceutical solids, which results in rather wide absorbance bands, which offers the advantage of a higher SNR. The spectral range of modern FT-NIR spectrometers is mainly limited by the sensitivity of the detector material, rather than the mechanical stability of the optical platform.

The polarizer interferometer (Ciurczak 2005) relies on a two-piece birefringent crystal wedge polarizer and birefringent compensator to modulate optical energy in the pattern of a Fourier interferogram. Figure 6 shows that randomly polarized radiation passes through a linear polarizer and a birefringent crystal, which separates the light into two orthogonally polarized parallel rays with a (wavelength specific) phase shift, thereby slightly rotating the plane of polarization. The phase-shifted rays are transmitted through the two-piece wedge polarizer, which then rotates the plane of polarization in the opposite direction, reducing the phase shift. The angle of polarization rotation is dependent on the effective pathlength through the wedge polarizer, and wavelength. At the initial position, the thickness of the wedge polarizer is set so that the polarization rotation angle (at all wavelengths) perfectly offsets the compensator, resetting the polarization state to that of the first polarizer. In this state, the maximum light energy at all wavelengths will pass through the second polarizer (DC intensity). As the thickness of

the wedge polarizer is varied, the polarization angle incident on the second polarizer will vary in a sinusoidal pattern between 0 and 100% transmittance; the frequency of the sinusoidal pattern will vary according to optical frequency. Therefore, the sum of the components incident on the detector will produce an optical interferogram. The optical efficiency of the device is limited by absorption in the beam path, especially as the thickness of the wedge polarizer reaches a maximum (which will limit maximum resolution).
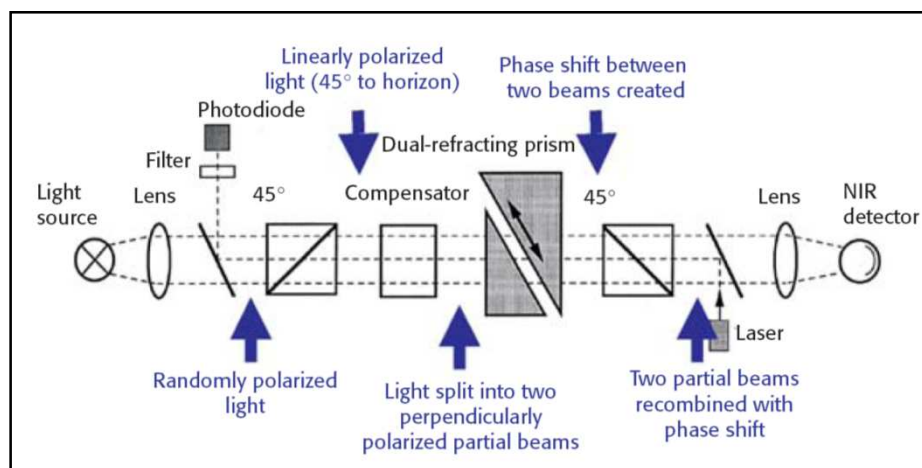
Figure 6: Overall schematic of the polarization interferometer. A sample is placed after the last lens and before the detector. A second lens then is needed to compensate for signal divergence through the sample. (Ciurczak 2005)

Early polarisation instrument models suffered from some wavelength stability problems, recent upgrades of the technology have yielded a very robust instrument with more than adequate resolution capability (Cogdill and James K. Drennen 2006), (Buchi). Because there is only a single optical path through the instrument (compared with the dual path of Michelson, Sagnac, or Mach-Zender interferometers), the polarization interferometer is less affected by small misalignments in the beam path, the sort of which might arise during at-line or in situ operation. Furthermore, the simple design is more cost-effective and can be produced with a smaller footprint.

1.6 Application-based instrument selection criteria

Modern NIR instrumentation for the analysis of pharmaceutical solids is best classified according to the demands of the application, as follows (FDA 2004):

At-line and off-line: Measurement where the sample is removed, isolated from, and analyzed in close proximity to (at-line) or away from (off-line) the process stream.

Applications include raw material identification, investigation of in-process (sampling) and finished materials, and data collection for method development. Many at-line NIR analyzers have automated sample conveyors and/or fibre-coupled probes. As they may be used for a wide variety of tasks, at-line analyzers generally offer the widest spectral range (often covering the entire NIR region), the highest spectral resolution, and internal means for background correction and performance qualification. These analyzers can be both interferometric, usually FT-NIR, or dispersive, typically utilizing a grating monochromator.

On-line: Measurement where the sample is diverted from the manufacturing process and may be returned to the process stream.

Process analyzers are often located in hazardous or controlled environments and their performance must be stable and robust to environmental variation. In addition, frequent instrument standardization and maintenance may be hindered by access or scheduling restrictions. Furthermore, frequent re-standardization or calibration updates can become a regulatory problem. The other critical factor affecting technology selection (and method development) is robustness (Zeaiter, Roger et al. 2004).

An at-line type of spectrometer can be adapted for on-line use by employing an automated sample handling mechanism if analysis speed was not critical. However, speed will often be a critical factor for on-line analyses of in-process materials or finished products. Thus, spectral range, resolution, sensitivity, or SNR may be sacrificed to increase the measurement speed. FT-NIR instruments have been developed for on-line applications by significantly reducing the length of measured interferograms. Grating monochromators can also be deployed effectively for some on-line applications. Acousto-optic tunable filter (AOTF) and holographic grating diode arrays have also some advantages in this field.

In-line: Measurement where the sample is not removed from the process stream.

The main difference from on-line instruments is the way the sensor interacts with the process. In-line measurements are typically performed by non-invasive or noncontact sensing directly through an optical window while the process is running.

Because the material being analyzed by in-line sensors is typically in motion, very high-speed spectrometers, especially diode array devices, are preferred. Slower-scanning instruments will often work for dynamic processes, provided that scan time is much less than the overall process time. In common with on-line applications, robust design of the sampling system is also a critical aspect of in-line sensor design. The spectrometer window should be resistant to material-wearing effects (e.g., sapphire) and might have an automated cleaning mechanism. In-line instruments may often be small and like to resemble a sensor much more than an analyzer. The use of RF wireless communication and battery-powered source illumination allow process spectrometers to be attached to moving equipment (e.g. blenders).

Diode array instruments are usually the most ideal for in-line use. Because in-line applications often involve long-term measurement of a single type of material, filter-type instruments (discrete photometers) are another option. Fast Fourier transform (FFT) of the detector signal can be used to isolate the spectral intensity data from instrumental noise effects, which, along with the simple, efficient design, make filter instruments very robust devices for single-material measurement.

Recently, NIR "micro-spectrometers" have been developed, which has the potential to greatly increase the pervasiveness of NIR process monitoring by producing extremely small, relatively inexpensive devices, based on microscopic tunable Fabry-Perot interferometers that are built into a single microchip. (Axsun)

2. Chemometrics

The term chemometrics was first used in 1971 to describe the growing use of mathematical models, statistical principles, and other logic-based methods in the field of chemistry and, in particular, the field of analytical chemistry. Chemometrics is an interdisciplinary field that involves multivariate statistics, mathematical modelling, computer science, and analytical chemistry.

Rapid technological advances, especially in the area of computerized instruments for analytical chemistry, have enabled and necessitated phenomenal growth in the field of chemometrics over the past 30 years.

Multivariate analysis

Because our environment is inherently multivariate, it is only logical to treat multiple measurements simultaneously in any data analysis procedure. By properly considering the distribution of multiple variables simultaneously, *more information* is obtained than could be obtained by considering each variable individually.

The additional information comes to us in the form of correlation which is overlooked if one variable at a time was examined. The advantages of chemometrics are often the consequence of using multivariate methods. Multivariate methods offer many advantages compared with univariate methods. Noise reduction is possible by eliminating redundant variables and partially selective measurements can be obtained free of the effects of interfering signals. Also, easier identification of false-identity or low-grade samples because the calibration is dependent on multiple factors which are more likely to point in the wrong direction in such cases (Bro 2003).

2.1 Spectral pre-processing (pretreatments)

The successful application of multivariate calibration methods is hindered by the presence of uninformative variance in the NIR spectra. Baseline effects may occur from small changes in sample properties (packing density, surface texture, temperature and humidity, inhomogeneities, etc.). In addition, uninformative variance may be introduced into a data set by changes in the operational parameters of the NIR spectrometer.

One approach to minimise these effects, is by applying mathematical pre-treatments to spectra. There are many types of such pre-treatments options, some of which are commonly indicated for certain conditions (like derivatives to exclude baseline shifts), while in many cases their use is strictly sample- and application-dependent.

2.1.1   Mean Centring and Variance Scaling

The application of mean centring and variance scaling is auto-scaling. Mean centring is applied by subtracting the mean spectrum of the data set from every spectrum in the data set, equation (0.4).

$$^{mc}R_{i,j} = R_{i,j} - \left(\sum_{j=1}^{J} \frac{R_{i,j}}{J} \right) \tag{0.4}$$

> *where*
> R =   Spectrum j in an array of J spectra
> i =   wavelength data point

In a multivariate sense, this pre-processing method translates the collection of data to the origin of the multivariate space where analysis will be performed. The practical consequence of mean-centring data is often a more simple and interpretable regression model. In effect, mean centring removes the need for an intercept from the regression model. Consequently, since fewer terms in the regression model may need to be estimated, estimated analyte concentrations may be more precise following mean centring of the data.

Variance scaling is applied to the jth wavelength of every spectrum by division of the standard deviation of the jth wavelength over all spectra in the calibration set. Thus, by variance scaling, the impact each variable has in determining the parameters of the calibration model is equalized.

$$^{vs}R_{i,j} = \frac{R_{i,j} - \sum_{i=1}^{J} \frac{R_{i,j}}{J}}{\sqrt{\sum_{i=1}^{J-1} \left(R_{i,j} - \sum_{i=1}^{J} \frac{R_{i,j}}{J} \right)^2}}$$
(0.5)

Equation (0.5) shows that variance scaling is performed by dividing mean centred spectra by variance at each wavelength over all wavelengths. Variance scaling is best employed when the variance of a particular wavelength has no correlation to the useful information content of that particular wavelength. Variance-scaled data gives equal weight to all wavelengths, regardless of whether they represent a vibrational overtone, scattering, or just baseline noise. Consequently, variance scaling is seldom beneficial for NIR calibration. However, in instances where the analytically useful signal is very weak compared to other absorbances, variable scaling can be essential.

2.1.2   Smoothing

With smoothing, it is possible to improve the signal-to-noise ratio of a signal recorded, for example, as a function of time or more commonly, wavelength.

Caution must be used when smoothing data. Strong smoothing gives better signal-to-noise ratios than weak smoothing, but strong smoothing may adversely reduce the resolution of the signal and hence affects methods involving spectra with sharp peaks or shoulders.

The simplest method of smoothing is to calculate a running average for a narrow window of points. The smoothed spectrum is generated by using the average value from the window. This causes problems at the endpoints of the curve, and numerous authors have described different methods for treating them.

The most commonly used type of smoothing is polynomial smoothing, also called Savitzky-Golay smoothing (Savitzky and Golay 1964). Polynomial smoothing works by fitting of a smooth polynomial function to the data in a sliding window of width w, where w is usually an odd number. Smoothed points are generated by evaluating the polynomial function at its midpoint. The window is moved to the right by dropping the oldest point from the window and adding the newest point to the window until the entire curve has been smoothed. The degree of smoothing is controlled by varying the width of the window, w, and by changing the degree of the fitted polynomial function.

2.1.3   First and second derivatives

Taking the derivative of a continuous function can be used to remove baseline offsets, because the derivative of a constant is zero. In practice, the derivative of a digitized curve can be closely approximated by numerical methods to effectively remove baseline offsets. (Brown, Vega-Montoto et al. 2000)

The derivative transformation is linear, and curves produced by taking the derivative retain the quantitative aspects of the original signal. The most commonly used method is based on polynomial smoothing. As in polynomial smoothing, a sliding window is used; however, the coefficients for the smoothing operation produce the derivative of the polynomial function fitted to the data. As in polynomial smoothing, the frequency-response function of these types of filters is not ideal, and it is possible to introduce distortions and artefacts if the technique is misused. Zero crossing points can be used to identify the location of peaks in the original spectra.

2.1.4   Normalisation

Here, each spectrum is normalized to constant area, thus removing the effect of the fluctuating signal. The simplest normalization technique is to simply set the sum of squares for each spectrum to 1, i.e., each spectrum has unit length. This procedure is similar to variance scaling, except the method is applied to rows in the data matrix rather than columns. Many other normalization schemes can be employed, depending on the needs dictated by the application. Normalisations by height, local band area or largest peak are other methods commonly used in spectroscopy.

2.1.5 *Multiplicative scatter correction (MSC) and standard normal variate (SNV)*

MSC is used a method to correct differences in baseline offsets and path length due to differences in particle-size distributions in near-infrared reflectance spectra of powdered samples. (Isaksson and Naes 1988)

In NIR reflectance measurements, there are two components of reflected light that reach the detector: specular reflectance (light reflected without being absorbed or interacting with the sample) and diffuse reflectance (light that is reflected by the sample after penetrating the sample particles, where some of the light is absorbed by the chemical components present in the particles). Powdered samples with very small uniform particles tend to pack very efficiently compared to samples with large, irregularly shaped particles. Samples with small, efficiently packed particles give a greater intensity of specular reflectance, and after transformation as log(1/reflectance), the higher levels of specular reflectance appear as increased baseline offsets; thus samples with smaller particle-size distributions tend to have larger baseline offsets. Beam penetration is shallow in samples with small, efficiently packed particles; thus these kinds of samples tend to have shorter effective path lengths compared to samples with larger irregularly shaped particles. MSC attempts to compensate these two measurement artefacts by making a simple linear regression of each spectrum against a reference spectrum. The mean spectrum of a set of training spectra or calibration spectra is usually used as the reference. The least-squares coefficients are first estimated and then used to calculate the MSC-corrected spectrum.

MSC has been shown to work well in several empirical studies, which showed an improvement in the performance of multivariate calibrations and a reduction in the number of factors in PCA. (Geladi, MacDougall et al. 1985)

However, in SNV transformation, the mean of each spectrum is subtracted and the length is normalized to 1, and it produces results similar to MSC in many cases, which sometimes makes it difficult to choose between the two methods. In practice, it is best to try both methods and select the pre-processing method that gives superior performance.

2.2 Multiple-linear regression (MLR)

MLR generalizes the simple linear regression model by allowing for many terms in a mean function rather than just one intercept and one slope.

Considering a response Y to a variable X_1 and the simple linear regression mean function with a slope of β_1 and an intercept of β_0:

$$E\left(Y \mid X_1 = x_1\right) = \beta_0 + \beta_1 x_1 \qquad (0.6)$$

By adding a second variable X_2, with which to predict the response, a mean function that depends on both the value of X_1 and the value of X_2 is needed:

$$E\left(Y \mid X_1 = x_1, X_2 = x_2\right) = \beta_0 + \beta_1 x_1 + \beta_2 x_2 \qquad (0.7)$$

The main idea in adding X_2 is to explain the part of Y that has not already been explained by X_1 (Weisberg 2005). The equation can be expanded to:

$$E\left(Y \mid X\right) = \beta_0 + \beta_1 x_1 + \ldots + \beta_p x_p \qquad (0.8)$$

With NIR spectroscopy, the correlation of absorbances (or transmissions) of adjacent wavelengths leads to collinearity. Also, there are usually fewer calibration samples available than there are recorded wavelengths in NIR spectra. Consequently, MLR often leads to unstable estimates of the response E. Also, the MLR model will fit the calibration set well, but if the regression vector is unstable, small random errors in future samples will be magnified. This may result in large prediction error in future samples.

However, MLR should not be summarily rejected. For applications with a small number of wavelengths (i.e., data from filter-wheel spectrometers), MLR is a potentially good method. In some cases, application of MLR following judicious selection of a wavelength may outperform other calibration methods. (Boysworth and Booksh 2001)

2.3 Principle component analysis (PCA) and regression (PCR)

The term principal component analysis (PCA) refers to a method of data analysis for building linear multivariate models of complex data sets (Thielemans and Massart 1985). The linear multivariate PCA models are developed using orthogonal basis vectors (**eigenvectors,** also called loadings), which are usually called **principal components**. One of the significant goals of PCA is to eliminate the principal components associated with noise, thereby reducing the dimensionality of complex problems and minimizing the effects of measurement error.

PCA is a statistical method that tries to explain the covariance structure of data by means of a small number of components. These components are linear combinations of the original variables, and often allow for an interpretation and a better understanding of the different sources of variation. Because PCA is concerned with data reduction, it is widely used for the analysis of high-dimensional data, which are frequently encountered in chemometrics. PCA is then often the first step of the data analysis, followed by classification, cluster analysis, or other multivariate techniques. It is thus important to find those principal components that contain most of the information (Hubert and Engelen 2004).

In the classical approach, the first principal component corresponds to the direction in which the projected observations have the largest variance. The second component is then orthogonal to the first and again maximizes the variance of the data points projected on it. Continuing in this way produces all the principal components, which correspond to the eigenvectors of the empirical covariance matrix.

This method would also be very sensitive to anomalous observations. Consequently, the first components are often attracted toward outlying points and thus may not capture the variation of the regular observations. Therefore, data reduction based on classical PCA (CPCA) becomes unreliable if outliers are present in the data.

2.3.1 Finding the factors

There are algorithms that can calculate the factors for a data matrix. The two most common are the NIPALS (nonlinear iterative partial least squares) algorithm, and SVD (singular value decomposition). In both, only the first N factors are calculated (primary PCs) where N is large enough to enable the determination of how many factors should be included in the basis space (secondary PCs).

$$ \mathbf{A} = \mathbf{T}_k \mathbf{V}_k^T + \varepsilon $$
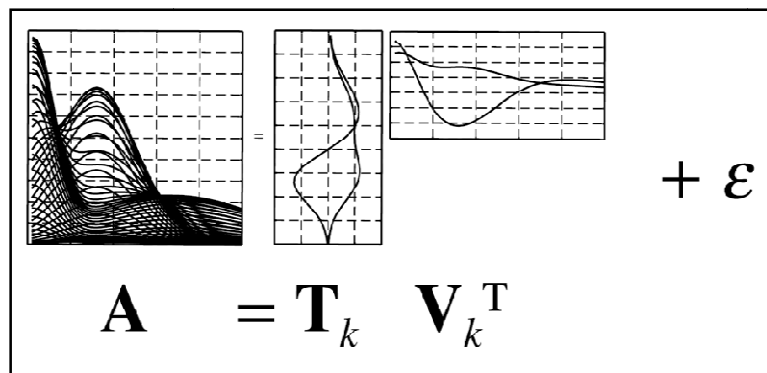
Figure 7: The PCA model. Spectral data matrix (A) is decomposed into eigenvectors (V) and their eigenvalues (T), plus additional non-explained variance (ε) (estimation error or noise). Modified from (Gemperline 2006)

SVD is a way of decomposing a data matrix into factors in a more general sense. Most SVD algorithms allow for proper management of the scale of the numbers to minimize problems of digital round-off error. The eigenvectors are organized into a matrix (V) which has as many rows as there are wavelengths in the original spectra (Figure 7). The length, or magnitude, of each eigenvector is normalized to unity. Thus, the vector cross product of each eigenvector multiplied with itself should be equal to 1. Also, all of the eigenvectors are mutually orthonormal. This means that the vector cross product of any eigenvector times any other eigenvector must equal 0. Each eigenvector in Vc has a corresponding **eigenvalue** which indicates the scale and direction of change in this vector. (Kramer 1998)

2.3.2 Factor selection

This is critical because retaining more factors than needed would only add more noise to predictions. On the other hand, if less than enough factors are kept, potentially meaningful information would be discarded that could be necessary for a successful calibration. There are a number of tools to help in the decision making process:

> **Indicator functions** (for data sets for which no reference values, or y-data, are available), which provide less reliable selection.
>
> PRESS for validation data
>
> One of the best ways to determine how many factors to use in a PCR calibration is to generate a calibration for every possible rank (number of factors retained) and use each calibration to predict the concentrations for a set of independently measured, independent validation samples. The predicted residual error sum-of-squares, or PRESS, is calculated for each calibration according, and the calibration that provides the best results is chosen. The number of factors used in that calibration is the optimal rank for that system.
>
> Cross-validation

In some cases, a sufficient set of independent validation samples with which to calculate PRESS is not available. In such instances, the original training set can be used to simulate a validation set. This approach is called *cross-validation.* The most common form of cross-validation is performed as follows:

> Calculate a calibration matrix using all of the training set samples except for one.
>
> Use the calibration to predict the concentrations of the components in the sample that was left out of the training set.
>
> Calculate the sum-squared of errors between the expected and predicted concentrations for the sample that was left out.
>
> Return the excluded sample to the training set, and leave out a different sample.
>
> Calculate a new calibration for this new subset of the original training set.
>
> Return to Step 2, above. Add the new PRESS value calculated in step 3, to the PRESS values calculated so far. Continue this process until PRESS values for all combinations of "leave one out" have been computed and summed.

Steps 1 - 6 are repeated for calibrations generated with every possible rank (number of factors). The PRESS is examined for each of the calibrations to choose the one that gives the best results. The number of factors used in that calibration is the rank of the system. This procedure is known as *"leave one out"* cross-validation. This is not the only cross-validation method, but rather the most popular. (Kramer 1998)

2.3.3   Spectral reconstruction and model calculation

By discarding the noise eigenvectors, it is possible to remove a portion of the noise from the data. The spectra which are generated after noise removal are the *reconstructed spectra.* When principal component regression, there is not really a separate, explicit data regeneration step, but by operating with the new coordinate system however, the spectra are automatically reconstructed with fewer noise using the factors that explain the spectral variation related to the change in the property under study rather than other influencing factors.

2.3.4   Predicting unknowns

To predict the concentrations in an unknown sample from its measured spectrum ($A_{unknwon}$), the calibration matrix (F_{cal}) calculated with the pre-selected factors is used to give:

$C_{unknown} = F_{cal} A_{unknwon}$

The prediction accuracy can be evaluated in light of the calibration model qualities obtained from validation (or cross-validation), as well as the closeness of the spectrum to the calibration data set (residual information – discussed in the following chapter).

2.4 Partial least squares (PLS) regression (PLSR)

PLS is a variation of PCR that takes its concept one step further by using a different strategy to find a coordinate system that can have advantages over the coordinate system used for PCR. This strategy involves finding factors for both the spectral and the referencing data.

The reasoning behind this approach is twofold: First, to utilize the noise removal capabilities of PCA and remove some of the noise from the reference data. Second, and because the noise in the spectral data will, in general, deflect each eigenvector slightly out of the plane containing the theoretical, noise-free data in some randomly different direction than the deflection of the corresponding spectral eigenvector (since noise in the reference and spectral data are independent of each other). PLS will rotate the vectors back toward each other until they are aligned, and provide better noise removal by bringing the vectors closer to the ideal planes containing the noise-free spectral and concentration data.

2.4.1 PLS principles

In addition to the set of new coordinate axes (basis space) for the spectral data (the x-block), we also find a set of new coordinate axes (basis space) for the referencing data (the y-block). These referencing data are expressed as projections onto the concentration factors (basis vectors) in a way similar to expressing the spectral data as projections onto the spectral factors (basis vectors).

Each pair of factors is rotated towards each other on a factor-by-factor basis to maximize the fit of the linear regression between the projections of the spectra onto the spectral factor with the projections of the reference data onto the concentration factor. The calibration (regression) coefficients are then calculated using linear regression between the projections of the spectra on each individual spectral factor with the projections of the reference data on each corresponding referencing factor of the same order.

The prediction step for PLS is also slightly different than for PCR where it is also performed on a rank-by-rank basis using pairs of spectral and referencing factors. Taking predicting concentration as an example, for each component, the projection of the unknown spectrum onto the first spectral factor is scaled by a response coefficient to become a corresponding projection on the first concentration factor. This yields the

contribution to the total concentration for that component that is captured by the first pair of spectral and concentration factors. The process is then repeated for the second pair of factors, adding its concentration contribution to the contribution from the first pair of factors, and continued until all of the factors in the basis space have been used.

2.4.2   Factor rotation in PLS

PLS will search for a single vector, W, that represents the best compromise between the spectral factor and the reference factor, which is not necessarily the factor that lies exactly half-way between them. It is, instead, the factor that maximizes the linear relationship between the projections (scores) of the spectral points onto the factor and the projections (scores) of the corresponding reference points onto this same factor and maximizes the covariance between the two.

2.5   Cluster analysis

The term "cluster" has the meaning of "concentrated" group. Cluster analysis tries to identify concentrated groups (i.e., clusters) of objects, while no information about any group membership is available, and usually not even the number of clusters is known. In other words, cluster analysis tries to find groups containing similar objects (Ripley 1996). The task of identifying concentrated groups of objects presumes that such a group structure is inherent in the data. This does not, however, lead to the assumption that an object belongs to only one group. Thus, clustering methods that perform a partitioning of the objects into separated groups will not always give the desired solution. For this reason many clustering algorithms have been proposed in the literature that do not only perform differently, but that even work on different principles.

2.5.1   Principal component analysis (PCA)

The first few principal components or factors represent a relevant part of the total data variance. Thus, when plotting pairs of principal component scores or factors, the data structure can be visually inspected in two dimensions in order to identify groups of objects. This approach works fine as long as objects of different groups are sufficiently different in the variable space, and the multidimensional space can be well represented by a projection (low intrinsic dimensionality), which is often the case.

Like PCR, PCA transforms a data matrix $X(n{\times}m)$, containing data for n objects with m variables, into a matrix of lower dimension $T(n{\times}a)$. In the matrix T, each object is characterized by a relative small number (a) of PCA scores (PCs, latent variables).

Score t_i of the ith object x_i is a linear combination of the vector components (variables) of vector x_i and the vector components (loadings) of a PCA loading vector p. The score vector t_k of PCA component k contains the scores for all n objects; T is the score matrix for n objects and a components; P is the corresponding loading matrix.

PCA is usually the first choice to visualize multivariate data by scatter plots and transform highly correlating variables into a smaller set of uncorrelated variables. Outliers may heavily influence the result of PCA and diagnostic plots help to find outliers (leverage points and orthogonal outliers) falling outside the hyper-ellipsoid which defines the PCA model.

In cases where PCA fails because of a complicated data structure, nonlinear methods like Kohonen mapping, Sammon's NLM, and cluster analysis with a dendogram can be useful alternatives, which are beyond the scope of this research.

3. Calibration model development

Univariate calibration is specific to situations where the instrument response depends only on the target analyte concentration. With *multivariate calibration*, however, model parameters can be estimated where responses depend on the target analyte in addition to other chemical or physical variables and, hence, multivariate calibration corrects for these interfering effects.

With multivariate calibration, wavelengths no longer have to be selective for only the analyte, but can now respond to other chemical species in the samples. Additionally, a set of calibration standards must be selected that are representative of the samples containing any interfering species. It would be possible to build a calibration model that compensates for the interfering species. However, due to spectroscopic noise and spectral collinearity (spectral overlap or selectivity), concentration estimates can be seriously degraded. Thus, selection of specific wavelengths to be included in the model is critical to the performance of the model.

3.1   Data sets and representative sampling

Calibration samples must include representation for every responding chemical species in a system under study. Spectral shifts and changes in instrument readings for mixtures due to interactions between components, changes in pH, temperature, ionic strength, and index of refraction are well known. The use of mixtures instead of pure standards during calibration enables multivariate calibration methods to form approximate linear models for such interactions over narrow assay working ranges, thereby providing more precise results.

The calibration samples must cover a sufficiently broad range of composition that a suitable change in measured response is instrumentally detectable. For simple systems, it is usually possible to prepare mixtures according to the principles of experimental design, where concentrations for all ingredients are varied over a suitable range. Because it is more desirable to make interpolations rather than extrapolations when making predictions from a calibration model, the range of concentrations in the calibration standards should exceed the expected working range of the assay. Calibration sample compositions should give a fairly uniform coverage across the range of interest. However, if the range is too large, deviations from linearity could begin to appear. The recommended minimum number of calibration samples is 30 to 50, although this depends on the complexity of the problem (ASTM 1999).

It is very important that validation sets do not contain aliquots of samples used for calibration. The validation sample set must form a truly independent set of samples. Another equally important point is that the composition of validation samples should be designed to lie at points in between calibration points, so as to exercise the interpolating ability of the calibration model.

Different validation data sets should be prepared to investigate every source of expected variation in the instrument response, operational environment changes, as well as expected sample variability.

Proper setup of calibration sets yields calibrations that are superior in terms of both precision and accuracy. The complexity of calibration development has not allowed, yet, completely automated mathematically modelling in any current software. In any case, the most critical step in calibration is the proper collection of samples to represent the population for routine analysis.

3.2   Method development and evaluation

It is the best mathematical model that when applied to photometric data obtained from a sample of unknown concentration will compute a reliable, accurate, and reproducible value of percent composition for the component(s) of interest. The ideal mathematical model will be "blind" to endogenous instrument variation, temperature effects, background interferences, and the like, and at the same time be most sensitive to changes in the concentration of the component(s) of interest. the commonly used calibration techniques include the rigor of experimental design, calibration modelling, and validation testing.

3.2.1   *Wavelength selection*

When performing multivariate analysis on such mixtures, the analyst musts elect wavelengths where the molar absorptivities for the components are most different. Only with perfectly error-free data will *any* wavelength set permit the generation of a calibration equation that fits the data perfectly.

With complex matrices, it is impossible to know if an ideal set of wavelengths has been selected for a calibration equation. Often when new instrumental effects are indicated and when new calibration sets are selected, new wavelengths are chosen for the same application.

Different wavelengths will, of course, give rise to different values for the calibration coefficients, reflecting the different values of the extinction coefficients at different wavelengths.

In simple calibrations, the differences between the spectra would be considerable and can be ascertained visually and the wavelengths to use for the discriminations selected manually. If the spectra are very similar, or if there are so many different materials involved that visual inspection becomes confusing, then such an a priori selection would not be possible. In the absence of a prior knowledge of which wavelengths are suitable for performing the desired discriminations, a method of selecting the optimum set of wavelengths is needed that maximizes the distances between groups that are close together in the multidimensional space, in other words, a criterion that emphasizes the differences between those materials that have similar spectra but different reference values. A solution to this problem would to compute all the intergroup distances and select the variables that maximize the distance between the closest pair of groups.

One method of wavelength selection that has been devised for implementation with the current algorithms in use in NIR is to calculate the distances D, between all pairs of groups i and j, and the sum of the inverse squared distance, in other words, $(1/D_{ij})$ is formed. The groups that are closest together will contribute most heavily to this sum; thus selecting those wavelengths that cause this sum to be smallest results in the selection of the wavelengths that best separate the closest groups, in other words, best distinguish the most similar spectra. This approach has an advantage over the simpler one in that this technique will optimize among all groups that are comparably closely spaced rather than concentrating on only the single closest pair (Mark 2001).

3.2.2   Model evaluation and optimisation

Many parameters can be used to assess the performance of NIR calibration models. Although automatic optimisation routines exist in literature and practice, manual intervention is needed because, depending on the application, each calibration will be evaluated differently.

3.2.2.1   *Coefficient of Multiple Determination (r^2 or R^2)*
Also termed total explained variation, this statistic allows us to determine the amount of variation in the data that is adequately modelled by the calibration equation as a total fraction of 1. Thus R^2 = 1.00 indicates the calibration equation models 100% of the variation within the data, while an R^2 = 0.50 indicates that 50% of the variation in the difference between the actual values for the data points and the predicted or estimated

values for these points are explained by the calibration equation (mathematical model), and 50% is not explained. R^2 values approaching 1.00 are attempted when developing calibration.

3.2.2.2 *Student's t value for regression or residuals (t, √F)*

This statistic is used to determine of the correlation between X and Y data. It can be used to determine whether there is a true correlation between an NIR value and the primary chemical analysis for that sample. It is used to test the hypothesis that the correlation really exists and has not happened only by chance. A large t value indicates a real (statistically significant) correlation between X and Y.

When used for residuals, the test allows evaluating criteria for assessing the variation between an NIR value and its primary chemical value, and *t* values greater than 2.5 are considered significant and such predictions may possibly be outliers. Most often, high t-test values here indicate poor laboratory results or a problem with sample presentation and positioning.

3.2.2.3 *Standard error of estimate (SEE), or standard error of calibration (SEC)*

This statistic, equation (0.9), is the standard deviation for the residuals due to differences between actual (primary wet laboratory analytical values) and the NIR predicted values for samples *within the calibration set*. It is an indication of the total residual error due to the particular regression equation to which it applies. The SEC will generally decrease with higher number of wavelengths (independent variable terms) used within an equation, indicating that increasing the number of terms will allow more variation within the data to be explained, or "fitted".

$$SEE = SEC = \sqrt{\frac{\sum_{i=1}^{N}\left(y_i - \hat{y}_i\right)^2}{N}} \qquad (0.9)$$

> *where*
> N = total number of samples used in the calibration
> y_i = a singular y value for the ith sample
> $\hat{y}_i$ = estimated y value given a regression line

The SEC statistic is a useful estimate of the theoretical "best" accuracy obtainable for a specified set of wavelengths used to develop a calibration equation.

3.2.2.4 *Standard Error of Prediction (SEP)*

The SEP is also termed the standard error of performance, is the standard deviation for the residuals due to differences between actual (primary wet chemical analytical values) and the NIR predicted values for samples *outside of the calibration set*. The SEP is calculated from equation (0.9) using validation instead of calibration samples. It allows for comparison between NIR-observed predicted values and wet laboratory values.

The SEP is generally greater than the SEC but could be smaller in some cases due to chance alone. When calculating the SEP, it is critical that the constituent distribution be uniform and the wet chemistry be very accurate for the validation sample set. If these criteria are not met for validation sample sets, the calculated SEP may not have validity as an accurate indicator of overall calibration performance.

3.2.2.5 *Standard Error of Cross-Validation (SECV)*

The calculation of SECV is a method for determining the "best" number of independent variables to use i n building a calibration equation. The SECV method is based on an iterative (repetitive) algorithm that selects samples from a sample set population to develop the calibration equation and then predicts on the remaining unselected samples. Some procedures for calculating SECV may calibrate using two-thirds of the samples while predicting on the remaining one-third of the samples. The SECV is an estimate of the SEP and is calculated as SEP or SECV as the square root of the mean square of the residuals for N - 1 degrees of freedom, where the residual equals the actual minus the predicted value.

3.2.2.6 *Bias-Corrected Standard Error*

Bias-corrected standard error measurements allow more accurate evaluation of error in cases where model bias has been evaluated. The bias value (b_0) is calculated as the mean difference between two columns of data, most commonly actual minus NIR predicted values.

$$SEC_C, SEP_C = \sqrt{\frac{\sum_{i=1}^{N}\left(y_i - \hat{y}_i + b_0\right)^2}{N}}$$

(0.10)

where
N	=	total number of samples used in the calibration
y_i	=	a singular y value for the ith sample
$\hat{y}_i$	=	estimated y value given a regression line

3.2.2.7   *PRESS (Prediction Sum of Squares)*

This statistic calculates the error sum square (between predicted and reference values) as a function of the number of factors (eigenvectors, principal components or principal factors). The optimum number of PC is always given by the smallest number of PC where the PRESS function for the calibration and validation sets is approximately equal and minimal.

$$PRESS = \sum_{i=1}^{N} \left(y_i - \hat{y}_i \right)^2 \qquad (0.11)$$

where

N	=	total number of samples used in the calibration
y_i	=	a singular y value for the ith sample
$\hat{y}_i$	=	estimated y value given a regression line

3.2.2.8   *Other performance indicators*

3.2.2.8.1   SEC / SEP RATIO

This describes the relation between the standard errors of the calibration and validation sets. An SEC much higher than SEP indicates over-fitting of the model to the calibration samples.

3.2.2.8.2   BIAS

This is the average deviation between the calibration and validation predictions, calculated from equation (0.12) below.

$$Bias = \frac{\sum_{i=1}^{N} y_i - \hat{y}_i}{N} \qquad (0.12)$$

where

N	=	total number of samples used in the calibration
y_i	=	a singular y value for the ith sample
$\hat{y}_i$	=	estimated y value given a regression line

3.2.2.8.3   REGRESSION COEFFICIENT, INTERCEPT AND SLOPE

Absolute regression coefficient near 1.0 shows that two properties are linearly dependent. Slope should be as close as possible to 1.0 and intercept to 0.

3.2.2.8.4 DURBIN-WATSON STATISTIC

This statistic can be used to assess the lack of inter-correlation between data points in the regression. Since the correlation coefficient R only describes the tendency of the line, not the trueness of fit to a linear model. If there is no inter-correlation of the residuals described by the Durbin–Watson statistic, then a linear model is appropriate and may be used. A value closest to 2 indicates good linear correlation referenced and predicted values.

3.2.2.8.5 LEVERAGE

The concept of leverage in statistics is comparable to the physical model of a lever. The hinge for the calibration line lies the centre of the x-values. Calibration samples close to the mean of the x-values tend to exert little force on the slope of the calibration curve. Calibration samples farthest from the mean of the x-values can put forth a greater force on the slope of the calibration curve, so that their residuals are made as small as possible. Leverage plots can be used to find optimal factors or to detect outliers.

3.3 Method validation

Validation of a multivariate calibration model is a critical step that must take place prior to widespread adoption and use of the calibration model for routine assays or in production environments. Many official monograms, standards, papers and published guidelines exist, directed both to NIR use in general, or specific for pharmaceutical release purposes. Of these, the most notable guidelines are through:

USP (USP 30 NF25 2007)

> 1119 – Near-infrared spectrophotometry
> 1225 – Validation of compendia procedures
> EP and BP (BP 2007, EP 5.5)
> Ph. Eur. method 2.2.40 – Near-infrared spectrophotometry
> SC III F. Validation of analytical procedures
> EMEA
> "Note for guidance on the use of near infrared spectroscopy by the pharmaceutical industry and the data requirements for new submissions and variations" , 2003
> ICH guidelines
> Q2(R1) "Validation of analytical procedures: text and methodology"
> PASG

Guidelines for the development and validation of near infrared (NIR) spectroscopic methods, 2001

Assuming that an appropriate quality assurance program is in place, three criteria must be met: validation of the software; validation of the hardware; and validation of the NIR spectroscopic method (or any analytical method). Currently, reputable NIR software and hardware manufacturers provide considerable regular automated suitability tests using approved standards in order to validate NIR software and hardware.

The purpose of method (or model) validation is to determine the reproducibility of a multivariate calibration, its bias against a known method or accepted values, and its long-term ruggedness (robustness). Regardless of the numerous sources providing general direction to the method developer, validation is an extremely complex regulatory issue that is not easily defined.

The term validation, in the regulatory context of a NIR method, refers to the establishment of appropriate data and documentation to certify that the method performs as intended.

Provided that instrument and software validation have been established, as well as following cGMP and cGLP guidelines, NIR method validation can be achieved by observing the points outlined below.

3.3.1   Specificity

Specificity is the ability to assess unequivocally the analyte in the presence of components that may be expected to be present. A major problem with utilizing NIR to accurately determine concentrations of actives in solid dosage forms is that the analysis is performed without removing the analyte from its matrix.

The very property that makes NIR so attractive, allowing analysis of intact dosage forms and intermediate products without dissolution/extraction of the active agent, is also the issue that could potentially limit its application to pharmaceutical analysis, if we are restricted to current validation regulations.

Because NIR spectra represent all materials present in the formulation, including the active, specificity is a major validation hurdle that must be overcome if NIR is to be used as a release testing technique.

One mechanism that is proposed to address this problem is to first identify the product being tested before quantifying the analyte of interest, using several lots of product with varying analyte values.

3.3.2   Linearity

The linearity of a NIR spectroscopic method is determined from the multiple correlation coefficients (R) of the NIR predicted values of either the calibration or validation set with respect to reference values. It may be argued that this is an insufficient proof of linearity since the analyst is comparing information from two separate instrumental methods, and thus simple linearity correlation of NIR data through regression versus some primary method is largely inappropriate without other supporting statistics.

A potentially more appropriate statistical tool, that being the Durbin–Watson statistic (d) (Draper and Smith 1998), can be used to assess the lack of inter-correlation between data points in the regression. The Durbin–Watson statistic is more of a test for nonlinearity, calculated from residuals obtained from fitting a straight line. The statistic evaluates for sequential dependence in which error is correlated with those before and after the sequence.

If successive residuals are positively serially correlated, that is, positively correlated in their sequence, d will be near zero. If successive residuals are negatively correlated, d will be near 4, so that 4 - d will be near zero. The distribution of d is symmetric about 2.

3.3.3   Range

The ICH guidelines recommend a minimum range of 80 to 120% of the test concentrations for assay of a drug substance or a finished product and 70 to 130% of the test concentration for content uniformity.

This brings about the need for out-of-specification samples to extend the very narrow concentration ranges from production samples to this range. This might seem trivial, but in reality, is not so simple. The first problem is that it would mostly be impossible to provide out-of-specification product in the production environment.

Manufacturing these out-of-specification samples in a pilot plant or laboratory will lead to further problems. Despite the use of identical raw materials (relative to the production samples), the "process signature" is often so significantly different from laboratory to production to pilot scale that significant calibration errors will arise. For

example, the dwell time, compaction force, and feed rate variations that exist between the different scales of manufacturing can cause significant variations in sample properties and hence NIR spectra, even when formulations are identical. Thus, expansion of the range of concentration values through the use of laboratory or pilot plant samples is, in most cases, impractical. It is possible that the range problem is the single most significant issue prohibiting a uniform approach in wide implementation of quantitative NIR techniques in the industry.

3.3.4   Ruggedness/Robustness

The robustness of any method may be measured by inflicting small, deliberate variations in the method and ascertaining whether any changes in the predictions gleaned are significant, e.g. turning the tablet over from one side to the other. Method developers must consider tests to evaluate algorithm stability during the development and validation processes.

For solid dosage forms in particular, this issue is of prime importance, and if the variation in physical parameters as a result of small process variability is not sufficient to flag the sample as an outlier, it is still unknown whether or not this variation would contribute to significant prediction errors. This issue is one the topics investigated in this research.

The evaluation of robustness should be considered during the development phase and depends on the type of procedure under study. It should show the reliability of an analysis with respect to deliberate variations in method parameters. One consequence of the evaluation of robustness should be that a series of system suitability parameters (e.g., resolution test) is established to ensure that the validity of the analytical procedure is maintained whenever used. (ICH 2005)

3.3.5   Accuracy

The accuracy of an analytical procedure expresses the closeness of agreement between the value which is accepted either as a conventional true value or an accepted reference value and the value found (trueness).   There are several methods of establishing accuracy (ICH 2005):

> Application of the analytical procedure to synthetic mixtures of the drug product components to which known quantities of the drug substance to be analysed have been added.

Compare the results obtained from a second, well characterized procedure, the accuracy of which is stated and/or defined.

Accuracy may be inferred once precision, linearity and specificity have been established.

3.3.6 *Precision*

Precision of any analytical procedure describes how close the agreement is, between a series of measurements obtained from multiple sampling of the same homogenous sample under the prescribed conditions. The precision of an analytical procedure is usually expressed as the variance, standard deviation or coefficient of variation of a series of measurements and can be described in terms of:

Repeatability

This is precision under the same operating conditions over a short interval of time. Repeatability is also termed intra-assay precision and should be assessed using:

Minimum of 9 determinations covering the specified range for the procedure (e.g. 3 concentrations/3 replicates each); or

Minimum of 6 determinations at 100% of the test concentration.

Intermediate precision

This expresses within-laboratories variations and should establish the effects of random events on the precision of the analytical procedure. Typical variations to be studied include days, analysts, equipment, etc. It is not considered necessary to study these effects individually.

Reproducibility

This describes the precision between laboratories (collaborative studies, usually applied to standardization of methodology).

Since this discussion is specific to intact dosage forms, repeatability takes on a slightly different colour than for HPLC methods. While sample preparation is usually significantly reduced for NIR methods in comparison to traditional wet chemical methods, thus reducing method error from dissolution, extraction, and the like, the diffuse reflectance and diffuse transmittance methods common to NIR practice are susceptible to other factors that can ultimately reduce precision. The "repack error" once described for ground grain samples that were repacked into the traditional NIR sample cup may more aptly be described as a "positioning error" for today's non-destructive analyses of intact dosage forms. Appropriate sample handling and various

mathematical routines allow minimization of the spectral variability and imprecision arising from this type of error.

3.3.7   Detection and quantification limits

The detection limit of an individual analytical procedure is the lowest amount of analyte in a sample which can be detected but not necessarily quantified as an exact value, while the quantification limit is the lowest amount of analyte in a sample which can be quantitatively determined with suitable precision and accuracy. The quantification limit is a parameter of quantitative assays for low levels of compounds in sample matrices, and is used particularly for the determination of impurities and/or degradation products.

4. NIRS and process analytics

In 2004, the US FDA announced their guidance document on process analytical technology (PAT) and triggered a rapidly growing movement within the pharmaceutical industry. In the FDA definition, PAT consists of "*Systems for the analysis and control of manufacturing processes based on timely measurements, during processing of critical quality parameters and performance attributes of raw materials and in-process materials and processes to assure acceptable end product quality at the completion of the process*" (Hussain 2002).

From this definition, the PAT toolbox consists of four main elements:

> Multivariate data acquisition and analysis tools
> Modern process analysers or process analytical chemistry tools
> Process and endpoint monitoring and control tools
> continuous improvement and knowledge management tools

Since then, PAT has been an important subject of research and industry, suppliers, government, and academia are still wrestling with a huge number of method development and implementation issues. Despite this tremendous effort, PAT is in an early stage of development in the pharmaceutical manufacturing industry.

Although PAT has been applied extensively in other industries (e.g., chemical and food processing), the nature of pharmaceutical manufacturing presents new challenges in terms of regulation, risk, and complexity. In addition, PAT applications will place new demands on the existing industrial infrastructure and a significant amount of practical, application-specific research is required to support the deployment, operation, and maintenance of associated analytical methods.

Critical issues that must be considered during PAT method development include (Cogdill, Anderson et al. 2004):

> risk analysis of the process
> feasibility studies
> experimental design
> sensors and technology selection
> model development and transfer
> process sampling

information management

The integration of these concepts and issues into the development effort will produce a more effective method and a better grasp of the technology. This understanding corresponds to fundamental knowledge about the basis for method operation and critical factors affecting method performance. The result of integrated development is a validated method that provides information about the process.

Near infrared (NIR) spectroscopy is an important process analyser and is perhaps the most dominant technology within this group of process analysers. Because NIR spectra are capable of providing a very detailed physical and chemical picture of the process at many positions in the manufacturing line, this makes NIR such a versatile and powerful instrument for PAT applications.

5. Sample properties affecting spectra

As has been discussed in previous sections, NIR spectra are the convolution of chemical and physical interactions between the sample and NIR radiation.

Although the value of the chemical information in NIR spectra is obvious, the physical factors, which affect NIR spectra may also yield useful information related to the quality (state) of the sample material. In other cases, the presence of strong variations in concomitant physical parameters may overwhelm the analytical signal of interest.

5.1 Particle Size

The particle size distribution (PSD) and mean particle size are critical quality control factors for pharmaceutical solids (e.g. raw material quality or process control). Drug and excipient PSD variability can affect dosage form performance by altering dissolution rate or bioavailability, or it can affect drug product quality in manufacturing by altering the flow properties of the materials.

Since the angle of optical diffraction for a single-particle event is inversely proportional to particle size, the actual angle of diffraction will depend not only on particle size and wavelength of incident light but also on particle morphology and refractive index, as described by Mie and Fraunhofer theories of optical scattering (Ingle and Crouch 1988).

Thus, as particle size varies, the relative level of forward and backward scattering events will vary as well, causing a change in apparent optical absorption. Larger particles, for example, will have a greater proportion of forward scatter, which reduces the probability that a diffusely scattered photon from an incident beam will be returned to the surface of a sample in DR (Figure 8).
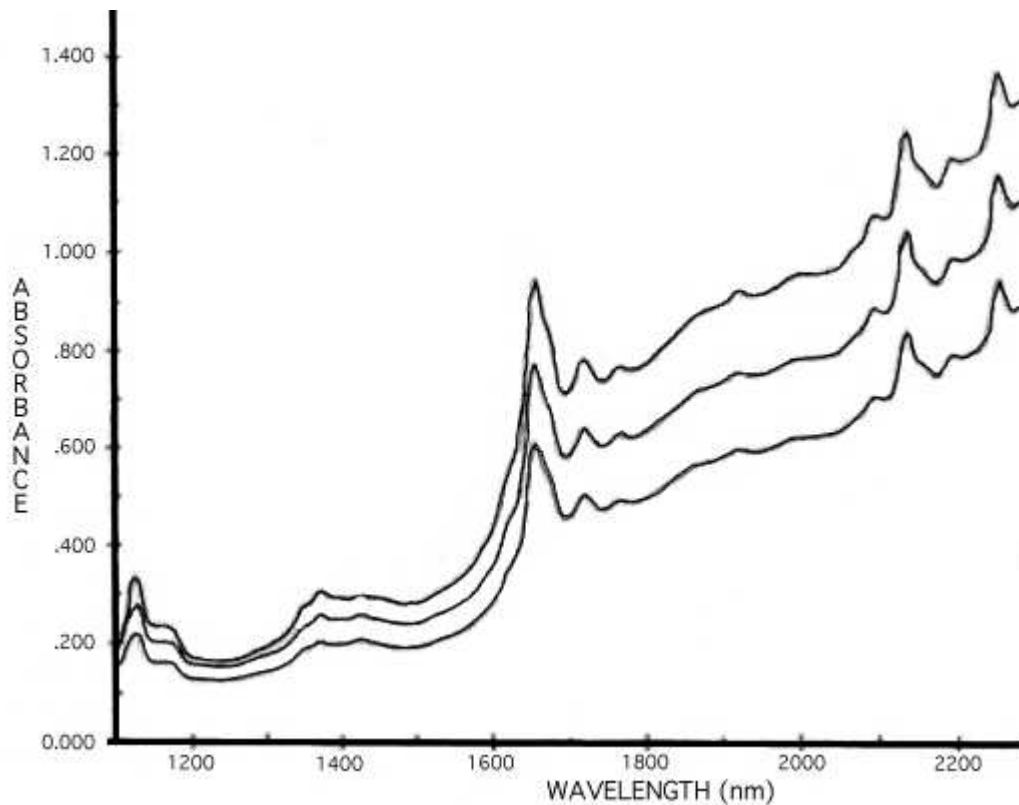
Figure 8: NIR DR spectra of (from below up) 40, 100, and 200μ aspirin powder samples

Particle size variation will also affect particle packing characteristics, leading to more complex spectral effects. Hence, there has been great interest in using NIR spectroscopy for rapidly determining MMPS or PSD of pharmaceutical solids and granules. Ciurczak (1986) published some of the first pharmaceutical work relating the particle size of pharmaceutical raw materials to variation in NIR spectra, demonstrating a linear relationship between the absorbance at any wavelength and the reciprocal of particle size as measured using low-angle laser light scattering.

Numerous references on the use of NIR for particle size analysis followed. Examples include the application of NIR for real-time median particle size determination during granulation (Rantanen and Yliruusi 1998) and MPS of API in a binary mixture (Frake, Luscombe et al. 1998). Laser diffraction or sieve analysis was used for reference testing in all cases.

5.2 Crushing strength-related physical properties

Crushing strength (hardness) has been observed to have a measurable effect on NIR spectra. Tablet crushing strength is a common product release parameter and is important for process control, because varying crushing strength might affect product friability, disintegration, dissolution, and ultimately, bioavailability. The crushing strength and apparent density (or porosity, solid fraction) are common parameters for process control during roller compaction.

Drennen published the first examples of using NIR spectroscopy and chemometrics for non-destructive tablet crushing strength in 1991. Subsequent publications by Ciurczak and Drennen (1992) and Drennen and Lodder (1993) further explored the application using both quantitative and qualitative methods. It was observed in all of these experiments that changes in dosage form crushing strength are indicated by a sloping baseline shift of the apparent absorption spectrum measured in reflectance.

As the tablet (or compact) crushing strength increases, the apparent absorption baseline increases. Although the root cause of the spectral effect is not conclusively established, some references do posit hypotheses. It is suggested however, that as tablet crushing strength increases (and the total surface area of inter-particle contact increases), less fraction of the radiation is backscattered due to the air–particle interface, reducing the magnitude of reverse flux. At the same time, a greater fraction of the radiation propagates through points of inter-particle intimate contact, increasing the magnitude of forward flux. As fewer scattered photons reach the reflectance detector via reverse flux, the apparent absorbance increases (measured reflectance decreases). This hypothesis is supported by the observed relationship between the tablet crushing strength and NIR transmittance, whereby increasing crushing strength reduces the apparent tablet absorbance.
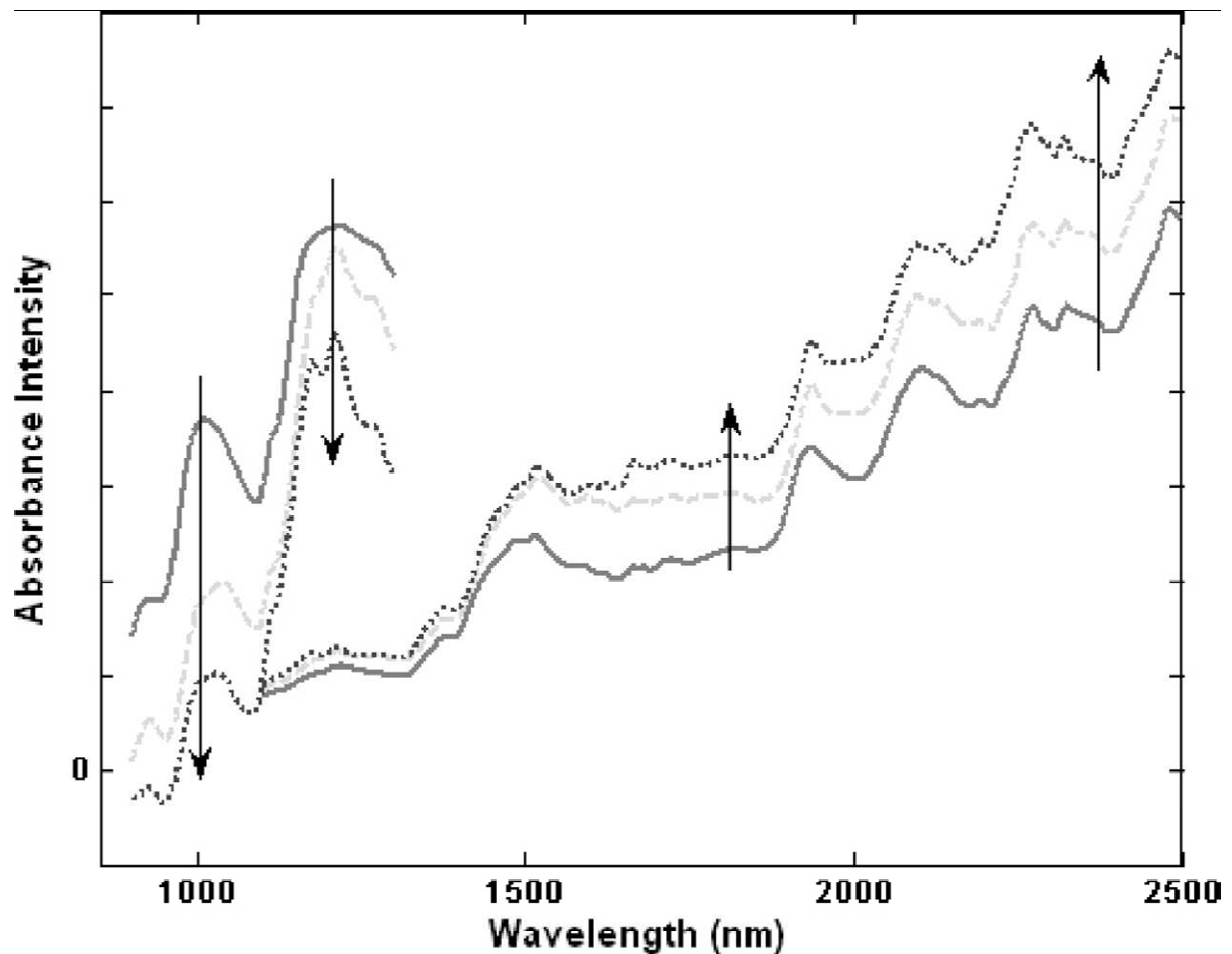
Figure 9: Effect of increasing crushing strength on NIR Transmittance (downward arrows) and reflectance spectra (upward arrows). Arrows indicate direction of increasing crushing strength. (Cogdill and James K. Drennen 2006)

As is for the effect of particle size, the rate of baseline increase is more pronounced near strong absorption bands. Although baseline shifting is the most pronounced spectral change observed with varying tablet crushing strength, other spectral changes (e.g., peak shifting) have been observed.

It has been shown that the crushing strength can be predicted with reasonable accuracy by simply fitting linear or nonlinear functions to the NIR baseline (Guo, Skinner et al. 1999) and then correlating crushing strength to selected coefficients of the baseline fit.

5.3   NIR sampling span

The need for effective sampling is common to all analytical techniques. With NIR spectroscopy, a great deal of attention is usually given in the selection of calibration samples highly representative of end product units over different batches. However, another aspect of sampling is as equally important and sometimes overlooked. NIR radiation in classical diffuse reflection mode is reflected from a central area of the surface and is only assumed rather than proven representative of the whole tablet.

The scale of mass to be assayed 'scale of scrutiny' (Donoso, Kildsig et al. 2003), (Berntsson, Danielsson et al. 1998) by any method depends on both the magnitude of the unit dose in question and the application. For example, monitoring blend uniformity requires minimal effective sampling mass, while the reverse is true for individual dosage forms. Moreover, the effective sampling mass has a complex and nonlinear effect on NIR transmittance and reflectance spectra. (Bull 1990)

5.3.1   *Diffuse reflectance*

There is little experimental evidence of how deep the radiation penetrates the surface in diffuse reflection. This penetration is sample-dependant and the difference between loose and compacted powders is significant.

Few researchers have tried to DR estimate information depth for powder mixtures. Olinger and Griffiths (2001) used absorbance values for mixtures with known absorptivities and particle size values and reported an upper boundary of 1 mm at 1653 nm. It was also reported that if scattering effect was to be considered, this range would unlikely be more than 300 µm. Others have reported different values but without supporting experimental or theoretical evidence: 5 mm (MacDonald and Prebble 1993), 1-2 cm (Ciurczak 1991), 1-4 mm (Olinger and Griffiths 1992), 0.5 mm (Stephen Victor Hammond 1997).

The evidence is even smaller for compacted solids. Iyer (Iyer, Morris et al. 2002) have tried to estimate the sampled mass in DR using single and double-layered tablets and second derivative spectra. He concluded that the effective sampling depth was between 1.9 and 2.7 mm depending on the wavelength. Another study by Andersson (Andersson, Josefson et al. 1999) showed different values and suggested an information depth of 0.1 - 0.2 mm using incremental coating and tablets with 2 different components. The authors however maintained that these figures are only rough estimates because the

results were obtained using extrapolation and may only be valid for specific materials and instruments.

Because of such varying views on DR information depth, the exact value is still not clear to operators of the method. Additionally, since the majority of pharmaceutical tablets range in thickness between 1 – 4 mm, determining this depth is crucial to the selection of appropriate measurement modes for different coated, uncoated and multi-layered tablets and can provide better understanding of the performance differences between DR and DT modes.

5.3.2   Diffuse transmission

Diffuse transmission mode penetrates the whole thickness of the tablet and would theoretically be more representative of the whole tablet (Berntsson, Burger et al. 1999) especially for low-dose units where aggregation has a higher effect. It is not clear, however, what path the radiation follows inside the tablet and hence the percentage actually being scanned. Moreover, transmission is more sensitive to path-length and density variability. Iyer *et al.* (2002) did a series of experiments to address this issue. They calculated a wavelength-dependent information depth for reflection ranging between 1.9 to 2.7 mm using second derivative spectra from tablets of increasing thickness. They also showed a limiting tablet thickness of 3.5 – 4.8 mm for transmission. Another set of experiments showed an effective transmission diameter of 7 mm and concluded that the mass sampled for both modes was comparable and around 200 mg. However, the radiation intensity inside this diameter is fading towards the periphery in all directions making the mass over-estimated in this case, especially for reflection. Also, the fact that sampled mass is largely dependent on physical properties of the sample, mainly crushing strength and packing, makes this issue an open question.

6. Pharmaceutical Tableting

The oral route is the most common way of administering drugs, and among the oral dosage forms tablets of various different types are the most common. The EP defines tablets as 'solid preparations each containing a single dose of one or more active ingredients and obtained by compressing uniform volumes of particles' (EP 2006).

Tablets are prepared by forcing particles into close proximity to each other by powder compaction, which enables the particles to cohere into a porous, solid specimen of specified geometry. This compaction takes place in a die by the action of two punches, the lower and the upper, by which the compressive force is applied.

Powder compaction is the reduction in volume of a powder by the application of a force. Because of the increased proximity of particle surfaces accomplished during compaction, bonds are formed between particles which provides coherency to the powder, i.e. a compact is formed.
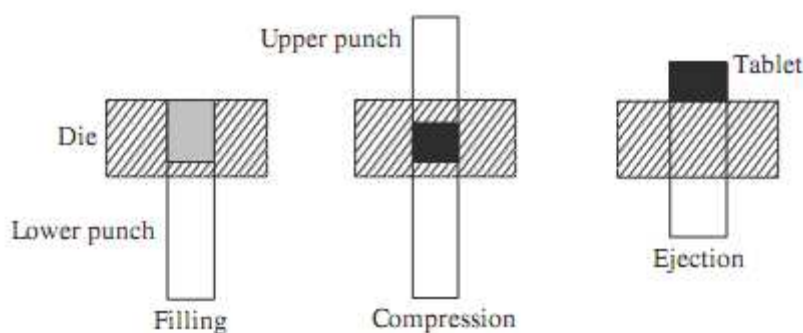
Figure 10: Stages of tablet manufacture (encyclopaedia of ph tech, p 3654)

Irrespective of the press type used, a complete tablet manufacturing cycle occurs in the following steps (Figure 10): *(i)* the die is filled and adjusted (scraped), *(ii)* the tablet is compacted, and *(iii)* the tablet ejected from the die.

6.1 Single-punch press (eccentric press)

Eccentric tablet presses are single station tablet presses that use an eccentric shaft connected to a rotating wheel to control the displacement of the upper punch into the die. In an eccentric press, the displacement profile of the upper punch is sinusoidal and the displacement rate is controlled by adjusting the rotation rate of the eccentric wheel (Figure 11). The lower punch remains stationary during the compaction and acts only to enable uniform die filling prior to tablet formation and tablet ejection after tablet formation. Eccentric presses utilize single-sided compaction to make tablets, where as rotary presses use double-sided compaction. Also, eccentric press compaction cycles do not have a dwell time, where rotary presses typically use a punch head flat which enables a dwell time as the punch passes under the compaction roller. Finally, the degree of machine deflection is different for these different presses. (Augsburger and Hoag 2008)
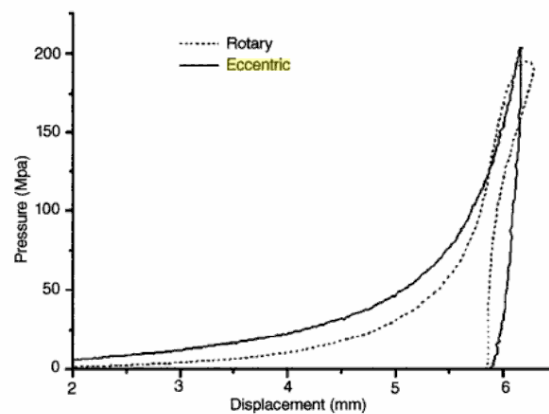
Figure 11: Displacement profile of an eccentric press compared to a rotary press
(Augsburger and Hoag 2008)

6.2   Rotary press

The rotary press was developed to increase the output rate of tablet production. A rotary press operates with a number of dies and sets of punches. The dies are mounted in a circle in the die table and both the die table and the punches rotate together during operation of the machine, so that one die is always associated with one pair of punches. The vertical movement of the punches is controlled by tracks that pass over cams and rolls used to control the volume of powder fed into the die and the pressure applied during compaction. The powder is held in a hopper whose lower opening is located just above the die table. The powder flows by gravity on to the die table and is fed into the die by a feed frame. The reproducibility of the die feeding can be improved by a rotating device, referred to as a force-feeding device. During powder compaction both punches operate by vertical movement. After tablet ejection, the tablet is knocked away as the die passes the feed frame.

1. die table
2. fill cam
3. feed wheel with paddles
4. die fill area
5. metering wheel with paddles
6. pre-compression roller
7. main compression roller
8. ejection cam
9. upper punch
10. die
11. lower punch
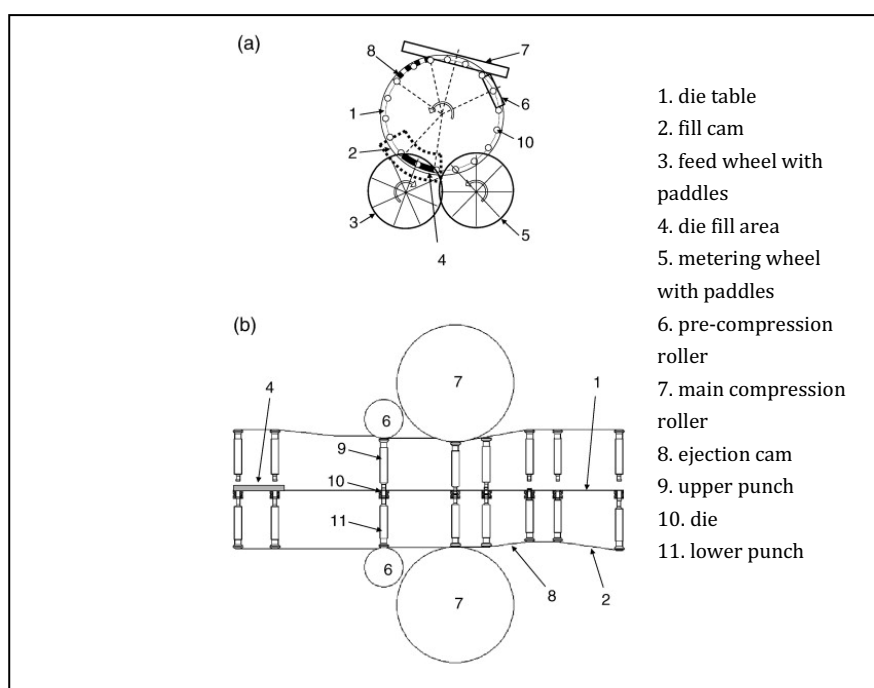
Figure 12: Rotary press production cycle a) top view, b) unfolded view (Sinka and Motazedian 2009)

The location of the compaction roll on the punch head determines the phase of compaction. The loading phase begins when the upper punch first makes contact with the compaction roller, and lasts until the compaction roller reaches the edge of the flat portion of the punch head. At this point the dwell phase begins and continues until the compaction roller rolls off the top of the torus (Augsburger and Hoag 2008). During the dwell phase the strain is constant, with unloading beginning at roll-off and continues until the punch stress drops to zero; this point is called lift-off. Once the punch stress is

zero the relaxation phase begins and continues until the tablet is ejected from the die. The stress created during compaction is a consequence of a reduction in tableting material volume.

6.3 Compaction mechanics

The compaction process can be described by a series of sequential phases:

> Particle rearrangement
> Elastic, viscoelastic, and plastic deformation of particles
> Fragmentation of particles
> Formation of inter-particulate bonds

As the powder volume is reduced, the particles become rearranged into a closer packing structure. At a certain point, the packing characteristics of the particles and inter-particulate friction between particles will prevent any further particle rearrangement. At this point, the further reduction in compact volume results in the elastic, viscoelastic, and plastic deformation of the particles. (Wu, Ruddy et al. 2005)

Elastic deformation is reversible, whereas the plastic deformation is irreversible. In addition, particle fragmentation or breakage results in smaller particles, which further decreases in compact volume. As the volume is further reduced, the smaller particles formed by fragmentation can undergo deformation. As a consequence of these processes, particle surfaces are brought into close proximity to each other which can lead to the formation of inter-particulate bonds. These bonds may later break which facilitates further compaction.

All materials posses varying degrees of elastic, viscoelastic, plastic, and brittle characteristics, and the type of volume reduction mechanism that will predominate for a specific material is dependent on factors such as temperature and compaction rate.

Three types of bond mechanisms can occur during tableting: mechanical interlocking between irregularly shaped particles, inter-particulate attraction forces (Van der Waal forces, hydrogen and electrostatic forces) and melting solid bridges.

6.4   Tablet production by direct compaction

The aim of direct compaction, as opposed to tableting via granulation, is to minimize the number of operations involved in the pre-treatment of the powder mixture before tableting. Tablet production by direct compaction involves only two operations in sequence, powder mixing and tableting. The advantage with direct compaction is primarily a reduced production cost. However, in a direct compactable formulation, specially designed fillers and dry binders are normally required, which usually are more expensive than the traditional ones. They may also require a larger number of quality tests before processing. As heat and water are not involved, product stability can be improved. Finally, drug dissolution is generally faster from a tablet prepared by direct compaction owing to fast tablet disintegration into primary drug particles (depending on formulation). (Göran Alderborn 1995)

The disadvantages of direct compaction are mainly technological. In order to handle a powder of acceptable flowability and bulk density, relatively large particles must be used which, firstly, may be difficult to mix to a high homogeneity; and secondly are prone to segregate. Moreover, a powder consisting mainly of drug will be difficult to form into tablets if the drug itself has poor compactibility. Finally, an even colouring of tablets can be difficult to achieve with a colourant in dry particulate form.

6.5 Tableting excipients

In addition to the active ingredient(s), a series of excipients are normally included in a tablet; their role is to ensure that the tableting operation can run satisfactorily and to ensure that tablets of specified quality are prepared. Depending on the intended main function, excipients to be used in tablets are subcategorized into different groups. However, one excipient can affect the properties of a powder or the tablet in a series of ways, and many substances used in tablet formulations can thus be described as multifunctional. The functions of the most common types of excipients used in tablets are given in Table 1 (Aulton 2002).

Table 1: Common tableting excipients

Excipient category	Examples
Filler	Lactose
	Sucrose
	Glucose
	Mannitol
	Sorbitol
	Calcium phosphate
	Calcium carbonate
	Cellulose
Disintegrate	Starch
	Cellulose
	Cross-linked polyvinyl pyrrolidone
	Sodium starch glycolate
	Sodium carboxymethyl cellulose
Solution binder	Gelatine
	Polyvinyl pyrrolidone
	Cellulose derivatives
	(e.g. hydroxypropylmethyl cellulose)
	Polyethylene glycol
	Sucrose
	Starch
Dry binder	Cellulose
	Methyl cellulose
	Polyvinyl pyrrolidone
	Polyethylene glycol
Glidant	Silica
	Magnesium stearate
	Talc
Lubricant	Magnesium stearate
	Stearic acid
	Polyethylene glycol
	Sodium lauryl sulphate
	Sodium stearyl fumarate
	Liquid paraffin
Antiadherent	Magnesium stearate
	Talc
	Starch
	Cellulose

6.6 Determinants of the compaction process

As discussed previously, the bulk volume reduction during compaction (compression) is a complex process involving several events. Thus, the success and efficiency of compact formation can be influenced by numerous factors. These factors could be product/formulation related, process/equipment related and/or environment related. Some of the most important factors affecting the compressibility/compactibility of pharmaceutical materials are:

6.6.1 Crystallinity/Polymorphism

Polymorphism, pseudo-polymorphism, and the crystal ordering/disordering of pharmaceutical materials are known to affect their densification behaviour and the final compact attributes. Typically, crystalline materials undergo brittle fragmentation whereas amorphous materials undergo plastic deformation (Singhal and Curatolo 2004).

6.6.2 Porosity and Bulk Density

The relative density and hence porosity vary largely among pharmaceutical materials. Moreover, the porosity of these materials may change significantly during processing. Since the process of compaction is aimed at reducing the porosity of a powder or granule, the initial porosity largely determines the extent to which the porosity can be reduced in a given tablet press. Also, increases in the original intra-granular porosity increased the compressibility at a given applied pressure (Eriksson and Alderborn 1995).

6.6.3 Particle size and shape

The particle size, size distribution, and shape are among the important determinants of the deformation behaviour of pharmaceutical powders and granules. Increasing the irregularity and roughness of granules changed the compaction behaviour from plastic deformation towards a more complex process including fragmentation and attrition of the granules. Compressibility is generally better in larger particle size systems due to a greater degree of densification. This is attributed to increased frictional and cohesive forces associated with the smaller size range; which tends to restrict particle flow and thus reduce densification (Fichtner, Rasmuson et al. 2005).

6.6.4 Compaction Force

Compaction force is the major driving force in the powder densification process. The rate and extent of the applied force on the powder bed not only affects the way particles physically deform but also determines the integrity of the compact formed (crushing strength/tensile strength). There is a positive correlation between compaction force and compactibility of the material up to a threshold pressure beyond which either the crushing force of compact remains unchanged, decreases or results in manufacturing problems like capping and lamination (Wu, Ruddy et al. 2005).

6.6.5 Lubricants and Glidants

Lubricants are usually added to formulations to reduce die-wall friction, although they may also help improve flow properties (those having a glidant characteristic), as well as function as anti-adherents. The amount of lubricant added and the extent or duration of mixing a lubricant have been shown to affect several formulation properties including powder flow, deformation behaviour, crushing strength, and dissolution rate. It has been traditionally observed that increasing the concentration of lubricant in a formulation results in tablets with decreased crushing strength. This effect is attributed to a decrease in the degree of cohesiveness between the particles as well as decreased frictional effects at the punch faces and die-wall (Moody, Rubinstein et al. 1981).

Glidants are typically incorporated in solid dosage formulations to improve the flow properties of granules or powders. There are several mechanisms by with a glidant can increase the flowability of formulations, including

- Decreasing surface roughness of the particles by forming a uniform coating around them; thus, reducing the frictional drag between the particles.
- Acting as physical barriers between particles which reduces attractive forces between particles.
- Removing absorbed moisture from the surface of the particles, making them drier and more flowable.

6.6.6 Moisture

Moisture is known to affect a wide range of properties, such as powder flow, compactibility, and stability (physical chemical and microbiological). The interaction between moisture and a solid is complex and can occur in a variety of ways. For example, water can be stoichiometrically incorporated into a solid's crystal structure in

the form of a hydrate (pseudo-hydrate). In addition, moisture can have nonspecific interactions with a solid by adsorbing on the surface or being absorbed into the material and acting as a plasticizer, and these interactions are more common in amorphous or semi crystalline materials.

Absorbed moisture increases the deformability of the material by facilitating a temporary transition of the amorphous material from a glassy to a rubbery state (particularly for long chain polymeric materials), occurring during the compaction phase, resulting in the formation of solid bridges (due to evaporation of moisture during processing) with a subsequent increased inter-particulate bonding area, which increases the deformability of the particles (Sun 2008).

6.6.7   Tableting speed

The deformation behaviour of many pharmaceutical materials is time-dependent and the nature of this time dependency is often related to the mechanism of compaction for a given material. It is thought that time dependency or speed sensitivity arises from the viscoelastic or viscoplastic characteristics of a material. In contrast, studies have shown that brittle materials are much less speed dependent that ductile materials because yielding and fragmentation are not as dependent on the rate of compaction. It is also believed that the particle size and size distribution of the powder or granules have an important role in the speed sensitivity due to the fact that this property affects the pre-dominant mechanism of deformation.

The speed sensitivity of pharmaceutical materials can have serious implications on the final tablet attributes. The effect of punch velocity can be pronounced when a material is transferred from a single station laboratory press to a rotary press or scaled up to a very high speed industrial press. Several studies have found that materials that have a high degree of elastic recovery or deform via plastic deformation tend to show a decrease in tablet strength with increase in tableting speed, and problems like capping and lamination are more likely to occur when such materials are scaled up to a high-speed press (Akande, Rubinstein et al. 1997).

6.7 Compaction simulators

A compaction simulator is a tool for the characterization, scale-up, and troubleshooting of powder compaction performance. In the simplest of terms, a compaction simulator is a highly instrumented single station compaction machine fitted with an upper punch, lower punch, and die that is capable of mimicking a modelled compaction event. These machines are either hydraulically or mechanically powered to deliver a range of compaction forces using highly controlled punch displacement profiles. Compaction simulators use sophisticated instrumentation to monitor, at minimum, the displacement and force profiles associated with the compaction event. Therefore, the data generated while using a compaction simulator offers a significant advantage over traditional pharmaceutical unit operations for studying and understanding powder compaction behaviour.

6.7.1 Hydraulic Compaction Simulators

The hydraulic system is electronically controlled, with either compaction force cycles or movement of the punches being freely adjustable. The primary aim is to mimic the densification process of a rotary machine and the mechanical factors influencing it.

The force-time profile of a rotary tableting machine can be theoretically deduced and calculated using machine geometries (Oates and Mitchell 1989). But this is only possible to a certain extent, because of the amount of factors influencing the measured force outside the simulation, e.g. the tableted material, the geometries of the machine, the machine wear time, tableting speed, and tableting tools (Pudipeddi , Venkatesh et al. 1993). Similarly, the displacement-time profile of a tableting machine, especially a rotary tableting machine, is very difficult to calculate. Thus either an approximated displacement-time profile can be used for programming the compaction simulator or approximation of real punch movement is only possible using recorded data from real tableting machines

However, hydraulic compaction simulators are still used in research for basic material characterization. They show the advantage of controlling speed exactly and of using low and high punch travel speeds, between 10 and 300 mm s^{-1}.

6.7.2 Mechanical Compaction Simulators

These employ a single pair of punches moving linearly forth and back on a lower and an upper punch track. For tableting, the punches pass along exchangeable compaction wheels which are equivalent in dimensions to those of rotary tableting machines used in practice (Natoli, Levin et al. 2009).

Tableting speed can be varied and different tableting machines are simulated by using similar dwell times. In addition, pre-compaction wheels can also be mounted to simulate pre-compaction. Therefore, mechanical compaction simulators allow process simulation of rotary tableting machines to a greater extent than when using hydraulic compaction simulators when used for formulation development and scale-up (e.g. Presster™, section 12.2.1 - page 159).

6.7.2.1 Dwell time

Because different presses employ different number of stations and pitch circle diameters, matching tablet press speed (rpm) has no real scientific value. The solution would be to express tableting speed in terms of dwell time or contact time.

Functionally, the effective dwell time (EDT) can be defined as the time it taken by the force–time curve to traverse the 90% of the peak height (with effective contact time (ECT) being the time between points at 10% of the peak height).

Mechanical Definitions of dwell and contact times disregard material properties and concentrate on press and punch geometry. They would be preferred for dwell time calculations because they serve as an objective material-independent measure of compaction speed:

1. *Contact time* can be defined as the time the punch is in contact with the compaction wheel; and
2. *Dwell time*, equation (0.13), is defined as the time the flat portion of punch head is in contact with the compaction wheel (time at maximum punch displacement, or time when the punch does not move in vertical direction).

$$DT\left(\text{mesc}\right)=\frac{L\cdot NS\cdot 3,600,000}{\pi\cdot PCD\cdot TPH}$$ (0.13)

    where
       DT   =   dwell time in (msec)
       L   =   length of the flat portion of the punch head (mm)

NS	=	number of stations
PCD	=	pitch circle diameter of the turret (mm)
TPH	=	tableting speed (tablets per hour)

6.8 Powder deformation during compaction

The material property that predominantly affects the tableting of powders is the deformation behaviour of powder under stress. The deformation characteristics may be elastic, plastic, brittle fracture or a combination of these deformation mechanisms. Various parameters that characterize the deformation characteristics of powders include Young's modulus, Poisson's ratio, yield stress, and fracture toughness.

Elastic deformation is time independent, reversible deformation of a particle, and can create residual stresses within the compact during the decompression phase of the compaction cycle. The force applied on a compact or powder divided by the surface area of a compact causes a change in dimensions. The linear portion of the stress-strain plot and the proportionality constant between stress and strain is given by the Young's modulus (DWIDEDI, OATES et al. 1992).

For elastic deformation:

$$\sigma_d = \varepsilon_E \qquad\qquad (0.14)$$

Where E is the Young's modulus of elasticity of material, ε is the deformation strain and σ_d is the deformation stress (Rowe and Roberts 1996).

Plastic deformation is the permanent deformation of a particle that is controlled by the applied stress. The amount of plastic deformation depends on the overall time of compaction, contact time or rate of application of compaction force and the time during which the material is subjected to maximum force (dwell time). Plastic deformation facilitates the formation of permanent particle–particle contact regions during compaction, and is given by:

$$\sigma_d = \sigma_y \qquad\qquad (0.15)$$

Where σ_y is the yield stress of material, which is the stress beyond which material is not elastic. When the yield stress is exceeded, the material may either flow or break upon compaction (Cartensen 1993).

And for brittle fracture:

$$\sigma_d = \frac{A K_{ic}}{\sqrt{d}}$$
(0.16)

Where K_{ic} is the critical stress intensity factor of material that provides an indication of the stress required to produce propagation of crack, d is the particle size diameter and A is a constant depending on geometry and stress application. K_{ic} describes the state of stress around an unstable crack, and is a measure of the resistance of material to cracking via tensile stresses normal to the crack walls (Roberts, Rowe et al. 1993).

6.9   Analysis of the tableting process

Instrumented tableting variables, namely force, time, displacement, and temperature, can be combined differently and can be analyzed afterward. From the functional relations, conclusions can be drawn about the compaction and compaction behaviour of the materials.

6.9.1   *Changes in bed density or porosity during compaction*

During tableting, the bed density or porosity of the powder changes as the compaction force is applied. This reduction in volume or density of the compact upon application of force can be calculated using the Heckel equation (Heckel 1061), and is given by the mean yield pressure, P_Y:

$$\mathrm{Ln}(1/1-D) = KP + A$$
(0.17)

Where D is the relative density of the compact in die at the pressure P. K and A are regression coefficients of the linear portion of the curve, and the reciprocal of K is the mean yield pressure, P_Y.

The Heckel equation is applicable to systems that deform plastically, but deviations from linearity at low applied stress tend to suggest alternative compaction mechanisms such as brittle fracture. The Heckel equation has been used to distinguish three types of volume reduction mechanisms based on the effect of stress on initial powder bed density.
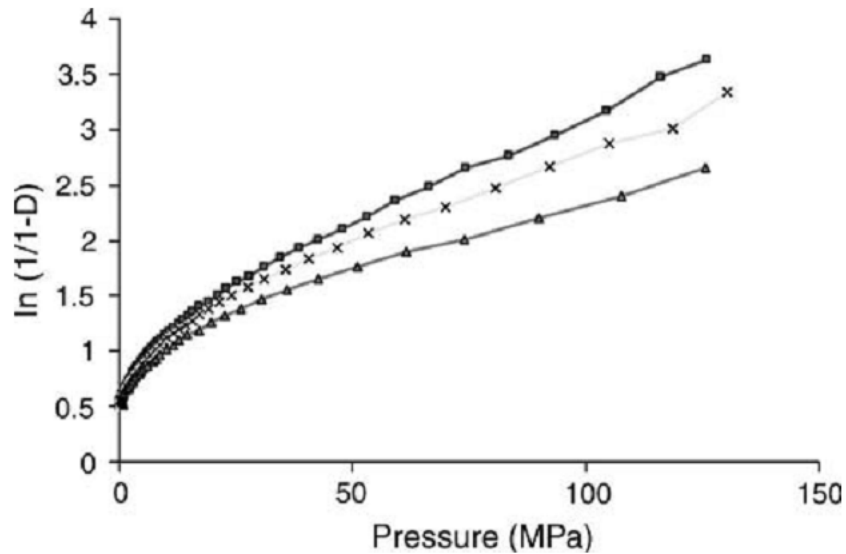
Figure 13: Heckel plot (Ruegger, Royce et al. 2007)

These materials were categorized by compressing different particle size fractions of various powders. In type A materials, the variation in initial bed densities results in different final bed densities under applied stress. Particle size fractions had different initial packing fractions and the plots remained parallel as the compaction pressure was increased. In these densification takes place by plastic flow preceded by particle rearrangement. In type B materials, irrespective of the initial bed density, a single linear relationship occurs above certain pressures. Below this pressure plots are slightly curved at initial stages of compaction. Powder densification happens by fragmentation of particles. The initial structure of the powder column is completely destroyed by fragmentation and hence differences in initial packing have no effect on further densification. In type C materials, the plots have an initial steep linear portion after which they become coincidental with only trivial volume reduction. Powder densification occurs by plastic flow but no initial particle rearrangement is observed. (Paronen and Iikka 1996)

6.9.2   Tablet indices

Strain index, P/E', is obtained from dynamic indentation hardness, P, and the reduced Young's Modulus, E'. E' is given by:

$$E' = \frac{E_1}{\left(1 - \upsilon_1^{\,2}\right)} \qquad (0.18)$$

Where E_1 is the elastic modulus of the compact and v_1 its Poisson's ratio. Strain index is indicative of the relative strain or change in size during elastic recovery after plastic deformation, and is indirectly related to the proximity of surfaces that remain in contact after decompression. The values of P/E range from 0–0.04. A high P/E implies potential structural failures such as capping or lamination (Shah and Davar 1995).

Brittle Fracture Index (BFI) is the ratio of the tensile strength of the tablets with, (σ_T), and without a hole, (α_{To}), at their centre. This ratio may indicate the ability or inability of compact to relieve stress at a crack tip within the compact by plastic deformation.

$$\text{BFI} = \frac{\sigma_T / \sigma_{To} - 1}{2}$$
(0.19)

BFI is a measure of brittleness, which is the principal cause of capping and lamination. A BFI of <0.2 indicates better compacting properties, whereas values >0.2 indicate tendencies to cap and laminate (Shah and Davar 1995).

6.9.3   Force displacement curves

By adding a displacement transducer to the instrumented press, the upper punch force is measured against punch-tip displacement. The resulting curve shows a progressively increasing slope, reaching maximum force as the punch achieves maximum penetration. The characteristic shape of the force-displacement curves, recognizable in terms of its slope and elastic recovery, can be correlated to the ability of material to undergo plastic deformation and form strong compacts.

The gross work done in compaction and the proportion of the total applied energy absorbed by the material are indicated by the area under the curve and are considered a measure of the tablet strength, although this value includes the work done to overcome die wall friction. Several limitations to the use of this approach include concerns with accurate measurement of punch displacement, errors introduced because of multiplication of a large number (punch pressure) with a small number (punch displacement at maximum pressure), die wall friction, deformation of machine parts under pressure, and separation of net work from gross work (Watt 1988).
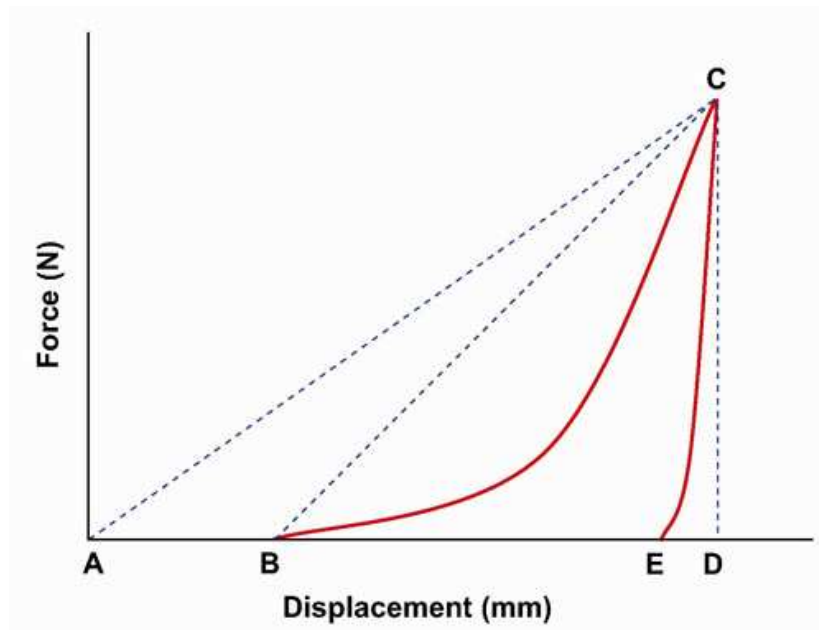
Figure 14: A theoretical force-displacement compaction profile.

Triangle ACD describes the mechanical energy (energy of compaction); triangle BCD is the theoretical energy (energy of compaction, excluding initial packing phase, AB); curve BCD is the total energy (energy involved during compaction, excluding initial packing and interparticulate friction); curve BCB is the frictional energy (friction arising due to particle-particle and particle-die wall friction, i.e., difference between theoretical energy and total energy); curve CDE is the elastic energy (energy released as a result of elastic deformation during compaction unloading); and curve BCE is the net energy (energy required to yield a particle under force). (Patel, Kaushal et al. 2007)

6.9.4   *Elastic recovery during multiple compaction*

Work done in each compaction cycle is calculated by integration of each force/displacement curve. When this work becomes constant, this force-displacement value is assumed as the work done to produce the elastic deformation during compaction and is an indicator of the elasticity of material. Elastic recovery (ER) is defined as percentage of axial expansion of the compact after ejection, relative to its height at maximum pressure:

$$\text{ER} = \left(\frac{h - h_c}{h_c} \right) \cdot 100 \qquad (0.20)$$

Where h_c and h are the heights under compaction and after ejection, respectively. The plastic deformation takes place during initial compaction and, after a certain number of compaction cycles, elastic deformation is predominant. The fewer the number of compaction cycles required for arriving at constant work, the more readily is plastic deformation completed, exhibiting increased plasticity (Watt 1988).

6.9.5   Deformation hardness

Deformation hardness of a tablet can be correlated with the compressive stresses during compaction (Leuenberger and Rohera 1986), assuming that increasing the relative density of the compact allows more particles to come into contact and increases the deformation hardness, P:

$$P = P_{max}(1 - e^{-y\,Sc\,\pi})$$ (0.21)

P_{max} denotes the theoretical maximum deformation (Brinell) hardness when the number of non-bonding points is reduced to zero and the applied compressive stress, Sc, is highest or infinite. A low P_{max} value shows a relatively poor compactibility, for even with high compaction stress this limiting value cannot be exceeded. The parameter γ specifies the rate at which the compact hardness P builds-up with an increase in applied compaction stress and provides information about compressibility. A high value of γ will imply $P = P_{max}$ and a sharp decrease in compact porosity may be attained with low compaction forces. A plastically deforming material will have a high value of γ and a low value of P_{max}, whereas the reverse is the case for brittle materials.

6.9.6   Compaction force versus tablet strength

The effect of compaction force on tablet strength is obtained by operating the tablet press at any given speed for an extended range of compaction forces. The crushing strength and friability of the resulting tablets are evaluated to obtain the range of compaction parameters in which the formulation performs best. Tablet compaction profiles and crushing-strength data provide useful information for limiting compaction forces during tableting and can provide additional information about lamination or capping. The slope of a compaction-force versus crushing-strength profile provides qualitative information about the ability of material to produce strong tablets. A very high slope value may suggest potential problems in production processes as a small change in the compaction force could cause significant increases in the tablet crushing strength, which could result in capping or variability in disintegration and dissolution of resultant tablets.

Crushing strength or breaking force F measures the force, which when applied across a specific plane of a compact produces fracture in tablets. It is a function of compact geometry and does not take into account the mode of fracture or the dimensions of the tablet (Davies and Newton 1996). Crushing strength can be affected by the presence of lubricant, its concentration, and state of subdivision and location of particles; pre-

compaction processing, including wet or dry processes; time and scale of mixing; storage condition; compaction force; variations in time of consolidation, dwell and contact; die residence and ejection; amount of bound or free moisture and initial porosity of the powder bed. (Shotton and Lewis 1964)

Crushing strength is only a limited index of the compaction properties of starting materials. Most materials will either deform elastically or plastically, or fracture under the influence of applied stress. Therefore, measuring the final force required to produce fracture does not truly reflect the conditions during compaction. The strain rate and thus the time during which materials are subjected to compressive stress is another important variable for consideration.

6.9.7   Tensile strength

The radial tensile strength, which measures the tablet failure as a result of the application of tensile stress only, is given by the relationship:

$$\sigma_x = \frac{2F}{\pi DT} \tag{0.22}$$

Where σ_x is the tensile strength, F is the force required to break the tablet, D is the diameter of the tablet, and T is the tablet thickness. Various factors, such as test conditions, deformation properties of the material, homogeneity of the compact, adhesion conditions between the compact and its support, and tablet shape, may influence the tensile strength measurement (David and Augsberger 1974).

In the axial tensile strength test, the tablet cleaves in a plane along its axis. It is measured by straining the face of the tablet, mounted between a pair of adapters, and determining the maximum force required to cause failure due to tensile stresses (Leuenberger and Rohera 1986). The axial tensile strength, σ_z, is given by:

$$\sigma_z = \frac{4F}{\pi D^2} \tag{0.23}$$

Where F is the force required to break the tablet and D is the diameter of the tablet. A comparison of radial and axial tensile strengths is indicative of the bonding strength in two directions and may provide information about the laminating and capping tendencies of the material (Alderborn and Nystrom 1984).

7. Research aims

This research aims to evaluate various factors affecting NIRS applications, in particular quantitative methods.

The first study aims to assess the effects of tablet press variability, in terms of compaction force, on content predictions for low-dose tablets. Calibration model performance, as well as the effects on spectra, are investigated.

The second study examines the horizontal sampling span for pharmaceutical tablets in DT mode.

The third study is a series of experiments aiming to investigate and estimate the information depth for DR mode in pharmaceutical tablets.

The three studies would provide better evidence and understanding on the use and applicability of both DR and DT modes for pharmaceutical tablets, and the critical aspects affecting their performance and selection criteria.

8. Press effect on NIR predictions of low-dose tablets and DT sampling span

The work on this section is summarised in the original scientific publication from the author (below), with detailed experimental methods and results in Appendices I & II.

8.1 Assessment of diffuse transmission mode in near-infrared quantification - part I: The press effect on low-dose pharmaceutical tablets (original paper)

8.1.1   Keywords

8.1.2   Abstract

Quantitative applications for pharmaceutical solid dosage forms using near-infrared (NIR) spectroscopy are central to process analytical technology (PAT) manufacturing designs. A series of studies were conducted to evaluate the use of NIR transmission mode under various pharmaceutical settings. The spectral variability in relation to tablet physical parameters were investigated using placebo tablets with different thickness and porosity steps and both variables showed an exponential relationship with the detected transmittance signal drop. The drug content of 2.5% m/m folic acid tablets produced under extremely different compaction conditions was predicted and found to agree with UV assay results after inclusion of extreme physical outliers to the training sets. NIR transmission was also shown to traverse a wide section of the tablet by comparing relative blocking intensities from different regions of the tablet surface and >90% of the signal was detected through a central area of 7 mm diameters of the tablet surface. NIR Quantification of both film thickness and active ingredient for film-coated tablets are examined in part II of this study. © 2009 Wiley-Liss, Inc. and the American Pharmacists Association J Pharm Sci 98:4877-4886, 2009

8.1.3   Introduction

8.1.3.1   NIR Spectroscopy and PAT

Near-infrared (NIR) spectroscopy is the measurement of absorbed radiation in the spectral region of 780-2500 nm (12,800-4000 cm^{-1}). The absorption bands arise from overtones and combinations of fundamental mid-IR stretching and bending modes. It offers unique advantages of being fast, non-destructive, with no sample preparation requirements and strong identification and quantification abilities. Therefore, NIR

spectroscopy possesses great potentials for in-process control and end-product analytics.

The recent developments in the applications of near-infrared spectroscopy (NIRS) for pharmaceutical manufacturing have been the strongest manifestation of the push for successful implementations of process analytical technology (PAT) applications, and were facilitated by the explosive growth in both the types and sophistication of NIR equipment and software. If successful, PAT manufacturing can deliver quality products that require minimal or no end-product testing (real-time release), owing to the fact that they will be produced through critically controlled processes designed to produce in-spec products (Davies 2004).

Although NIR spectroscopy has now been long-investigated for a vast range of applications, from fuels to food and feed industries, its use in the pharmaceutical field has picked up momentum only recently. One issue for NIR in this tightly regulated industry is the fact that use of this technique involves careful 'risk-assessment', mainly because predictions are the result of statistical correlations with established assays rather than being a primary assay. This logically leads to the need for establishing concrete methodology for NIR quantification which is specific for solid dosage forms and thus minimising (rather than completely eliminating) physical properties effects that dominate the spectra down to an acceptable threshold of error (Blanco, Eustaquio et al. 2000).

8.1.3.2 *Quantification Using NIR Spectroscopy*

The work by Sherken (1968) contained the earliest published NIR determination of actives in tablets after extraction. The analysis of intact dosage forms, however, was reported as early as 1987 through the works of Lodder et al (1987). In common with other spectroscopic methods, NIR quantification relies on regression over variations in one or more spectral regions, which follow the change of one component's concentration in the sample relative to the rest. However, unlike UV assays where very dilute concentrations of samples are needed to avoid nonlinearity and deviations from Beer-Lambert law, NIR applications perform best with a 50:50 ratio of components (measured-entity relative to other entities), and difficulties start to materialise at either end of the scale. Low-dose (specifically low-concentration) tablets would have a higher relative standard error of estimation and smaller fluctuations in tableting parameters could have a bigger influence on NIR predictions in such conditions. Low-dose tablets are unavoidable with potent drugs and smaller tablets are usually utilised to minimise manufacturing problems. But there is a limit to how small a tablet can be manufactured

and yet easily handled by patients, which brings about the need for an evidence base supporting the use of NIR quantification under such conditions.

8.1.3.3 *NIR Transmission in the Solid State*

The combination of relatively weak absorbance and high scattering efficiency is an important characteristic of the interaction between NIR radiation and particulate solids. This combination allows the radiation to propagate through the voids inside tightly packed solid particles. However, transmittance is expected to deviate nonlinearly for Beer-Lambert law of absorption for very dilute and clear solutions, because it does not take into account the probability that incident photons will be scattered or reflected backward or forward relative to the incident beam direction. This produces changes in absorption coefficients across a wide range of concentrations as light takes a tortuous path through voids with continuous scattering and back-reflection. This makes the transmittance more and more diffuse as it travels through the sample before being detected (Birth and Hecht 1987).

It has still proved difficult to describe the nonlinearity from Beer-Lambert because the absorptivity/reflectance/scattering characteristics of a certain solid compact would be dependent on particle size and morphology, packing density, index of refraction and many other sample qualities. Nevertheless, many still consider Absorbance = log (1/Transmittance) as a simple, but working, approximation (Cogdill and Drennen 2006).

Micro-cavities inside tablets (porosity) cause light scattering due to rapid spatial changes in refractive index. Consequently, this scattering is very dependent on the manufacturing process, (compaction force, compacted mass, grain size, etc.). Abrahamsson et al. (2005) suggested that the scattering in a tablet is about 3-4 orders of magnitude larger than the absorption resulting in very long optical path lengths, so that a typical 3.5-mm thick tablet can have a mean optical transmission path length of 20-30 cm. This implies that some photons can find optical pathways of few millimetres while others span a meter before being detected. However, the high reproducibility of NIR spectra of the same sample in transmission indicates that this phenomenon is occurring in a consistent manner, but with great dependence on sample density (solid fraction or porosity) and thickness.

In his work on normalising weight variations of predicted samples, Baxter (1994) concluded that the variation in NIR reflection spectra is a picture of active per unit area and does not allow the detection of tablet weight, highlighting the need for correcting assay results from reference assay methods and again the NIR prediction results for

tablet weight. A reduction in residual values from 2.17% to 1.56% was reported by Baxter when he used this method.

Pretreatments, tighter wavelengths and various chemometric techniques have been used to minimise baseline effects for both reflection and transmission modes. The main problem in correcting density and thickness effects in transmission mode is the presence of nonlinear spectral scaling. This can also explain the difficulty in predicting tablets made with slightly different manufacturing conditions (e.g. different batches) from calibration samples (Blanco, Romero et al. 2004).

Numerous studies in literature examined the use of NIRS to predict tablet density and hardness. Many of the published papers describe baseline shifts in reflection mode in correlation with sample densities (Cogdill, Herkert et al. 2007), (Kirsch and Drennen 1999). Research from Ciurczak and Drennen (2001) on predicting tablet hardness using NIR suggested that the increased absorption in harder tablets is probably due to a reduction of light scattering on the smoother surface of these harder tablets, allowing more light to penetrate. The effect of hardness on spectra was so pronounced that the publisher indicated that level of error in NIR hardness prediction is in the neighbourhood of traditional destructive crushing-strength tests of 0.5 kP. On the other hand, there are no clear mathematical models that relate transmittance to apparent sample density and thickness because of the absence of a complete theory defining NIR transmittance.

8.1.3.4   *Effective Mass Sampled during NIR Analysis*

The need for effective sampling is common to all analytical techniques. With NIR spectroscopy, a great deal of attention is usually given in the selection of calibration samples highly representative of end product units over different batches. However, another aspect of sampling is sometimes overlooked. NIR radiation in classical diffuse reflection mode is reflected from a central area of the surface and is only assumed rather than proven representative of the whole tablet.

The scale of mass to be assayed 'scale of scrutiny' (Donoso, Kildsig et al. 2003), (Berntsson, Danielsson et al. 1998) by any method depends on both the magnitude of the unit dose in question and the application. For example, monitoring blend uniformity requires minimal effective sampling mass, while the reverse is true for individual dosage forms. Moreover, the effective sampling mass has a complex and nonlinear effect on NIR transmittance and reflectance spectra (Bull 1990).

There is little experimental evidence of how deep the radiation penetrates the surface in diffuse reflection. This penetration is sample-dependent and the difference between loose and compacted powders is significant. One paper assessed reflectance in NIR imaging and estimated a 50% signal drop over 27-180 μm depending on the wavelength (Clarke, Hammond et al. 2002). Other papers considered NIR reflection to have a penetration depth of less than 1 mm (Li, Bashai-Woldu et al. 2007). Olinger and Griffiths (1992),(2001) estimated an information depth around 1 mm using diffuse reflection and a mixture of powders. Considering that this penetration is occurring in a dissipating manner, this mode is logically even less useful for coated or multi-layered tablets. Diffuse transmission mode on the other hand penetrates the whole thickness of the tablet and would theoretically be more representative of the whole tablet, (Berntsson, Burger et al. 1999) especially for low-dose units where aggregation has a higher effect. It is not clear, however, what path the radiation follows inside the tablet and hence the percentage actually being scanned. Moreover, transmission is more sensitive to path-length and density variability. Iyer et al. (2002) did a series of experiments at Duquesne University to address this issue. They calculated a wavelength-dependent information depth for reflection ranging between 1.9 and 2.7 mm using second derivative spectra from tablets of increasing thickness. They also showed a limiting tablet thickness of 3.5-4.8 mm for transmission. Another set of experiments showed an effective transmission diameter of 7 mm and concluded that the mass sampled for both modes was comparable and around 200 mg. However, the radiation intensity inside this diameter is fading towards the periphery in all directions making the mass over-estimated in this case, especially for reflection. Also, the fact that sampled mass is largely dependent on physical properties of the sample, mainly hardness and packing, makes this issue an open question.

8.1.3.5 *Study Aims*

The aims of this study were to assess the effects of compaction variability introduced to the tableting process on the performance of content prediction using NIR diffuse transmission mode, as well as examining the effects of variation in tablet thickness and/or porosity on the spectra; and finally, to elucidate the proportional contribution of various areas of a tablet to the final NIR spectrum in diffuse transmission mode.

8.1.4 Experimental

8.1.4.1 Materials

Folic acid USP, *Sigma-Aldrich, USA*; Micro-crystalline cellulose (MCC) Sanaq 102G, *Pharmatrans Sanaq AG, Basel, Switzerland*; AcDiSol Croscarmellose Sodium, NF, Ph. Eur., *FMC Biopolymer, Brussels, Belgium*; Magnesium Stearate, *Novartis Pharma AG, Basel, Switzerland*.

8.1.4.2 Folic acid tablets

A directly-compactable tablet formulation was used to make 2 sets of 220 folic acid tablets in 11 batches per set (table 1) with an API range of 0-10 mg (0-5% *m/m in 0.5% steps and 20 tablets per step*). Optimizing particle size and mixing times was of prime importance to obtain a consistent API content within each batch. Powders were sieved with 90 μm mesh to minimise segregation potential and then mixed in a Turbula mixer for 12 minutes in a mix-sieve-mix manner.

TABLE 1: Folic acid tablet formulation

Substance	Percentage (m/m)	Function
Folic acid USP	0-5 %	active
MCC 102	93.75-88.75 %	filler
Ac-Di-Sol	6 %	disintegrant
Mg Stearate	0.25 %	lubricant

The tablets were produced by means of a tablet press compaction simulator (Presster™ - Metropolitan Computing Corporation) which is capable of constructing linear models of an industrial-scale rotary press by replicating its dwell time, compaction and pre-compaction forces, and ejection angle. Dwell time was adjusted by changing compaction speed while compaction force was a function of punch gap adjustments – hence the need for calibrating gap size against compaction force, tablet hardness and thickness. All press functions were instrumented and controlled by a computer terminal.

The first set of tablets was used to obtain NIR calibration models for low-dose folic acid tablets and test the model with an external 2.5% *m/m* batch (same formulation as the calibration set, but not involved in the calibration) while the second set was used to examine the press effect on predictions. Table 2 details the press settings and tablet specifications for the both sets.

Table 2: Tableting parameters

First Set	Average (SD)
Tablet mass	200.46 (0.31) mg
Diameter (flat face)	10.00 (0.01) mm
Thickness	2.39 (0.01) mm
Resistance to crushing	95.33 (1.51) N
Porosity	30.79 (0.26) %
Speed	10800 TPH
Dwell time	118.30 msec
Gap size	1.80 mm
Upper compaction force	3.90 kN
Pre-compaction	None
Second set – extra parameters	
Porosity range	18-40%
Gap size range	1.14-1.8 mm
Compaction force range	10-3 kN

8.1.4.3 *NIR measurements*

All NIR measurements were performed on NIRFlex-N500 Fourier transform NIR spectrometer with solids transmittance measurement cell from Büchi (Switzerland) in diffuse transmission mode, using 64 scans and 16 cm^{-1} resolution in the 11520 - 6000 cm^{-1} range. NIRCal 5.2 chemometrics software was used for calibration model development and predictions. All models used PLS (partial least squares) regression. Validation was through an independent validation set (1/3 of spectra) rather than cross validation.

8.1.4.4 *UV referencing*

Folic acid is soluble in slightly alkaline solutions. Sodium hydroxide solution (0.1 M) was used to dissolve each ground tablet and the filtered solution was measured in a 1 cm cell at 235 nm and a UV calibration line with $r^2 \geq 0.999$ was obtained in that medium.

2.5 Effect of porosity and thickness on spectra

Porosity in 6 tablets (formulation in table 1 with 0% fold acid) was fixed while varying thickness by adjusting tablet mass and compaction force. In the same manner, thickness was varied while keeping porosity constant in 3 more tablets (Table 3).

Table 3: Tablet porosity and thickness, varying one variable at a time

Tablet	Mass [mg]	Thickness [mm]	Porosity [%]
P1	200	2.66	38.00
P2	240	2.54	22.08
P3	280	2.61	11.53
T1	100	1.00	20.4
T2	200	1.99	20.0
T3	300	3.00	20.4
T4	400	4.06	21.6
T5	500	5.09	21.8
T6	600	6.10	21.7

8.1.4.5 *Radiation convergence*

Figure 15 illustrates how paper with LaserJet ink print (100% coverage) scales down the spectrum of a placebo tablet by at least 88%, compared to the same tablet covered with a blank paper.
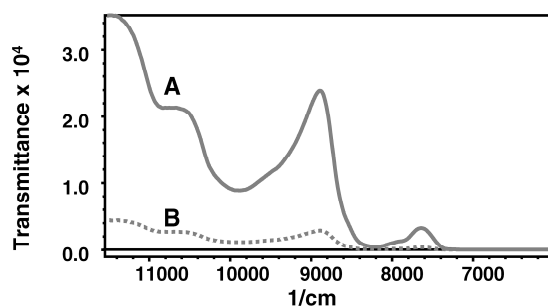
Figure 15: Transmission spectra of a 0% tablet (A) covered with white paper, (B) same tablet covered with LaserJet ink printed on paper

This can be exploited to examine the effect of blocking different areas of the surface of a single tablet using printed rings with varying internal diameters Figure 16. Each ring was sized such that fitting the paper inside any position on the tablet plate aligns the centres. These rings would block the tablet periphery, leaving a hole (white paper area) in the centre ranging between 9 to 1 mm in diameter. These paper filters were applied to the 0% batch with varying porosity and thickness. Each tablet/filter combination was scanned 3 times and the average of transmittance maximum at 8880 cm^{-1} was used.

Figure 16: 10-mm printed rings used to produce a block effect. The number indicates the internal diameter in mm. The block from each filter to that from F0 was used to calculate block percentage.

8.1.5 Results and discussion

8.1.5.1 *The first calibration*

Visual inspection of the pre-treated 0%, 2.5% and 5% spectra (normalisation by closure - ncl) showed wavelength regions related best with the folic acid property (Figure 17). It also showed the low signal of folic acid compared to the filler, which adds a further complication to the low-dose API problem.
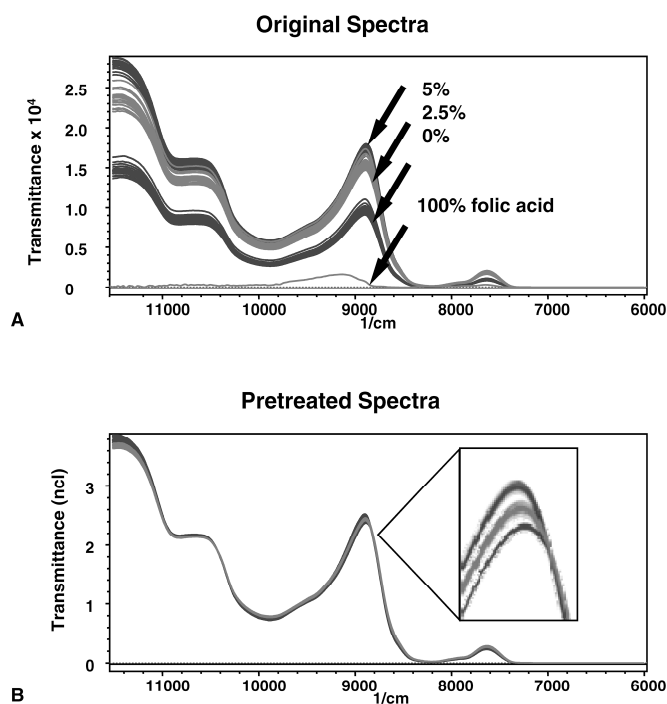
Figure 17: Transmission spectra of 0%, 2.5% and %5 m/m folic acid tablets before and after pre-treatments

Although ncl or SNV (standard normal variate) pre-treatments produced good order and grouping amongst the spectra (Figure 17, zoomed pane), the spectral noise from tablet-to-tablet variations in physical properties overwhelmed the element of folic acid in the spectra. The batches showed little difference in transmittance apart from a small shift in the transmission maximum at 8880 cm^{-1} and spectral scaling. At that point, to what extent the effect of small variations in tablet properties on spectral scale and hence predictions was unknown. Five PLS models were developed with different parameters and comparable performance (Table 4). Each model can be evaluated in accordance with the EMEA / ICH guidelines for new method development by inspecting its respective parameters.

Table 4: Calibration models' parameters

	NIRF1	NIRF2	NIRF3	NIRF4	NIRF5	NIRVAR
Wavelengths Calibration Set	6000-11520	7400-11520	8500-11520	6000-11520	7400-11520	6000-10600
Data Pretreatment Sequence	MSC full	MSC full	SNV	1st derivative BCAP, SNV	1st derivative BCAP, SNV	MSC full, normalisation by closure
PCs	7	7	6	3	3	12
V-Set BIAS	0.020901	-0.02879	0.017055	-0.000960	-0.001550	0.015475
C-Set SEE (SEC)	0.249761	0.323872	0.259507	0.286846	0.286303	0.312529
V-Set SEE (SEP)	0.258087	0.317960	0.254297	0.292198	0.290546	0.311205
Consistency	96.77390	101.8590	102.049	98.16820	98.53960	100.4260
						Regression linearity
C-Set Coefficient	0.997209	0.995125	0.996986	0.996318	0.996332	0.995599
V-Set Coefficient	0.995108	0.994061	0.995263	0.993946	0.994011	0.992966
C-Set Intercept	0.027482	0.049445	0.029669	0.036633	0.036495	0.042896
V-Set Intercept	0.039841	-0.01142	0.056711	0.037676	0.041552	0.019216
C-Set Slope	0.994425	0.990275	0.993981	0.99265	0.992678	0.991217
V-Set Slope	0.987660	1.008510	0.985014	0.992555	0.991889	0.992981
						Accuracy (n=20)
Mean	4.6663	4.5753	4.7229	4.7786	4.7784	4.7793
SD	0.2221	0.2527	0.2331	0.1845	0.1850	0.1849
t_{exp}	3.5304	3.8238	2.0392	1.3580	1.3702	1.3713
$t_{critical}$	1.7291	1.7291	1.7291	1.7291	1.7291	1.7282
P ($t_{exp} < t_{critical}$)	0.0011	0.0006	0.0278	0.0952	0.0933	0.0920
						Repeatability (1 tablet x 10, same operator)
SD	0.0381	0.0365	0.0448	0.0311	0.0306	0.0308
RSD	0.8165%	0.7978%	0.9486%	0.6508%	0.6404%	0.6446%

Figure 18 shows the difference between folic acid predictions and UV assay results for all five models using a 2.5% set external to the model. Models 4 and 5 had the best agreement. The same conclusion can be reached by inspecting model protocol produced in NIRCal (a compromise between best consistency, best correlation and least SEP).
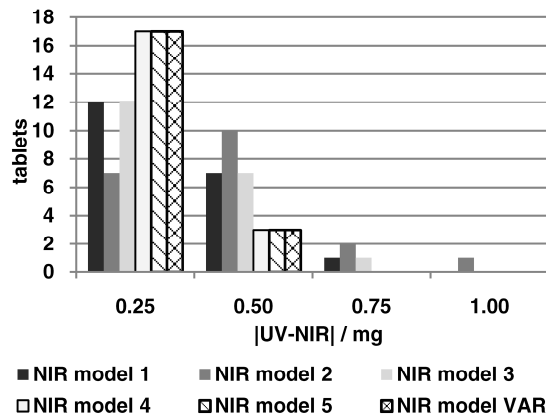
Figure 18: Absolute difference [mg folic a.] of NIR predictions from reference method for an external batch

8.1.5.2 *The press effect*

Figure 19A shows untreated transmission spectra for MCC placebo tablets made with varying porosity, thickness and hardness by applying increasing compaction force. There is a stark scaling effect, almost exponential, relating to apparent sample density (and hence tablet porosity and hardness) and thickness. This exaggeration in variability was used to demonstrate how difficult it is to completely remove the density and thickness element from spectra using pre-treatments (Figure 19B). A partial solution was to use multiple narrow wavelength regions where the spectra were grouped.
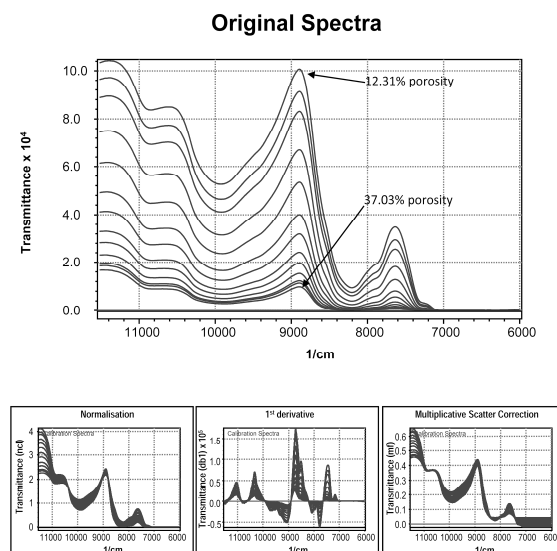
Figure 19: (A) Untreated spectra for placebo tablets made with varying compaction force. Thinner tablets with lower porosity have an upward scaled spectrum. (B) Pretreatment examples for same spectra, from left to right: normalization, 1st derivative and multiplicative scatter correction.

NIR predictions of the variable compaction force tablets are shown in Figure 20. Twenty 2.5% folic acid tablets made with varying porosities showed deviations from the reference method in varying degrees which are more pronounced on the high-porosity side (due to the exponential spectral relationship with thickness and density, *see below*). This highlights the need for careful model development for high density tablets.
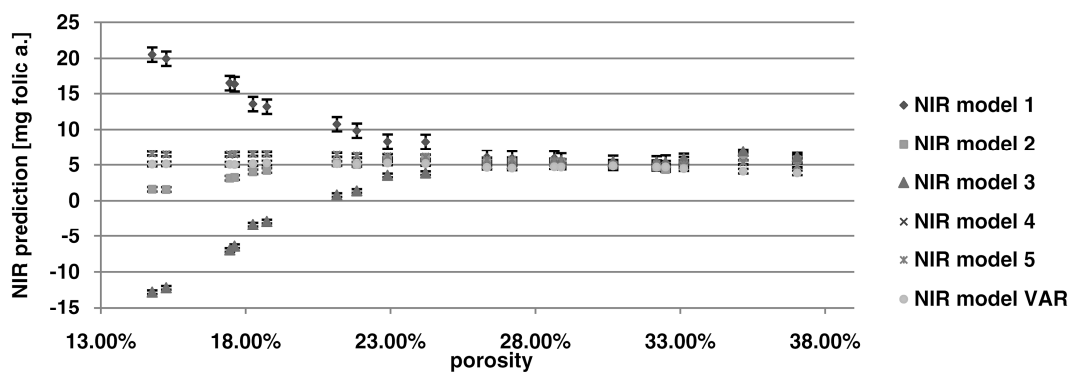
Figure 20: NIR predictions for 2.5% m/m folic acid tablets made with varying compaction force. All models perform well in a porosity range (31%) similar to that of calibration tablets. Calibration set with different porosities was added to model VAR which is more robust to porosity change.

Pharmaceutical tablets are made within a range of acceptable physical properties in line with friability requirements and desired dissolution/disintegration qualities. Although tablets are made within a narrow range of hardness (resistance to crushing – EP [25]) to obtain consistent properties and therapeutic effects, the limits are set by manufactures according to the formulation requirements, which can be broad. This means that a harder tablet that still complies with analytical limits would have a scaled spectrum and can either show up as an outlier when predicted with NIR or be over-/under-predicted. VAR is a sixth calibration model constructed from folic acid tablets with an extremely varying porosity range across all API concentrations for the calibration/validation set. This model (Table 4) had similar performance to the previous models but was much more robust in terms of tolerance to porosity variance (Figure 20).

However, the inclusion of samples with such extreme hardness variability makes the model very robust for hardness but would also render it more susceptible to other outlier effect, such as positioning, surface texture, particle size, raw material grades, etc. when tighter wavelengths and more principle components are used. A better compromise is the inclusion of maximum and minimum hardness samples from production batches to minimise the potential of future prediction errors and high spectral residuals.

8.1.5.3 *Uniscalar effect of porosity and thickness*

A change in any of tablet mass, density (hence porosity and hardness) or thickness would affect the other two. To assess the effect of one variable at a time, mass had to be adjusted in order to fix porosity with different tablet thickness values or vice versa (Table 3). Transmittance at 8880 cm^{-1} showed an exponential relationship with porosity (Figure 21A) and thickness (Figure 21B). The effects from these two variables were additive when tablets were pressed with varying compaction force and the resulting spectral scale was inversely related to both thickness and porosity (Figure 19A). These results offer a better understanding of the spectral relationship with tablet hardness presented in literature. (Cogdill, Herkert et al. 2007), (Kirsch and Drennen 1999), (Ciurczak and Drennen 2001) This also illustrates why tablets with thickness of less than 4 mm can have a significant spectral scaling when produced with a thickness SD as low as 0.1 mm, which can add to prediction errors and outlier potential (Figure 19B and Figure 21).
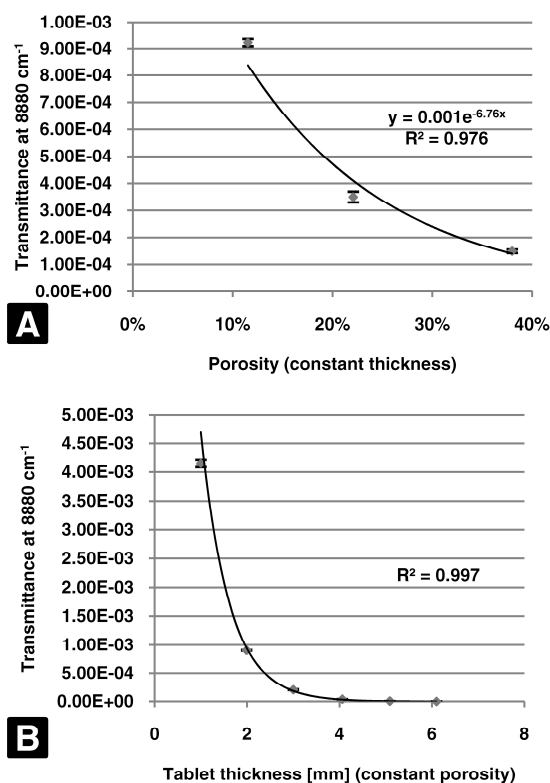
Figure 21: Transmittance at 8800 cm-1 of untreated placebo tablet spectra. (A) variable porosity and fixed thickness (B) variable thickness and fixed porosity

8.1.5.4 *Transmittance through the tablet*

To obtain an estimation of what percentage of the tablet volume is scanned in NIR transmission spectroscopy, untreated transmittance values at 8880 cm^{-1} were compared

as the same tablet was covered with laser-jet printed rings of different inner diameters (Figure 16). Tablets of varying porosities were used to examine different settings. Figure 22 shows that increasing the block area over a tablet towards its centre reduced the signal at the detector (transmittance at 8880 cm^{-1}) in a sigmoidal pattern, which was similar across different porosities. This suggests that porosity has little or no role in the distribution of NIR radiation coming out of the tablet surface.
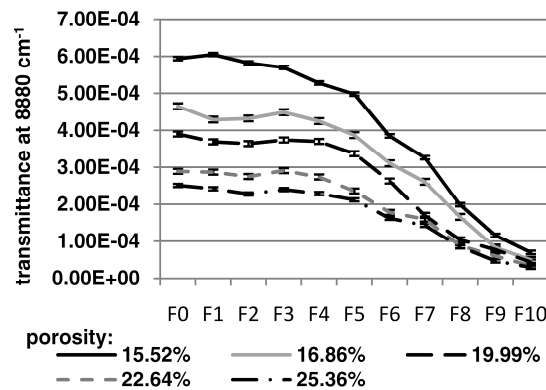
Figure 22: Reduction of detected signal with different paper filters. Different porosities show similar shape but different scale.

In Figure 23, average transmittance values from 10 tablets after block from all filters were expressed in relative terms to the intensity of a tablet covered by a white paper with no ink. This was also compared to the ratio of white area of each filter to the whole tablet surface area (drop in the signal if distribution was assumed to be equal across the tablet surface, Figure 23 - dark line).
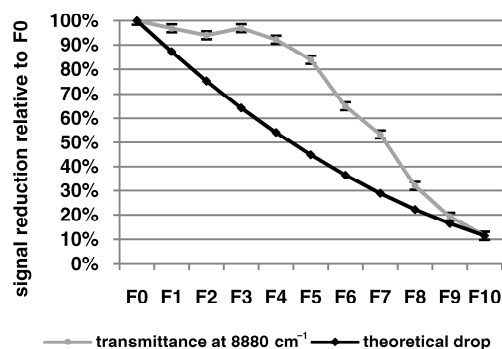
Figure 23: Reduction of detected signal with different paper filters relative to blank paper (grey) compared to ideal reduction if distribution was assumed equal across all regions of the tablet (black). Central regions carry more signal than peripheral.

If the tablet was visualised to be composed of 1 mm rings of decreasing internal diameters, the intensities from each ring can be estimated from the experimental data

above and compared to the theoretical intensity that the ring should transmit according to its area. This is also shown in Figure 23 and Figure 24 and modelled in Figure 25.
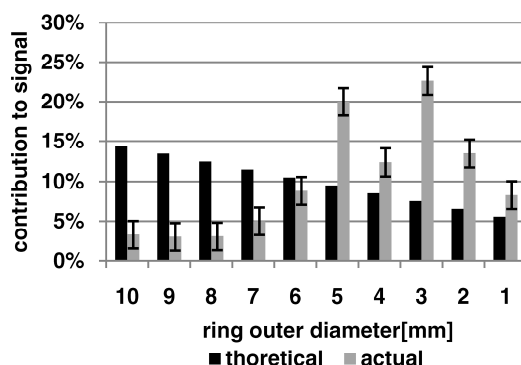
Figure 24: Actual distribution of transmittance through 1mm ring sections of a tablet from periphery to centre (grey) compared to ideal distribution if distribution was assumed equal across all regions of the tablet (black). Central rings carry more than their relative surface area.

A gradual reduction of the signal was followed by a sharp drop beyond a diameter of 7 mm across the tablet centre. However, the peripheral 3 mm also contributed by a small amount to the signal (<10%). Similar results were described by Iyer *et al.* [21] This also means that for a 10 mm tablet, the central 5 mm of a tablet carry 77% of the signal (area 25% of the whole surface) and the peripheral 5 mm of the tablet carry 23% of the signal (area 75% of the whole surface). This modelled distribution, coupled with the fact that radiation traverses the whole thickness, provides evidence that NIR transmission mode holds information representative of a big percentage of the tablet space. In addition, the fact that spectral representation of the tablet fades towards the periphery makes estimation of the sampled mass for both diffuse reflection and transmission modes overestimated and very much dependant on the tablet physical properties.
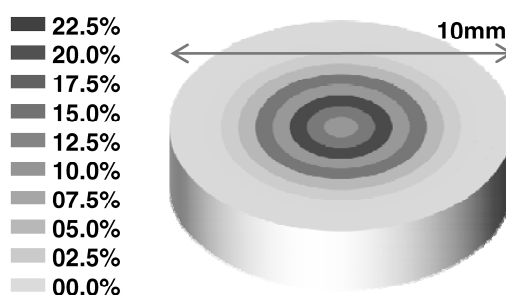
Figure 25: Final model representing NIR transmission through a 10-mm pharmaceutical tablet with a flat surface. Darker areas indicate higher signal contribution. There is a gradual fade from the centre with >90% of the signal carried through the central 7mm.

8.1.6 Conclusions

The time- and cost-saving benefits of NIR spectroscopy in quantifying solid dosage forms are too big to be ignored. Transmission mode is highly representative of pharmaceutical tablets but much more liable for interference from physical variations. This brings about the need for careful calibration model planning at the outset, with the inclusion of intended physical outliers in various possibilities in the calibration and validation sets, while employing representative sampling techniques and possibly partial factorial design for complex systems. On the other hand, the element of tableting parameters in spectra is a valuable resource in understanding the process, which is the rationale behind PAT manufacturing.

The technique was shown to perform well compared to the UV assay even under very challenging parameters (minimal spectral variation related to active principal and maximum density and thickness interference) but only after proper sampling design.

The arrangement and actual length of NIR optical pathways through a tablet have a major impact on spectra and, if not accounted for, predictions. Sources of variability such as pore size, shape, arrangement and total percentage inside a compacted tablet are important determinants of detected NIR absorption and intensity as well as the robustness of calibration models and can have potential answers for many issues related to prediction outliers.

8.2 Supplementary discussion to the published paper

8.2.1 Sample preparation

Folic acid is a water-insoluble and light sensitive drug and hence a good example where NIR spectroscopic analytics present clear advantages over wet-chemistry assays. Moreover, it is administered in very low doses (typically 5 mg), which would present more challenge to NIR methods.

Direct-compaction was chosen as a method of tableting for this experiment and tablets were compressed directly from mixtures of the drug and excipients without any preliminary treatment (granulation, pelletisation, etc.).

The mixture to be compacted must have adequate flow properties and cohere under pressure. Since most active compounds have less of such properties, they are mixed with other materials are directly compactable and serve as tablet diluents. This means that direct-compaction properties usually derive from the diluent, and potent drugs (like folic acid) which are presented in low doses can be mixed with generous amounts of diluent and still have a low table mass.

With direct-compaction, the original individual particles are still present and influence the compact properties and add to batch-to-batch variation problems. Further disadvantages of direct-compaction are segregation of mixture components which can further compromise tablet properties, adversely affect content uniformity and, in the case of NIR content analysis, present question marks on the validity of prediction.

The most frequently used direct-compaction diluent is microcrystalline cellulose which has a low bulk density and is highly compactable to form strong compacts that disintegrate readily in water. An important feature of direct compaction diluents is their capacity or dilution potential which is the amount by which they can incorporate substances which are not directly compactable and yet still produce acceptable tablets (Lund 1994).

An essential influence on the compaction process has likewise the crystal form and the grain size. A grain size between 0.5 and 1mm is regarded as optimal in direct-compaction. The requirement for the success of direct-compaction tableting is, that the

substances are dry, i.e. just showing a low residual moisture, which is the case in the prepared powder mixture (section 12.4.1.1).

Ideal directly compactable diluents should be physically and chemically inert and free flowing to ensure homogenous and rapid flow of powder for uniform die filling. High compactibility is also required and the mass must remain in the compact form once the compaction force is removed. Few excipients can be compacted directly without elastic recovery. Such fillers should also remain unchanged chemically and physically during the compaction process.

Diluents should have a particle size equivalent to the active ingredient present in the formulation which is consistent from batch to batch and produce uniform blending with and minimum segregation. This is why all mixture components were sieved with 90 μ sieve before mixing, without much sacrifice in tablet hardness (section 12.4.1.6).

Lubricants have a more adverse effect on the filler properties, and the softening effects as well as the hydrophobic effect of alkaline stearates can be controlled by optimising the length of blending time to as little as 2-5 min, as well as have lubricant concentration below 0.5%.

The Presster (section 12.2.1) was chosen because it presents a perfect tool to produce tablets of varying thickness, as well as its ability to simulate industrial-scale presses (dwell time). However, another aspect of tablet presses which is of prime importance to NIR methods is tablet mass and die filling variability, in relation to tablet press speed. This would mass variability would reflect on tablet thickness and porosity and hence might affect predictions. However, this variability is also dependant on the powder mix flow properties as well as feeding speed and container scale, and therefore is not a trivial factor to be simulated by lab-scale tools.

8.2.2 Calibration models

The use of NIR Flex N500 for analysis allowed spectral acquisition of tablets with high wavelength accuracy, good spectral resolution (16 cm^{-1}, capable of 8 cm^{-1}), and spectral reproducibility. The regular SST provided high reliability of the readings throughout the experiment.

The calibration range chosen (0-5% for testing 2.5% batches) was higher than the ICH guidelines of 70-130% of the SD of the target batch (around 1.75-3.25%) and big ranges have the potential for higher SEP. Slightly narrower range might achieve better predictions than in this experiment.

Another point is predicting total tablet API content (mg) versus predicting API concentration (mg mg^{-1}). NIRS like other spectroscopic techniques probe sample portions through their optical pathway, and hence optimally predict concentration (Figure 26).
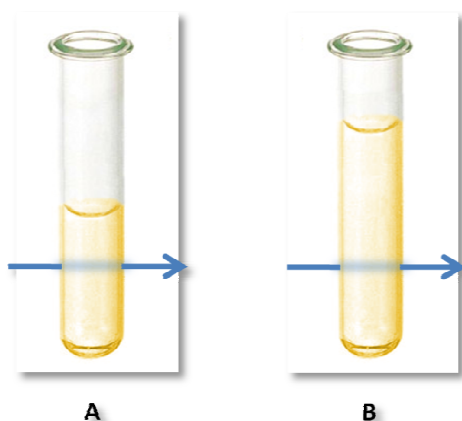
Figure 26: Spectroscopic assays, test tubes A and B are identical to the method because they have the same concentration, although B has more total drug content.

Although in DT, it is still not exactly known how much of the tablets are really scanned (also discussed in experiment II), but in all cases not all the tablet volume would be scanned. This means that NIR methods predicting total content are being able to do so because tablet mass variation is within a narrow range, and still this adds to the SE of prediction. Hence predicting percentage and converting to total content using precise tablet mass would be more accurate.

The UV method standard calibration curve was constructed from mixtures rather than folic acid stocks because the tablet contents would not be chromatically separated, like in HPLC, and all the components will be present in the sample solution. Although this was filtered before UV analysis and the components are not that soluble, but MCC is

slightly soluble in weak alkaline solutions and be might present in the cuvette during analysis. A calibration line made from such mixtures would perform in the same accuracy when a tablet is dissolved and assayed. The calibration fit had a zero intercept because the 0% tablets were inside the calibration and should not be assayed less than 0 (apart from –SD).

Because folic acid had very high UV absorption (light sensitive), 10.00 mg of the crushed tablet rather than the whole tablet was dissolved for assay sampling in order to remove the need for dilutions, the same applies to choosing 235 nm which is not the absorption peak, but rather 20 nm before it and lower in absorbance.

This might be argued as adding error to the method, but dilutions would be more problematic, especially the need for huge amounts of NaOH stocks (which need dilution) and the fact that the drug is light sensitive.

Every analytic method has its SD (or SE), and this is different than the SD of the UV apparatus itself. The SE of the whole method stems from errors in each step in the method, and in this experiment could be: sampling errors and scale SE, inhomogeneities not sampled (minimized by crushing and grinding), NaOH stock preparation, dissolution (complete or not), filtration (efficiency), cuvette cleanliness, and UV accuracy (wavelength and absorbance). To estimate the UV SEE, a more accurate analytic method needs to be available for comparison, and since that was not the case, SD can be used as a measure of SEE, in this case it was 0.1133 mg. This means that the NIR method will never have an SEP less than this figure, and in best cases will be 2 times that SEP.

With regards to the calibration model set, excluding the 0 and 5% API batches from the validation was needed, otherwise the calibration performance would be understated, because these spectra are at the periphery of the property space and their predictions would be in most cases extrapolated and hence fall as outliers or potential outliers. The limits of any calibration model should not be the target for validation, but rather the centre.

Outliers are spectra which, when applied to the constructed PCR or PLS calibration, cannot be fitted with the majority of the calibration model data. They can be identified by having residuals or scores outside the normally distributed SDs of the calibration model residuals and scores. There are many *possible* causes for outliers, but can generally classified into:

a. Abnormal sample (true outlier), e.g. wrong constituents or physical properties of the tablet

b. Abnormal spectral acquisition, e.g. tablets out of position in the sampling plate or instrument problems. This can sometimes be excluded by re-scanning the sample.

c. Abnormal referencing, e.g. errors in UV or HPLC dilutions, sampling, measurements, etc. This is difficult to detect due to the destructive nature of the referencing methods.

d. Poor calibration model, e.g. models with numerous outliers should be re-evaluated.

In Figure 68, an outlier can be visually detected in the "predicted vs. original", as well as the leverage plots. In many cases, it would be safe to exclude outliers from the model, especially if they are very infrequent. In other cases however, they might be an important indicator of the model's performance, especially in terms of robustness.

Although this amount of validation spectra are good enough to generate data that can fully validate the method, an external prediction batch that was not involved in the model development is needed, especially when model robustness is in question. In such cases, external batches taken at different points of time over the process life time would be the best approach.

In NIRCal, there are two aspects unique to the software, namely Q-value and the model wizard. Both were researched and patented (Bossart and Grabinski 2002) and ultimately included in NIRCal in attempt to simplify calibration model optimization and evaluation. The Q-value (Figure 27) is a pool of *weighted* model indicators that sum up to a value between 0 and 1. Models above Q-value of 0.75 are claimed to be useful and those above 0.95 excellent.

This Q-value is also used to find *near* optimum model optimization by changing the model variables (pretreatments, wavelength regions, number of PCs, and even sample sets) until the best Q-value is found.
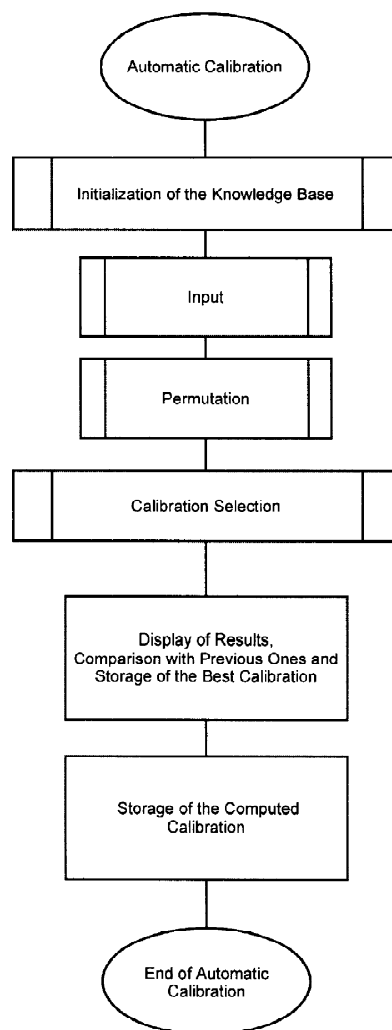
Figure 27: NIRCal's Q-value overview (Bossart and Grabinski 2002)

During this experiment, both tools proved to be as good as (in some cases better than) manual optimization and evaluation of models. The only aspect where manual intervention is needed was wavelength selection.

An SEP of 0.2731 mg (5.452% of prediction batch content) is 2.4 times the SD of the reference method and can be considered adequate. It must be noted however, the SEP is normally distributed and it means that 95% of the samples will be ±2×SD and 68% within 1×±SD (Figure 28).
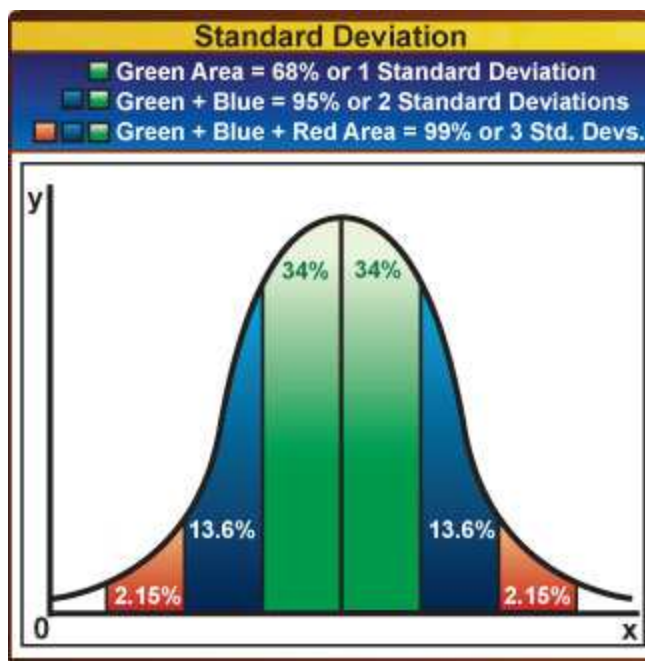
Figure 28: Normal distribution of standard error

The t-test results show that there is significant difference between the three models and the UV reference method. This shows typically how NIR models can be over-fitted to the training set, and fail with external prediction (see section 12.4.3, page 192 for better models). However this result should also be viewed in light of the low (20) sample size. Moreover, ICH guidelines permit for accuracy to be inferred once other parameters have been validated (page 58).

8.2.3   Press effect

It is known that density affects NIR spectra in both DT and DR modes. In tablets, however, there is a complex relationship between compaction force, tablet thickness and porosity (apparent density), which is further affected by fluctuations in tablet mass (Figure 29).

Therefore, it is essential to investigate these effects on spectra, both in combination and singularly. The normal variability range might not show a clear effect on NIR spectra, apart from contributing to the SEP of prediction. However, when this variability was extended, the dependency of the spectra in DT mode to the compaction force was very clear (Figure 75).

The spectral scale was non-linearly proportional to compaction force, and as the powder particles were more compacted and voids became smaller and less numerous (less porous), the air/solid interface total area became also smaller and therefore scatter was reduced. This meant that photons had a greater chance of escaping to the other side and

be detected. The accompanying reduction in tablet thickness produced a reduction in voids independent from porosity.
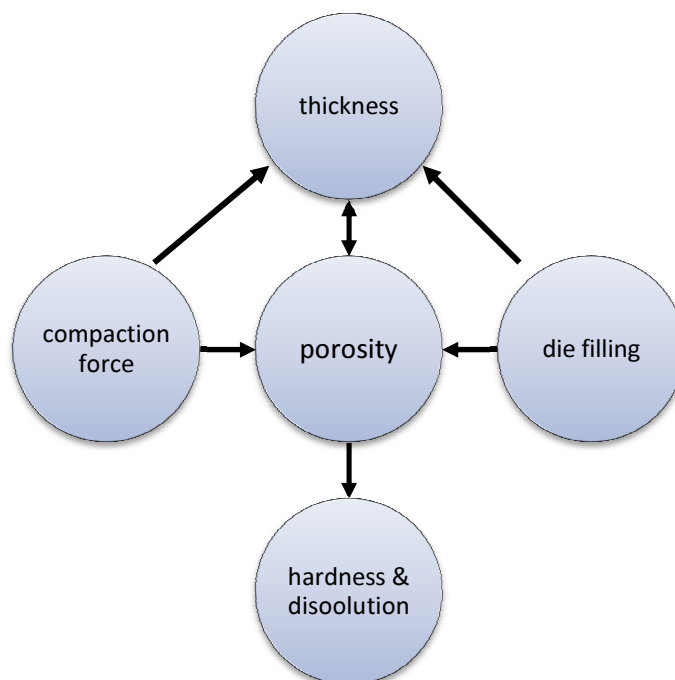
Figure 29: Relationship between compaction force and tablet parameters. Compaction will affect thickness and porosity, so does die filling (tablet mass). Porosity will in turn affect tablet hardness and dissolution profile.

The scale was bigger in spectral regions that had more transmittance (less absorbance). This dependency on absorbance was the main reason why all pre-treatments failed to group the spectra (Figure 79), and this failure on big-scale would be reflected on small-scale variations, meaning there is a limit to how much pre-treatments can correct, and the remainder will be prediction errors. Therefore, novel pretreatments that can take this effect into account (sample-dependent) would potentially improve predictions.

Compaction speed, on the other hand, can also contribute to the variability picture. However, and in the case of the MCC diluent, there was no clear relationship between tableting speed and any of the tablet physical parameters, and hence predictions (Figure 75 and Figure 78). Other diluents which have compaction profile that are more clearly dependent on compaction duration might show a different picture and are yet to be investigated.

The effect of compaction force variability on predictions is clearly illustrated in Figure 80 when all models show gradual drift in prediction from the referenced content, except in the porosity region they were trained for.

It was possible, however, to develop a model that was robust to this variability by adding spectra of variable compaction force across all calibration concentrations (Figure 81). Only then was the content predicted across the whole porosity range, of course with higher SEP and using much bigger number of PCs.

Finally, the spectral scale relation to tablet thickness and porosity, each singularly is illustrated in Figure 82 and Figure 83. The scaling in both cases was exponential and running in the same direction of the compaction force change.

8.2.4   *Tablet sampling span in diffuse transmission*

The effect of placing a black paper over a tablet on DT spectra had to be tested first, and Figure 15 shows the scaled-down spectrum of an MCC tablet and blank paper. It also shows the effect of laser ink 100% coverage on paper over the tablet. The spectrum was scaled-down even further but in both cases preserved the same MCC spectral features. This meant that scaling, represented by transmittance at a single wavenumber can be taken to represent the degree of block, hence the maximum at 8880 cm-1 was chosen.

With the application of paper filters F0 – F10 (from Figure 16) on the tablet, the DT spectra were scaled-down gradually with each increase in the block inner diameter (Figure 69). F1 and F2 block was small and difficult to judge whether due to positioning noise effect (most peripheral blocks) or real signal block. From F3 onwards, the block was strongly evident.

In Figure 22, all porosity ranges tested showed similar sigmoidal block pattern, an indication that porosity change (in that range), was not affecting the signal distribution to a big degree. The plots do, however, have different scales, and it is due to due increase in radiation scatter at lower sample densities (higher porosity) – see press effect, chapter 8.

The decrease in absolute transmittance at 8880 cm-1 was taken as a measure of the drop, and converted to proportional drop in comparison to F0 spectrum (section 11.2.4). Because F10 (100% coverage) would never scale-down the signal to 0%, the corresponding theoretical (ideal) distribution was also scaled-up to match this partial block.

The theoretical block describes how the block pattern should be if the DT radiation was assumed uniform across tablet surface, and used for comparison to appreciate the area of the block.

The central areas were found to carry represent more of the signal than their proportional area (as expected). However, the representation of the tablet was continued up to 7 mm in diameter (90.6% of signal). However, although much less, the outer area is still represented in the spectrum, but eventually, tablets with bigger diameters have even smaller area sampled by the NIR radiation. Such big tablets in most cases have higher drug loadings (main reason behind increased tablet size) and would have less problems of drug segregation.

9. Tablet sampling span in diffuse reflection

The work on this section is summarised in the original scientific publication from the author (below), with more detailed experimental methods and results sections in Appendix III.

9.1 Assessment of diffuse transmission and reflection modes in near-infrared quantification – part II: diffuse reflection information depth (original paper)

9.1.1 Keywords

9.1.2 Abstract

Near-infrared (NIR) spectroscopy offers tremendous advantages for pharmaceutical manufacturing as a fast and non-destructive method of quantitative and qualitative analysis. Content uniformity (end product analytics) and process analytics are two important applications of the method. In part I of the study, diffuse transmission (DT) and the effect of tableting press and horizontal sampling span were discussed. Experimental evidence showed that 90% of the signal was detectable from a diameter of up to 7 mm.

On the other hand, DR information depth (vertical sampling span) assessment is of equal importance in content prediction applications and to understand the effect of inhomogeneities in the sample. Three experiments were conducted: I. 0.5 – 10 mm incremental thickness MCC tablets with constant porosity, II. MCC/Phenylbutazone (PBZ) double layered (DL) tablets (PBZ layer 0-100% in 0.5 mm steps) and III. Comparison of placebo and 30% caffeine tablet cores with incremental film coating (film thickness of 0 – 0.35 mm). Incremental thickness and cluster analysis of DL tablets showed that DR information depth was < 0.5 mm, while the data fitting from incremental coating showed that signal drop reached 50% at 0.05 – 0.07 mm depending on the wavenumber and 90% signal drop (10% information content) can be seen between 0.2 – 0.25 mm without extrapolation.

9.1.3   *Introduction*

Near infrared (NIR) spectroscopic methods have been widely used in pharmaceutical analysis for both qualitative and quantitative purposes, providing results of comparable quality in a more simple and expeditious manner. Therefore, they constitute effective alternatives to chromatographic techniques in many cases, encouraged by additional factors such as the ease of sample preparation and the reproducibility of measurements, which have often dictated their use in quality control analyses of both raw materials and finished products. The differential sensitivity and selectivity of spectroscopic techniques have so far dictated their specific uses. For example, UV-Vis spectroscopy has typically been used for quantitative analysis by virtue of its high sensitivity, while infrared (IR) spectrometry has been employed mainly for the identification of chemical compounds on account of its high selectivity.

9.1.3.1   *Theoretical aspects of diffuse reflection*

In NIR spectroscopy (NIRS), X-H (X is C, N or O) functional groups are almost exclusively involved in NIR spectroscopy (NIRS) because the overtones and combinations of their fundamental frequencies in the mid-IR and produce absorption bands of useful intensity in the NIR. The absorptivities of these overtone and combination bands are so much weaker than in mid-IR spectroscopy, and it is due to this fact that spectra of condensed phase, physically thick samples can be measured without sample dilution (non-destructive analysis) and hence no sample preparation. The other advantage of low absorptivity is that measurements involving scattering effects are possible (diffuse transmission and refection). (Simpson 2005)

Reflectance (R%) can be interpreted from equation (0.24), where I_R is the intensity of the diffusely reflected light and I_0 is the intensity of the incident light. Absorbance can be approximated as log of reciprocal reflectance, equation (0.25).

$$R\% = \frac{I_R}{I_0} \times 100 \qquad\qquad (0.24)$$

$$A = \log\frac{1}{R} \qquad\qquad (0.25)$$

Diffuse reflectance (DR) differs from specular reflectance in that light penetrates the material up to some distance, where it is partially scattered on the surface of particles, as well as being partially absorbed. Therefore, considerable attempts have been made to describe it mathematically, the earliest being Lambert cosine law (Lambert 1760) in

which he proposed a correlation between the remitted radiation and the angle of observation for matte surfaces. Kortüm (1969) suggested that this law can be derived from the second law of thermodynamics but valid only for ideal diffuse reflectors and hence deviation from this law will occur in practice.

Mie (1908) developed a more accepted theory that described the angular distribution of intensity and polarization of scattered radiation for a single scattering by one particle. This makes it applicable only to chemical systems in which particles are well separated. In practice, samples are expected to have multiple scattering taking place which led Theissing (1950) to take this theory a step further by including multiple scattering, but still particles in NIR/DR analyses are so densely packed that phase relations and interferences between scattered beams which have not been accounted for do exist. Thus for samples of this type no general quantitative solution to the problem of multiple scattering has been found. (Griffiths and Olinger 2002)

Most other theories have evolved from energy transfer treatments, which describe the change in intensity of a beam of radiation of a given wavelength in a sample of a given density and pathlength due to total radiation loss from scattering and absorption that corresponds an attenuation coefficient, (Truelove 1988) and (Craig and Incropera 1984). Schuster (1905) made an attempt to find simpler solutions to the radiation transfer equations by using different vectors for the light being incident or being remitted by the sample.

Kubelka and Munk (1931) made more assumptions in their derivation of a simplified solution to the radiation transfer equation. The final derivation is shown in equation (0.26) and shows that the measured DR (R_∞) is dependent on the ratio of K and S (absorption and scattering coefficients respectively). Kubelka and Munk's solution is the most widely accepted DR explanation since it is a two-constant equation and therefore experimentally testable. Moreover, many other derivations by other workers like Smith (1931), Amy (1937) and Bruce (1926) have been shown to be derivable from Kubelka and Munk's work.

$$f\left(R_\infty\right) = \frac{K}{S} = \frac{1 - 2R_\infty + R_\infty^2}{2R_\infty} = \frac{\left(1 - R_\infty\right)^2}{2R_\infty} \tag{0.26}$$

For diffuse transmission (DT) on the other hand, light travelling in a medium is attenuated by absorption and scattering. The energy that is transmitted along the regular path is reduced more the longer it propagates in the medium or when the

concentration of the absorbing ingredient in the medium is higher. For a medium that does not cause significant multiple scattering, the radiant flux density of the transmitted light is related to the radiant flux density of the incident light by Beer-Lambert law, which holds true only when the effect of multiple scattering is negligible because the energy scattered forwards by one particle can be scattered backwards by a second particle. Although the interaction of light with materials was studied extensively, especially at the visual range (light propagation theory and optical dispersion (Lee 2005), the complexity of the optical path inside a compacted material and the dependence of this path on physical properties of the compact (packing density, particle size, thickness, absorbing species concentration and distribution, etc.) hindered the development of a complete theory describing (DT) to date.

As mentioned before, variations in the physical properties of samples can have significant effects on spectra. For tablets, mainly variation in bulk density (porosity and hardness); and in particle size range of compacted material would change the total surface area of the compacted particles and the ratio of voids to solids, hence spectral scaling will be evident for both effects. In DR mode, this will show as baseline shifts that can complicate content analysis or form the basis for hardness predictions (Short 2009 and Blanco 2006), and is one of the reasons for using various pre-processing techniques (Shi and Anderson 2009).

Another important aspect in the determination of content uniformity (CU) in pharmaceutical tablets is portion being sampled. The higher this portion is, the less likely the predictions will be affected by non-homogeneity in the tablet contents. In DT mode, experimental evidence have shown that >90% of the spectral information is from the central 7-mm of a typical pharmaceutical tablet, (Saeed et al, 2009) and the fact that radiation traverses the whole thickness of the sample means that this mode scans a considerable portion of the tablet volume.

In DR mode however, the information depth (the depth of the sample contributing to the final detected radiation and for which the spectrum is representative) would determine the sampled portion of the tablet. Moreover, the extent of this depth would determine the applicability of this mode to coated or multi-layered tablets.

9.1.3.2 *Current evidence on DR information depth*
Few researchers have tried to DR estimate information depth for powder mixtures. Olinger and Griffiths (1992), (2002) used absorbance values for mixtures with known absorptivities and particle size values and reported an upper boundary of 1 mm at 1653 nm. It was also reported that if scattering effect was to be considered, this range would

unlikely be more than 300 μm. Others have reported different values but without supporting experimental or theoretical evidence: 5 mm (MacDonald and Prebble 1993), 1-2 cm (Ciurczak 1991), 1-4 mm (Olinger and Griffiths 1992), 0.5 mm (Stephen Victor Hammond 1997).

The evidence is even smaller for compacted solids. Iyer et al. (2002) have tried to estimate the sampled mass in DR using single and double-layered tablets and second derivative spectra. He concluded that the effective sampling depth was between 1.9 and 2.7 mm depending on the wavelength. Another study by Andersson et al. (1999) showed different values and suggested an information depth of 0.1 - 0.2 mm using incremental coating and tablets with 2 different components. The authors however maintained that these figures are only rough estimates because the results were obtained using extrapolation and may only be valid for specific materials and instruments.

Because of such varying views on DR information depth, the exact value is still not clear to operators of the method. Additionally, since the majority of pharmaceutical tablets range in thickness between 1 – 4 mm, determining this depth is crucial to the selection of appropriate measurement modes for different coated, uncoated and multi-layered tablets and can provide better understanding of the performance differences between DR and DT modes.

9.1.3.3 *Study aims*
The study aims to determine the portion of the tablet contributing to DR spectral information (DR information depth). Because the evidence would be experimental and in many cases indirect, three different studies are made using tablets with increasing thickness, double-layered and incrementally coated tablets. Finally, an estimation of the pharmaceutical tablet depth at which 50% and 95% drop in the DR information is to be proposed.

9.1.4 Experimental

9.1.4.1 *Materials*

Microcrystalline cellulose 102 (MCC SANAQ 102 G) (Pharmatrans SANAQ AG, Basel, Switzerland), Phenylbutazone (Sigma-Aldrich, Buchs, Switzerland), Caffeine anhydrous powder (BASF AG, Schaffhausen, Switzerland), Magnesium Stearate (Sigma-Aldrich, Buchs, Switzerland), FD+C Red 3 LA (Sigma-Aldrich, Buchs, Switzerland), Pharmacoat 603 (HPMC) (Novartis Pharma AG, Basel, Switzerland), Aquacoat ECD 30 (FMC Biopolymer, Houston, TX), Triethylcitrate (Sigma-Aldrich, Buchs, Switzerland).

9.1.4.2   *Tableting*

Variable thickness tablets were compacted on a Zwick Material Testing Machine (Zwick GmbH & Co., Ulm, Germany). Double layer tablets were compacted on a Presster™ tablet press simulator (Metropolitan Computing Corporation, East Hanover, New Jersey). Tablets for coating were compacted on an eccentric press (Korsch Schweiz GmbH, Trimbach, Switzerland).

True density measurements were performed using a helium pycnometer (AccuPyc 1330, Micromeritics, Norcross, GA, USA) at room temperature. Air was extracted to generate a vacuum and then Helium was pumped-in 5 times until equilibrium was reached. Tablet thickness was measured using a digital calliper (Mitutoyo, Tokyo, Japan), and tablet mass was measured using an analytical scale AX204 (Mettler Toledo, Switzerland).

Detailed method description is given in sections 14.3.1-14.3.3.

9.1.4.3   *Coating*

Tablets were coated inside Strea-1 laboratory fluid-bed (Aeromatic AG, Muttenz, Switzerland) and coat material was fed using a rotary pump.

9.1.4.4   *NIR measurements*

Tablets were scanned with NIRFlex N-500 (Büchi Labortechnik, Flawil, Switzerland), a Fourier-Transform spectrometer based on quartz polarization interferometer and a Tungsten halogen source. DR measurements used NIRFlex Solids cell with tablets add-on and DT measurements used NIRFlex Solids Transmission cell with a sample size-adjustable sample holder. Both cells use an extended range InGaAs detector (temperature controlled). More details are given in section 14.2.2.

9.1.4.5   *Data processing*

Data was fitted in a 3-way curve using Tablecurve 3D (Statcon, Germany). Spectral data processing and chemometrics were performed using NIRCal v5 (Büchi, Flawil, Switzerland). Exported spectra were averaged and correlated using standard Microsoft Excel functions and a VB macro to examine the entire wavenumber regions.

9.1.4.6   *Experiment 1: Variable-thickness tablets*

MCC powder was compacted into 0.5 – 10 mm thick tablets in a porosity range of 25 – 33% using the Zwick. The mass of each tablet was calculated from the porosity equation (0.27) where porosity of the tablet (F) is related to the density of the compact (ρ) and

the true density of the powder mix (ρ_0). P was simply the tablet mass (m) over its volume (V).

$$F = 1 - \frac{\rho}{\rho_0} = 1 - \frac{\dfrac{m}{V}}{\rho_0} \tag{0.27}$$

Because the Zwick is a hydraulic press where the force of compaction rather than the gap is set, and because this force is dependent on both the final tablet thickness and mass for the same powder mix, the press was calibrated using different powder masses and different tablet thickness and the data was fitted on a 3-dimensional calibration curve (Figure 30) to calculate compaction forces for all tablets made (Table 5). DR spectra where then collected from all tablets, both the upper and lower surfaces. The collected DR spectra were processed with and without pre-treatments (normalisations, 1st and 2nd derivatives, standard normal variate and multiplicative scatter corrections). However, non-pretreated spectra in this case showed the best grouping, because the sample density was tightly controlled.

Table 5: Incremental thickness tablet details

| Tablet mass [mg]	Thickness [mm] after 24h	Porosity
41.90	0.50	25.68%
83.80	1.00	25.39%
125.50	1.52	26.24%
167.20	2.01	25.86%
208.90	2.50	25.63%
252.80	3.01	25.24%
293.30	3.52	25.85%
335.20	4.05	26.27%
380.00	4.56	25.72%
419.80	5.06	26.06%
461.40	5.55	25.91%
504.20	6.07	25.99%
545.90	6.58	26.09%
589.70	7.07	25.75%
630.30	7.57	25.84%
672.40	8.05	25.65%
714.00	8.57	25.83%
757.00	9.12	26.06%
799.90	9.54	25.35%
840.30	10.06	25.63%
	Mean	25.80%
	SD	2.79E-03
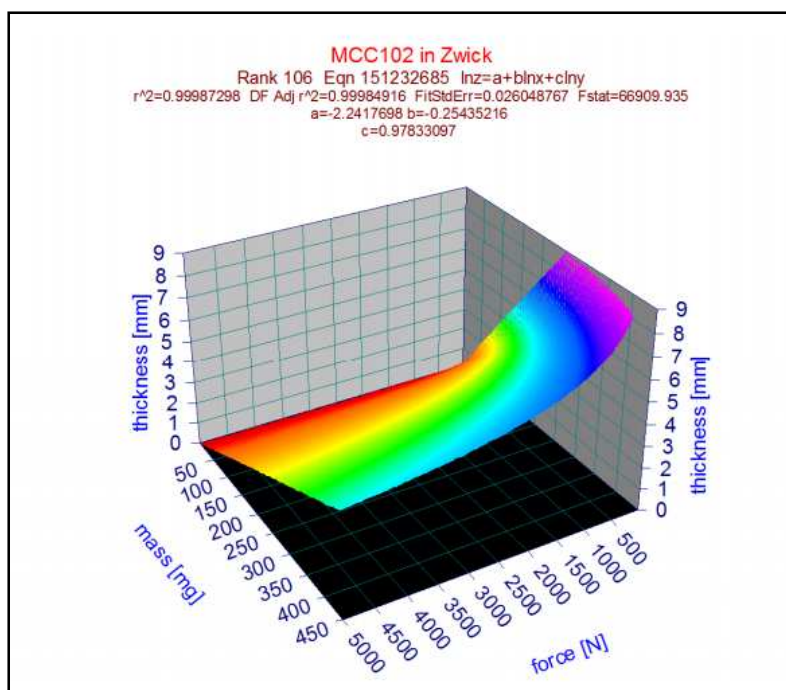
Figure 30: Three-factorial fitting of tablet thickness, mass and compaction force of MCC 102 on Zwick

9.1.4.7 *Experiment 2: double-layered tablets*

In these tablets, the lower layer contained phenylbutazone (PBZ), pigment and lubricant while the upper layer contained MCC and lubricant only (Table 6). The tablets where compacted in Presster™ using a flat face 10 mm punch. The powders where manually fed for each tablet. The lower layer was fed first and loosely compacted. The compaction was interrupted before ejection and the upper layer was fed on top and both where compacted and the double-layered tablet was ejected. Table 6 also lists the proportions of each layer, compaction forces used and compacted thickness. DR and DT spectra where then collected from both sides of the tablets and a principal component analysis (PCA) cluster models were constructed using different pretreatments, wavelength regions and number of PCs, and models with the best clustering (least amount of SE) were selected.

Table 6: Double-layered tableting

	Upper layer (PBZ)				Lower layer (MCC)			Final tablet	
mass	Comp-action gap	Thickness after compaction		mass	Comp-action gap	Thickness after compaction		mass	Thickness
mg	mm	mm	% tablet	mg	mm	mm	% tablet	mg	mm
0	0.0	0.00	0.0	400	3.2	4.27	100.0	394.7	4.27
50	0.6	0.50	11.7	350	3.2	3.77	88.3	391.0	4.27
100	1.8	0.95	23.5	300	3.2	3.10	76.5	396.6	4.05
150	2.8	1.58	38.7	250	3.2	2.50	61.3	394.1	4.08
200	3	2.09	49.2	200	3.2	2.16	50.8	388.5	4.25
250	3	2.7	65.1	150	3.2	1.45	34.9	391.1	4.15
300	3.4	3.21	75.5	100	3.2	1.04	24.5	393.2	4.25
350	3.4	3.8	88.4	50	3.2	0.50	11.6	392.9	4.30
400	3.2	4.45	100.0	0	0	0.00	0.0	389.4	4.45

9.1.4.8 *Experiment 3: Coating experiment*

Placebo (99% MCC and 1% MgSt) and caffeine (30% caffeine, 69% MCC and 1% MgSt) tablets where compacted using a Korsch eccentric press and 7 mm concave punch with a 5.5 mm curvature radius. Tableting involved strict and frequent in-process-control sampling. Both batches produced tablets with 100.57 mg (SD 1.03) mass and 3.16 mm (SD 0.022) thickness.

Both placebo and caffeine tablets were coated (separately) with a typical film coat formulation (Aquacoat ECD – Table 7) inside a fluidized bed. The process was stopped every 50 g of coat sprayed and samples were collected for analysis. The process was stopped after 6 batches because the coating started to be non-homogeneous. Figure 31 shows the weight and thickness gain along the process. It is noticeable that coating was continued much beyond normal film coating (10 – 100 μm) (Swarbrick and Boylan 1988) in order to investigate the DR information depth. NIR DR and DT spectra were then collected for all coat levels. The spectral data were then exported to Excel for analysis.

Table 7: Film coat formulation

| Component	Proportion %
Aquacoat ECD-30 (30% w/w)	22.22
Pharmacoat 603 (19% w/w)	35.09
Triethylcitrate	1.33
FD+C Red 3 LA	7
Water (dist.)	34.36
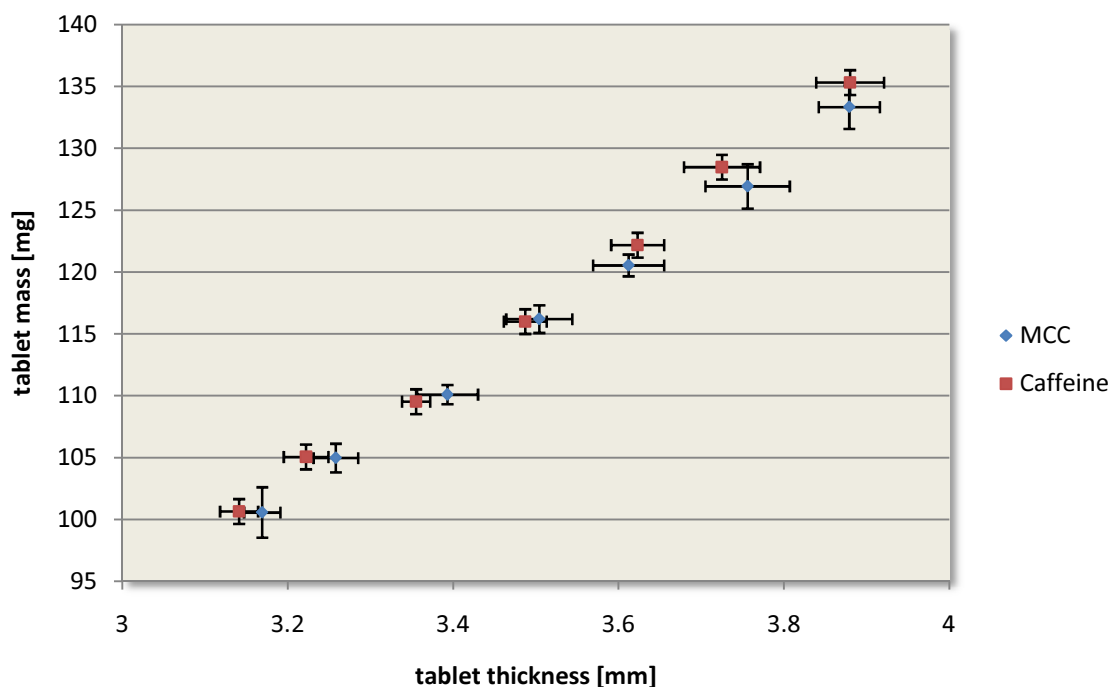
Figure 31: Film-coat increase for both MCC and Caffeine batches

9.1.5   *Results and discussion*

9.1.5.1 *Incremental thickness tablets*

Table 5 shows the gradual and uniform increase in tablets thickness, from 0.5 mm to 10 mm. It was not possible to manufacture a tablet with a thickness of less than 0.5 mm, and 10 mm was chosen because it was higher than any published data on DR depth. The tablets had a uniform porosity (mean of 25.8%), as shown from the small SD and graphically in Figure 32 (no correlation with thickness). Any changes in porosity with thickness would make interpretation of the spectra very difficult.
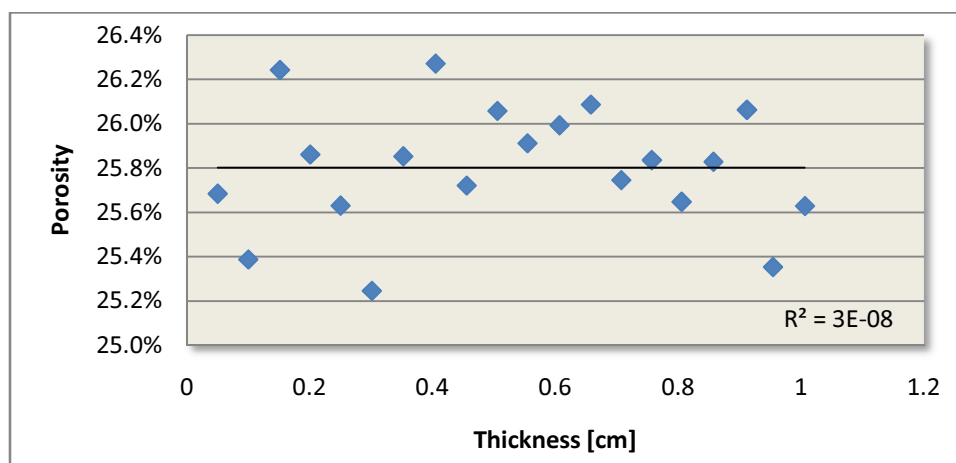

Figure 32: Plot of tablet thickness against porosity for incremental thickness tablets showing no correlation

Figure 33 shows a plot of several DR spectral maxima of the increasing thickness tablets, from both upper and lower surface scans. There was a gradual increase in reflectance with thickness, until 2-3 mm, followed by a gradual drop until 7 mm, and then another increase. This pattern was seen in all scans and cannot be relied upon for estimation of the depth with any certainty. One possibility was that the information depth was already missed with the thinnest tablet (0.5 mm). Both the upper and lower surfaces were scanned because tablets compacted in Zwick have different density distributions across its surfaces. However, the same pattern was observed.
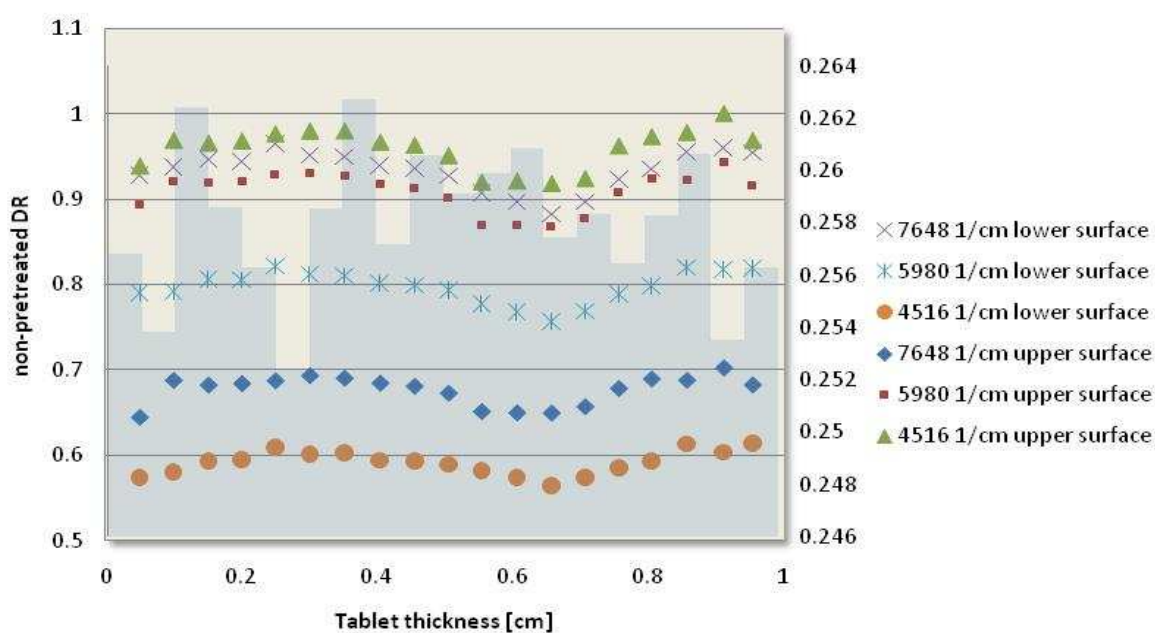

Figure 33: DR spectral changes with increasing tablet thickness, both for the upper and lower tablet surfaces and different spectral maxima. The blue bars indicate porosity of the same tablets (secondary axis)

Since all the tablets were produced from the same raw material batch (MCC only) with excluded effect of porosity (Figure 34), the pattern could also be due to instrument-related density distribution or tablet surface texture changes with different compaction force/tablet mass profiles. This meant that the experiment did not yield useful information and other approaches had to be tried.

9.1.5.2 *Double-layer tablets*

The selected Presster compaction scheme was able to produce double-layered tablets of uniform layers (Table 6 and Figure 35). Again, the thinnest layer was 0.5 mm and less than that cannot achieve homogenous and complete layer. Figure 36 shows SNV pretreated DR spectra of double-layered tablets, scanned with the PBZ layer downwards, as well as single layered MCC and PBZ tablets (white and pink respectively).

There was a marked spectral difference between the MCC- and PBZ-only tablets in several regions (marked red) which enabled a good interpretation of the results.


Figure 34: Plot of DR against tablet porosity of increasing thickness tablets, for upper and lower surface at different spectral maxima. No correlation was observed.


Figure 35: Layer thickness of double-layered tablets versus layer mass, showing uniform layers

Figure 36: Double-layer tablets DR spectra (PBZ downwards, SNV pretreatment). All spectra are non-distinguishable from PBZ, except the single layer MCC tablet.

If there was any DR radiation penetration beyond the thinnest PBZ layer (0.5 mm) into the MCC layer, the spectra of these tablets should have carried some features of the MCC spectrum, which was not the case in Figure 36. The picture becomes more clear when compared with DT spectra of the same tablets in the same orientation (Figure 37). In this mode which penetrates both layers, there was a gradual change of spectral features from the PBZ-only tablets, and then the double layers with decreasing PBZ layer thickness, until the MCC-only tablet. Because this picture is not shown in any of the double-layered tablets, the conclusion would be that DR information depth should be less than 0.5 mm.
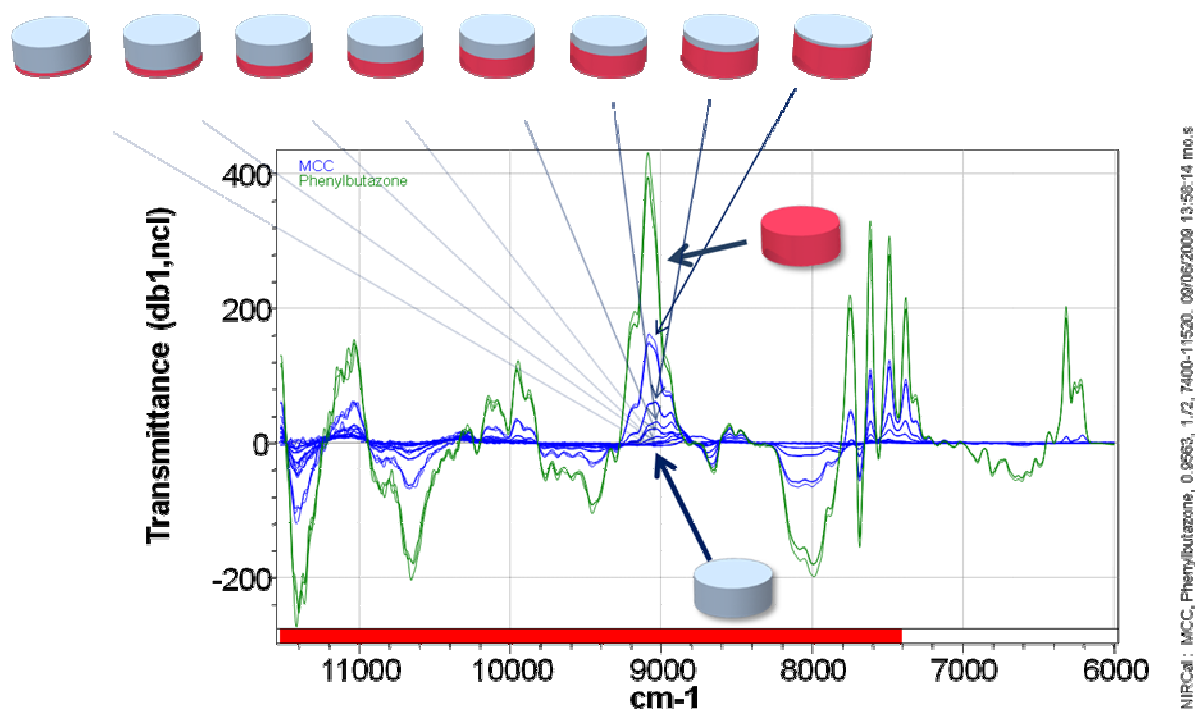
Figure 37: Double-layer tablets DT spectra (PBZ downwards, db1 and ncl pretreatments). Spectra feature change gradually from PBZ to MCC as PBZ layer thickness decreases

Because the results above depended on visual inspection of the spectra, they had to be confirmed by cluster analysis chemometric models. Figure 38 shows PC 1 versus PC 2 scores of the DR spectra, referenced as MCC property (blue), except the PBZ-only tablet labelled as PBZ (green). This was to see if the model can identify any of the double-layered tablets as MCC when the MCC layer is upwards (and hence DR penetration across PBZ). The score plot very clearly shows that all the double-layered tablets were grouped with the PBZ-only tablet away from the MCC-only tablet because no MCC spectral features are available to distinguish them. The model had a very low Q-value (<0.4).
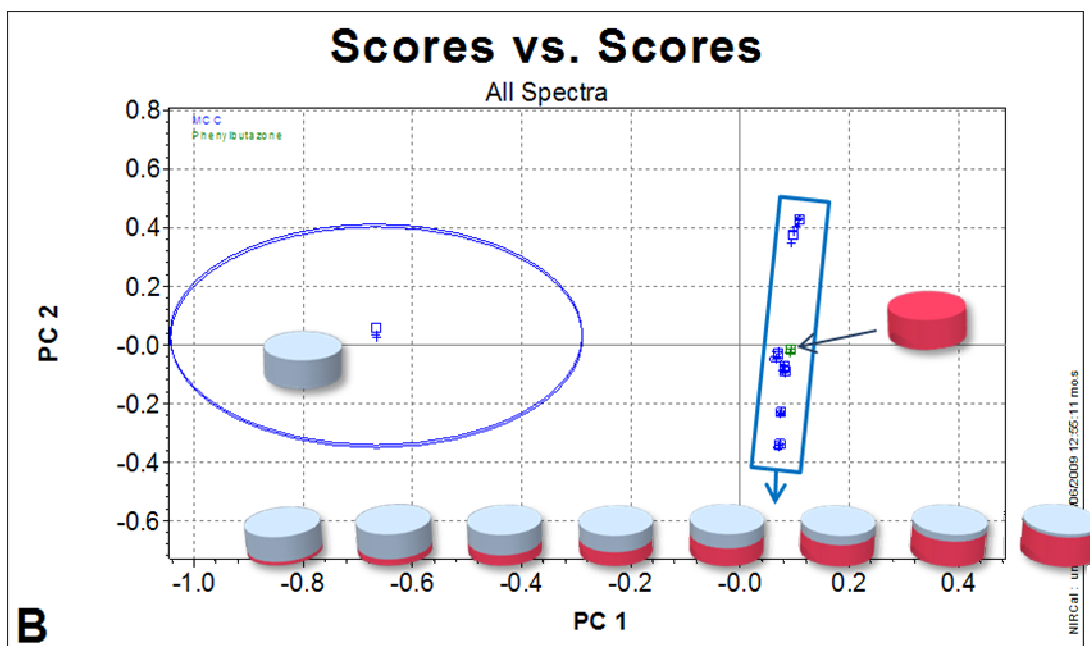
Figure 38: Cluster analysis of double-layer tablets in DR mode. None of the double-layer tablets labelled as MCC (upper layer) was grouped with the MCC-only tablet, and instead had scores similar to the PBZ-only tablet

This was not the case with DT cluster analysis of the same tablets (Figure 39) where all the double-layered tablets were correctly identified and clustered with the MCC-only tablet, with scores moving towards the PBZ with increasing PBZ content. The model had a very high Q-value (>0.9) and other models consisting of one PC were also possible.
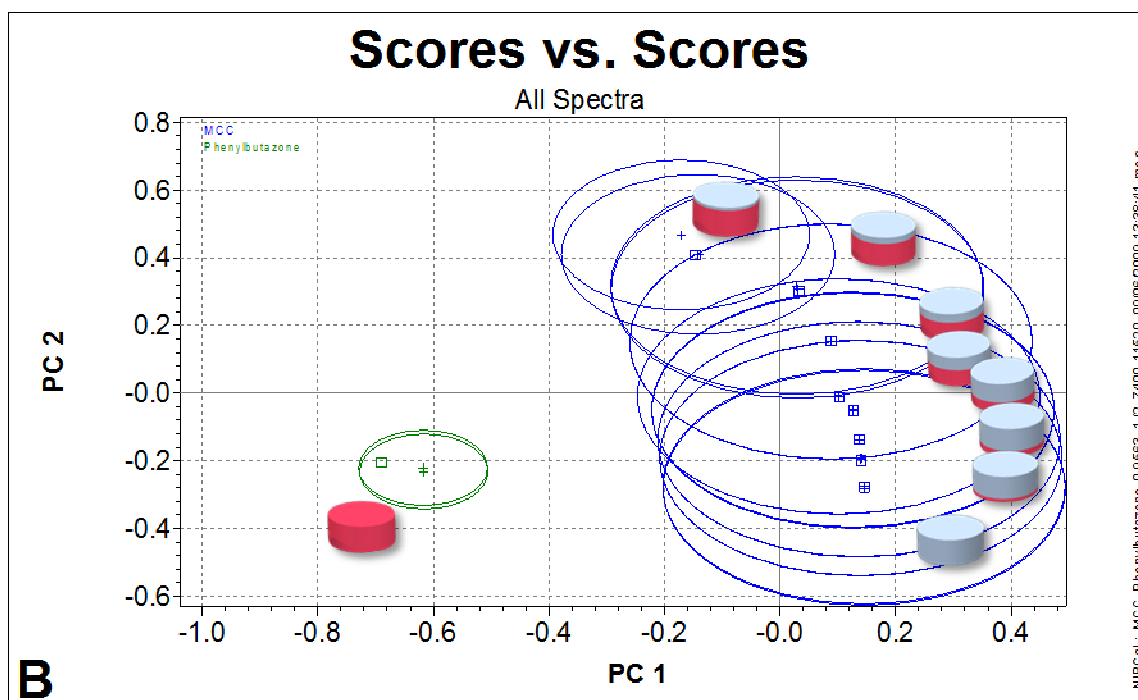
Figure 39: Cluster analysis of double-layer tablets in DT mode. All of the double-layer tablets labelled as MCC (upper layer) were grouped with the MCC-only tablet, with scores gradually moving to the PBZ cluster as its layer gets bigger

9.1.5.3 *Incremental tablet coating*

The coating process for both tablet batches (MCC and caffeine tablets) produced uniform incremental coatings, as shown from the thickness and mass-gain data (Table 8). Another crucial fact was to have comparable coating thickness mean at each coating step for both batches (Figure 31), otherwise data analysis and interpretation would be very difficult. The maximum coat thickness possibly was 0.35 – 0.37 mm, beyond that the coats were pitted and cracking and therefore useless.

Table 8: Incremental coating details, showing mass and thickness increasing with coating (average of 10 tablets). Coat thickness from one side was calculated by dividing thickness gain by 2.

	Coat level	0	1	2	3	4	5	6
MCC tablets	mass [mg]	100.57	104.97	110.10	116.20	120.54	126.93	133.34
	Mass SD	1.03	1.05	1.29	1.03	1.90	1.86	2.03
	Mass gain [mg]	0.00	4.40	9.53	15.63	19.97	26.36	32.77
	Thickness [mm]	3.169	3.258	3.393	3.504	3.612	3.756	3.879
	Thickness SD	0.022	0.027	0.037	0.040	0.043	0.051	0.037
	Coat thickness [mm]	0.000	0.045	0.112	0.168	0.222	0.294	0.355
caffeine tablets	mass [mg]	100.65	105.06	109.53	116.00	122.18	128.48	135.32
	Mass SD	2.04	1.16	0.78	1.12	0.88	1.79	1.76
	Mass gain [mg]	0.00	4.41	8.88	15.35	21.53	27.83	34.67
	Thickness [mm]	3.141	3.222	3.355	3.487	3.623	3.725	3.880
	Thickness SD	0.023	0.027	0.017	0.026	0.032	0.046	0.041
	Coat thickness [mm]	0.000	0.041	0.107	0.173	0.241	0.292	0.370

Figure 40 (lower part) shows the DR spectra of both batches. The MCC tablets (blue) and caffeine tablets (green) spectra have different spectral features (example $6000 - 7000$ cm^{-1} shown in the zoomed pane) that are evident for uncoated tablets, and start to decrease gradually with incremental coatings of both batches until both MCC and caffeine spectra are indistinguishable, an indication that the spectrum carried information from the coat only. DT scans of these tablets show a different picture (Figure 31, upper part). Here, spectral features for both MCC and caffeine batches were preserved in all coating steps, because the radiation was always probing the tablet core, even at exaggerated film coat thickness.
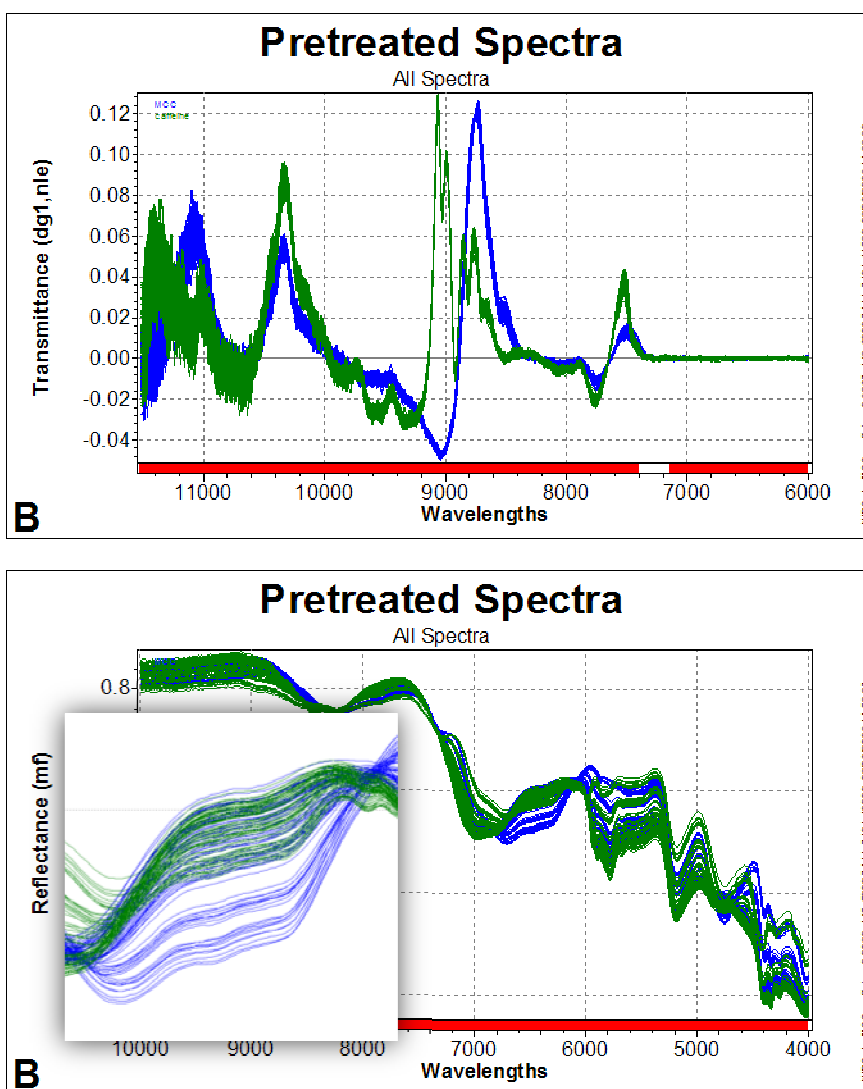
Figure 40: Pretreated spectra of MCC and caffeine incrementally coated tablets in DT (above) and DR (below) modes, with the area between 6000-7000 cm^{-1} zoomed.

Cluster analysis of these spectra was also performed, and PC plots are shown in Figure 41 (upper part DT and lower part DR spectra). In DR mode, it was not possible to classify all the MCC and caffeine spectra separately with any number of PCs, because there are spectra with indistinguishable features (hence coat information only). In DT, all the spectra from each batch (MCC and caffeine) were clearly separable with only one PC.
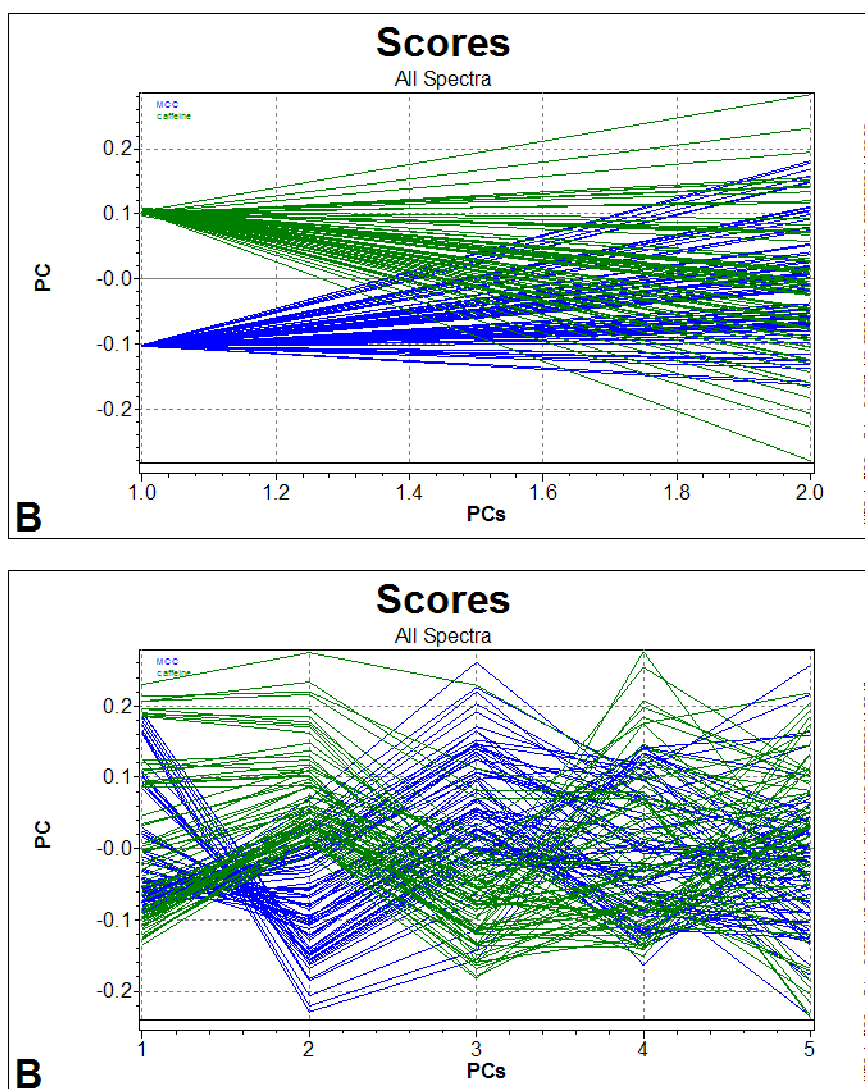
Figure 41: Cluster analysis of coated tablets in DT (above) and DR (below) modes, showing scores vs. PCs plots. Calibration and validation spectra are identified by pluses and squares, respectively.

In Figure 42, the cluster analysis results are very striking when "scores versus scores" plot is viewed. In DT, all spectra are grouped separately with one PC, while in DR, the spectra are only well separated in the uncoated and thin coated batches, and move closer together until inseparable at the 4th and 5th coating levels. This clearly suggests that the DR information depth and radiation penetration should be less than the maximum coat thickness reached (0.37 mm).
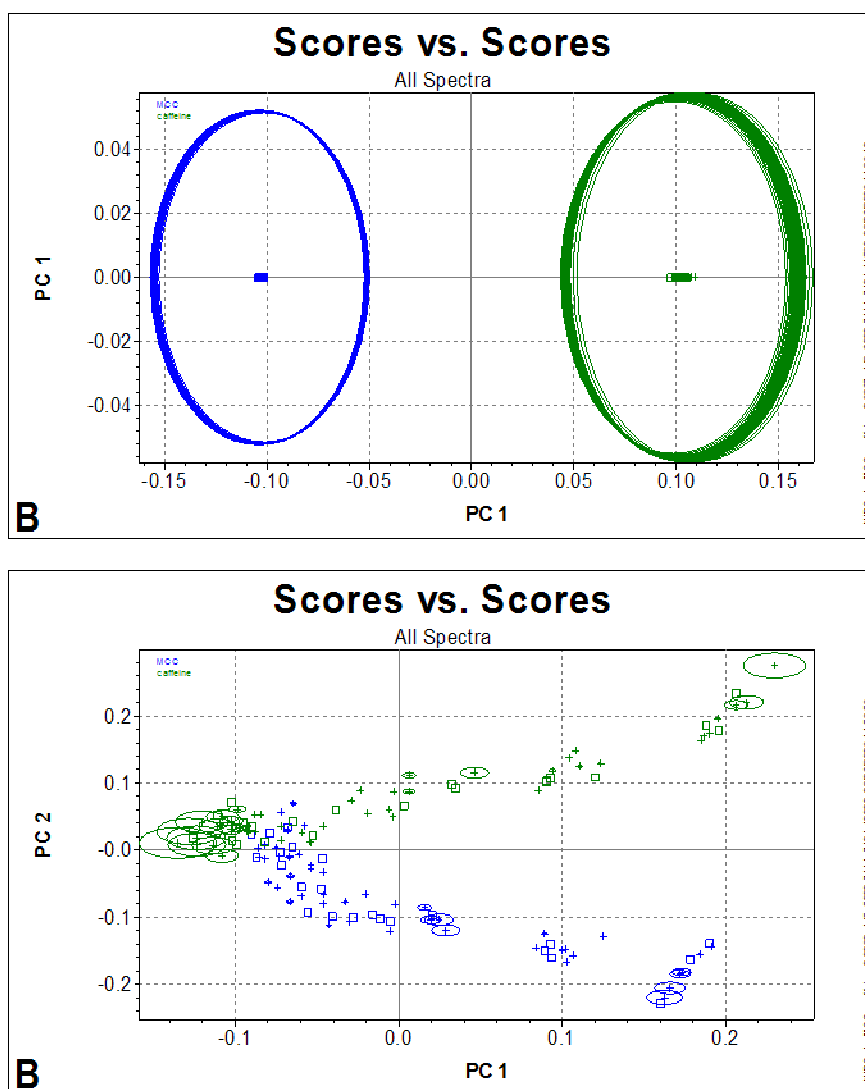
Figure 42: Cluster analysis of coated tablets in DT (above) and DR (below) modes, showing scores vs. scores plots. Calibration and validation spectra are identified by pluses and squares, respectively.

From the DR spectra analysed above, different spectral regions can from both MCC and caffeine batches can be plotted together against coat thickness (Figure 43). These plots showed how the spectral differences decreased gradually between the two batches. These differences can be expressed in terms of percentage from the maximum spectral difference in the uncoated tablets (100% difference = 100% information between MCC and caffeine DR spectra). This is shown in Figure 44 which also show an exponential drop in spectra differentiation (= DR spectral information) with coat thickness and a very high correlation coefficient ($r^2 > 0.99$).
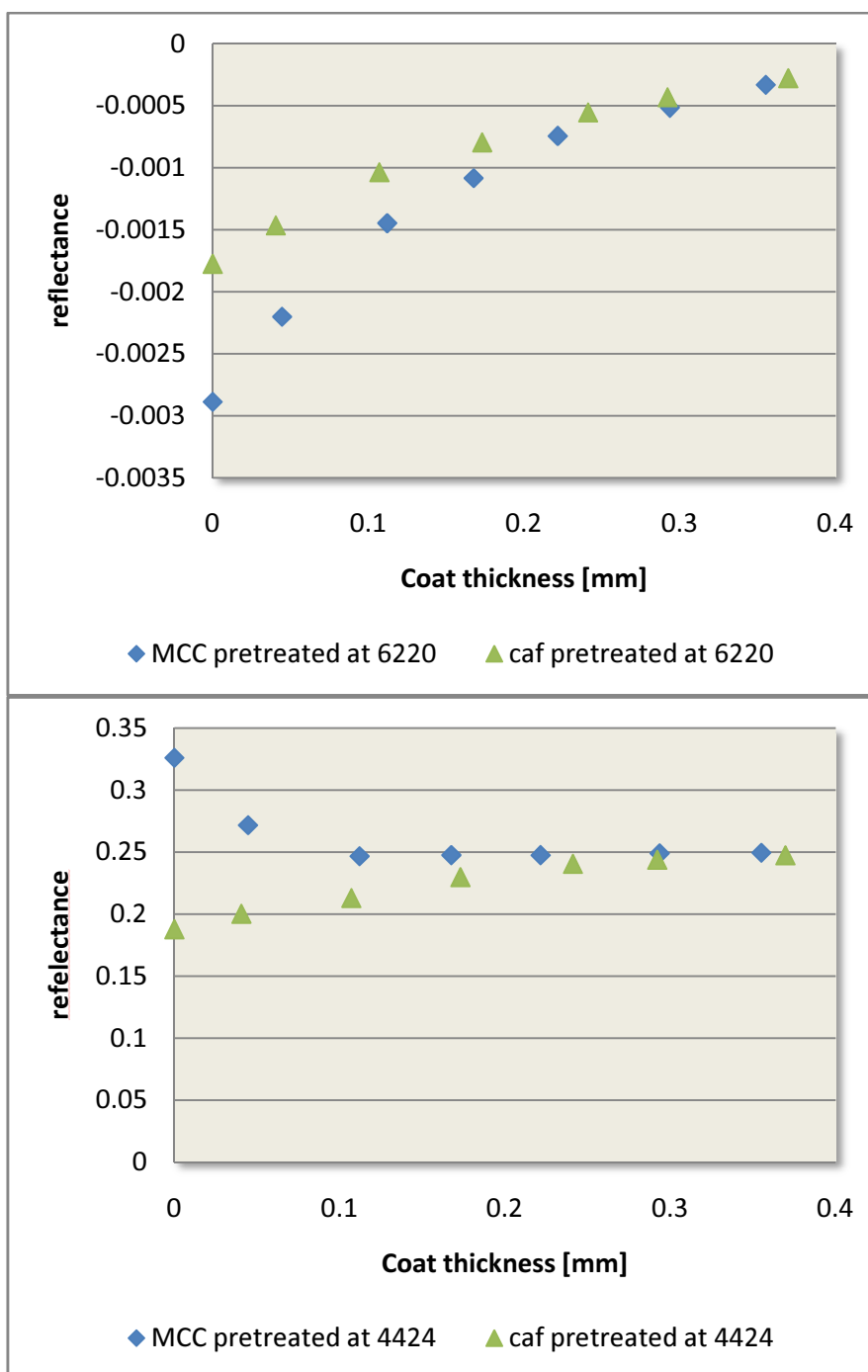
Figure 43: DR values of both MCC and caffeine tablets against coat thickness, at 6220 cm^{-1} and db1 pretreatment (above); and 4420 cm^{-1} and mf pretreatment (below)

The drop reached 50% at 0.05 – 0.07 mm depending on the wavenumber (Figure 44 and Figure 45). The 90% signal drop (10% information content) can be seen between 0.2 – 0.25 mm without extrapolation, while the 99% drop is a bit further at 0.3 – 0.4 mm (extrapolated and higher SD).

mf at 4420-4428 cm^{-1}

y = 89.198e$^{-11.51x}$
R^2 = 0.9923

db1 (smoothed) at 6220 cm^{-1}

y = 98.227e$^{-8.231x}$
R^2 = 0.9921
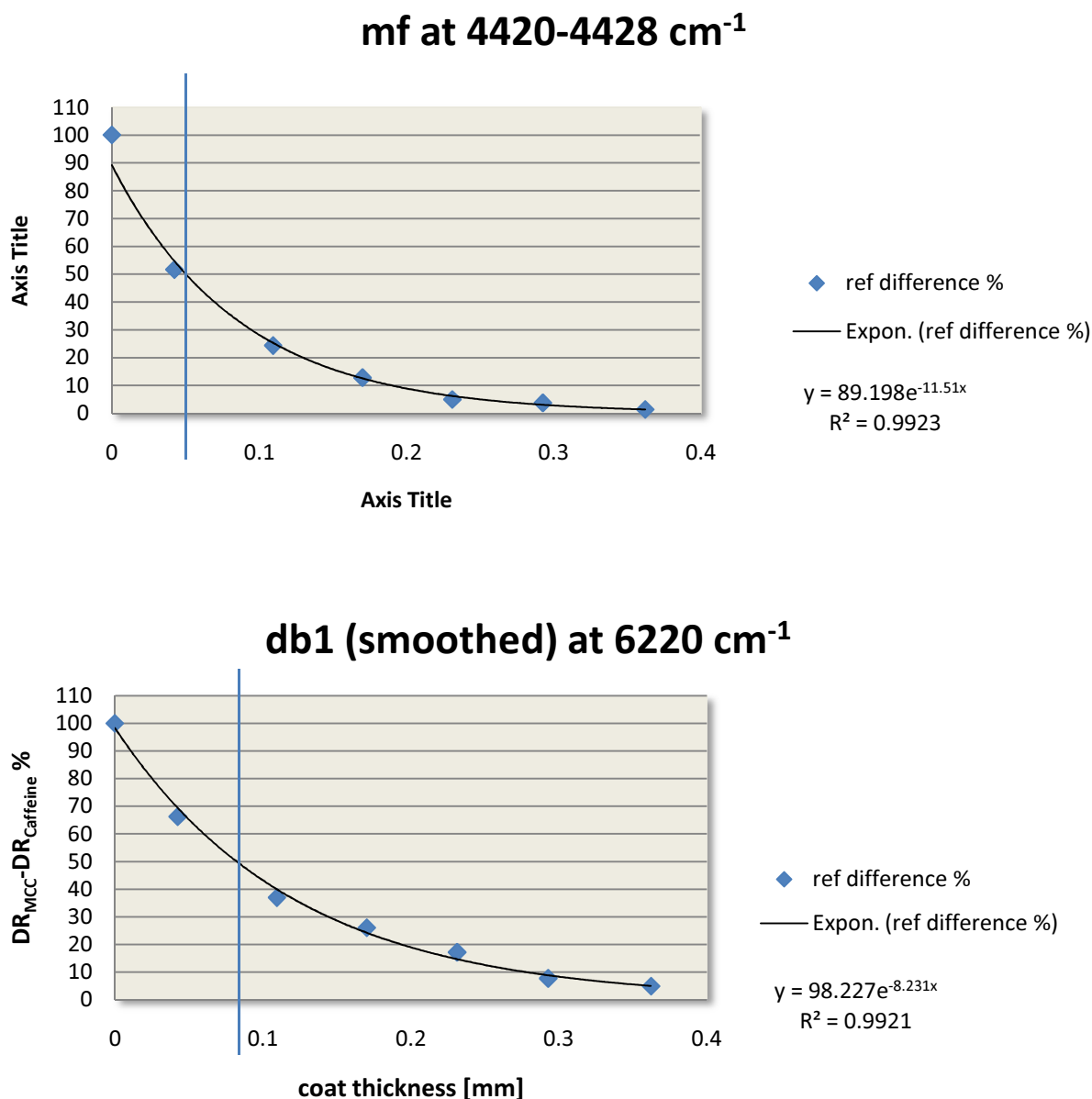
Figure 44: Plot of DR spectral difference between MCC and caffeine tablets against coat thickness. The difference was taken as percentage of the maximum difference at coat level 0 (uncoated tablets). Two different spectral positions and pretreatments are shown.

As shown, this signal drop depth decreased with decreasing wavenumbers (increasing wavelength). Figure 46 show a 3.5 mm-thick tablet model with the DR information percentage from the experimental exponential fit represented converted to red colour values, fading gradually with increasing penetration depth. This illustrated clearly how small the DR sampling span is for typical pharmaceutical tablets, taking into account that not the entire lower surface area is scanned, but only a central area (no determined yet) that depends on the instrument setup and the sampling slit.
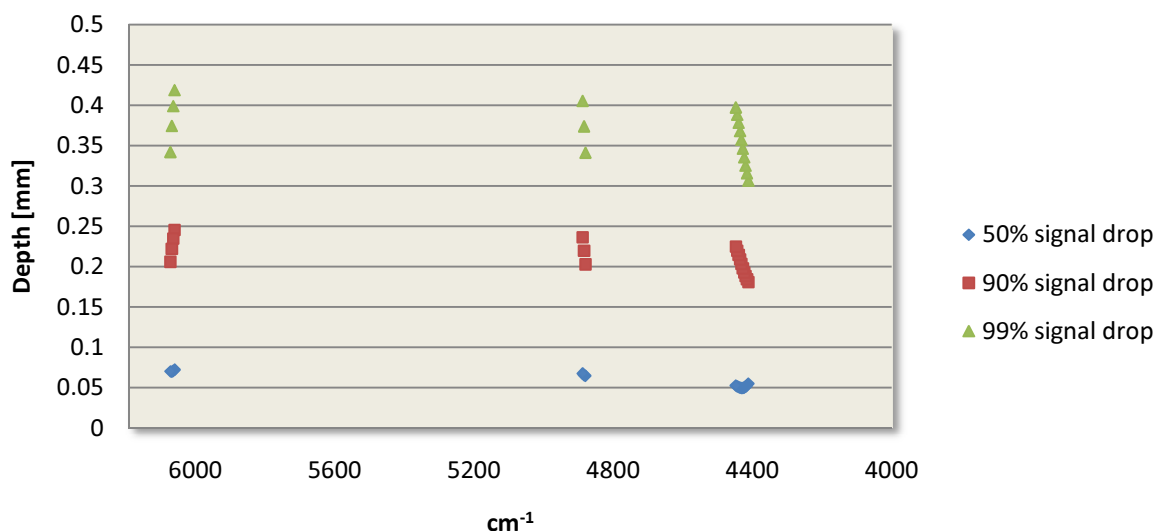
Figure 45: DR Signal drop at various NIR wavelengths based on the coating experiment and mf pretreatment. Only data with $R^2>0.99$ are shown

9.1.6   Conclusion

The evidence collected to determine DR information depth was three-fold. Incremental tablet thickness showed no constant relationship to spectra and indicated that this depth was less than 0.5 mm. The double-layered tablets confirmed this assumption through cluster analysis and finally, incremental coatings of tablets with different cores permitted the estimation of pattern and extent of the DR information drop across sample depth.

The radiation in DR mode was found to be decaying exponentially after penetrating the tablet's surface; hence no single depth can be defined as a margin for the sampled mass. Instead, the percentage of spectral information representing a certain tablet depth can be expressed. 50% of the spectral information represented 0.05 – 0.07 mm, and 90% of the spectrum represented no more than 0.2 - 0.25 mm of the tablet. This means that NIR in DR mode is really a surface-effect phenomenon, and content predictions using this mode are only possible when the tablet surface contain accurate proportional representation of all the tablet contents, hence more potential for errors.

The other aspect is its applicability to coated tablets. Most film-coated tablets are manufactured with coat thickness of 10 – 100 μm; hence DR mode is in effect capable of probing the core and predicting content. In thicker coats, however, DR mode core quantification would not be that successful and DT mode in such cases is more suitable (e.g. thin layer coating – 0.2-1.0 mm and sugar coating – few millimetres). On the other

hand, DR mode would be the ideal tool to study surface qualities, most importantly film-coat thickness, homogeneity and quality.
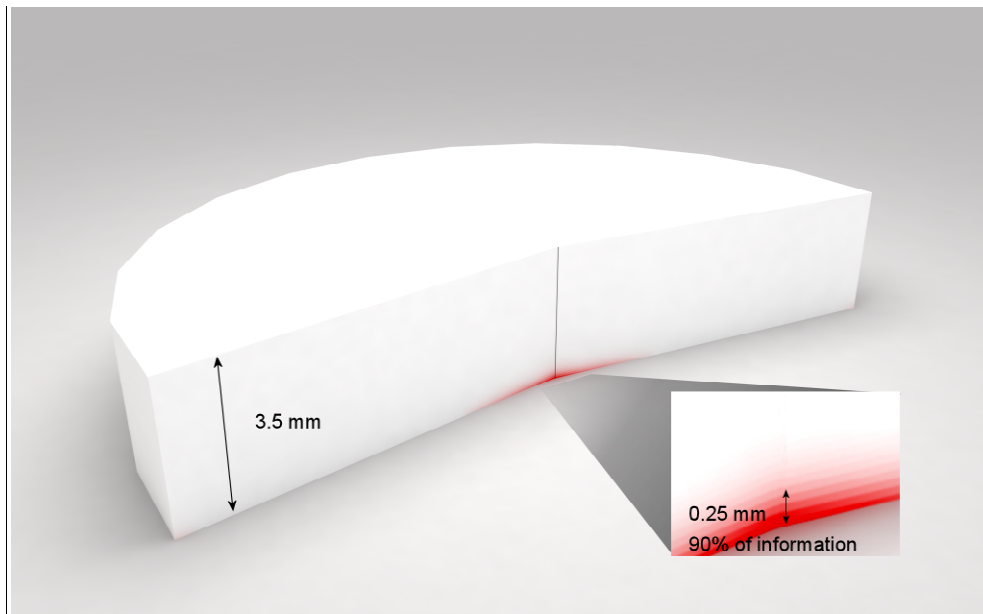

Figure 46: DR information depth for a typical pharmaceutical tablet, based on the exponential fitting in Figure 44 (lower plot). The 90% of information from 0.25 mm estimate was based on area under curve calculation.

10. Research conclusions and prospective

Throughout this research, different aspects of NIR spectroscopy for pharmaceutical tablets were assessed. These aspects are of prime practical importance to using the method in various applications, especially content determination.

DT measurement mode was found able to perform well with quantification applications tablets, even for low-dose tablets. Such applications have the potential of completely replacing wet-chemistry assays and offer tremendous time, cost and even environmental savings.

A crucial issue in such applications was seen to be method development and validation, which in some cases not a trivial matter, especially when the method was to be tested over extended production time-lines and potentially varying process conditions in response to varying starting materials.

This leads to the second issue in method development, which is robustness, and a wait-and-see approach to collect and include predictions outliers over time in hope of a robust model would not constitute a system that fits any PAT definition. Instead, all the parameters that have the potential of variability which would critically affect the method should be identified, studied and included in the model from the outset.

Tableting press variability was seen to present potential problems for NIR methods. The radiation in DT mode traverses the entire thickness of the tablet, and hence is more liable for any variation that affects the internal structure, geometry, percentage and distribution of the voids within the tablet, hence porosity and tablet thickness variability was found to contribute significantly to prediction error or most importantly prediction failure and outliers. Pretreatments can minimise such effects but never completely remove them, and at a higher variability scale can introduce more errors. The best solution is a model with all possible variability sources included at their full possible scale (or even bigger scale).

Another issue in DT mode is that the radiation interaction with compacted particulate solids remains little understood to date, and attempts to describe the spectral relationship to sample properties mathematically is as important as the development of high precision instruments. The experiments conducted studied the effects of tablets

12.2.2   NIRFlex N-500

This is an FT NIR spectrometer from Büchi Labortechnik AG (Flawil, Switzerland). It is a quartz polarization interferometer consisting of two crystal wedges which splits 45° polarized light into two vectors, which traverse the crystal at different phase velocities. By moving one wedge relative to the other, the vectors undergo a systematically varied phase shift relative to each other. This changes the polarization of the combined beam. For monochromatic light, this results in a sinusoidal variation of the radiation after the second polarizer, while for polychromatic light an interferogram is formed.

The spectrometer also has various gray filters and a wavelength standard, enabling wavelength accuracy, signal-to-noise ratio, and linearity to be checked in a series of tests (System Suitability Test - SST) to ensure validation of the spectrometer before any measurement session, including qualification and performance verification requirements of pharmacopoeial chapters "1119" (USP) and 2.2.40 (EP) on Near-Infrared. The SST produces automatic validation reports and complies with 21 CFR Part 11.

Dimensions housing (W x H x D)	350 x 250 x 450 mm
Spectral range	800–2500 nm (recommended 1000–2500 nm)
	12500–4000 cm^{-1} (recommended 10000–4000 cm^{-1})
	(if not specified differently for measuring cell)
Resolution	8 cm^{-1} (with boxcar apodization)
Type of interferometer	Polarisation interferometer with TeO_2 wedges
Wavenumber accuracy	± 0.2 cm^{-1} (measured with HF gascell at an ambient temperature of 25 °C ± 5 °C)
Signal-to-noise ratio	10000 (peak-to-peak noise)
Number of scans/sec.	2–4
Analog digital converter	24 bit
Ambient temperature	5–35 °C (25 ± 5 °C recommended)
Type of lamp/lifetime lamp (MTBF)	Tungsten halogen lamp / 12000 h (2x 6000 h)
Type of laser	12 VDC HeNe, wavelength at 632.992 nm
Ethernet connection	100 Mbit/s
Electric power supply	100–230 VAC ± 10%, 50/60 Hz, 350 W

Figure 58: NIRFlex N-500 specifications

12.2.2.1 NIRFlex Solids Transmittance

NIRFlex is a modular spectrometer enabling the use of different modules depending on the application. The "Solids Transmittance" module is optimized to perform transmission measurements of solid dosage forms, like tablets or capsules, using custom-made sample plates which are also designed and coated to prevent stray light.

Detector	InGaAs (temperature controlled)
Spectral range	12 500–6000 cm⁻¹
	(recommended range 11 520–6000 cm⁻¹)
	800–1660 nm (recommended range 870–1660 nm)
Photometric dynamic range	0–6 AU
Photometric linearity	The "addition of filter technique" has been used.
	A 2% transmission filter and a wavelength standard (Rare Earth Oxide mixture) were used for the addition. Both filters were measured individually and together in series. The addition of the individual measurements has been compared with the measurement of both filters ihn series. The difference was < 2x 10⁻⁷ T at 7876 cm⁻¹
Typical signal-to-noise ratio	Rms for spectral segments of 300 cm⁻¹ in the range of 11 000–6500 cm⁻¹
– open beam	Mean 2x 10⁻⁵ AU (16 scans; Blackman apodization)
– 5 mm Spectralon®	Mean 10x 10⁻⁵ AU (64 scans; Blackman apodization)
Electric power supply	100–230 VAC +/– 10%, 50/60 Hz, 20 W

Figure 59: Specifications of NIRFlex Solids Transmittance module

12.2.3 Other apparatus

12.2.3.1 *UV spectrophotometer*

- Beckman - Du ® Series 500, instrument type UV-DU 530, series N° U 300 2050, (Beckman, Germany)

12.2.3.2 *Turbula mixer*

- Turbula, type T2A (Wily A Bachofen AG, Switzerland)

12.2.3.3 *Pycnometer*

- AccuPyc1330 (Micromeritics, Norcross, GA)
- helium gas at room temperature

12.2.3.4 *Digital callipers*

12.2.3.5 *Electron microscope*

- Philips XL30 ESEM (Philips, Eindhoven, Netherlands)

12.2.3.6 *Disintegration tester*

- DT2, Sotax, Switzerland

12.2.3.7 *Infrared balance*

- Mettler Toledo Type LP 16M (Mettler instruments, Switzerland)

12.2.3.8 *Scales*

- Delta Range®, instrument type AX204, (Mettler Toledo, Switzerland)

12.3 Methods

12.3.1 Powder characterisation

12.3.1.1 Residual moisture content

USP30-NF25, 731: Loss on drying

The residual moisture of a powder mixture is calculated from the moisture content of its components, equation (0.28), where w_{tot} is the water content of the compound, a_i is the fraction of the component in % (m/m) and w_i is the residual moisture of the mixture in % (m/m).

$$w_{tot} = \sum_{i=1}^{n} \frac{a_i \cdot w_i}{100} = \frac{a_1 \cdot w_1 + a_2 \cdot w_2 + ... + a_n \cdot w_n}{100} \tag{0.28}$$

Moisture content was determined using the loss on drying method with an infrared balance Mettler Toledo Type LP 16M (Mettler instruments, Switzerland) and standard USP methods. Samples of 1.0-1.5 g were heated for 15 min at 105°C and the mass loss was reported in percent to sampled mass.

12.3.1.2 Bulk and tapped density

USP30-NF25: Bulk and tapped density (method I)

A comparison of the bulk and tapped densities can be often used as an index of the ability of the powder to flow. The bulk density often is the bulk density of the powder "as poured" or as passively filled into a measuring vessel. The tapped density is a limiting density attained after tapping down, usually in a device that lifts and drops a volumetric measuring cylinder containing the powder a fixed distance.

1. A quantity of material sufficient to complete the test was passed through a 1.00-mm (No. 18) screen to break up agglomerates .
2. Approximately 100 g (M) of powder was introduced in a dry 250-mL cylinder, without compacting.
3. The powder was levelled carefully without compacting and read the apparent volume, V_0 to the nearest graduated unit.
4. Bulk density, in g per cm^3, was calculated by the formula: (M) / (V_0).
5. The cylinder was mechanically tapped (STAV 2003, J. Engelsmann AG) 500 times initially and the tapped volume V_a was measured.

6. Tapping was repeated an additional 750 times the tapped volume, V_b, was measured.

7. When the difference between the two volumes was < 2%, V_b was taken as the final tapped volume, V_f, otherwise tapping was repeated in increments of 1250 taps until the difference between succeeding measurements was < 2%.

8. The tapped density, in g per mL, was calculated by the formula: $(M) / (V_f)$.

12.3.1.3 *Compressibility and Hausner factor*

The Compressibility Index, equation (0.29), and Hausner factor (or ratio), equation (0.30), are measures of the degree to which a powder can be compressed. As such, they are measures of the relative importance of inter-particulate interactions.

In a free-flowing powder, such interactions are generally less significant, and the bulk and tapped densities will be closer in value.

For poorer flowing materials, there are frequently greater inter-particle interactions, and a greater difference between the bulk and tapped densities will be observed. These differences are reflected in the Compressibility Index and the Hausner factor.

$$\text{Compressibility index} = 100 \cdot \frac{V_0 - V_f}{V_0} \qquad (0.29)$$

$$\text{Hausner Factor} = \frac{V_f}{V_0} \qquad (0.30)$$

12.3.1.4 *Particle Size Measurement*

A laser scattering particle sizer (MasterSizer X Long Bed, Malvern Instruments, UK) was used to determine the particle size distribution, employing an MSX64 – Manual Dry Powder Feeder (Malvern Instruments, UK) to apply a dry analysis method. Data analysis of the results and the apparatus system were operated using MasterSizer X version 2.19 software (Malvern Instruments, UK).

12.3.1.5 *True density*

The true density powders and powder mixtures were measured with a helium pycnometer (AccuPyc 1330, Micromeritics, Norcross, GA) at room temperature. Air was extracted to generate a vacuum and then Helium was pumped-in 5 times until equilibrium was reached.

12.3.1.6 *Scanning Electron Microscopy (SEM)*

Images were taken using a Philips XL30 ESEM (Philips, Eindhoven, Netherlands) electron microscope. Powder samples were mounted on aluminium stubs and sputtered with Platinum coating of 20nm.

12.3.2   Low-dose folic acid tablets

12.3.2.1 *Formulation*

- A directly compactable folic acid tablet formulation was devised using MCC 102 as filler, Ac Di Sol as disintegrant and magnesium stearate as lubricant (Gohel 2005).
- Tablet weight was 200 mg.
- The nominal dose of folic acid was 5 mg per tablet (2.5%)
- NIR calibration batches had folic acid content varying from 0 to 5%. Other components were kept constant and the filler was adjusted to accommodate the change.
- Of each concentration step (batch), 20 tablets where compacted to make a total of 220 calibration and validation samples.
- The formulations of the 11 folic acid batches in the API range of 0 to 5% are summarized in Table 9.

Table 9: Formulation of folic acid tablets (calibration and validation batches)

Folic acid % m/m	MCC % m/m	Ac-Di-Sol % m/m	Mg-stearate % m/m
0.0	93.75	6.0	0.25
0.5	93.25	6.0	0.25
1.0	92.75	6.0	0.25
1.5	92.25	6.0	0.25
2.0	91.75	6.0	0.25
2.5	91.25	6.0	0.25
3.0	90.75	6.0	0.25
3.5	90.25	6.0	0.25
4.0	89.75	6.0	0.25
4.5	89.25	6.0	0.25
5.0	88.75	6.0	0.25

12.3.2.2 *Powder preparation and mixing*

- Foe each batch, the powdered components were screened through a 90 μm mesh before weighing on Mettler Toledo scales - Delta Range ®, instrument type AX204, series N° 1121140335, Switzerland).

- Powder mixtures ware transferred to 100 mL amber glass bottles
- Mixing was made using a Turbula blender (type T2A, Wily A Bachofen AG, Switzerland).
- Folic acid was pre-mixed with MCC for 5 minutes.
- The remaining excipients, except of magnesium stearate, were added and lot mixed for 5 minutes.
- Magnesium stearate was finally added and the mixture was blended for another 2 minutes.

12.3.2.3 *Powder compaction*

The tableting process was controlled using the Presster™ (MCC, NJ, USA) with software version 3.8.4.

- Korsch rotary press PH336 was selected for simulation.
- The default press speed (10800 TPH) and dwell time (118.3 msec) were used.
- A flat face punch with a diameter of 10.0 mm was used for compaction.
- Gap vs. thickness and gap vs. hardness plots for 200 mg tablet mixtures was performed (*see* Appendix I.1-2, Figure 60 and Figure 61)
  - The gap size was decreased gradually from 2.7 mm until satisfactory tablet crushing strength was reached.
  - Tablet thickness and crushing strength was measured with each adjustment step.
- A crushing strength around 104 N, a thickness around 2.41 mm and an upper compaction around 3.9 kN were achieved with a gap size of 1.8 mm.
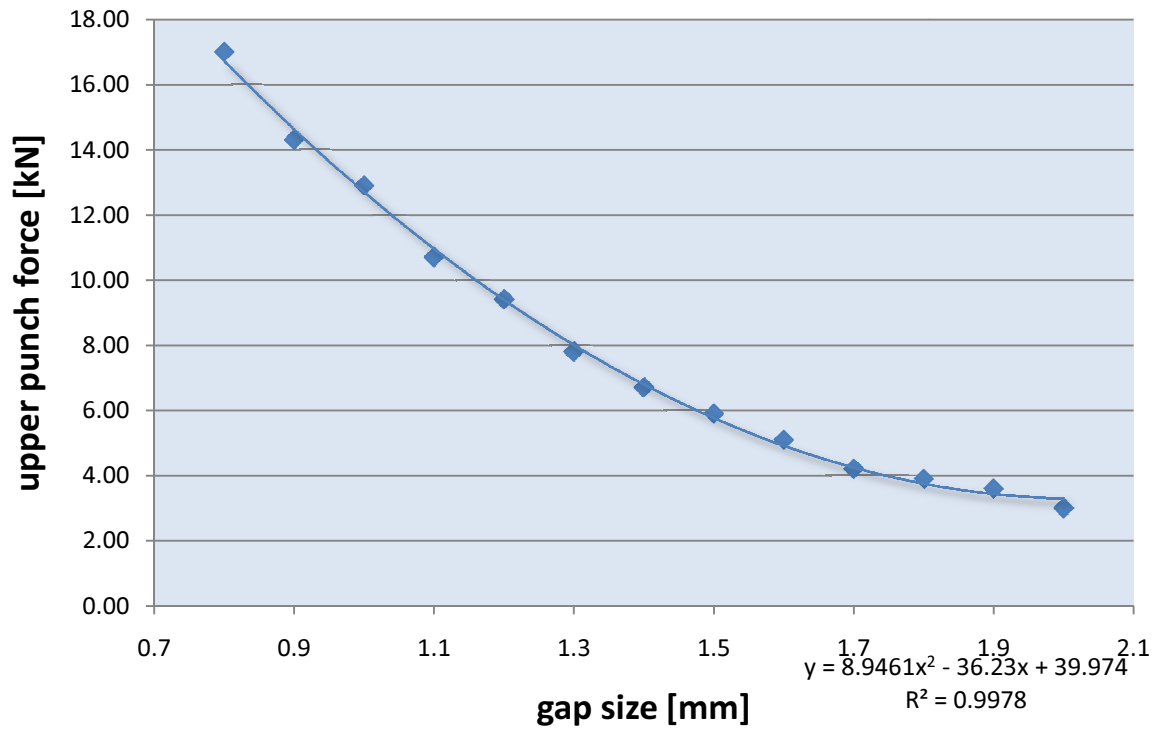
Figure 60: Presster plot: gap size vs. upper punch force for 200 mg tablets
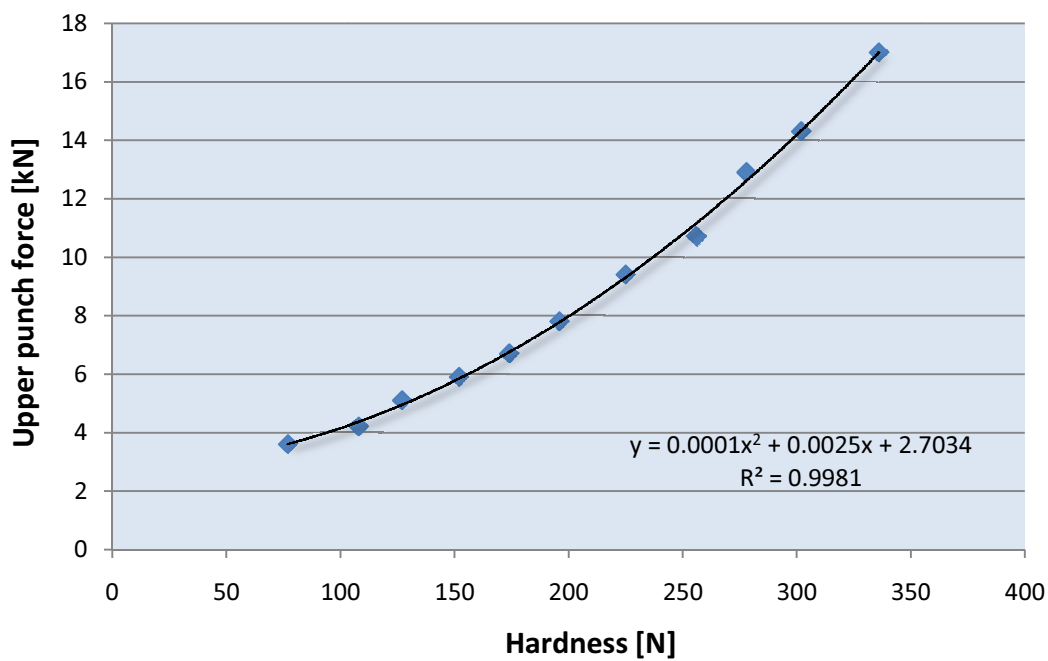

Figure 61: Hardness vs. upper punch force

12.3.2.4 *Tablet production*

- Powder mixture mass for each tablet (around 208 mg to accommodate for loss during compaction) was weighted manually for each tablet by using an analytical balance.
- The powder mixture was filled carefully inside the press well.
- "One tablet" was ordered from Presster software
- 24 hours after the compaction of the tablet the thickness was measured by a digital calliper and the tablet mass was measured by an analytical balance. (*see* Appendix IV.3)
- The tablets were put in tablet holders and were provided with batch and tablet number and stored protected from light inside a box.
- Two batches of the 2.5% tablets were manufactured. One set was referenced by the UV analytical method before light exposure and the other set of ten 2.5% tablets after light exposure.
- To exclude the effect of light exposure on predictions, ten 2.5% tablets were used as light exposure control and were exposed to light whenever any batch was handled to record the NIR spectra for the development of the calibration model.

12.3.3   Tablet characterisation

12.3.3.1 *Resistance to crushing (hardness')*

Ph. Eur. 5, method 2.9.8: Resistance to Crushing of Tablets

Crushing strength is a measure of the load where the tablet breaks under diametrical compaction between two flat platens.

Tablets crushing strength was measured after 24 hours using an automated tablet hardness tester Dr. Schleuniger® (Tablet Tester 8M, Pharmatron, Switzerland).

12.3.3.2 *Tensile strength*

Tensile strength is a fundamental measurement of the resistance to fracture. Crushing strength can be converted into tensile strength (σ in [N/cm^2]) using equation (0.31).

$$\sigma = \frac{2 \cdot S_c}{\pi \cdot D \cdot T} \tag{0.31}$$

where

S_c	=	crushing strength in N
D	=	tablet diameter in cm
T	=	tablet thickness in cm

However, this equation is only applicable to round flat-faced tablets when they fail in tension by splitting cleanly into halves under diametric compaction.

12.3.3.3 *Porosity*

The porosity of the tablets was calculated from equation (0.32).

$$\varepsilon = \left(1 - \frac{M}{V} \cdot \frac{1}{\rho}\right) \times 100 \qquad (0.32)$$

where

ε	=	porosity in % (v/v)
M	=	tablet mass in g
V	=	tablet volume in cm^3
ρ	=	true density of the powder mixture in g cm^{-3}

12.3.3.4 *Disintegration time*

USP30 NF25, 701: Disintegration

Disintegration time of three tablets was measured using a disintegration tester (DT2, Sotax, Switzerland) with a disk. The disintegration medium consisted of distilled water maintained at 37°C $\pm$ 0.5.

12.3.3.5 *Scanning Electron Microscopy (SEM)*

Refer to "Scanning Electron Microscopy (SEM)" page 165.

12.3.4   NIR quantitative model development

12.3.4.1 *NIR spectral collection*

- Tablets from all batches were scanned on NIRFlex N-500 spectrometer using the solids transmittance mode and adjustable plate using default instrument settings.
- The spectra were labelled so as to identify each spectrum to its tablet.
- Two quantitative properties were created (folic acid nominal and UV) and added to the spectral set.
- Nominal content of each tablet was referenced for each spectrum in the nominal property field.

12.3.4.2 *UV assay standardisation*

- 0.1 M NaOH (molar mass = 40 g/mol) was used as a solvent for folic acid in the UV assay.
- 4 grams of NaOH were dissolved in 1 L distilled water to produce NaOH 0.1 M solution.
- For added accuracy, the UV calibration curve was constructed from tablet mixtures with standard folic acid concentration rather than from folic acid alone.
- 10 mg of every 200 mg powder mixture with folic acid in an API range of 0 to 5% was dissolved in 10 ml NaOH 0.1M of a test tube.
- A 1ml syringe with a filter attachment was used to take some of the solution out of the test tube after dissolution of folic acid into a 1 cm quartz glass cuvette of 1 cm.
- UV absorbance at 235 nm was measured and NaOH 0.1M stock solution as blank.
- The powder mixtures of all 11 batches were used to create a linear calibration line with the UV spectrophotometer with a zero intercept. (*see* Appendix IV.4-5)
- To get an estimation of the assay SD, 10 absorption measurements of the 1% powder mixture had been taken to calculate the average and the standard deviation of the content.

12.3.4.3 *UV Content determination (spectral referencing)*

- Each tablet was weighed, crushed and homogenised using a pestle and mortar.
- 10 mg was sampled and dissolved, similar to the above method and UV absorbance taken and content per tablet calculated in mg using:

$$API_{tablet} = Slope_{calib} \times UV_{abs} \times 100 \times \frac{mass_{tablet}}{10mg}$$

- shows the referenced data for all tablets
- API reference value (in mg per tablet) for each tablet was added in the "folic acid UV" property field of its respective NIR spectrum in the database.

12.3.4.4 *NIR Calibration model development*

- A new project was created in NIRCal and tablet spectra imported from the database

- One third of the spectra set to validation (except 0% and 5% batches), the rest set to calibration spectra

- One property was selected for the model (first nominal folic acid and then UV reference)

- Both manual (Figure 62) and automatic (Q value wizard) were tried to search for best model optimisation.

- Models were evaluated using
    - Q-value: as close to 1 as possible
    - SEP: as low as possible
    - consistency: as close to 100 as possible
    - bias: as low as possible
    - regression coefficient and slope: as close to 0.999 as possible
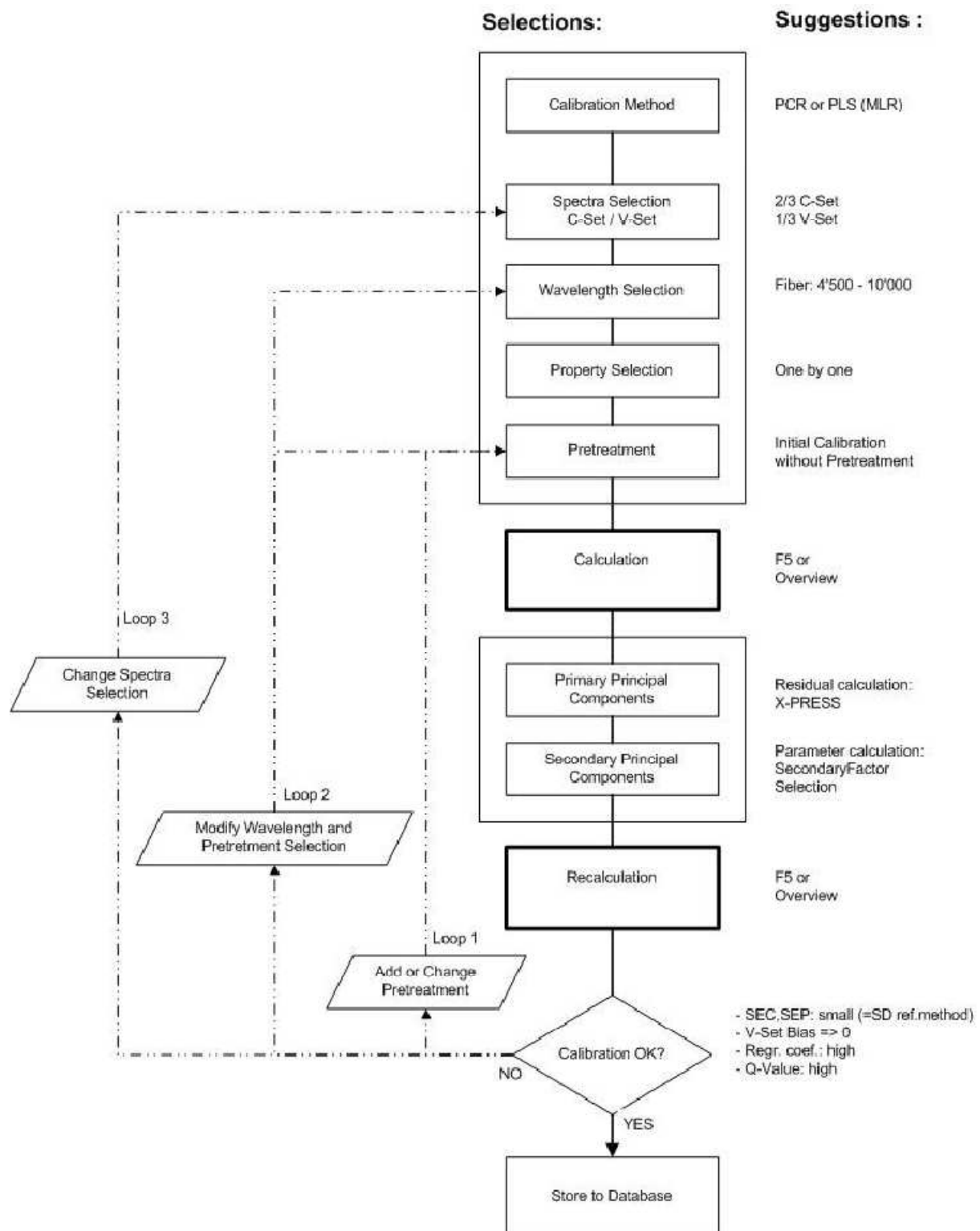
Figure 62: Suggested calibration model flow-chart (NIRCal 5.2 user manual)

12.3.4.5 *External prediction*

- The selected optimal calibration models were used to predict the content of 2.5% folic acid tablets which were not used for developing the calibration model.

- The spectra of the 2.5% folic acid tablets were recorded and the API content of these tablets was predicted.
- To evaluate the calibration model the predicted values were compared with the values obtained in the UV reference method.
- An independent t-test for the significance of the difference between the means of two samples, was applied to assess a possible significant difference between the NIR and the UV reference method:
    - H_0: there is no significant difference between the UV assay results and NIR predictions of folic acid content in tablets
      against
    - H_1: there is a significant difference
    - *Rejecting H_0 indicates that the differences between UV and NIR are significant and not due to chance only.*
    - *H_0 can be rejected with 95% confidence if P<0.05*

12.3.5   Press effect on NIRS predictions

12.3.5.1 *Porosity and thickness outliers (i)*
* The same folic acid tablet formulation was used (Table 9, page 165)
* For each batch (0%-5% API), the same method for making the fixed porosity tablets was repeated, except the following:
    * Presster gap size set for 1.0 mm
    * 2 tablets made
    * Gap increased by 0.1 mm
    * 2 more tablets and gap increments until gap size of 1.9 mm was reached and 20 tablets were made
* Tablets were weighed, stored, thickness measured after 24h, and UV referenced (Appendix V.1).

12.3.5.2 *Porosity and thickness outlier external prediction (ii)*
* An 2.5% API external prediction batch (20 tablets) was also manufactured with the same gap range as above (Appendix V.2)

12.3.5.3 *Tableting speed (possible) outliers (iii)*
* 15 2.5% API folic acid tablets (Table 9, page 165) were manufactured in Presster:
    * 1.8 mm gap size
    * Tableting speed range from 15,000 – 135,000 TPH (85.2-9.5 ms dwell time)
* Tablets were weighed, stored, thickness measured after 24h, and UV referenced

12.3.5.4 *Testing model robustness*
* 5 different NIR calibration models (F1-F5) developed using previous folic acid calibration spectra.
* Batches from items (ii) and (iii) above where predicted using these models and predictions compared to their UV assay content.
* A further model (FV) constructed by adding spectra of variable compaction force (item i above) and prediction batch (item ii above) was predicted and evaluated.

12.3.5.5 *Effect of tablet porosity and thickness change on spectra*
* 2 sets of placebo tablets (formulation Table 9, page 165) manufactured on Presster:
    * Varying porosity and constant thickness, mass-adjusted tablets (Table 3, P1-3)

- o Varying thickness and constant porosity, mass adjusted tablets (Table 3, T1-6)
- Tablets were scanned on NIRFlex N-500 solids transmittance and maximum at 8880 cm^{-1} plotted against thickness and porosity

12.4 Results

12.4.1 Characterisation

12.4.1.1 *Loss on drying*

Table 10: water content in excipients

excipient	water content in % [m/m]
Ac-Di-Sol®	7.3
MCC	4.2
Mg-stearate	3.9

- The theoretical residual moisture was 4.39%
- Powder mixture loss on drying for all mixtures was 4.45 ($\pm$0.08) %

12.4.1.2 *Bulk and tapped density, Hausner factor*

- Bulk and tapped volumes are listed in Appendix I.6
- Hausner Factor of 2.5 powder mix = 1.1951

12.4.1.3 *Particle Size Measurement*

- 90% of the MCC 102 particles were $\leq$ 111.12 µm
- 90% of the Ac-Di-Sol® particles were $\leq$ 78.0 µm
- 90% of the folic acid particles were $\leq$ 62.5 µm
- 90% of the Magnesium Stearate particles were $\leq$ 25.4 µm

12.4.1.4 *True density*

- Average true density was 1.544 ($\pm$0.0046) g cm^{-3} for 5 runs

Table 11: True density of 2.5% powder mixture

run	density [g cm^{-3}]
1	1.540
2	1.551
3	1.546
4	1.541
5	1.543

12.4.1.5 *Scanning Electron Microscopy (SEM)*

- The SEM images of excipients are shown in the methods section (pages 152-158)

- The SEM images of the 2.5% powder mixture is shown in SEM of 2.5% powder mixture (Figure 63)
- The SEM images of a 2.5% API tablet surface is shown Figure 64
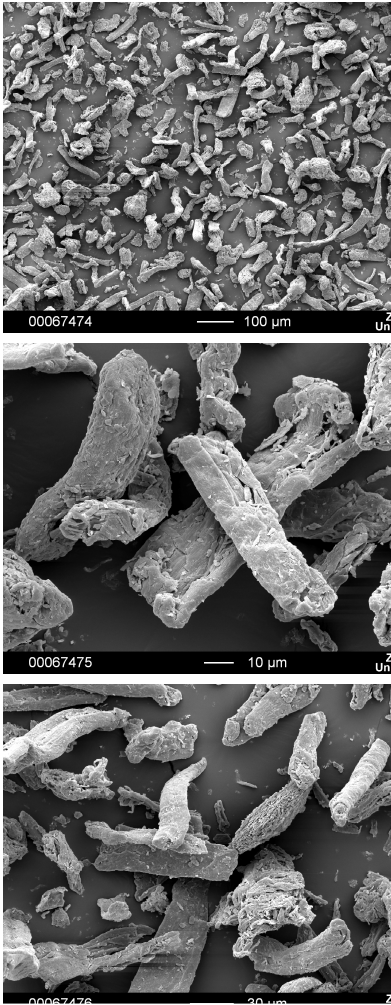

Figure 63: SEM of 2.5% powder mixture
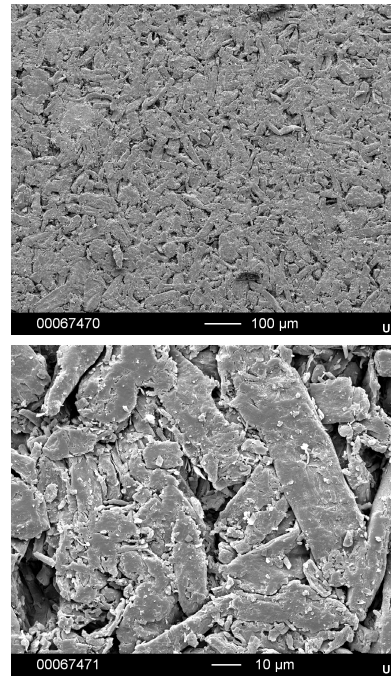
Figure 64: SEM of 2.5% tablet surface

12.4.1.6 *Tablets physical parameters*

Description

- The tablets had a flat smooth surface, sharp edges and colour varying from white to faint yellow to yellow, increasing with the API content (Figure 65).
- No signs of capping or lamination were observed on any of the tablets.

Figure 65: 1 tablet of each of the 11 batches of folic acid tablets, from 0% (far left) to 5% (far right) API

Thickness and crushing strength

- The diameter, the thickness and the crushing strength was measured for 2.5% (m/m) folic acid tablets.

Table 12: Tablet thickness and crushing strength for 2.5% batch

tablet	diameter [mm]	thickness [cm]	crushing strength [N]
1	10.00	2.39	95
2	10.00	2.38	94
3	10.00	2.39	96
4	10.00	2.40	98
5	10.00	2.39	95
6	10.00	2.38	94
Average (SD)	**10.00 (0)**	**2.39 (0.007)**	**95.33 (1.52)**

Tensile strength:

- $$\sigma = \frac{2 \cdot S_c}{\pi \cdot D \cdot T} = \frac{2 \cdot 95.33N}{\pi \cdot 1cm \cdot 0.239cm} = 253.93 \frac{N}{cm^2} = 253.93 \text{ N cm}^{-1}$$

Porosity

- $$\varepsilon = \left(1 - \frac{M}{V} \cdot \frac{1}{p}\right) \times 100 = \left(1 - \frac{0.2g}{0.187cm^3} \cdot \frac{1}{1.544g/cm^3}\right) \times 100 = 30.73\%$$

Disintegration time

- The tablets disintegrated within 34.5 ($\pm$2.3) seconds

12.4.2   First calibration models

12.4.2.1 *SD of UV method*

- The average of the content was 2.2089 mg and the standard deviation of the content was 0.1133 mg. The recorded absorption values and the calculated content of folic acid are shown below (Table 13).

Table 13: UV standard deviation for a 10 mg 1% API powder mixture

UV A	UV content [mg]
0.243	2.3729
0.211	2.0604
0.229	2.2362
0.213	2.0800
0.230	2.2460
0.223	2.1776
0.223	2.1776
0.237	2.3143
0.240	2.3436
0.213	2.0800
mean	2.2089
SD	0.1133

12.4.2.2 *Calibration models*

- Calibration project is shown in Figure 67, using nominal content as calibration property. Spectra showed no visible peak changes with folic acid concentration, except scaling. Figure 66 show the spectra of MCC and folic acid and gives an idea why there is no obvious peak shifts with the API change.
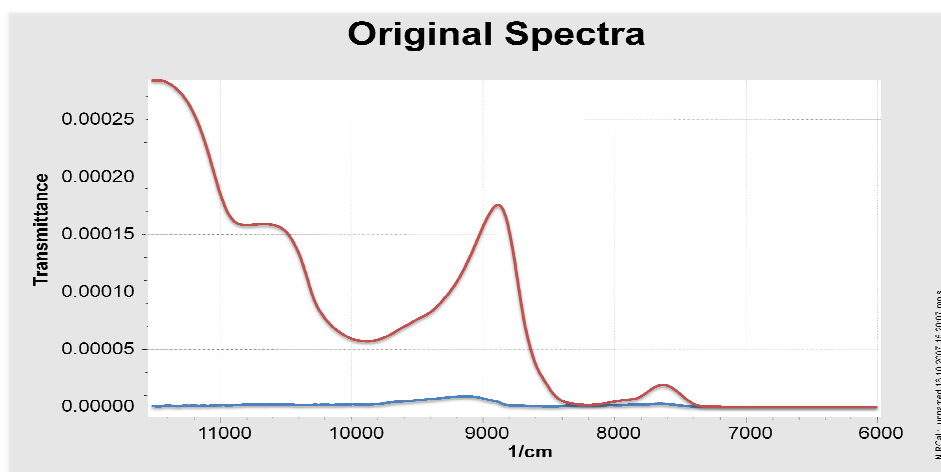
Figure 66: NIR spectra of a 100% filler (MCC) tablet (red), and 100% API (folic acid) tablet (blue)

- Leverage plot showed 2 potential outliers (Figure 67).

- Applying normalisation, first derivative and 1 PC selection improved the model (consistency) and leverage showed 1 outlier (Figure 68).

- Figure 69 show the model (A1) with UV reference data used as calibration property, with still 2 prediction outliers.

- Two more calibration models developed, A2 (Figure 70 and Figure 71) and A3 (Figure 72 and Figure 73) employing different pretreatments, wavelength selection and wavelength regions.

- First derivative reveal 2 small peak changes at 8500 and 8800 cm-1 (Figure 70).

- NIRCal data (Table 16) show that A1 is the best model (lowest SEP, highest r^2, best consistency). The software's Q-value agreed with this evaluation and was a good total evaluation tool. (Full calibration protocols in appendices I.7,8,9)
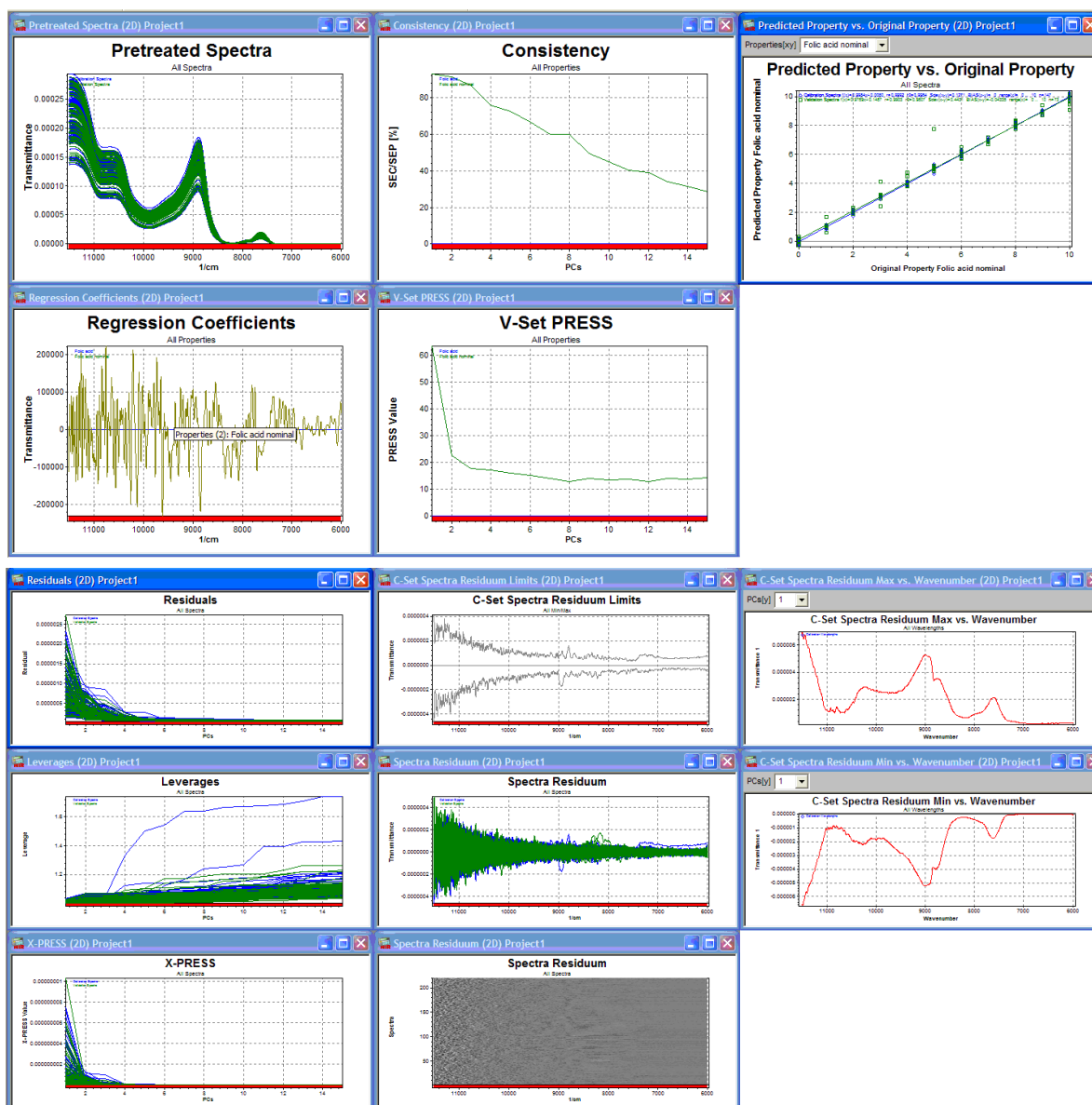
Figure 67: A new NIRCal project with folic acid spectra (before optimization)
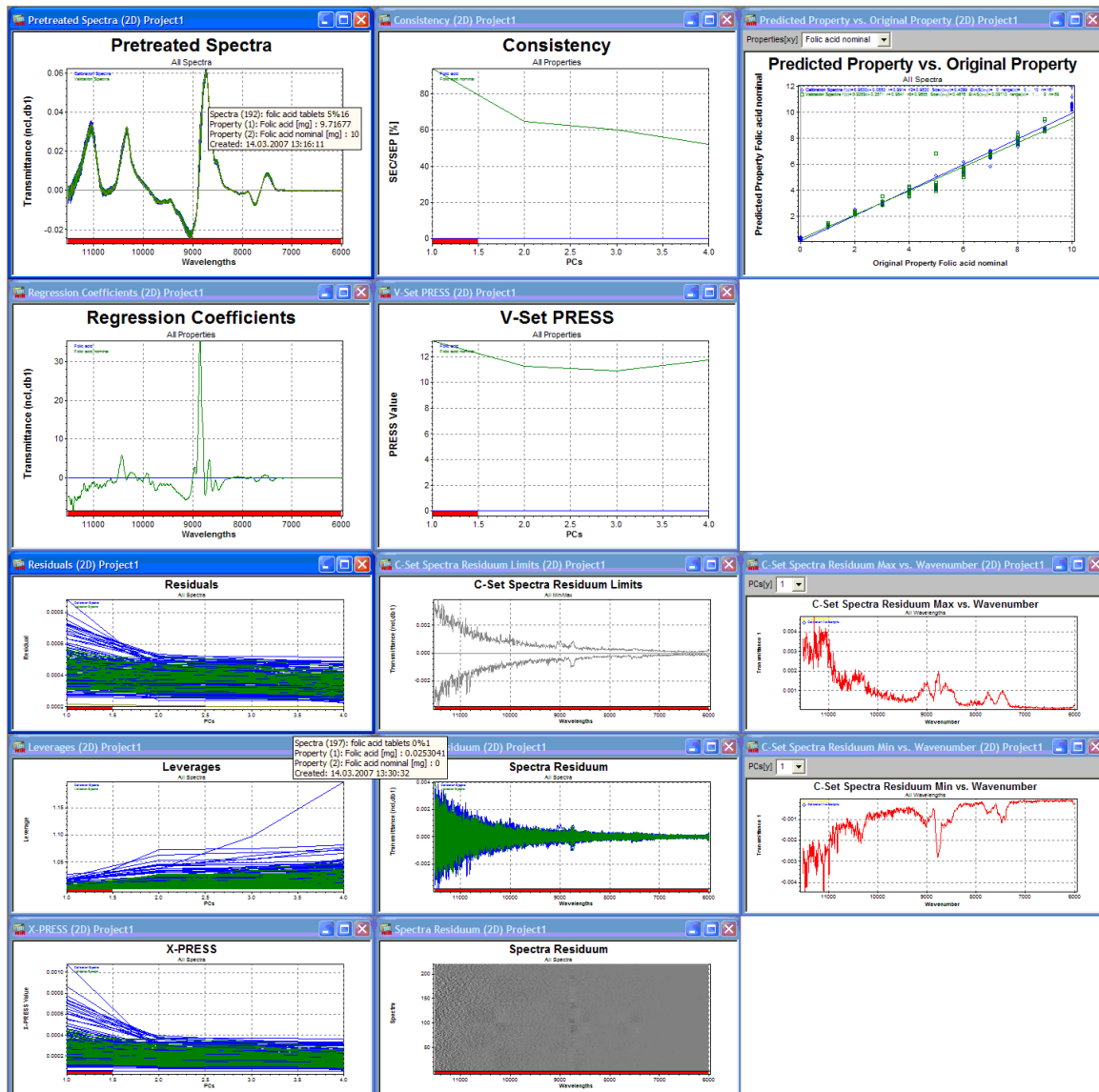
Figure 68: Applying ncl and db1 pretreatments and fact selection (1 PC)
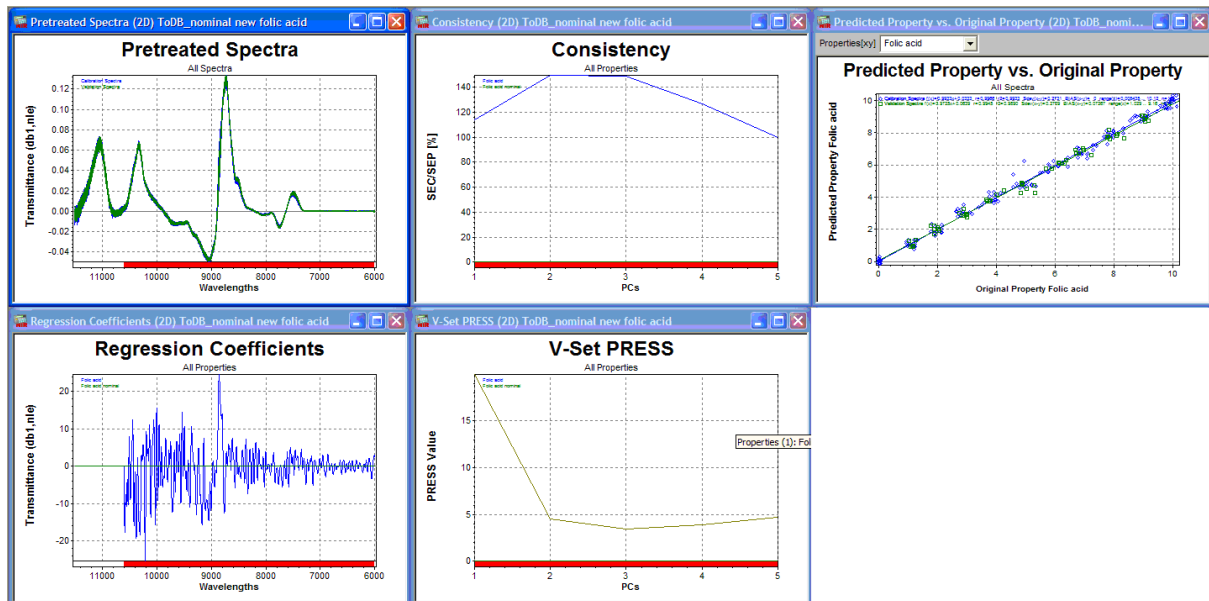
Figure 69: Calibration model (A1) applying db1 and nle pretreatments and 5 PCs
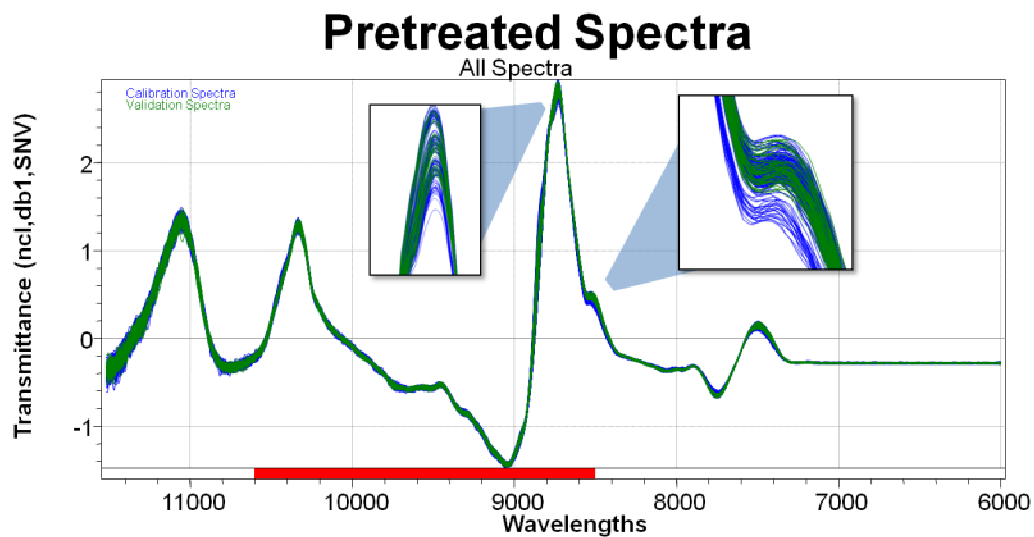
Figure 70: Calibration model (A2) applying ncl, db1 and SNV pretreatments and 4 PCs
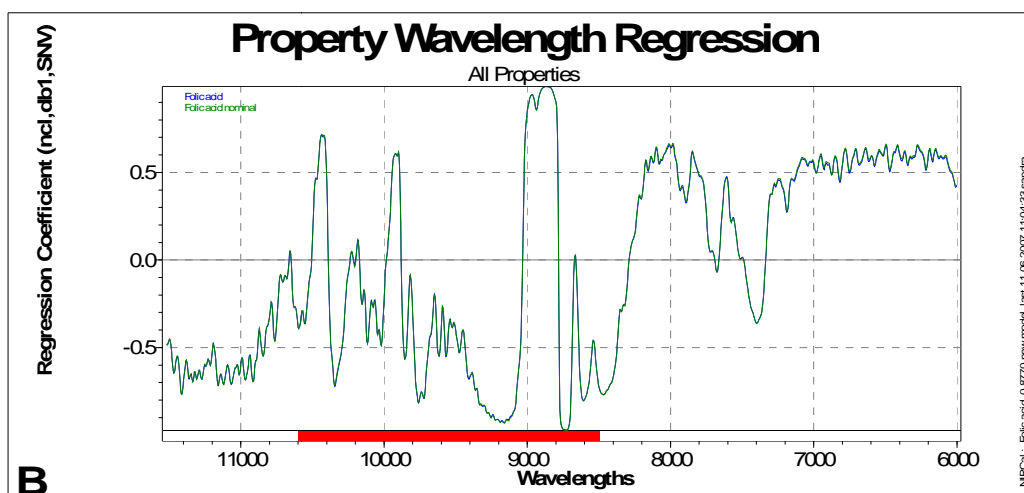
Figure 71: Calibration model (A2) wavelength regression
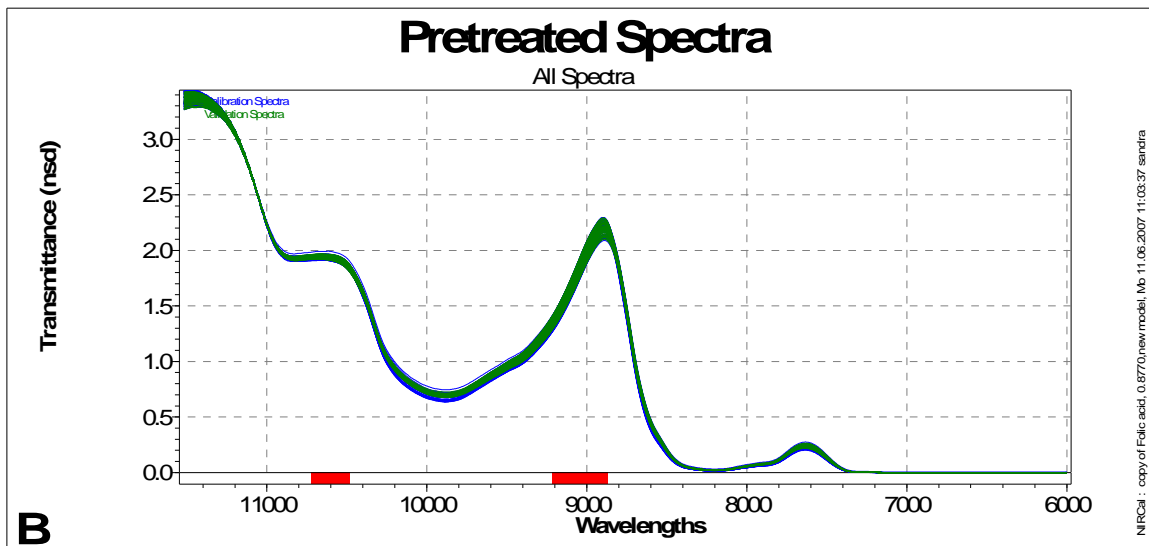
Figure 72: Calibration model (A3) applying nsd pretreatment, 8 PCs and tight wavelength selection
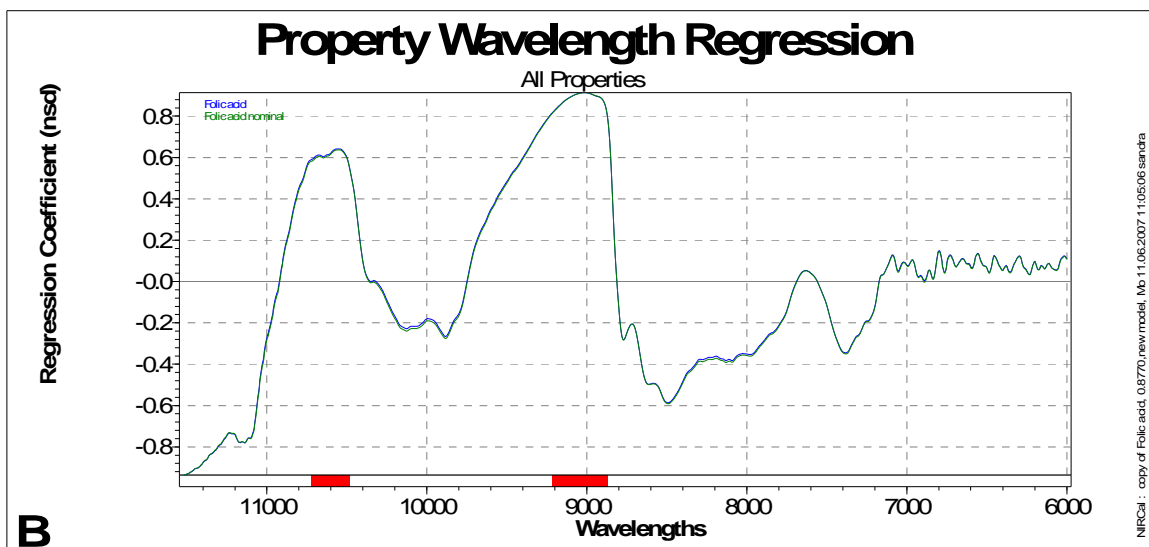
Figure 73: Calibration model (A3) wavelength regression

- NIR SEP (0.2731 mg) should be evaluated in terms of the UV own SE (SD=0.1133 mg), 2.4 times larger.
- SEP should also be evaluated in terms of the target content evaluated (5 mg folic acid per 2.5% tablet) and relative NIR SEP was 5.462%.
- External prediction by the three models is shown in Figure 74.. Tablets 1,2,8,15 and 19 show relatively big differences from UV method.
- A two-tailed student t-test show that all three models are statistically different from the UV method, with A1 being the best model (Table 17).

- Light effect (Table 18) was small and the average drop in folic acid content was 0.0733 mg over the whole process (tablet analytics, referencing and NIR scanning). This should be much less if the referencing step was omitted (after complete NIR method development).
- If the referencing method was HPLC, this light effect is expected to be much higher due to longer analysis time and NIR prediction would have had more benefit.

Table 14: External prediction set tablets (mass and UV content)

tablet number	mass [mg]	UV A 1	UV A 2	UV A 3	UV A 4	UV A 5	UV A average	UV content [mg]
1	205.50	0.697	0.697	0.698	0.698	0.698	0.698	6.045
2	200.40	0.749	0.751	0.751	0.750	0.750	0.750	6.340
3	198.40	0.577	0.577	0.577	0.577	0.578	0.577	4.829
4	204.10	0.543	0.543	0.543	0.543	0.544	0.543	4.675
5	200.30	0.609	0.609	0.609	0.609	0.609	0.609	5.144
6	202.40	0.651	0.651	0.651	0.650	0.650	0.651	5.553
7	202.00	0.580	0.581	0.581	0.582	0.582	0.581	4.951
8	205.40	0.720	0.720	0.720	0.720	0.719	0.720	6.235
9	199.40	0.627	0.627	0.627	0.627	0.628	0.627	5.274
10	202.80	0.573	0.573	0.573	0.573	0.572	0.573	4.899
11	203.50	0.594	0.594	0.594	0.594	0.594	0.594	5.097
12	198.00	0.576	0.577	0.577	0.578	0.578	0.577	4.819
13	204.20	0.566	0.564	0.565	0.567	0.565	0.565	4.869
14	200.90	0.608	0.607	0.607	0.607	0.607	0.607	5.144
15	204.40	0.688	0.689	0.689	0.689	0.689	0.689	5.937
16	201.50	0.589	0.589	0.589	0.588	0.588	0.589	5.001
17	200.40	0.633	0.635	0.635	0.635	0.635	0.635	5.363
18	204.00	0.617	0.617	0.619	0.619	0.619	0.618	5.318
19	203.90	0.551	0.551	0.551	0.550	0.550	0.551	4.734
20	204.40	0.657	0.659	0.659	0.658	0.658	0.658	5.673

Table 15: UV content and NIR external prediction from 3 calibration models

tablet number	mass [mg]	UV [mg]	NIR A1 [mg]	NIR A2 [mg]	NIR A3 [mg]	Residuals		
						A1	A2	A3
1	205.5	6.045	4.953	4.562	4.678	0.000450	0.019094	0.000569
2	200.4	6.340	5.079	4.795	4.984	0.000492	0.018114	0.000624
3	198.4	4.829	5.000	4.773	5.091	0.000484	0.017422	0.000666
4	204.1	4.675	5.269	4.686	5.421	0.000548	0.020807	0.000776
5	200.3	5.144	5.009	4.626	5.241	0.000416	0.016324	0.000592
6	202.4	5.553	5.359	4.890	5.306	0.000538	0.019485	0.000986
7	202.0	4.951	5.236	4.794	5.450	0.000449	0.018312	0.000498
8	205.4	6.235	5.391	4.984	4.716	0.000444	0.017114	0.000754
9	199.4	5.274	4.589	4.367	4.700	0.000454	0.017491	0.00057
10	202.8	4.899	5.088	4.733	5.318	0.000433	0.016305	0.000516
11	203.5	5.097	5.013	4.694	4.748	0.000412	0.016304	0.000601
12	198.0	4.819	4.865	4.589	5.110	0.000442	0.017455	0.000625
13	204.2	4.869	5.153	4.718	4.999	0.000440	0.017268	0.000449
14	200.9	5.144	4.753	4.598	4.560	0.000433	0.016335	0.000634
15	204.4	5.937	4.885	4.561	4.676	0.000406	0.016557	0.000631
16	201.5	5.001	4.919	4.666	4.749	0.000439	0.016356	0.000463
17	200.4	5.363	4.880	4.529	4.428	0.000416	0.016017	0.000406
18	204.0	5.318	5.111	4.677	4.716	0.000488	0.019164	0.000615
19	203.9	4.734	5.079	4.732	4.506	0.000403	0.016390	0.000446
20	204.4	5.673	4.815	4.539	4.574	0.000501	0.018945	0.000616
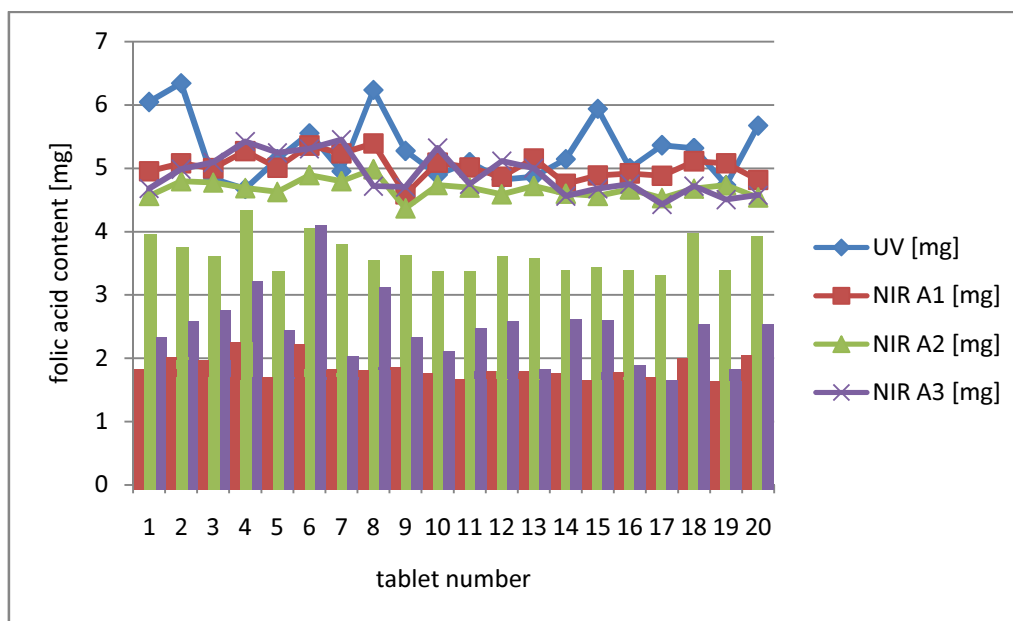
Figure 74: Folic acid content in external prediction set, UV assay vs. three NIR models. Bars indicate residuals of respective model, with A2 residuals (green) scaled down 20 times for clarity.

Table 16: Overview of the 3 NIR calibration models

calibration model	A1	A2	A3
method	PLS	PLS	PLS
pretreatments	db1,nle	ncl,db1, SNV	nsd
wavelength selection [cm^{-1}]	6000-10600	8500-10600	8876-9216, 10488-10724
PCs	5	4	8
Q-value	0.8782	0.877	0.862
SEC [mg]	0.2731	0.2958	0.3365
SEP [mg]	0.2739	0.291	0.3385
consistency	99.72	101.67	99.4
V-set Bias [mg]	0.0727	0.0208	0.0277
V-set regression coefficient	0.9945	0.9936	0.9913

Table 17: Statistical evaluation of the 3 NIR models

	UV	NIR A1	NIR A2	NIR A3
Mean	5.289471	5.022145	4.675565	4.89848
Variance	0.263305	0.04077	0.019195	0.104224
Observations	20	20	20	20
Hypothesized Mean Difference		0	0	0
df		25	22	32
t Stat		2.16803	5.16544	2.884266
P(T<=t) one-tail		0.019939	1.77E-05	0.003482
t Critical one-tail		1.708141	1.717144	1.693889
P(T<=t) two-tail		0.039878	3.53E-05	0.006963
t Critical two-tail		2.059539	2.073873	2.036933

Table 18: Possible light effect on predictions during whole experiment

tablet number	Without light exposure			With light exposure		
	tablet mass [mg]	thickness [mm]	UV content [mg]	tablet mass [mg]	thickness [mm]	UV content [mg]
1	0.2005	2.41	5.0777	0.2003	2.39	4.8500
2	0.1995	2.37	4.9596	0.2004	2.39	5.0693
3	0.2008	2.39	5.0524	0.2008	2.40	4.7825
4	0.2009	2.40	5.0861	0.2005	2.40	5.0440
5	0.2004	2.40	5.1199	0.2009	2.41	4.8415
6	0.2006	2.39	5.0271	0.2008	2.39	5.1199
7	0.2004	2.38	4.9596	0.2008	2.39	5.0271
8	0.2009	2.39	5.0355	0.2008	2.39	5.0440
9	0.2002	2.38	4.8668	0.2004	2.38	4.7825
10	0.2009	2.39	4.9933	0.2009	2.39	4.8837
Average (SD)	0.2005 (0.0004332)	2.39 (0.01155)	5.0178 (0.07487)	0.2007 (0.0002319)	2.39 (0.008233)	4.9445 (0.1285)

12.4.3   Tablet press effect

- As the upper punch compaction force increased, the tablets became thinner and denser (less porous). They also became slightly darker in colour (Figure 76).

- In terms of NIR, transmittance spectra showed upward scaling with increased compaction force. One factor is reduced scattering and more light reaching the detector. This can also be considered reduction in apparent absorption (Figure 75).

- Although pretreatments are considered as a tool to reduce baseline and scale effects on spectra, this was not the case for such a wide change in compaction differences, as shown in Figure 79. No single pretreatment was able to group the spectra because scaling was not only higher with higher frequency (in transmittance), but also absorption dependant.
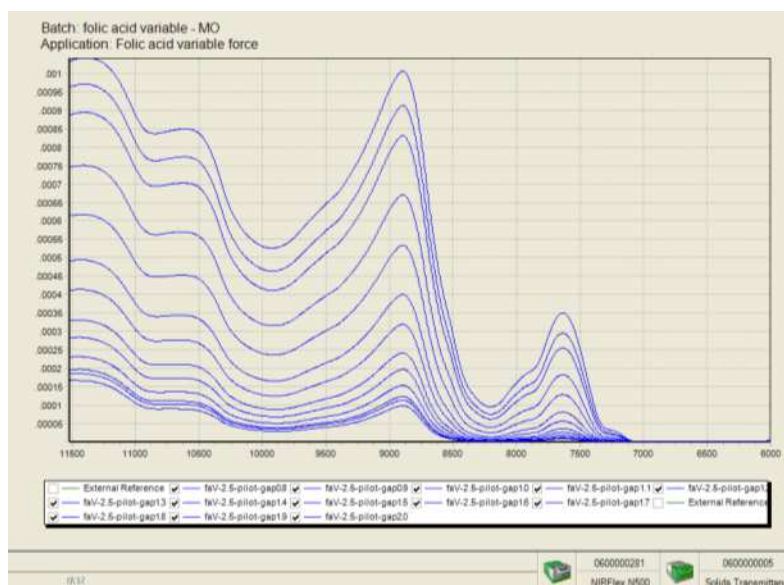
Figure 75: Raw spectra of placebo tablets with increasing compaction force. Gap size from 0.8 mm (biggest spectrum) to 1.7 (smallest spectrum)
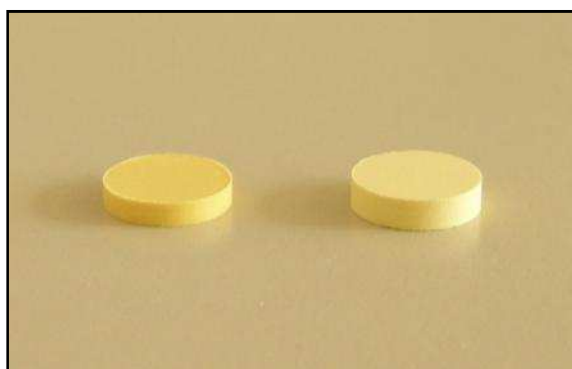
Figure 76: 2.5% folic acid tablet compacted with gap 0.8 mm (left) and 1.8 mm (right)

- Increasing tableting speed, in terms of dwell time (Table 19) had no observable effect on NIR spectra (Figure 77).
- Prediction of this variable speed batch also showed no difference pattern from the UV-assayed content (Figure 78), indicating that tableting speed (for the current tablet formulation) had no effect on NIR predictions. This cannot be generalised however, and other diluents may show different behaviour.

Table 19: Presster tableting to assess speed (dwell time) effect on predictions

No.	Gap / mm	Thickness / mm	Upper Force / kN	Powder mass / mg	Speed / TPH	Dwell time / ms	UV	NIR F2	NIR F3
1	1.8	2.40	3.5	202.6	15000	85.2	5.200	5.092	5.216
2	1.8	2.41	3.5	201.2	25000	51.1	5.175	5.135	5.157
3	1.8	2.43	3.6	202.1	35000	36.5	5.225	5.339	5.176
4	1.8	2.42	3.7	201.3	45000	28.4	5.075	5.154	5.174
5	1.8	2.44	3.7	201.7	55000	23.2	5.250	5.368	5.274
6	1.8	2.42	3.7	202.0	65000	19.7	5.075	5.287	5.198
7	1.8	2.43	3.6	202.0	75000	17.0	5.200	5.308	5.264
8	1.8	2.43	3.9	202.0	85000	15.0	5.250	5.454	5.237
9	1.8	2.43	3.7	202.9	95000	13.5	5.125	5.375	5.193
10	1.8	2.45	4.0	203.0	105000	12.2	5.250	5.435	5.324
11	1.8	2.45	3.8	202.3	115000	11.1	5.058	4.832	4.987
12	1.8	2.42	2.7	202.2	125000	10.2	5.065	5.004	5.054
13	1.8	2.42	3.6	201.2	135000	9.5	5.020	5.028	5.043
14	1.8	2.43	3.6	201.6	145000	8.8	5.033	4.969	5.062
15	1.8	2.46	3.7	202.3	155000	8.2	5.025	5.017	5.096
mean		2.43	3.6385	202.0	n/a	n/a	5.135	5.186	5.164
SD		0.01183	0.3070	0.5317	n/a	n/a	0.08939	0.1932	0.09668
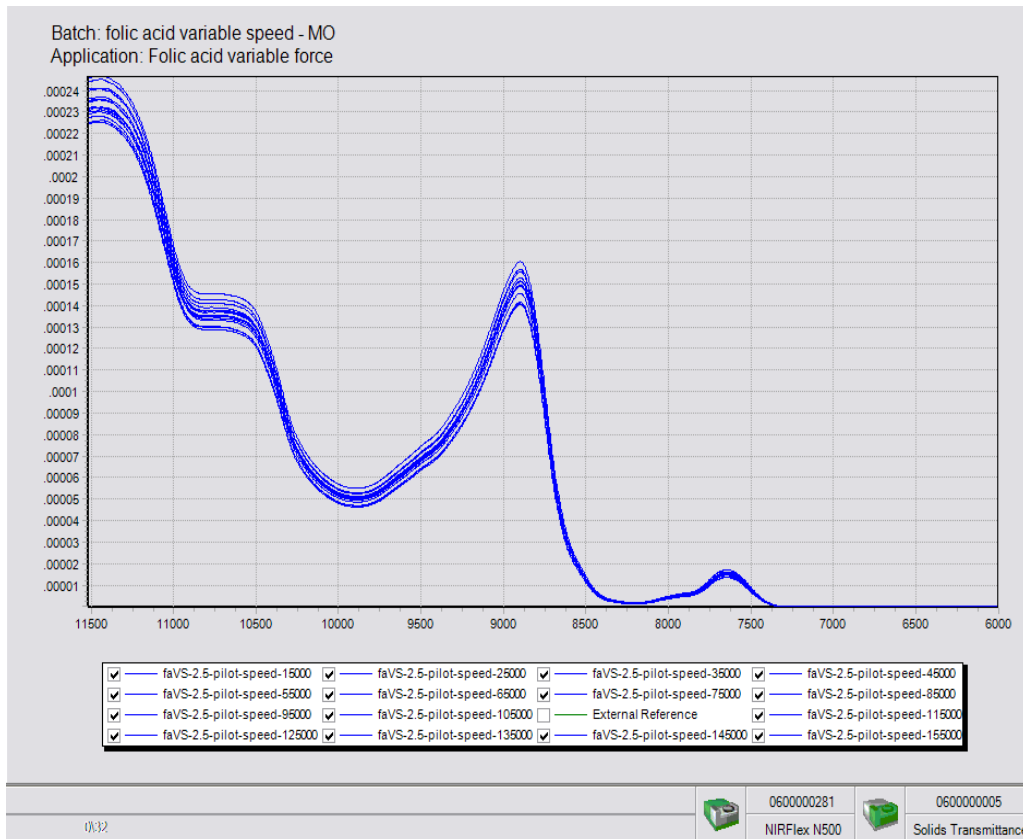
Figure 77: Raw spectra of 2.5% folic acid tablets compacted in a dwell time range of 85.2 – 8.2 msec

Figure 78: Prediction of variable compaction speed tablets by two NIR models, compared to the UV assay content
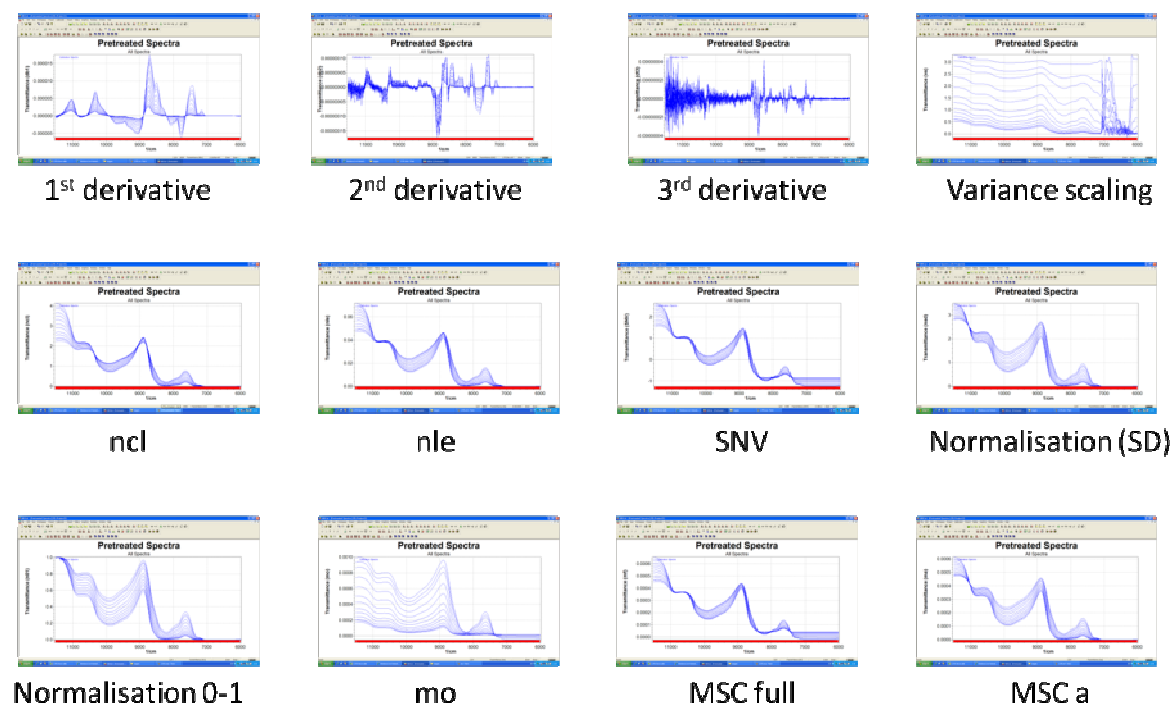
Figure 79: Various pretreatments applied to transmittance spectra of variable compaction force tablets
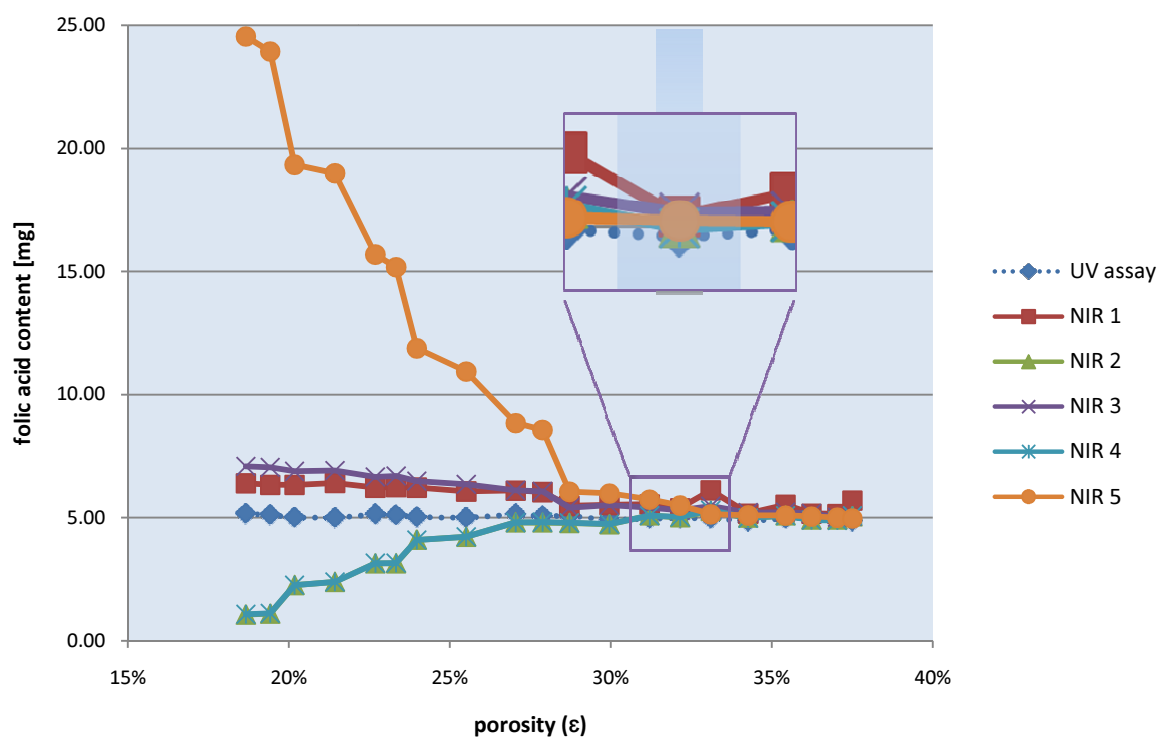
Figure 80: UV assay vs. NIR predictions for variable compaction force tablets

Table 20: Variable compaction force prediction set, UV content and NIR predictions

#	Mass	Thick ness	Poros ity	UV	F1	F2	F3	F4	F5	FV
	mg	mm	%	mg	mg	mg	mg	mg	mg	mg
1	204.5	1.99	0.15	5.17	19.96	1.58	-12.19	6.43	6.48	5.13
2	206.7	2.00	0.15	5.11	20.53	1.60	-12.80	6.57	6.61	5.10
3	200.2	2.00	0.17	5.01	16.45	3.14	-6.95	6.40	6.46	5.08
4	199.8	2.00	0.18	5.00	16.31	3.23	-6.43	6.46	6.52	5.04
5	204.0	2.07	0.19	5.14	13.18	4.21	-2.87	6.48	6.54	5.25
6	205.7	2.08	0.18	5.10	13.56	4.02	-3.31	6.48	6.53	5.15
7	200.8	2.10	0.21	5.02	10.76	5.19	0.80	6.37	6.42	5.16
8	200.0	2.11	0.22	5.00	9.86	5.05	1.37	6.24	6.29	5.09
9	202.2	2.20	0.24	5.14	8.31	6.04	3.85	6.11	6.14	5.17
10	205.7	2.20	0.23	5.06	8.34	5.70	3.53	6.17	6.20	5.25
11	196.0	2.22	0.27	5.09	5.91	5.35	5.11	5.70	5.74	4.56
12	203.7	2.28	0.26	4.90	6.05	5.28	5.15	5.69	5.71	4.66
13	199.2	2.31	0.29	4.98	5.62	5.42	5.55	5.47	5.49	4.69
14	199.0	2.30	0.29	4.98	5.93	5.30	5.61	5.52	5.54	4.74
15	194.5	2.37	0.32	4.97	5.20	4.73	5.36	5.10	5.10	4.68
16	200.9	2.39	0.31	4.86	5.27	4.95	5.41	5.00	5.02	4.85
17	198.7	2.45	0.33	4.97	5.55	5.36	5.85	5.05	5.04	4.47
18	202.2	2.47	0.32	5.02	5.32	4.33	5.29	4.87	4.87	4.70
19	198.9	2.53	0.35	5.06	5.99	5.95	6.95	5.37	5.31	4.12
20	194.7	2.55	0.37	4.87	5.67	5.69	6.11	4.91	4.88	3.87

- The five NIR models details constructed from fixed compaction folic acid tablets (F1-F5) are shown in Table 21. F4 and F5 had no statistically significant difference from the UV assay, as shown from Table 22.
- Predicting the variable compaction tablets by F1-F5 models showed gradual drift with the change of tablets porosity (and thickness) from UV content and accuracy only in the porosity region of 33%, in which the calibration tablets are made (Figure 80 and Table 20).

Table 21: Overview of fixed compaction force calibration models (F0-F5) and model with additional variable compaction force spectra (FV)

	F1	F2	F3	F4	F5	FV
Wavelengths Project Set	6000-11520. (total 1381/1381)	6000-11520. (total 1381/1381)	6000-11520. (total 1381/1381)	6000-11520. (total 1381/1381)	6000-11520. (total 1381/1381)	6000-11520. (total 1381/1381)
Wavelengths Calibration Set	6000-11520. (total 1381/1381)	7400-11520. (total 1031/1381)	8500-11520. (total 756/1381)	6000-11520. (total 1381/1381)	7400-11520. (total 1031/1381)	6000-10600. (total 1151/1381)
Data Pretreatment Sequence (short form)	mf	mf	SNV	db1,SNV	db1,SNV	mf, ncl
Method	PLS	PLS	PLS	PLS	PLS	PLS
Max Iterations	3000	3000	3000	3000	3000	3000
Mean Centring	yes	yes	yes	yes	yes	yes
Number of Primary PCs	9	9	8	3	3	14
Secondary/Calibration PCs	1-7. (total 7/9)	1-7. (total 7/9)	1-6. (total 6/8)	1-3. (total 3/3)	1-3. (total 3/3)	1-12. (total 12/14)
V-Set BIAS	0.020901	-0.02879	0.017055	-0.00096	-0.00155	0.0154753
C-Set SEE (SEC)	0.249761	0.323872	0.259507	0.286846	0.286303	0.312529
V-Set SEE (SEP)	0.258087	0.31796	0.254297	0.292198	0.290546	0.311205
Consistency	96.7739	101.859	102.049	98.1682	98.5396	100.426
C-Set Regression Coefficient	0.997209	0.995125	0.996986	0.996318	0.996332	0.995599
V-Set Regression Coefficient	0.995108	0.994061	0.995263	0.993946	0.994011	0.992966
C-Set Regression Intercept	0.027482	0.049445	0.029669	0.036633	0.036495	0.0428957
V-Set Regression Intercept	0.039841	-0.01142	0.056711	0.037676	0.041552	0.0192164
C-Set Regression Slope	0.994425	0.990275	0.993981	0.99265	0.992678	0.991217
V-Set Regression Slope	0.98766	1.00851	0.985014	0.992555	0.991889	0.992981
V-Set t-value	0.600605	0.799727	0.497373	0.024149	0.039284	0.540175
Confidence %	44.9384	57.3671	37.9055	1.91752	3.11883	40.9897

- Model FV consisted of 440 calibration/validation spectra, by adding the variable compaction calibration set (appendix V.1) to the previous set (appendix I.3). The model details are set in Table 21.
- This model (FV) was able to predict the variable compaction tablets across the whole porosity range and is hence completely robust to press compaction variability (Figure 81 and Table 20).
- Although FV model has slightly worse SEP (0.31 mg) than models F4 and F5 (0.29 mg), it was still statistically equivalent to the UV method (Table 22).

Table 22: Statistical evaluation of the fixed- and variable compaction models

	UV	F1	F2	F3	F4	F5	FV
					t-Test: Two-Sample Assuming Equal Variances		
Mean	4.832661	4.666275	4.575305	4.72289	4.778595	4.77842	4.77842
Variance	0.085586	0.049345	0.063881	0.054344	0.034057	0.03421	0.034210211
Observations	20	20	20	20	20	20	20
Pooled Variance		0.696352	0.398076	0.600993	0.81445	0.817354	0.817354149
Hypothesized Mean Difference		0	0	0	0	0	0
df		19	19	19	19	19	19
t Stat		-3.53039	-3.82375	-2.03918	-1.35803	-1.3702	-1.370196485
P(T<=t) one-tail		0.001118	0.000573	0.027795	0.095182	0.0933	0.093299869
t Critical one-tail		1.729133	1.729133	1.729133	1.729133	1.729133	1.729132792
P(T<=t) two-tail		0.002236	0.001146	0.055589	0.190363	0.1866	0.186599738
t Critical two-tail		2.093024	2.093024	2.093024	2.093024	2.093024	2.09302405
Mean	4.832661	4.666275	4.575305	4.72289	4.778595	4.77842	4.77842
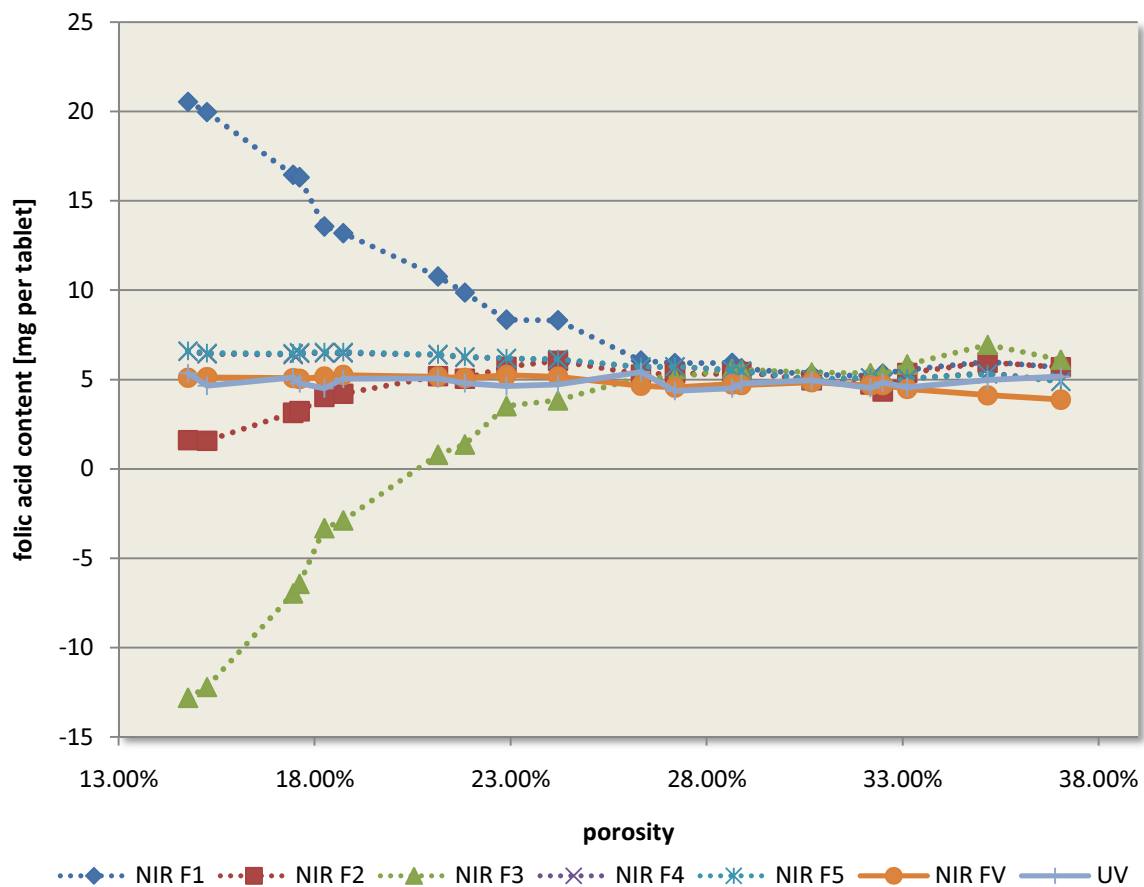
Figure 81: Prediction of variable compaction force tablets using the new model FV

- Figure 82 shows the spectral down-scaling at one wavenumber position (8880 cm^{-1}) with increasing tablet thickness and constant porosity. The drop was exponential and relates to decreasing NIR radiation reaching the detector in diffuse transmittance as the tablets became thicker and thicker. Beyond is 5 mm the spectrum was very small but still preserved its shape and whether a calibration model is achievable at such tablet thickness remains to be investigated.

- Increasing porosity in tablets with constant thickness (Figure 83) caused a similar effect, but this time less radiation is being detected due to more scattering (forward as well as backward) in higher porosity and less chances for photons to find their way to the tablet's other surface. The drop was also exponential and the porosity range chosen represents the normal manufacturing range of commercial tablets.

- The two parameters, tablet thickness and porosity are both exerting an exponential scaling effect, in the same direction, during compaction variability (Figure 75).

$$y = 0.0236e^{-1.614x}$$
$$R^2 = 0.9974$$
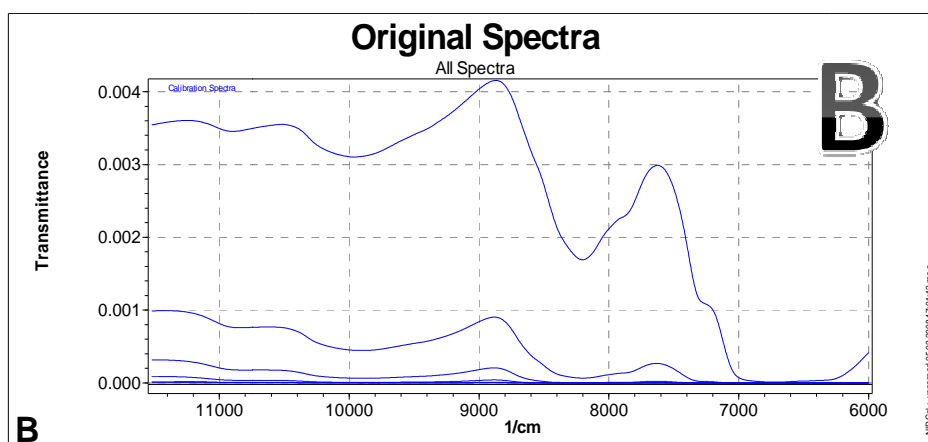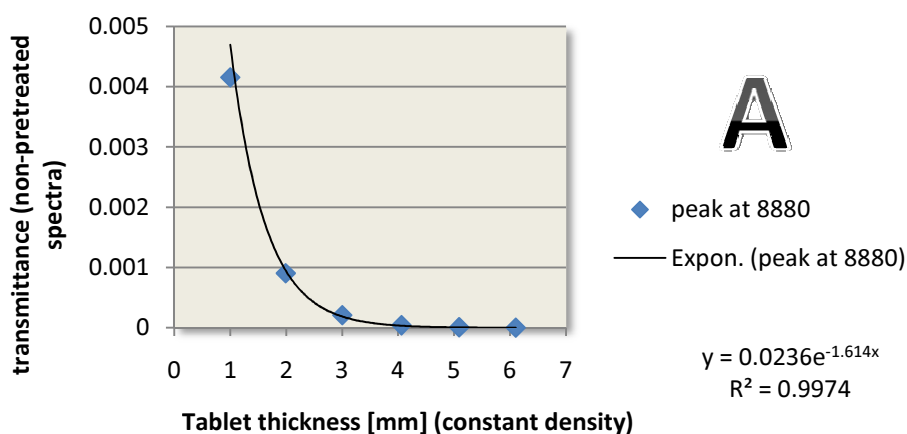
Figure 82: Effect of tablet thickness on transmittance spectra, with fixed porosity (apparent density)
(A) Plot of maximum (B) Raw spectra
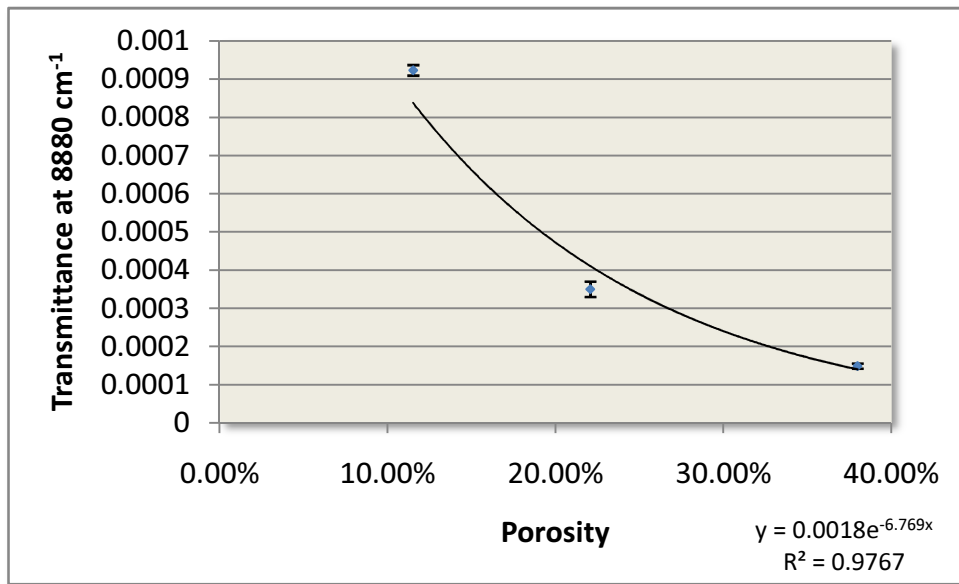
Figure 83: Effect of tablet porosity on transmittance spectra, with fixed tablet thickness

13. Appendix II

Expanded methods and results sections: Tablet sampling span in diffuse transmittance

13.1 Materials and instruments

13.1.1   Micro-crystalline cellulose

Please refer to section 12.1.2, page 153.

13.1.2   Carboxymethylcellulose sodium

Please refer to section 12.1.3 page 155.

13.1.3   Magnesium stearate

Please refer to section 12.1.4, page 157.

13.1.4   White paper

- A4 standard printer paper
- 80 g m^{-2}

13.1.5   Laser printer

- HP LaserJet 2200dn network printer
- 1200×1200 dpi
- HP LaserJet C4096 family printer cartridge

13.1.6   Presster

Please refer to sections 12.2.1, page 159.

13.1.7   NIRFlex N-500 with Solids Transmittance cell

Please refer to section 12.2.2, page 161.

13.2 Methods

13.2.1   Tableting

- Placebo tablet mixture was prepared from formulation in Table 9.
- 200 mg tablets were compacted in Presster.
- Korsch rotary press PH336 was selected for simulation, with of a speed 10800 TPH and dwell time of 118.3 msec.
- A flat face punch with a diameter of 10.0 mm was used for compaction.
- Presster gap size set for 1.0 mm
- 1 tablets made
- Gap increased by 0.1 mm
- 1 more tablets and gap increments until gap size of 1.4 mm was reached and 5 tablets were made.

13.2.2   Paper filters

- 10 boxes were drawn in word, with 13 mm width and height.
- Over each box, a circle of 10 mm diameter and black fill was drawn, centre-align to the box above.
- Over the above circle, another white-filled circle, centre-aligned was drawn. The diameter of that circle was decreasing from 9 (filter F1) to 1 mm filter (F9).
- Filter F10 had no white circle (complete block).
- Filter F0 had no circles (no block).
- Figure 16 shows the filters and their labelling and Appendix VI.1 shows an exact print-out of the filters.
- After printing, each box was carefully cut and kept for scanning.
- 3 sets of each filter were made to assess experimental error.

13.2.3   NIR Spectral collection

- Each tablet was placed on the DT sample tray, and one type of paper filter placed on top of the tablet with forceps, so that the box corners align with the tablet tray position walls.
- The tablet was scanned.
- The filter was carefully removed and another placed on the same way and the tablet was scanned.
- The process was repeated until all filters are used.
- The second tablet was taken and the same steps undertaken until spectra of the five tablets, each covered by all filter types were obtained.

13.2.4   Data processing and calculations

- Transmittance at 8880 cm^{-1} for one tablet (one porosity) was plotted against filter types (average of 3 measurements for three filters of the same type).
- This was also compared with the same for other tablets (different porosities).
- **Theoretical signal drop** for filter Fx was calculated as a ratio between the block (black) area and tablet surface area:

$$_x Drop_{theor} = \frac{_x A_{block}}{A_{tablet}} \cdot 100\%$$

  o This represents the block ratio of each filter if the NIR radiation was equally distributed across the whole tablet surface.
  o This was scaled because complete block was not 100% according to the DT data (*see discussion).*

- **Actual (measured) signal drop** for filter Fx was calculated as a ratio between transmittance at 8800 cm^{-1} from filter Fx and the transmittance at 8800 cm^{-1} from filter F0:

$$_x Drop_{actual} = \frac{^{8880}DT_{Fx}}{^{8880}DT_{F0}} \cdot 100\%$$

- **Theoretical signal drop for each ring** was calculated by subtracting the $Drop_{theor}$ of each filter, from $Drop_{theor}$ of the subsequent filter:

$$_x Ring_{theor} = _x Drop_{theor} - _{x+1}Drop_{theor}$$

  o This made the tablet surface consist of 10 rings, each 1 mm thick.
  o It represents the signal drop due to the block of one ring, if the NIR radiation was equally distributed across the whole tablet surface.

- **Actual (measured) signal drop for each ring** was calculated by subtracting the actual drop $Drop_{actual}$ of each filter, from $Drop_{actual}$ of the subsequent filter:

$$\,_xRing_{actual} = \,_xDrop_{actual} - \,_{x+1}Drop_{actual}$$

- o It represents the measured signal drop due to the block of one ring.
- **Theoretical signal distribution** for each ring was calculated by dividing the theoretical signal drop from each ring by the sum of theoretical signal drop due to all rings, multiplied by 100%:

$$\,_xContribution_{theor} = \frac{\,_xRing_{theor}}{\displaystyle\sum_{i=0}^{9} \,_iRing_{theor}} \cdot 100\%$$

- o This represents the share of each ring in the total signal drop in that filter, if the NIR radiation was equally distributed across the tablet surface.
- o In this case it will be simply related to the ring area.
- **Measured signal distribution** for each ring was calculated by dividing the measured signal drop from each ring by the sum of measured signal drop due to all rings, multiplied by 100%:

$$\,_xContribution_{actual} = \frac{\,_xRing_{actual}}{\displaystyle\sum_{i=0}^{9} \,_iRing_{actual}} \cdot 100\%$$

- o This represents the measured share of each ring in the total signal drop in that filter in DT mode
- o Plotting this for all filters gives a picture of the distribution of the radiation emerging from the tablet surface in DT mode.

13.3 Results

With the application of paper filters F0 – F10 (from Figure 16) on the tablet, the DT spectra were scaled-down gradually with each increase in the block inner diameter (Figure 84). F1 and F2 block was small and difficult to judge whether due to positioning noise effect (most peripheral blocks) or real signal block. From F3 onwards, the block was strongly evident.

In Figure 22, the DT filters block test was repeated for tablets with different porosities (15 - 25%) and 8880 cm^{-1} maxima plotted. All the tablets showed similar sigmoidal block pattern, an indication that porosity change (in that range), was not affecting the signal distribution to a big degree. The plots do, however, have different scales, and it is due to due increase in radiation scatter at lower sample densities (higher porosity) – *see press effect, chapter 8.*
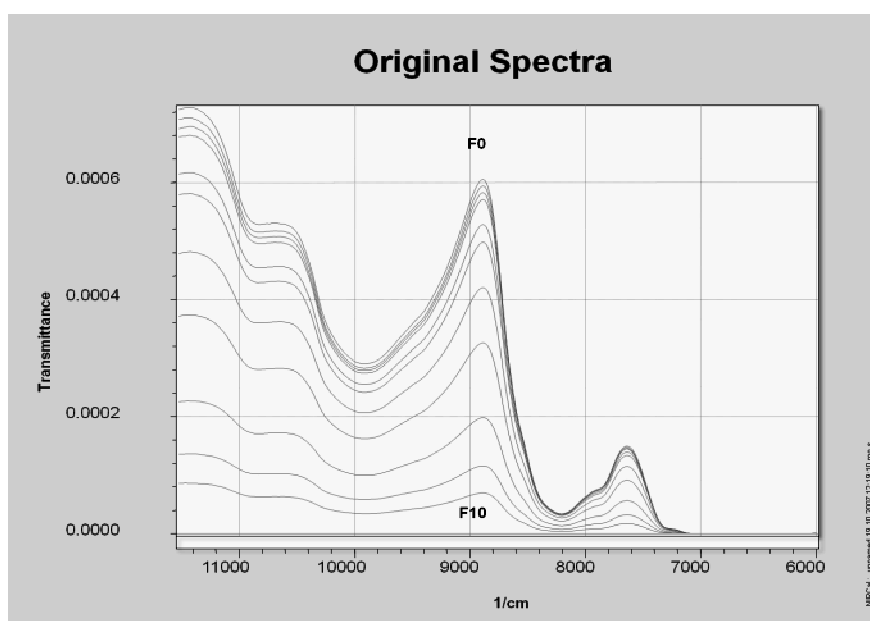
Figure 84: DT spectra of MCC tablet covered with paper filters F0-F10, showing spectral down-scaling with increasing block.

Table 23 shows the calculated actual and theoretical signal drop, and drop due to each 1-mm ring of gradually decreasing diameters. The latter values were converted to proportions of the total block due to all rings and would represent the distribution of the drop across tablet surface. This was also graphically illustrated in Figure 24 which shows that central areas carry represent more of the signal than their proportional area

(as expected). However, the representation of the tablet was continued up to 7 mm in diameter (90.6% of signal).

Table 23: Measured and theoretical relative drops with each filter, and respective drop for block rings.

Filter	Drop$_{actual}$	Drop$_{theor}$	Ring #	Ring$_{actual}$	Ring$_{theor}$	Contribution$_{actual}$	Contribution$_{theor}$
F0	100.00%	100.00%					
F1	96.89%	87.24%	1	3.11%	12.76%	3.30%	14.43%
F2	94.04%	75.34%	2	2.85%	11.89%	3.02%	13.45%
F3	96.95%	64.32%	3	2.90%	11.02%	3.08%	12.46%
F4	92.24%	54.17%	4	4.70%	10.15%	4.99%	11.48%
F5	83.92%	44.89%	5	8.32%	9.28%	8.82%	10.49%
F6	65.05%	36.48%	6	18.87%	8.41%	20.01%	9.51%
F7	53.39%	28.94%	7	11.67%	7.54%	12.37%	8.52%
F8	32.04%	22.28%	8	21.35%	6.67%	22.64%	7.54%
F9	19.32%	16.48%	9	12.71%	5.79%	13.48%	6.55%
F10	11.51%	11.56%	10	7.81%	4.92%	8.29%	5.57%
			Sum			100.00%	100.00%

14. Appendix III

Expanded methods section: Tablet sampling span in diffuse reflection

14.1 Materials

14.1.1   Micro-crystalline cellulose

Please refer to section 12.1.2, page 153.

14.1.2   Phenylbutazone

- *source*
  - Sigma-Aldrich, Buchs, Switzerland
- *functional category*
  - API
  - Cyclo-oxygenase inhibitor; pyrazolone analgesic
- empirical formula: $C_{19}H_{20}N_2O_2$
- *molecular mass*: 308.37 g mol^{-1}
- *structural formula* (Figure 85)
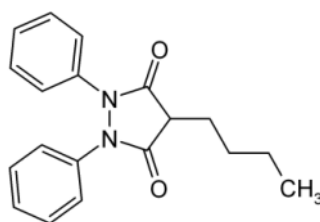
Figure 85: Molecular structure of phenylbutazone

- *Appearance*
  - White or almost white, crystalline powder.
- *Solubility*
  - Practically insoluble in water, sparingly soluble in alcohol. It dissolves in alkaline solutions.
- *Storage*
  - Store in an air-tight container
- *Particle size*
  - 90% of the particles < 38.2 μm

14.1.3   Caffeine (anhydrous)

- *source*
  - BASF AG, Schaffhausen, Switzerland
- *functional category*
  - API
  - Central nervous system stimulant
- *empirical formula:* $C_8H_{10}N_4O_2$
- *molecular mass*: 194.19 g mol^{-1}
- *structural formula* (Figure 86)
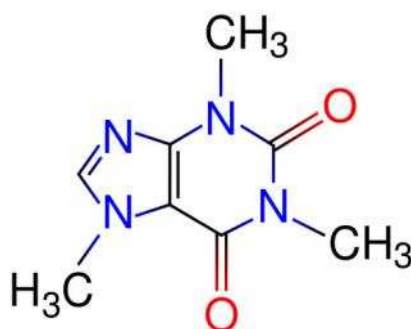
Figure 86: Molecular structure of caffeine

- *Appearance*
  - White or almost white, crystalline powder or silky, white or almost white, crystals.
- *Solubility*
  - Sparingly soluble in water, freely soluble in boiling water, slightly soluble in ethanol (96 per cent).
  - Dissolves in concentrated solutions of alkali benzoates or salicylates.
  - Readily sublimes.
- *Storage*
  - Store in an air-tight container
- *Particle size*
  - 90% of the particles < 37 µm

14.1.4   *Magnesium stearate*

Please refer to section 12.1.4, page 157.

14.1.5   *FD+C Red 3 LA*

- *E number*
  - E127
- *Common name*
  - Erythrosine
- *source*
  - Sandoz Pharma, Switzerland
- *functional category*
  - Colouring agent
- empirical formula: $C_{20}H_6I_4Na_2O_5$
- *molecular mass*: 879.86 g mol^{-1}
- *structural formula* (Figure 87)
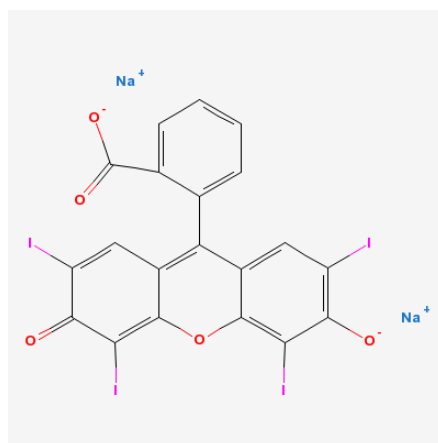
Figure 87: Molecular structure of erythrosine

- *Appearance*
  - Cherry red powder.
- *Solubility*
  - Soluble in water and alcohol and acidic solutions.
  - Insoluble in alkaline solutions.
- *Storage*
  - Store in an air-tight container

14.1.6   Hydroxypropylmethylcellulose

- *source*
  - *Pharmacoat 603,* Novartis Pharma AG, Basel*, Switzerland*
- *functional category*
  - sustained release; stabilizing agent; suspending agent; tablet binder; viscosity-increasing agent.
- *non-proprietary name*
  - Hypromellosum (Ph. Eur.)
- *empirical formula*: $C_6H_7O_2(OH)_x(OCH_3)_y(OC_3H_7)_z$
- *molecular mass*: 10 000–1 500 000 g mol^{-1}
- *structural formula* (Figure 88)
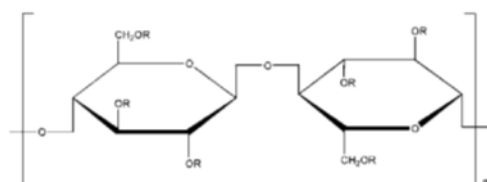
where R is H, CH$_3$, or CH$_3$CH(OH)CH$_2$

Figure 88: Molecular structure of HPMC

- *pharmaceutical applications*
  - In oral products, HPMC is primarily used as a tablet binder, in film-coating, and as a matrix for use in extended-release tablet formulations. Concentrations of 2–20% w/w are used for film-forming solutions to film-coat tablets. Lower-viscosity grades are used in aqueous film-coating solutions, while higher-viscosity grades are used with organic solvents.
- *appearance and characteristics*
  - odourless and tasteless, white or creamy white fibrous or granular powder.
- *stability and storage conditions*
  - should be stored in a well-closed container in a cool, dry place.
- *incompatibilities*
  - Since it is non-ionic, hypromellose will not complex with metallic salts or ionic organics to form insoluble precipitates.
- *safety*
  - generally regarded as a nontoxic and non-irritant material.
- *Solubility*

o   soluble in cold water, forming a viscous colloidal solution; practically insoluble in chloroform, ethanol (95%), and ether.

14.1.7   Ethylcellulose

- *source*
  o   Aquacoat ECD 30, FMC Biopolymer, Houston, TX
- *functional category*
  o   Coating agent; viscosity-increasing agent.
- *non-proprietary name*
  o   Ethylcellulosum (Ph. Eur.)
- *empirical formula*: $C_{12}H_{23}O_6(C_{12}H_{22}O_5)_nC_{12}H_{23}O_5$
- *structural formula* (Figure 88)
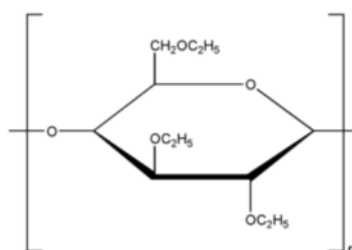
Figure 89: Molecular structure of ethylcellulose

- *pharmaceutical applications*
  o   The main use of ethylcellulose in oral formulations is as a hydrophobic coating agent for tablets and granules and modify the release of a drug, to mask an unpleasant taste, or to improve the stability of a formulation. Higher-viscosity ethylcellulose grades tend to produce stronger and more durable films. Ethylcellulose films may be modified to alter their solubility, by the addition of hypromellose or a plasticizer. An aqueous polymer dispersion of ethylcellulose such as Aquacoat ECD may also be used to produce ethylcellulose films without the need for organic solvents.
- *Glass transition temperature:* 129–133°C
- *appearance and characteristics*
  o   tasteless, free-flowing, white powder.
- *incompatibilities*
  o   Incompatible with paraffin wax and microcrystalline wax.
- *safety*
  o   safe, used in food products, not metabolised enterally.
- *Solubility*

- o practically insoluble in glycerine, propylene glycol, and water. Solubility depends on the percentage of ethoxyl groups.

14.1.8   Triethyl citrate

- *source*
  - o Triethyl citrate, FCC FEMA 3083, Sigma-Aldrich, Buchs, Switzerland.
- *functional category*
  - o Plasticizer
- *non-proprietary name*
  - o Triethylis citras (Ph. Eur.)
- *empirical formula*: C12H20O7 276.29
- *molecular mass*: 276.29 g mol^{-1}
- *structural formula* (Figure 90)
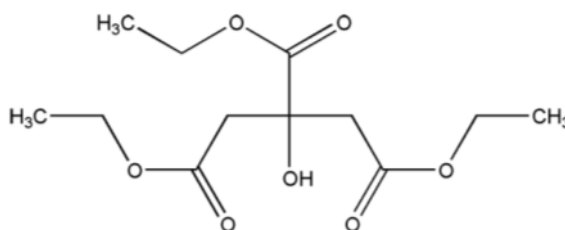
Figure 90: Molecular structure of triethyl citrate

- *pharmaceutical applications*
  - o Used to plasticize polymers in formulated pharmaceutical coatings.
- *appearance and characteristics*
  - o a clear, odourless, practically colourless, oily liquid.
- *incompatibilities*
  - o Incompatible with strong alkalis and oxidizing materials.
- *safety*
  - o Generally regarded as a nontoxic and non-irritant material.
- *Solubility*
  - o soluble 1 in 15 of water. Miscible with ethanol (95%), acetone, and propan-2-ol.
- *Viscosity (dynamic)*
  - o 35.2 mPa s (35.2 cP) at 25°C

14.2 Instruments, apparatus and software

14.2.1   *Zwick Material Tester*

This is a hydraulic press (Type 1478TM, Wick Roell, Germany) designed to mimic the compaction cycle of any prescribed shape by using hydraulic control mechanisms that are driving a punch in and out of the die.

Under computer control, the hydraulic actuator maintain load, position, and strain associated with the punch. The simulation can be achieved by controlling the force (load control) or punch displacement at any given moment of time, while the machine plots the compaction and punch displacement profiles.

14.2.2   *NIRFlex N-500 with solids measurement cell*

Please refer to section 12.2.2, page 161. The solids measurements cell scans samples in diffuse reflection mode (Figure 91). The tablets where mounted on a tablet sample plate with adjustable holding mechanism.

Detector	Extended range InGaAs (temperature controlled)			
Electric power supply	100–230 VAC ± 10%, 50/60 Hz, 20 W			

	Petri dish add-on	Vial add-on	Tablet add-on	XL add-on
Max. number of samples per sequence	1	6	10	1
Measurement based on diffuse reflection	x	x	x	x
Measurement based on transflectance	x	–	–	–
Measurement with petri dishes	x	–	–	–
Measurement with vials	–	x	–	–
Measurement of tablets	–	–	x	–
Measurement using small plastic bags	–	–	–	x
Environmental working conditions 5–35 °C	x	x	x	x
Internal reference	x	–	–	–
External reference	x	x	x	x
Sample dimensions	Petri dish 100 mm	Glass vials 10–15 mm	Tablets 5–10 mm	

Figure 91: Specifications of the Solids measurement cell

14.2.3   *Strea-1™ Fluid-bed*

This is a fluid-bed coater/dryer/granulator from Aeromatic-Fielder (Bubendorf, Switzerland), with a 16.5 l container and 2 m^3 min^{-1} air flow. Spraying is possible from top or bottom and product temperature, air volume, filter resistance are continuously instrumented.

14.2.4   Eccentric tablet press

This is an electric, single station eccentric tableting machine from Korsch (Germany) with adjustable tableting speed, lower punch filling position and upper punch gap position.

14.2.5   Presster™ tablet press simulator

Please refer to section 12.2.1, page 159.

14.2.6   Other instruments

For scales, Turbula mixer, micrometer, *please refer to section 12.2.3, page 162.*

14.2.7   Software

14.2.7.1 NIR Cal

This is a chemometrics software from Büchi, used for spectral pretreatments and calibration model development.

14.2.7.2 Table Curve 3D

This is a n-factorial fitting software from Statcon (Wizenhausen, Germany).

14.2.7.3 Excel 2007 with VBA

This is a spreadsheet software, used with the built-in Visual Basic for Applications module to write and run macros.

14.3 Methods

14.3.1   *Incremental thickness tablets*

This experiment was used to test the effect of increasing tablet thickness (with fixed tablet composition and density) on DR spectra, and hence the possibility of reaching a thickness with minimum spectral variability that may present a candidate for determining DR information depth.

- Zwick hydraulic press was used with a 10 mm die and flat punches.
- A 3D curve fitting was calculated using TableCurve3D between tablet mass, thickness and compaction force was calculated:
  - o Powder masses of 30, 100, 200, 300 and 430 mg were fed in the die.
  - o For each powder mass, 500 – 5000 N compaction forces were tried in 4 steps
  - o With each trial, the tablet mass was measured.
  - o The mass, thickness and force data were imported in TableCruve3D and the best and simplest fitting was selected (Figure 30).
  - o The fitting equation was used to determine the compaction force for experimental samples.
- 20 MCC tablets with thickness of 0.5 – 10 mm (in 0.5 mm steps) and a porosity of 25% were compacted in the Zwick using compaction force determined from the fitting equation (Appendix VII.3).
- Tablet thickness and porosity were determined after 24h, and a plot of tablet thickness against porosity was used to determine whether or not porosity and thickness variabilities were co-related.
- Tablets were scanned in DR mode and spectra imported in NIRCal.
- Spectral data table was obtained by clicking "G" and imported in Excel.
- Various spectral positions, with and without pretreatments, were examined for correlation with tablet thickness.

14.3.2   Double-layer tablets

Tablets consisting of 2 layers (PBZ-phenylbutazone and MCC) of varying layer thicknesses were used to possibility of detecting DR spectral features of one layer through the other. The DR information depth would be less than the lower layer thickness if the upper layer is undistinguishable.
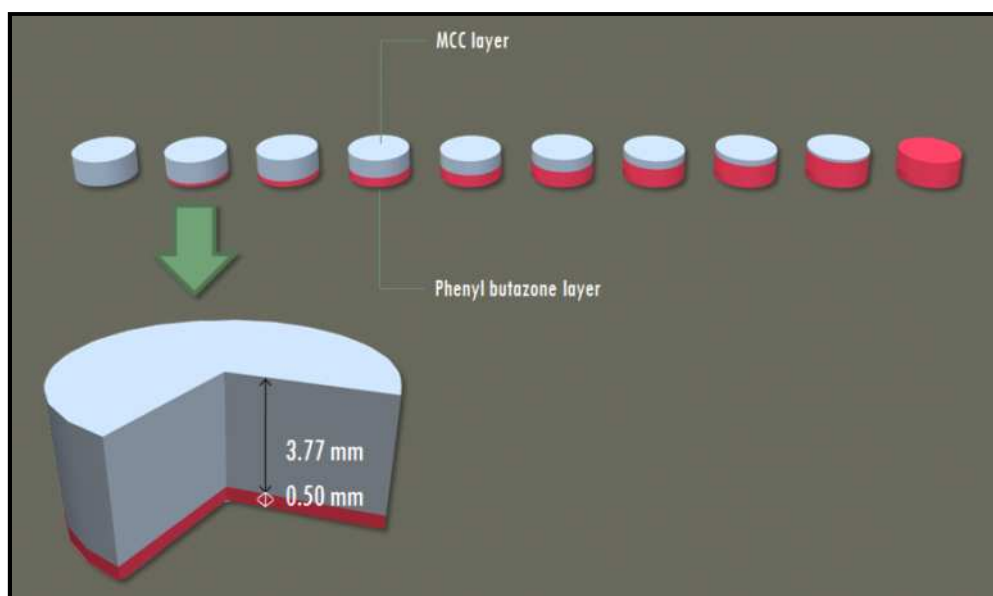
Figure 92: Overview of double layer tablets

- The formulations of upper and lower layers are shown in table.
- Samples were tabled in Presster with a 10-mm flat punch and Korsch PH 336 press simulation.
- The PBZ layer was fed first and pre-compacted.
- The station was moved back to home position and the upper punch was cleaned.
- The MCC layer powder was fed and both layers were compacted and tablet ejected.
- Tablets were weighed, thickness measured and DR were spectra collected for both sides by flipping the tablets.
- Spectra were imported in NIRCal and layer features inspected in comparison to tablets 1 and 10 using different pretreatments.
- Each spectrum was assigned 2 qualitative properties, PBZ and MCC. Tablets scanned with PBZ layer down were checked as PBZ and those with MCC layer down as MCC. Tablet 1 was MCC and 10 PBZ (Figure 92). Same applied to spectra of flipped tablets.
- Cluster analysis models were started in NIRCal, one for each qualitative property. PC scores were used to analyse the ability to cluster tablets:

     ○ For PBZ property, clustering tablets scanned with the PBZ layer down with MCC-only tablet.

     ○ For MCC property, clustering tablets scanned with the MCC layer down with PBZ-only tablet.

Table 24: Double-layered tablets formulation

	Phenylbutazone	Pigment	MCC 102	MgSt	Total
MCC layer	-	-	99%	1%	100%
PBZ layer	98%	1%	-	1%	100%

14.3.3 *Incremental tablet coating*

This experiment was used to examine DR information depth by scanning tablets coated with increasingly thicker coats. This depth is reached after spectral variability reaches its minimum. A second batch of tablets of different core and same coating conditions was used to confirm this estimation of information depth.
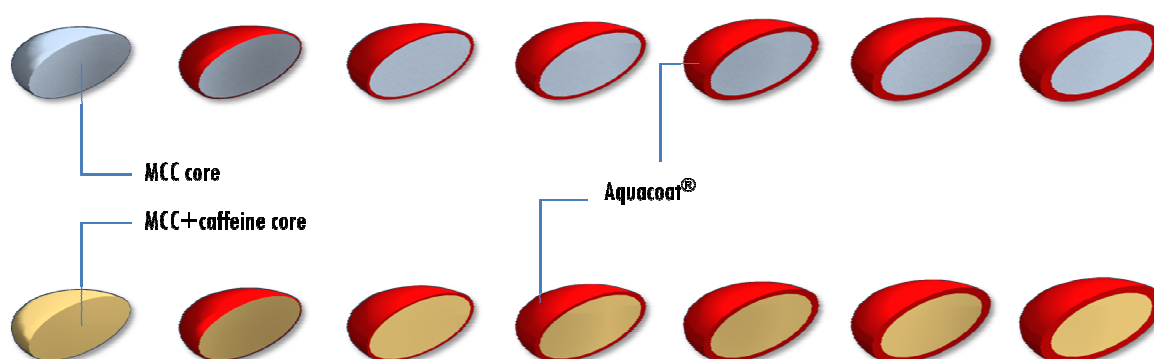
Figure 93: Overview of incremental coating experiment

• A simple directly compactable tablet formulation was used to make to batches of tablets, MCC placebo and 30% caffeine tablets (Table 25).

• Tablets were compacted on en eccentric Korsch press with a concave punch (7 mm diameter, 5.5 dome height).

• The tableting mixture was fed into the hopper and the press was manually adjusted to produce tablet having:

     ○ Mass 100 ±1.5% mg

     ○ Thickness 3.1 – 3.2 mm

     ○ Hardness 90-110 N

• The press was then run and tableting continued with IPC every 50 samples.

• The same procedure was used for the second batch.

Table 25: MCC and caffeine tablet formulation

	MCC tablets	Caffeine tablets
MCC 102	99 %	69 %
Caffeine	-	30 %
MgSt	1 %	1 %
Total	**100 %**	**100 %**

- An Aquacoat film coat formulation was derived from Aquacoat ECD product manual (FMC Biopolymer, PA, USA) to coat the tablets (Table 26):
  o 19% Pharmacoat 603 solution was prepared.
  o (A) Triethylcitrate and Aquacoat were added to a beaker and mixed for 30 minute with a magnetic stirrer.
  o (B) The dye powder was sieved over the Pharmacoat solution and mixed for 5 minutes.
  o (A) and (B) were mixed together with stirred with paddle throughout the coating process

Table 26: Aquacoat film coat formulation

Component	Percentage [%]
Aquacoat ECD 30 (30% m/m)	22.22
Pharmacoat 603 (19% m/m)	35.09
Triethylcitrate	1.33
Fd+C Red 3 LA	7.00
Water (dist.)	34.36
Total	**100.00**

Table 27: Aeromatic process parameter for Aquacoat film coating

Parameter	Value	
Inlet temperature	60 .0	°C
Outlet temperature	35 .0	°C
Product temperature	47.5	°C
Atomising pressure	0.8	Bar
Spray rate	52.4	mg s^{-1}

- The tablets were incrementally coated inside the Aeromatic fluid bed:
  o 250 g of tablets were fed in the product chamber and preheated to the product temperature (Table 27).
  o The coat suspension was fed using a pump at the specified rate.
  o Coating was interrupted after 50 g of coat suspension was used.
  o Tablets were dried for 1 minute and 10 tablets were sampled for analysis and then coating was continued for another 50 g of coat suspension.

- o 5 coating steps were possible (+1 uncoated) before tablets showed cracked, and pitted surfaces and coating was terminated.
  - o The same coating process was repeated for the caffeine tablets using the same film coat formulation.
- Mass and thickness of tablets from all coating steps and for both tablet batches were determined.
- DR and DT spectra were collected from all tablets.
- 2 qualitative properties (MCC and Caffeine) were created and assigned for the respective tablets' DR and DT spectra.
- The decay curve in different spectral regions was estimated:
  - o The spectra were imported in NIRCal and spectral data were exported to excel using different pre-treatments (each spectrum in a column).
  - o An Excel macro (Appendix VII.2) was used to search for spectral regions with difference between MCC and caffeine DR spectra of the same coating level highly correlating with the coat thickness; using r^2 of an exponential fit (other fittings did not produce any correlation).
  - o When the DR difference was converted to percentage, (100% being the maximum difference of the uncoated tablets), the fit represented the DR signal decay with increasing coat thickness.
- The spectra were also investigated using cluster analysis to assess the possibility of predicting a tablet correctly (MCC or Caffeine) with increasing coat thickness:
  - o DR spectra were imported in a qualitative CLU model in NIRCal.
  - o One third of the spectra were assigned as validation.
  - o Best qualitative model was searched for using manual and automatic model optimizations, using Q value as a performance indicator.
  - o Clustering was visualized using the Scores vs. Scores plot.
  - o The same was repeated for the DT spectra and the results were compared with DR.

15. Appendix IV

Appendix IV.1: Presster compaction profile for folic acid tablets

tablet number	tablet mass [mg]	thick ness [mm]	crushin g strength [N]	CO step motor position (gap size) [mm]	upper compaction [kN]
1	203.2	3.31	27	2.7	1.4
2	198.1	2.90	40	2.3	1.9
3	201.3	2.92	47	2.3	2.1
4	200.1	2.67	75	2.0	2.8
5	201.6	2.44	104	1.8	4.0
6	200.3	2.44	104	1.8	3.9
7	201.8	2.48	109	1.8	3.9

Appendix IV.2: Complete data from Presster compaction profile for folic acid tablets

batch #	batch tablet #	press brand	press model	desired press speed [TPH]	desired dwell time [ms]	achieved dwell time [ms]
0	0	KORSCH	PH336	10'800	118.3	31.1
0	0	KORSCH	PH336	10'800	118.3	31.1
0	0	KORSCH	PH336	10'800	118.3	31.6
0	0	KORSCH	PH336	10'800	118.3	31.1
0	0	KORSCH	PH336	10'800	118.3	31.1
0	0	KORSCH	PH336	10'800	118.3	31.1
0	0	KORSCH	PH336	10'800	118.3	31.1

batch #	batch tablet #	effective dwell time [ms]	upper pre-compression peak [kN]	lower pre-compression peak [kN]	upper compression peak [kN]	lower compression peak [kN]
0	0	5.1	0.1	0.1	1.4	0.6
0	0	15.2	0.2	0.1	1.9	1.2
0	0	5.1	0.1	0.1	2.1	1.2
0	0	17.7	0.1	0.1	2.8	2.1
0	0	10.1	0.1	0.1	4.0	3.0
0	0	10.1	0.1	0.1	3.9	2.9
0	0	12.6	0.1	0.1	3.9	3.0

batch #	batch tablet #	maximum upper punch displacement [mm]	maximum lower punch displacement [mm]	peak ejection [N]	peak take-off [N]	peak radial die wall pressure [MPa]
0	0	4.300	6.670	119.4	16.0500	20.5100
0	0	4.290	6.280	156.3	16.0500	24.3600
0	0	4.300	6.290	139.9	16.0500	21.4300
0	0	4.290	6.030	144.0	16.0500	24.0400
0	0	4.300	5.850	139.9	16.0500	24.1000
0	0	4.300	5.840	115.4	16.0500	23.7400
0	0	4.290	5.850	107.2	16.0500	27.2100

batch #	batch tablet #	punch ID	tool type	effective contact time [ms]	effective rise time [ms]	effective fall time [ms]
0	0	Flat Face 10.0 mm	EU B	75.8	53.0	17.7
0	0	Flat Face 10.0 mm	EU B	73.2	35.4	22.7
0	0	Flat Face 10.0 mm	EU B	101.0	45.5	50.5
0	0	Flat Face 10.0 mm	EU B	75.8	37.9	20.2
0	0	Flat Face 10.0 mm	EU B	83.3	48.0	25.3
0	0	Flat Face 10.0 mm	EU B	85.9	53.0	22.7
0	0	Flat Face 10.0 mm	EU B	80.8	40.4	27.8

batch #	batch tablet #	minimum punch gap [mm]	corrected gap [mm]	CO step motor position [mm]	dosing step motor position [mm]	PCO step motor position [mm]
0	0	2.82		2.7	17.4	14.3
0	0	2.47		2.3	17.4	14.3
0	0	2.46		2.3	17.4	14.3
0	0	2.23		2.0	17.4	14.3
0	0	2.05		1.8	17.4	14.3
0	0	2.05		1.8	17.4	14.3
0	0	2.06		1.8	17.4	14.3

batch #	batch tablet #	EJ step motor position [deg]	number of stations	achieved RPM	sampling rate [Hz]	achieved linear speed [m/s]
0	0	10.9	36.0	19.0	396.0	0.408
0	0	10.9	36.0	19.0	396.0	0.408
0	0	10.9	36.0	18.7	396.0	0.402
0	0	10.9	36.0	19.0	396.0	0.408
0	0	10.9	36.0	19.0	396.0	0.408
0	0	10.9	36.0	19.0	396.0	0.408

b atch #	bat ch tablet #	desired RPM	desired linear speed [m/s]	punch head flat [mm]	achieved press speed [TPH]	depth of fill [mm]
0	0	10.9	36.0	19.0	396.0	0.408
0	0	5.0	0.107	12.7	41'037	11.3
0	0	5.0	0.107	12.7	41'037	10.8
0	0	5.0	0.107	12.7	40'489	11.1
0	0	5.0	0.107	12.7	41'037	10.6
0	0	5.0	0.107	12.7	41'037	10.5
0	0	5.0	0.107	12.7	41'037	10.5
0	0	5.0	0.107	12.7	41'037	10.5

Appendix IV.3: Calibration/validation folic acid tablets physical parameters

#	Batch	tablet	tablet [mg]	thickness [mm]	Porosity [%]
1	0.0%	1	200.5	2.40	31.10845
2	0.0%	2	200.3	2.39	30.88921
3	0.0%	3	200.4	2.40	31.14281
4	0.0%	4	200.2	2.38	30.63347
5	0.0%	5	200.3	2.38	30.59883
6	0.0%	6	200.6	2.39	30.78570
7	0.0%	7	200.1	2.38	30.66812
8	0.0%	8	200.2	2.38	30.63347
9	0.0%	9	200.2	2.38	30.63347
10	0.0%	10	200.2	2.39	30.92371
11	0.0%	11	200.6	2.39	30.78570
12	0.0%	12	200.5	2.40	31.10845
13	0.0%	13	200.4	2.39	30.85470
14	0.0%	14	200.5	2.39	30.82020
15	0.0%	15	200.6	2.40	31.07409
16	0.0%	16	200.5	2.40	31.10845
17	0.0%	17	200.5	2.39	30.82020
18	0.0%	18	200.3	2.38	30.59883
19	0.0%	19	200.1	2.37	30.37558
20	0.0%	20	200.5	2.39	30.82020
21	0.5%	1	200.0	2.38	30.70277
22	0.5%	2	200.2	2.38	30.63347
23	0.5%	3	200.3	2.39	30.88921
24	0.5%	4	200.4	2.40	31.14281
25	0.5%	5	200.4	2.39	30.85470
26	0.5%	6	200.6	2.39	30.78570
27	0.5%	7	200.2	2.38	30.63347
28	0.5%	8	200.9	2.40	30.97101
29	0.5%	9	200.6	2.39	30.78570
30	0.5%	10	200.5	2.38	30.52953
31	0.5%	11	200.0	2.38	30.70277
32	0.5%	12	200.4	2.39	30.85470
33	0.5%	13	200.9	2.40	30.97101
34	0.5%	14	200.2	2.39	30.92371
35	0.5%	15	200.3	2.39	30.88921
36	0.5%	16	200.8	2.38	30.42558
37	0.5%	17	200.4	2.40	31.14281
38	0.5%	18	201.1	2.40	30.90229
39	0.5%	19	200.5	2.39	30.82020
40	0.5%	20	200.7	2.40	31.03973
41	1.0%	1	200.6	2.39	30.78570
42	1.0%	2	200.0	2.38	30.70277
43	1.0%	3	200.6	2.40	31.07409
44	1.0%	4	201.0	2.41	31.22322

45	1.0%	5	200.8	2.40	31.00537
46	1.0%	6	200.9	2.41	31.25744
47	1.0%	7	200.1	2.39	30.95822
48	1.0%	8	200.2	2.39	30.92371
49	1.0%	9	201.1	2.41	31.18900
50	1.0%	10	200.6	2.39	30.78570
51	1.0%	11	200.5	2.39	30.82020
52	1.0%	12	200.9	2.38	30.39093
53	1.0%	13	200.6	2.39	30.78570
54	1.0%	14	200.6	2.40	31.07409
55	1.0%	15	200.6	2.39	30.78570
56	1.0%	16	200.2	2.38	30.63347
57	1.0%	17	200.6	2.40	31.07409
58	1.0%	18	200.6	2.39	30.78570
59	1.0%	19	200.5	2.39	30.82020
60	1.0%	20	200.8	2.39	30.71669
61	1.5%	1	200.7	2.41	31.32587
62	1.5%	2	200.2	2.39	30.92371
63	1.5%	3	200.5	2.38	30.52953
64	1.5%	4	200.6	2.40	31.07409
65	1.5%	5	201.0	2.40	30.93665
66	1.5%	6	199.9	2.37	30.44517
67	1.5%	7	200.0	2.40	31.28025
68	1.5%	8	200.6	2.38	30.49488
69	1.5%	9	200.4	2.40	31.14281
70	1.5%	10	200.8	2.40	31.00537
71	1.5%	11	200.8	2.40	31.00537
72	1.5%	12	200.7	2.38	30.46023
73	1.5%	13	200.0	2.37	30.41038
74	1.5%	14	200.5	2.38	30.52953
75	1.5%	15	200.6	2.39	30.78570
76	1.5%	16	200.9	2.40	30.97101
77	1.5%	17	200.2	2.38	30.63347
78	1.5%	18	200.3	2.37	30.30599
79	1.5%	19	200.8	2.38	30.42558
80	1.5%	20	200.6	2.39	30.78570
81	2.0%	1	200.2	2.38	30.63347
82	2.0%	2	200.5	2.38	30.52953
83	2.0%	3	200.1	2.39	30.95822
84	2.0%	4	200.3	2.37	30.30599
85	2.0%	5	200.4	2.40	31.14281
86	2.0%	6	200.6	2.40	31.07409
87	2.0%	7	200.1	2.39	30.95822
88	2.0%	8	200.1	2.39	30.95822
89	2.0%	9	200.4	2.39	30.85470
90	2.0%	10	200.8	2.39	30.71669
91	2.0%	11	200.3	2.39	30.88921

92	2.0%	12	200.1	2.38	30.66812
93	2.0%	13	200.8	2.38	30.42558
94	2.0%	14	200.3	2.39	30.88921
95	2.0%	15	200.3	2.39	30.88921
96	2.0%	16	200.5	2.39	30.82020
97	2.0%	17	200.3	2.38	30.59883
98	2.0%	18	200.3	2.38	30.59883
99	2.0%	19	200.3	2.38	30.59883
100	2.0%	20	200.4	2.39	30.85470
101	2.5%	1	200.9	2.39	30.68219
102	2.5%	2	201.1	2.40	30.90229
103	2.5%	3	201.1	2.41	31.18900
104	2.5%	4	201.0	2.38	30.35629
105	2.5%	5	200.9	2.37	30.09723
106	2.5%	6	200.2	2.36	30.04562
107	2.5%	7	201.0	2.40	30.93665
108	2.5%	8	200.4	2.40	31.14281
109	2.5%	9	200.9	2.39	30.68219
110	2.5%	10	200.4	2.41	31.42852
111	2.5%	11	200.3	2.41	31.46274
112	2.5%	12	200.7	2.41	31.32587
113	2.5%	13	201.0	2.40	30.93665
114	2.5%	14	200.6	2.38	30.49488
115	2.5%	15	200.5	2.40	31.10845
116	2.5%	16	200.8	2.39	30.71669
117	2.5%	17	201.0	2.40	30.93665
118	2.5%	18	200.9	2.40	30.97101
119	2.5%	19	200.6	2.40	31.07409
120	2.5%	20	200.5	2.39	30.82020
121	3.0%	1	199.8	2.37	30.47997
122	3.0%	2	200.5	2.39	30.82020
123	3.0%	3	200.1	2.40	31.24589
124	3.0%	4	200.1	2.40	31.24589
125	3.0%	5	200.0	2.37	30.41038
126	3.0%	6	200.6	2.39	30.78570
127	3.0%	7	200.7	2.40	31.03973
128	3.0%	8	200.0	2.37	30.41038
129	3.0%	9	201.0	2.38	30.35629
130	3.0%	10	200.9	2.41	31.25744
131	3.0%	11	200.3	2.38	30.59883
132	3.0%	12	200.8	2.40	31.00537
133	3.0%	13	200.7	2.39	30.75119
134	3.0%	14	200.1	2.37	30.37558
135	3.0%	15	200.6	2.39	30.78570
136	3.0%	16	200.9	2.41	31.25744
137	3.0%	17	200.6	2.39	30.78570
138	3.0%	18	200.4	2.38	30.56418

139	3.0%	19	200.6	2.40	31.07409
140	3.0%	20	200.5	2.40	31.10845
141	3.5%	1	200.4	2.39	30.85470
142	3.5%	2	200.3	2.39	30.88921
143	3.5%	3	200.3	2.39	30.88921
144	3.5%	4	200.8	2.40	31.00537
145	3.5%	5	200.4	2.40	31.14281
146	3.5%	6	200.4	2.39	30.85470
147	3.5%	7	200.8	2.39	30.71669
148	3.5%	8	200.6	2.39	30.78570
149	3.5%	9	200.7	2.39	30.75119
150	3.5%	10	200.7	2.38	30.46023
151	3.5%	11	200.1	2.38	30.66812
152	3.5%	12	200.6	2.40	31.07409
153	3.5%	13	200.2	2.38	30.63347
154	3.5%	14	200.3	2.38	30.59883
155	3.5%	15	200.6	2.40	31.07409
156	3.5%	16	200.6	2.39	30.78570
157	3.5%	17	199.9	2.37	30.44517
158	3.5%	18	200.6	2.40	31.07409
159	3.5%	19	200.9	2.37	30.09723
160	3.5%	20	200.7	2.38	30.46023
161	4.0%	1	200.2	2.38	30.63347
162	4.0%	2	199.8	2.37	30.47997
163	4.0%	3	200.5	2.39	30.82020
164	4.0%	4	200.6	2.40	31.07409
165	4.0%	5	200.5	2.39	30.82020
166	4.0%	6	201.0	2.41	31.22322
167	4.0%	7	200.6	2.39	30.78570
168	4.0%	8	199.8	2.37	30.47997
169	4.0%	9	200.2	2.38	30.63347
170	4.0%	10	200.6	2.39	30.78570
171	4.0%	11	200.4	2.38	30.56418
172	4.0%	12	200.2	2.38	30.63347
173	4.0%	13	200.3	2.39	30.88921
174	4.0%	14	200.1	2.38	30.66812
175	4.0%	15	200.0	2.37	30.41038
176	4.0%	16	200.3	2.38	30.59883
177	4.0%	17	200.1	2.38	30.66812
178	4.0%	18	200.7	2.39	30.75119
179	4.0%	19	200.2	2.38	30.63347
180	4.0%	20	200.5	2.40	31.10845
181	4.5%	1	200.0	2.37	30.41038
182	4.5%	2	200.4	2.38	30.56418
183	4.5%	3	200.1	2.38	30.66812
184	4.5%	4	200.4	2.38	30.56418
185	4.5%	5	200.0	2.37	30.41038

186	4.5%	6	200.9	2.41	31.25744
187	4.5%	7	200.4	2.39	30.85470
188	4.5%	8	200.3	2.38	30.59883
189	4.5%	9	200.2	2.38	30.63347
190	4.5%	10	201.0	2.41	31.22322
191	4.5%	11	200.1	2.38	30.66812
192	4.5%	12	200.5	2.39	30.82020
193	4.5%	13	200.8	2.40	31.00537
194	4.5%	14	200.8	2.40	31.00537
195	4.5%	15	200.6	2.39	30.78570
196	4.5%	16	200.8	2.39	30.71669
197	4.5%	17	200.4	2.38	30.56418
198	4.5%	18	200.3	2.38	30.59883
199	4.5%	19	200.5	2.39	30.82020
200	4.5%	20	200.4	2.38	30.56418
201	5.0%	1	200.0	2.38	30.70277
202	5.0%	2	200.8	2.39	30.71669
203	5.0%	3	200.3	2.38	30.59883
204	5.0%	4	200.3	2.38	30.59883
205	5.0%	5	200.5	2.39	30.82020
206	5.0%	6	201.0	2.41	31.22322
207	5.0%	7	200.4	2.38	30.56418
208	5.0%	8	200.4	2.38	30.56418
209	5.0%	9	200.6	2.38	30.49488
210	5.0%	10	199.8	2.39	31.06173
211	5.0%	11	200.2	2.38	30.63347
212	5.0%	12	200.6	2.39	30.78570
213	5.0%	13	199.7	2.37	30.51476
214	5.0%	14	199.8	2.37	30.47997
215	5.0%	15	200.2	2.38	30.63347
216	5.0%	16	200.2	2.38	30.63347
217	5.0%	17	200.5	2.39	30.82020
218	5.0%	18	200.2	2.38	30.63347
219	5.0%	19	200.5	2.39	30.82020
220	5.0%	20	199.9	2.37	30.44517

Appendix IV.4: UV assay calibration

folic acid in tablet [%]	nominal content [mg]	conc. [g/100ml]	UV A
0.0	0	0.0000	0.002
0.5	1	0.0005	0.119
1.0	2	0.0010	0.234
1.5	3	0.0015	0.343
2.0	4	0.0020	0.456
2.5	5	0.0025	0.581
3.0	6	0.0030	0.724
3.5	7	0.0035	0.839
4.0	8	0.0040	0.947
4.5	9	0.0045	1.071
5.0	10	0.0050	1.186

UV calibration line for folic acid tablets

◆ UV assay
—— Linear (UV assay)
y = 4.217x
$R^2 > 0.999$

folic acid % / 1000 (vertical axis)
absorbance at 235nm (horizontal axis)
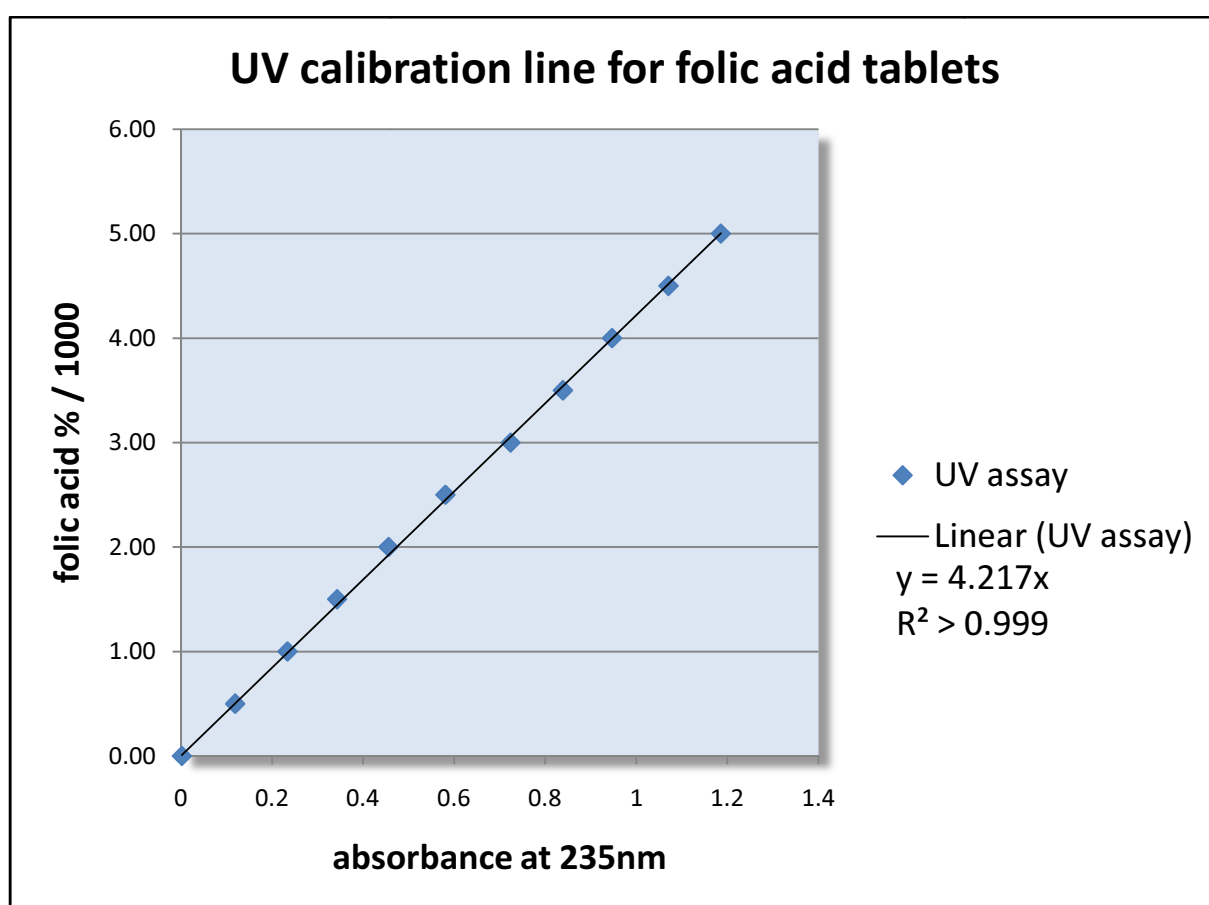
Appendix IV.5: UV assay calibration line for folic acid tablets

Appendix IV.1: UV referencing for calibration / validation folic acid tablets

#	tablet	tablet mass[mg]	UV Abs	nominal [mg]	referenced content [mg]
1	1	200.5	0.00300	0.00000	0.02537
2	2	200.3	0.00200	0.00000	0.01689
3	3	200.4	0.00400	0.00000	0.03381
4	4	200.2	0.00500	0.00000	0.04222
5	5	200.3	0.00500	0.00000	0.04224
6	6	200.6	0.00100	0.00000	0.00846
7	7	200.1	0.00200	0.00000	0.01688
8	8	200.2	0.00600	0.00000	0.05066
9	9	200.2	0.00300	0.00000	0.02533
10	10	200.2	0.00400	0.00000	0.03377
11	11	200.6	0.00300	0.00000	0.02538
12	12	200.5	0.00200	0.00000	0.01691
13	13	200.4	0.00200	0.00000	0.01690
14	14	200.5	0.00100	0.00000	0.00846
15	15	200.6	0.00300	0.00000	0.02538
16	16	200.5	0.00100	0.00000	0.00846
17	17	200.5	0.00200	0.00000	0.01691
18	18	200.3	0.00100	0.00000	0.00845
19	19	200.1	0.00300	0.00000	0.02532
20	20	200.5	0.00100	0.00000	0.00846
21	1	200.0	0.14400	1.00000	1.21460
22	2	200.2	0.15400	1.00000	1.30024
23	3	200.3	0.13400	1.00000	1.13195
24	4	200.4	0.13100	1.00000	1.10716
25	5	200.4	0.14600	1.00000	1.23393
26	6	200.6	0.14700	1.00000	1.24362
27	7	200.2	0.14600	1.00000	1.23270
28	8	200.9	0.11200	1.00000	0.94894
29	9	200.6	0.14000	1.00000	1.18440
30	10	200.5	0.14100	1.00000	1.19227
31	11	200.0	0.14100	1.00000	1.18929
32	12	200.4	0.12900	1.00000	1.09025
33	13	200.9	0.11600	1.00000	0.98283
34	14	200.2	0.11900	1.00000	1.00473
35	15	200.3	0.12200	1.00000	1.03058
36	16	200.8	0.14200	1.00000	1.20252
37	17	200.4	0.11200	1.00000	0.94658
38	18	201.1	0.13400	1.00000	1.13647
39	19	200.5	0.14100	1.00000	1.19227
40	20	200.7	0.12100	1.00000	1.02417
41	1	200.6	0.23500	2.00000	1.98810
42	2	200.0	0.22500	2.00000	1.89781
43	3	200.6	0.25400	2.00000	2.14884
44	4	201.0	0.24300	2.00000	2.05988

#	tablet	tablet mass[mg]	UV Abs	nominal [mg]	referenced content [mg]
45	5	200.8	0.22000	2.00000	1.86306
46	6	200.9	0.22600	2.00000	1.91482
47	7	200.1	0.22400	2.00000	1.89032
48	8	200.2	0.25200	2.00000	2.12767
49	9	201.1	0.25500	2.00000	2.16268
50	10	200.6	0.22200	2.00000	1.87812
51	11	200.5	0.23400	2.00000	1.97865
52	12	200.9	0.22700	2.00000	1.92329
53	13	200.6	0.21000	2.00000	1.77660
54	14	200.6	0.21400	2.00000	1.81044
55	15	200.6	0.25100	2.00000	2.12346
56	16	200.2	0.24100	2.00000	2.03480
57	17	200.6	0.24000	2.00000	2.03040
58	18	200.6	0.20800	2.00000	1.75968
59	19	200.5	0.22300	2.00000	1.88564
60	20	200.8	0.25300	2.00000	2.14252
61	1	200.7	0.31900	3.00000	2.70009
62	2	200.2	0.35600	3.00000	3.00576
63	3	200.5	0.31500	3.00000	2.66357
64	4	200.6	0.33300	3.00000	2.81718
65	5	201.0	0.34400	3.00000	2.91604
66	6	199.9	0.31200	3.00000	2.63031
67	7	200.0	0.33600	3.00000	2.83406
68	8	200.6	0.34100	3.00000	2.88486
69	9	200.4	0.36400	3.00000	3.07637
70	10	200.8	0.33900	3.00000	2.87080
71	11	200.8	0.32600	3.00000	2.76071
72	12	200.7	0.36700	3.00000	3.10637
73	13	200.0	0.37400	3.00000	3.15458
74	14	200.5	0.35100	3.00000	2.96798
75	15	200.6	0.32900	3.00000	2.78334
76	16	200.9	0.33700	3.00000	2.85529
77	17	200.2	0.35500	3.00000	2.99731
78	18	200.3	0.33200	3.00000	2.80452
79	19	200.8	0.31900	3.00000	2.70143
80	20	200.6	0.34300	3.00000	2.90178
81	1	200.2	0.40400	4.00000	3.41103
82	2	200.5	0.46400	4.00000	3.92349
83	3	200.1	0.43400	4.00000	3.66249
84	4	200.3	0.46200	4.00000	3.90268
85	5	200.4	0.46400	4.00000	3.92153
86	6	200.6	0.45000	4.00000	3.80700
87	7	200.1	0.44500	4.00000	3.75532
88	8	200.1	0.41500	4.00000	3.50215
89	9	200.4	0.44800	4.00000	3.78630

#	tablet	tablet mass[mg]	UV Abs	nominal [mg]	referenced content [mg]
90	10	200.8	0.46600	4.00000	3.94629
91	11	200.3	0.45300	4.00000	3.82665
92	12	200.1	0.47400	4.00000	4.00005
93	13	200.8	0.47700	4.00000	4.03945
94	14	200.3	0.42600	4.00000	3.59857
95	15	200.3	0.50300	4.00000	4.24902
96	16	200.5	0.49100	4.00000	4.15179
97	17	200.3	0.44400	4.00000	3.75062
98	18	200.3	0.43600	4.00000	3.68305
99	19	200.3	0.48000	4.00000	4.05473
100	20	200.4	0.46900	4.00000	3.96379
101	1	200.9	0.55500	5.00000	4.70232
102	2	201.1	0.58000	5.00000	4.91903
103	3	201.1	0.59800	5.00000	5.07169
104	4	201.0	0.59400	5.00000	5.03526
105	5	200.9	0.58500	5.00000	4.95650
106	6	200.2	0.54200	5.00000	4.57618
107	7	201.0	0.57500	5.00000	4.87420
108	8	200.4	0.54100	5.00000	4.57230
109	9	200.9	0.61500	5.00000	5.21068
110	10	200.4	0.62700	5.00000	5.29913
111	11	200.3	0.61700	5.00000	5.21202
112	12	200.7	0.56700	5.00000	4.79921
113	13	201.0	0.58600	5.00000	4.96745
114	14	200.6	0.58000	5.00000	4.90680
115	15	200.5	0.63200	5.00000	5.34406
116	16	200.8	0.63100	5.00000	5.34358
117	17	201.0	0.57300	5.00000	4.85725
118	18	200.9	0.57900	5.00000	4.90567
119	19	200.6	0.58700	5.00000	4.96602
120	20	200.5	0.59400	5.00000	5.02274
121	1	199.8	0.76000	6.00000	6.40396
122	2	200.5	0.66000	6.00000	5.58082
123	3	200.1	0.76200	6.00000	6.43046
124	4	200.1	0.64900	6.00000	5.47686
125	5	200.0	0.68100	6.00000	5.74403
126	6	200.6	0.70500	6.00000	5.96430
127	7	200.7	0.69700	6.00000	5.89956
128	8	200.0	0.67500	6.00000	5.69342
129	9	201.0	0.68300	6.00000	5.78970
130	10	200.9	0.74800	6.00000	6.33755
131	11	200.3	0.75600	6.00000	6.38620
132	12	200.8	0.72100	6.00000	6.10574
133	13	200.7	0.68500	6.00000	5.79799
134	14	200.1	0.72700	6.00000	6.13509

#	tablet	tablet mass[mg]	UV Abs	nominal [mg]	referenced content [mg]
135	15	200.6	0.68700	6.00000	5.81202
136	16	200.9	0.72300	6.00000	6.12573
137	17	200.6	0.72500	6.00000	6.13350
138	18	200.4	0.73900	6.00000	6.24571
139	19	200.6	0.74200	6.00000	6.27732
140	20	200.5	0.73800	6.00000	6.24037
141	1	200.4	0.80600	7.00000	6.81196
142	2	200.3	0.81200	7.00000	6.85925
143	3	200.3	0.79400	7.00000	6.70720
144	4	200.8	0.86300	7.00000	7.30826
145	5	200.4	0.79900	7.00000	6.75280
146	6	200.4	0.82200	7.00000	6.94719
147	7	200.8	0.83800	7.00000	7.09655
148	8	200.6	0.86200	7.00000	7.29252
149	9	200.7	0.85500	7.00000	7.23691
150	10	200.7	0.87300	7.00000	7.38927
151	11	200.1	0.80300	7.00000	6.77645
152	12	200.6	0.79300	7.00000	6.70878
153	13	200.2	0.81200	7.00000	6.85583
154	14	200.3	0.87700	7.00000	7.40833
155	15	200.6	0.80500	7.00000	6.81030
156	16	200.6	0.81800	7.00000	6.92028
157	17	199.9	0.83900	7.00000	7.07317
158	18	200.6	0.82700	7.00000	6.99642
159	19	200.9	0.84300	7.00000	7.14245
160	20	200.7	0.81600	7.00000	6.90680
161	1	200.2	0.94400	8.00000	7.97032
162	2	199.8	0.95700	8.00000	8.06394
163	3	200.5	0.93500	8.00000	7.90616
164	4	200.6	0.90600	8.00000	7.66476
165	5	200.5	0.96000	8.00000	8.11756
166	6	201.0	0.91600	8.00000	7.76482
167	7	200.6	0.91300	8.00000	7.72398
168	8	199.8	0.92500	8.00000	7.79430
169	9	200.2	0.94600	8.00000	7.98721
170	10	200.6	0.92200	8.00000	7.80012
171	11	200.4	0.98900	8.00000	8.35860
172	12	200.2	0.98400	8.00000	8.30804
173	13	200.3	0.92500	8.00000	7.81380
174	14	200.1	0.93100	8.00000	7.85663
175	15	200.0	0.92700	8.00000	7.81897
176	16	200.3	0.92100	8.00000	7.78001
177	17	200.1	0.92600	8.00000	7.81444
178	18	200.7	0.94600	8.00000	8.00715
179	19	200.2	0.98500	8.00000	8.31649

#	tablet	tablet mass[mg]	UV Abs	nominal [mg]	referenced content [mg]
180	20	200.5	0.92100	8.00000	7.78778
181	1	200.0	1.07400	9.00000	9.05887
182	2	200.4	1.03100	9.00000	8.71357
183	3	200.1	1.05900	9.00000	8.93681
184	4	200.4	1.05500	9.00000	8.91641
185	5	200.0	1.07000	9.00000	9.02513
186	6	200.9	1.07300	9.00000	9.09116
187	7	200.4	1.07100	9.00000	9.05163
188	8	200.3	1.01300	9.00000	8.55717
189	9	200.2	1.02100	9.00000	8.62044
190	10	201.0	1.07600	9.00000	9.12112
191	11	200.1	1.08400	9.00000	9.14779
192	12	200.5	1.04000	9.00000	8.79402
193	13	200.8	1.05300	9.00000	8.91727
194	14	200.8	1.08700	9.00000	9.20519
195	15	200.6	1.05700	9.00000	8.94222
196	16	200.8	1.08600	9.00000	9.19672
197	17	200.4	1.08200	9.00000	9.14460
198	18	200.3	1.07700	9.00000	9.09780
199	19	200.5	1.06300	9.00000	8.98850
200	20	200.4	1.06800	9.00000	9.02628
201	1	200.0	1.15300	10.00000	9.72521
202	2	200.8	1.18100	10.00000	10.00123
203	3	200.3	1.15300	10.00000	9.73980
204	4	200.3	1.17900	10.00000	9.95943
205	5	200.5	1.12200	10.00000	9.48739
206	6	201.0	1.20000	10.00000	10.17225
207	7	200.4	1.16900	10.00000	9.87988
208	8	200.4	1.18700	10.00000	10.03201
209	9	200.6	1.16900	10.00000	9.88974
210	10	199.8	1.17400	10.00000	9.89244
211	11	200.2	1.18600	10.00000	10.01356
212	12	200.6	1.18400	10.00000	10.01664
213	13	199.7	1.18900	10.00000	10.01382
214	14	199.8	1.13300	10.00000	9.54696
215	15	200.2	1.19700	10.00000	10.10643
216	16	200.2	1.15200	10.00000	9.72649
217	17	200.5	1.17800	10.00000	9.96092
218	18	200.2	1.17600	10.00000	9.92913
219	19	200.5	1.16300	10.00000	9.83408
220	20	199.9	1.15700	10.00000	9.75407
	Average	200.46			
	SD	0.031			
	Max	201.10			
	Min	199.70			

Appendix IV.6: Bulk and tapped volume data

	MCC	Ac-Di-Sol	Mg-stearate
mass [g]	43.75	73.17	22.91
bulk volume [ml]	112	132	96
tapped volume [ml]			
after 10 taps	110	126	94
after 500 taps	96	112	83
after 1250 taps	94	111	76
after 2500 taps			74

Appendix IV.7: Calibration protocol of NIR model A1

Software	NIRCal V5.2 (Build 1000)
Project File Name	folic acid
Project Comment	
Project GUID	{68EA7997-6ACB-4021-9791-F8D94B542C86}P
Calibration Name	A1
Calibration Comment	
Calibration GUID	{073F90A1-75C3-42B7-AB76-F87557A16636}
Calibration Version	0

_____
___

Properties in Project	Folic acid, Folic acid nominal. (total 2/2)
Properties in Calibration Set	Folic acid. (total 1/2)

_____
___

Spectra in Project	220
Spectra in Calibration Set	161
Spectra in Validation Set	59

Spectra in Calibration Set	1-2, 4-5, 7-8, 10-11, 13-14, 16-17, 19-20, 22-23,
	25-26, 28-29, 31-32, 34-35, 37-38, 40-41, 43-44, 46-47,
	49-50, 52-53, 55, 58-62, 64-65, 67-68, 70-71, 73-74, 76-77,
	79-83, 85-86, 88-89, 91-93, 95, 99-106, 109, 112-113,
	115-116, 118-119, 121-122, 124-125, 127-128, 130-131,
	133-134, 136-137, 139-140, 142-143, 145-146, 148-149,
	151-152, 154-155, 157-158, 160-164, 166-167, 169-170,
	172-173, 175-216, 218, 220.

Spectra in Validation Set	3, 6, 9, 12, 15, 18, 21, 24, 27, 30, 33, 36, 39, 42, 45, 48,
	51, 54, 56-57, 63, 66, 69, 72, 75, 78, 84, 87, 90, 94, 96-98,
	107-108, 110-111, 114, 117, 120, 123, 126, 129, 132, 135,
	138, 141, 144, 147, 150, 153, 156, 159, 165, 168, 171,)
	174, 217, 219.

Validation Method	Validation Set

C-Set Spectra	
Instrument type / serial	NIRFlex N500 / 600000281
y-Unit / Measurements / Scans	Transmittance / 1 / 64

V-Set Spectra	
Instrument type / serial	NIRFlex N500 / 600000281

y-Unit / Measurements / Scans	Transmittance / 1 / 64
Spectra Resolution	4 1/cm
Spectra y-Unit	Transmittance
Wavelengths Project Set	6000-11520. (total 1381/1381)
Wavelengths Calibration Set	6000-10600. (total 1151/1381)
Number of Data Pretreatments	2
Data Pretreatment Sequence	db1,nle
Data Pretreatment Sequence	1. First Derivative BCAP
	2. Normalization to Unit Length*,
	6000-10600.
Method	PLS
Max Iterations	3000
Mean Centring	yes
Number of Primary PCs	5
Secondary/Calibration PCs	1-5. (total 5/5)
Blow Up Parameter	
Residual Blow Up	2
Score Blow Up	1.05
Max C-Set Spectra Residual	0.000556
Max Allowed Residual for Calibration	0.001113
_____	
Q-Value V5	0.878166
Validation Method	Validation Set
C-Set Residual too big	0
V-Set Residual too big	0
Num Properties	1
Rel. Consistency	0.000604
Weighted BIAS	0.007186
Validity	0.005527
Comparability	0.002164
Precision	0.027079
Weighted Accuracy	0.088387
_____	
Property Statistics	Folic acid [mg]
C-Set BIAS	0
V-Set BIAS	0.072673
C-Set SEE (SEC)	0.273086
V-Set SEE (SEP)	0.273855
Consistency	99.7192

C-Set Regression Coefficient	0.996637
V-Set Regression Coefficient	0.994473
C-Set Regression Intercept	0.033263
V-Set Regression Intercept	0.063931
C-Set Regression Slope	0.993286
V-Set Regression Slope	0.972477
C-Set Orig. min	0.008435
V-Set Orig. min	1.02903
C-Set Orig. max	10.1216
V-Set Orig. max	9.16008
C-Set Orig. mean	4.954
V-Set Orig. mean	4.96332
C-Set Orig. sdev	3.3327
V-Set Orig. sdev	2.57637
C-Set Pred. min	-0.13916
V-Set Pred. min	0.893304
C-Set Pred. max	10.3353
V-Set Pred. max	9.07157
C-Set Pred. mean	4.954
V-Set Pred. mean	4.89065
C-Set Pred. sdev	3.32149
V-Set Pred. sdev	2.51938
C-Set RSS	11.9321
V-Set RSS	4.6614
C-Set Durbin-Watson	1.86243
C-Set Durbin-Watson in range 1.5 to 2.5	Yes
V-Set Durbin-Watson	1.28254
V-Set Durbin-Watson in range 1.5 to 2.5	No
C-Set Resid. min	-1.32909
V-Set Resid. min	-0.44622
C-Set Resid. max	0.643026
V-Set Resid. max	1.06942
V-Set t-value	2.03836
V-Set t-Test(n-1,2-tail) Confidence [%]	95.3918
C-Set n	161
V-Set n	59

Appendix IV.8: Calibration protocol of NIR model A2

Software	NIRCal V5.2 (Build 3000)
Project File Name	folic acid
Project Comment	
Project GUID	{9A382F82-8E6E-42E7-9C70-AFD3F9B17884}
Calibration Name	A2
Calibration Comment	
Calibration GUID	{DF1DCEDF-3DFA-410F-B9D0-EC5B7E510DCD}
Calibration Version	0

_____

____

Properties in Project	Folic acid, Folic acid nominal. (total 2/2)
Properties in Calibration Set	Folic acid. (total 1/2)

_____

____

Spectra in Project	220
Spectra in Calibration Set	161
Spectra in Validation Set	59

Spectra in Calibration Set	1-2, 4-5, 7-8, 10-11, 13-14, 16-17, 19-20, 22-23, 25-26, 28-29, 31-32, 34-35,
	37-38, 40-41, 43-44, 46-47, 49-50, 52-53, 55-56, 58-59, 61-62, 64-65, 67-68,
	70-71, 73-74, 76-77, 79-80, 82-83, 85, 88-89, 91-95, 97-98, 100-101, 103-104,
	106-107, 109-110, 112-113, 115-116, 118-119, 121-122, 124-125, 127-128, 130-131,
	133-134, 136-137, 139-140, 142-143, 145-146, 148-149, 151-152, 154-155, 157-158,
	160-161, 163-164, 166-167, 169-170, 172-173, 175-218, 220.

Spectra in Validation Set	3, 6, 9, 12, 15, 18, 21, 24, 27, 30, 33, 36, 39, 42, 45, 48, 51, 54, 57, 60, 63,
	66, 69, 72, 75, 78, 81, 84, 86-87, 90, 96, 99, 102, 105, 108, 111, 114, 117,
	120, 123, 126, 129, 132, 135, 138, 141, 144, 147, 150, 153, 156, 159, 162, 165, 168, 171, 174, 219

Validation Method	Validation Set

C-Set Spectra	
Instrument type / serial	NIRFlex N500 / 600000281
y-Unit / Measurements / Scans	Transmittance / 1 / 64
Spectra Resolution	4 1/cm
Spectra y-Unit	Transmittance

_____

____

Wavelengths Project Set	6000-11520. (total 1381/1381)
Wavelengths Calibration Set	8500-10600. (total 526/1381)
Number of Data Pretreatments	3
Data Pretreatment Sequence	ncl,db1,SNV
Data Pretreatment Sequence	1. Normalization by Closure*, 6000-11520.
	2. First Derivative BCAP
	3. SNV Standard Normal Variate*, 8500-10600.
Method	PLS
Max Iterations	3000
Mean Centring	yes
Number of Primary PCs	4
Secondary/Calibration PCs	1-4. (total 4/4)
Blow Up Parameter	
Residual Blow Up	2
Score Blow Up	1.05
Max C-Set Spectra Residual	0.019124
Max Allowed Residual for Calibration	0.038248

_____

____

Q-Value V5	0.876954
Validation Method	Validation Set
C-Set Residual too big	0
V-Set Residual too big	0
Num Properties	1
Rel. Consistency	0.003751
Weighted BIAS	0.00206
Validity	0.00645
Comparability	0.002509
Precision	0.028773
Weighted Accuracy	0.090958

_____

Property Statistics	Folic acid [mg]
C-Set BIAS	0
V-Set BIAS	0.02083
C-Set SEE (SEC)	0.295844
V-Set SEE (SEP)	0.290983
Consistency	101.67
C-Set Regression Coefficient	0.996059
V-Set Regression Coefficient	0.99355
C-Set Regression Intercept	0.039039

V-Set Regression Intercept	0.035007
C-Set Regression Slope	0.992134
V-Set Regression Slope	0.988696
C-Set Pred. min	-0.08475
V-Set Pred. min	0.880036
C-Set Pred. max	10.6774
V-Set Pred. max	9.42144
C-Set Pred. mean	4.96275
V-Set Pred. mean	4.91862
C-Set Pred. sdev	3.32248
V-Set Pred. sdev	2.55331
C-Set RSS	14.0038
V-Set RSS	4.93652
C-Set Durbin-Watson	1.97961
C-Set Durbin-Watson in range 1.5 to 2.5	Yes
V-Set Durbin-Watson	1.63596
V-Set Durbin-Watson in range 1.5 to 2.5	Yes
C-Set Resid. min	-1.69417
V-Set Resid. min	-0.86411
C-Set Resid. max	0.786573
V-Set Resid. max	1.02183
V-Set t-value	0.549857
V-Set t-Test(n-1,2-tail) Confidence [%]	41.5471
C-Set n	161
V-Set n	59

Appendix IV.9: Calibration protocol of NIR model A3

Software	NIRCal V5.2 (Build 3000)
Project File Name	folic acid
Project Comment	
Project GUID	{9A382F82-8E6E-42E7-9C70-AFD3F9B17884}
Calibration Name	A3
Calibration Comment	
Calibration GUID	{DF1DCEDF-3DFA-410F-B9D0-EC5B7E510DCD}
Calibration Version	1

_____

Properties in Project	Folic acid, Folic acid nominal. (total 2/2)
Properties in Calibration Set	Folic acid. (total 1/2)

_____

Spectra in Project	220
Spectra in Calibration Set	160
Spectra in Validation Set	59

Spectra in Calibration Set	1-2, 4-5, 7-8, 10-11, 13-14, 16-17, 19-20, 22-23, 25-26, 28-29, 31-32, 34-35,
	37-38, 40-41, 43-44, 46-47, 49-50, 52-53, 55-56, 58-59, 61-62, 64-65, 67-68,
	70-71, 73-74, 76-77, 79-80, 82-83, 85, 88-89, 91-92, 94-95, 97-98, 100-101, 103-104, 106-107, 109-110, 112-113, 115-116, 118-119, 121-122, 124-125, 127-128,
	130-131, 133-134, 136-137, 139-140, 142-143, 145-146, 148-149, 151-152, 154-155,
	157-158, 160-161, 163-164, 166-167, 169-170, 172-173, 175-218, 220.
Spectra in Validation Set	3, 6, 9, 12, 15, 18, 21, 24, 27, 30, 33, 36, 39, 42, 45, 48, 51, 54, 57, 60, 63, 66, 69, 72, 75, 78, 81, 84, 86-87, 90, 96, 99, 102, 105, 108, 111, 114, 117,
	120, 123, 126, 129, 132, 135, 138, 141, 144, 147, 150, 153, 156, 159, 162, 165,
	168, 171, 174, 219.
Validation Method	Validation Set
C-Set Spectra	
Instrument type / serial	NIRFlex N500 / 600000281
y-Unit / Measurements / Scans	Transmittance / 1 / 64
V-Set Spectra	
Instrument type / serial	NIRFlex N500 / 600000281
y-Unit / Measurements / Scans	Transmittance / 1 / 64
Spectra Resolution	4 1/cm
Spectra y-Unit	Transmittance

_____

Wavelengths Project Set	6000-11520. (total 1381/1381)
Wavelengths Calibration Set	8876-9216, 10488-10724. (total 146/1381)
Number of Data Pretreatments	1
Data Pretreatment Sequence	nsd
Data Pretreatment Sequence	1. Normalization by Sdev*, 6000-11520.
Method	PLS
Max Iterations	3000
Mean Centring	yes
Number of Primary PCs	8
Secondary/Calibration PCs	1-8. (total 8/8)
Blow Up Parameter	
Residual Blow Up	2
Score Blow Up	1.05
Max C-Set Spectra Residual	0.000995
Max Allowed Residual for Calibration	0.00199

_____

Q-Value V5	0.861954
Validation Method	Validation Set
C-Set Residual too big	0
V-Set Residual too big	0
Num Properties	1
Rel. Consistency	0.001525
Weighted BIAS	0.002738
Validity	0.008658
Comparability	0.003589
Precision	0.033474
Weighted Accuracy	0.105905

_____

Property Statistics	Folic acid [mg]
C-Set BIAS	0
V-Set BIAS	0.027694
C-Set SEE (SEC)	0.336494
V-Set SEE (SEP)	0.338533
Consistency	99.3978
C-Set Regression Coefficient	0.994931
V-Set Regression Coefficient	0.991342
C-Set Regression Intercept	0.050189
V-Set Regression Intercept	-0.00555

C-Set Regression Slope	0.989887
V-Set Regression Slope	0.995517
C-Set Orig. min	0.008435
V-Set Orig. min	1.02903
C-Set Orig. max	10.1216
V-Set Orig. max	9.16008
C-Set Orig. mean	4.96287
V-Set Orig. mean	4.93945
C-Set Orig. sdev	3.34609
V-Set Orig. sdev	2.56585
C-Set Pred. min	-0.07869
V-Set Pred. min	0.80691
C-Set Pred. max	11.5259
V-Set Pred. max	9.73067
C-Set Pred. mean	4.96287
V-Set Pred. mean	4.91175
C-Set Pred. sdev	3.32913
V-Set Pred. sdev	2.57666
C-Set RSS	18.0033
V-Set RSS	6.69232
C-Set Durbin-Watson	1.50282
C-Set Durbin-Watson in range 1.5 to 2.5	Yes
V-Set Durbin-Watson	1.69863
V-Set Durbin-Watson in range 1.5 to 2.5	Yes
C-Set Resid. min	-1.42957
V-Set Resid. min	-1.11547
C-Set Resid. max	0.798551
V-Set Resid. max	0.904472
V-Set t-value	0.628364
V-Set t-Test(n-1,2-tail) Confidence [%]	46.7768
C-Set n	160
V-Set n	59

16. Appendix V

Appendix V.1: Porosity and thickness outlier folic acid tablets

Batch	No.	Gap size [mm]	Upper force [kN]	Mass [mg]	Thickness [mm]	Volume [cm³]	Porosity [%]	UV Content
0.0%	1	1.00	12.87	199.30	1.98	0.1555	16.97	0.0000
0.0%	2	1.00	13.44	204.90	2.02	0.1590	16.53	0.0000
0.0%	3	1.10	10.49	196.40	2.02	0.1586	19.78	0.0000
0.0%	4	1.10	10.07	200.00	2.05	0.1608	19.46	0.0000
0.0%	5	1.20	9.52	200.20	2.11	0.1659	21.83	0.0000
0.0%	6	1.20	8.40	198.50	2.10	0.1648	21.99	0.0000
0.0%	7	1.30	7.94	199.10	2.17	0.1701	24.20	0.0000
0.0%	8	1.30	7.96	202.50	2.19	0.1722	23.86	0.0000
0.0%	9	1.40	7.47	198.20	2.22	0.1745	26.42	0.0000
0.0%	10	1.40	7.58	205.00	2.28	0.1787	25.72	0.0000
0.0%	11	1.50	6.65	196.70	2.27	0.1785	28.61	0.0000
0.0%	12	1.50	6.02	197.30	2.28	0.1788	28.54	0.0000
0.0%	13	1.60	4.00	203.00	2.39	0.1873	29.82	0.0000
0.0%	14	1.60	4.13	201.50	2.37	0.1864	29.98	0.0000
0.0%	15	1.70	4.31	198.00	2.41	0.1891	32.19	0.0000
0.0%	16	1.70	5.21	198.10	2.41	0.1892	32.18	0.0000
0.0%	17	1.80	3.23	200.80	2.49	0.1958	33.58	0.0000
0.0%	18	1.80	3.33	195.20	2.45	0.1923	34.25	0.0000
0.0%	19	1.90	3.91	203.70	2.58	0.2025	34.86	0.0000
0.0%	20	1.90	3.72	200.90	2.56	0.2008	35.20	0.0000
0.5%	1	1.00	12.03	202.50	2.01	0.1575	16.71	1.0125
0.5%	2	1.00	12.24	196.90	1.96	0.1540	17.17	0.9845
0.5%	3	1.10	11.35	204.50	2.08	0.1637	19.07	1.0225
0.5%	4	1.10	10.86	204.60	2.08	0.1637	19.06	1.0230
0.5%	5	1.20	10.20	203.00	2.13	0.1676	21.57	1.0150
0.5%	6	1.20	10.19	201.50	2.12	0.1667	21.71	1.0075
0.5%	7	1.30	8.98	200.20	2.17	0.1708	24.09	1.0010
0.5%	8	1.30	7.57	203.80	2.20	0.1731	23.73	1.0190
0.5%	9	1.40	6.74	200.50	2.24	0.1759	26.18	1.0025
0.5%	10	1.40	6.77	197.70	2.22	0.1742	26.48	0.9885
0.5%	11	1.50	5.04	193.80	2.25	0.1766	28.94	0.9690
0.5%	12	1.50	6.54	198.70	2.29	0.1797	28.39	0.9935
0.5%	13	1.60	4.93	191.70	2.29	0.1802	31.11	0.9585
0.5%	14	1.60	4.55	193.60	2.31	0.1814	30.89	0.9680
0.5%	15	1.70	4.58	195.50	2.39	0.1875	32.49	0.9775
0.5%	16	1.70	3.77	192.50	2.36	0.1857	32.85	0.9625
0.5%	17	1.80	4.59	194.80	2.45	0.1920	34.30	0.9740

Batch	No.	Gap size [mm]	Upper force [kN]	Mass [mg]	Thickness [mm]	Volume [cm³]	Porosity [%]	UV Content
0.5%	18	1.80	4.63	193.40	2.43	0.1912	34.47	0.9670
0.5%	19	1.90	3.11	197.00	2.53	0.1983	35.67	0.9850
0.5%	20	1.90	4.20	196.10	2.52	0.1978	35.78	0.9805
1.0%	1	1.00	11.76	202.40	2.00	0.1574	16.72	2.0240
1.0%	2	1.00	13.04	202.30	2.00	0.1573	16.73	2.0230
1.0%	3	1.10	11.51	201.60	2.06	0.1618	19.32	2.0160
1.0%	4	1.10	11.16	202.00	2.06	0.1621	19.28	2.0200
1.0%	5	1.20	10.18	200.40	2.11	0.1660	21.81	2.0040
1.0%	6	1.20	9.33	199.60	2.11	0.1655	21.89	1.9960
1.0%	7	1.30	8.54	198.90	2.16	0.1700	24.22	1.9890
1.0%	8	1.30	8.67	194.40	2.13	0.1672	24.68	1.9440
1.0%	9	1.40	6.38	197.50	2.22	0.1740	26.50	1.9750
1.0%	10	1.40	7.05	197.30	2.21	0.1739	26.52	1.9730
1.0%	11	1.50	5.34	204.30	2.33	0.1832	27.78	2.0430
1.0%	12	1.50	6.17	203.00	2.32	0.1824	27.92	2.0300
1.0%	13	1.60	3.93	197.40	2.34	0.1838	30.45	1.9740
1.0%	14	1.60	4.64	198.30	2.35	0.1844	30.34	1.9830
1.0%	15	1.70	4.86	196.60	2.40	0.1882	32.36	1.9660
1.0%	16	1.70	5.16	198.70	2.41	0.1896	32.11	1.9870
1.0%	17	1.80	4.32	189.90	2.41	0.1890	34.91	1.8990
1.0%	18	1.80	2.96	190.80	2.41	0.1895	34.79	1.9080
1.0%	19	1.90	4.26	193.90	2.50	0.1964	36.05	1.9390
1.0%	20	1.90	2.57	191.80	2.48	0.1951	36.32	1.9180
1.5%	1	1.00	11.88	213.60	2.09	0.1644	15.87	3.2040
1.5%	2	1.00	12.98	210.70	2.07	0.1626	16.09	3.1605
1.5%	3	1.10	11.79	206.30	2.10	0.1648	18.92	3.0945
1.5%	4	1.10	11.43	208.90	2.12	0.1664	18.70	3.1335
1.5%	5	1.20	8.75	209.40	2.19	0.1717	20.99	3.1410
1.5%	6	1.20	10.15	207.90	2.17	0.1707	21.13	3.1185
1.5%	7	1.30	7.17	206.40	2.22	0.1747	23.48	3.0960
1.5%	8	1.30	7.68	205.90	2.22	0.1744	23.53	3.0885
1.5%	9	1.40	6.70	203.00	2.26	0.1775	25.92	3.0450
1.5%	10	1.40	6.08	203.30	2.26	0.1777	25.89	3.0495
1.5%	11	1.50	5.58	201.60	2.31	0.1815	28.07	3.0240
1.5%	12	1.50	6.46	203.90	2.33	0.1830	27.83	3.0585
1.5%	13	1.60	5.19	200.00	2.36	0.1854	30.15	3.0000
1.5%	14	1.60	5.42	201.70	2.37	0.1865	29.96	3.0255
1.5%	15	1.70	3.63	197.90	2.41	0.1891	32.20	2.9685
1.5%	16	1.70	4.93	195.60	2.39	0.1876	32.47	2.9340
1.5%	17	1.80	2.99	199.30	2.48	0.1949	33.76	2.9895
1.5%	18	1.80	4.32	203.70	2.52	0.1976	33.24	3.0555
1.5%	19	1.90	2.84	189.00	2.46	0.1933	36.68	2.8350
1.5%	20	1.90	3.93	192.70	2.49	0.1956	36.20	2.8905

Batch	No.	Gap size [mm]	Upper force [kN]	Mass [mg]	Thickness [mm]	Volume [cm³]	Porosity [%]	UV Content
2.0%	1	1.00	12.12	207.40	2.04	0.1606	16.33	4.1480
2.0%	2	1.00	12.05	206.70	2.04	0.1601	16.39	4.1340
2.0%	3	1.10	11.93	203.80	2.08	0.1632	19.13	4.0760
2.0%	4	1.10	11.69	203.70	2.08	0.1632	19.14	4.0740
2.0%	5	1.20	8.88	204.20	2.14	0.1684	21.46	4.0840
2.0%	6	1.20	9.50	204.40	2.15	0.1685	21.44	4.0880
2.0%	7	1.30	7.19	203.70	2.20	0.1730	23.74	4.0740
2.0%	8	1.30	7.37	204.00	2.21	0.1732	23.71	4.0800
2.0%	9	1.40	5.94	204.00	2.27	0.1781	25.82	4.0800
2.0%	10	1.40	5.83	202.40	2.26	0.1771	25.98	4.0480
2.0%	11	1.50	5.81	198.40	2.29	0.1795	28.42	3.9680
2.0%	12	1.50	4.81	197.10	2.28	0.1787	28.57	3.9420
2.0%	13	1.60	4.45	198.90	2.35	0.1848	30.28	3.9780
2.0%	14	1.60	4.60	197.40	2.34	0.1838	30.45	3.9480
2.0%	15	1.70	3.58	207.30	2.48	0.1950	31.13	4.1460
2.0%	16	1.70	5.14	206.60	2.48	0.1945	31.21	4.1320
2.0%	17	1.80	4.63	201.80	2.50	0.1964	33.46	4.0360
2.0%	18	1.80	4.23	198.50	2.47	0.1944	33.85	3.9700
2.0%	19	1.90	2.87	195.20	2.51	0.1972	35.89	3.9040
2.0%	20	1.90	4.02	191.80	2.48	0.1951	36.32	3.8360
2.5%	1	1.00	12.48	202.00	2.00	0.1572	16.75	6.0338
2.5%	2	1.00	12.74	200.20	1.99	0.1560	16.90	5.6306
2.5%	3	1.10	10.15	198.20	2.03	0.1597	19.62	5.6361
2.5%	4	1.10	11.78	196.10	2.02	0.1584	19.81	5.3084
2.5%	5	1.20	9.35	198.00	2.09	0.1645	22.04	5.3442
2.5%	6	1.20	9.70	200.60	2.12	0.1661	21.79	4.8061
2.5%	7	1.30	8.95	195.90	2.14	0.1681	24.52	4.9318
2.5%	8	1.30	7.65	201.10	2.18	0.1714	24.00	4.9550
2.5%	9	1.40	7.54	195.90	2.20	0.1730	26.67	5.1005
2.5%	10	1.40	6.83	197.60	2.22	0.1741	26.49	5.2911
2.5%	11	1.50	6.51	200.50	2.30	0.1808	28.19	4.5771
2.5%	12	1.50	4.85	199.70	2.30	0.1803	28.28	4.5889
2.5%	13	1.60	4.47	203.20	2.39	0.1875	29.79	4.6009
2.5%	14	1.60	5.48	198.00	2.35	0.1842	30.38	5.0326
2.5%	15	1.70	4.36	201.50	2.44	0.1913	31.79	4.7504
2.5%	16	1.70	3.38	203.30	2.45	0.1924	31.58	5.0950
2.5%	17	1.80	4.02	197.70	2.47	0.1939	33.95	4.8643
2.5%	18	1.80	3.23	197.20	2.46	0.1935	34.01	4.9474
2.5%	19	1.90	2.59	204.20	2.58	0.2029	34.81	4.9098
2.5%	20	1.90	4.35	201.20	2.56	0.2010	35.16	4.8904
3.0%	1	1.00	13.19	201.70	2.00	0.1570	16.78	4.7589
3.0%	2	1.00	12.78	202.50	2.01	0.1575	16.71	5.5332

Batch	No.	Gap size [mm]	Upper force [kN]	Mass [mg]	Thickness [mm]	Volume [cm³]	Porosity [%]	UV Content
3.0%	3	1.10	10.05	203.90	2.08	0.1633	19.12	5.7137
3.0%	4	1.10	10.58	204.90	2.09	0.1639	19.03	5.9321
3.0%	5	1.20	10.26	208.50	2.18	0.1711	21.07	6.3522
3.0%	6	1.20	9.61	202.50	2.13	0.1673	21.62	5.7970
3.0%	7	1.30	8.09	205.40	2.22	0.1741	23.58	5.9251
3.0%	8	1.30	7.99	202.00	2.19	0.1719	23.91	5.5902
3.0%	9	1.40	6.67	203.60	2.26	0.1779	25.86	6.0681
3.0%	10	1.40	7.19	197.70	2.22	0.1742	26.48	5.8722
3.0%	11	1.50	5.71	202.60	2.32	0.1822	27.96	7.3678
3.0%	12	1.50	5.13	203.40	2.33	0.1827	27.88	6.7621
3.0%	13	1.60	5.16	202.30	2.38	0.1869	29.89	5.9944
3.0%	14	1.60	4.84	200.90	2.37	0.1860	30.05	6.0639
3.0%	15	1.70	4.01	198.40	2.41	0.1894	32.14	5.5717
3.0%	16	1.70	5.00	200.90	2.43	0.1909	31.85	5.8893
3.0%	17	1.80	3.42	201.50	2.50	0.1962	33.50	6.0658
3.0%	18	1.80	3.87	196.20	2.46	0.1929	34.13	5.9427
3.0%	19	1.90	2.49	198.00	2.53	0.1990	35.55	6.0381
3.0%	20	1.90	3.52	194.30	2.50	0.1966	36.00	5.7991
3.5%	1	1.00	12.76	204.40	2.02	0.1587	16.56	7.1540
3.5%	2	1.00	13.47	203.30	2.01	0.1580	16.65	7.1155
3.5%	3	1.10	11.46	208.40	2.11	0.1661	18.74	7.2940
3.5%	4	1.10	11.55	206.30	2.10	0.1648	18.92	7.2205
3.5%	5	1.20	8.54	207.60	2.17	0.1705	21.15	7.2660
3.5%	6	1.20	9.55	202.10	2.13	0.1671	21.65	7.0735
3.5%	7	1.30	7.07	206.50	2.23	0.1748	23.47	7.2275
3.5%	8	1.30	7.93	200.70	2.18	0.1711	24.04	7.0245
3.5%	9	1.40	7.77	209.90	2.32	0.1818	25.23	7.3465
3.5%	10	1.40	7.13	197.50	2.22	0.1740	26.50	6.9125
3.5%	11	1.50	6.19	200.50	2.30	0.1808	28.19	7.0175
3.5%	12	1.50	6.07	202.20	2.32	0.1819	28.01	7.0770
3.5%	13	1.60	4.30	202.70	2.38	0.1871	29.85	7.0945
3.5%	14	1.60	4.80	201.50	2.37	0.1864	29.98	7.0525
3.5%	15	1.70	4.15	200.60	2.43	0.1907	31.89	7.0210
3.5%	16	1.70	3.68	203.00	2.45	0.1923	31.61	7.1050
3.5%	17	1.80	4.50	206.80	2.54	0.1996	32.89	7.2380
3.5%	18	1.80	2.79	198.50	2.47	0.1944	33.85	6.9475
3.5%	19	1.90	2.60	194.40	2.50	0.1967	35.99	6.8040
3.5%	20	1.90	2.77	194.30	2.50	0.1966	36.00	6.8005
4.0%	1	1.00	12.27	194.40	1.94	0.1524	17.37	7.7760
4.0%	2	1.00	12.20	197.40	1.96	0.1543	17.12	7.8960
4.0%	3	1.10	11.85	206.40	2.10	0.1648	18.91	8.2560
4.0%	4	1.10	11.11	197.50	2.03	0.1593	19.68	7.9000
4.0%	5	1.20	10.19	204.60	2.15	0.1686	21.42	8.1840

Batch	No.	Gap size [mm]	Upper force [kN]	Mass [mg]	Thickness [mm]	Volume [cm³]	Porosity [%]	UV Content
4.0%	6	1.20	10.24	196.60	2.08	0.1636	22.18	7.8640
4.0%	7	1.30	7.89	200.20	2.17	0.1708	24.09	8.0080
4.0%	8	1.30	8.23	201.50	2.19	0.1716	23.96	8.0600
4.0%	9	1.40	7.02	202.20	2.25	0.1770	26.00	8.0880
4.0%	10	1.40	7.53	205.60	2.28	0.1791	25.66	8.2240
4.0%	11	1.50	6.35	202.00	2.31	0.1818	28.03	8.0800
4.0%	12	1.50	5.25	203.50	2.33	0.1827	27.87	8.1400
4.0%	13	1.60	4.78	201.10	2.37	0.1861	30.03	8.0440
4.0%	14	1.60	5.18	197.70	2.34	0.1840	30.41	7.9080
4.0%	15	1.70	3.92	198.10	2.41	0.1892	32.18	7.9240
4.0%	16	1.70	3.83	201.20	2.43	0.1911	31.82	8.0480
4.0%	17	1.80	3.20	195.80	2.45	0.1927	34.18	7.8320
4.0%	18	1.80	4.36	194.20	2.44	0.1917	34.37	7.7680
4.0%	19	1.90	2.98	197.30	2.53	0.1985	35.63	7.8920
4.0%	20	1.90	2.44	196.90	2.52	0.1983	35.68	7.8760
4.5%	1	1.00	13.16	200.10	1.99	0.1560	16.91	9.0045
4.5%	2	1.00	12.76	202.30	2.00	0.1573	16.73	9.1035
4.5%	3	1.10	9.95	201.40	2.06	0.1617	19.33	9.0630
4.5%	4	1.10	10.47	203.00	2.07	0.1627	19.20	9.1350
4.5%	5	1.20	10.19	203.80	2.14	0.1681	21.50	9.1710
4.5%	6	1.20	8.94	202.20	2.13	0.1671	21.64	9.0990
4.5%	7	1.30	8.26	203.10	2.20	0.1726	23.80	9.1395
4.5%	8	1.30	8.66	197.70	2.15	0.1692	24.34	8.8965
4.5%	9	1.40	7.17	201.00	2.24	0.1762	26.13	9.0450
4.5%	10	1.40	7.11	199.80	2.23	0.1755	26.25	8.9910
4.5%	11	1.50	6.40	200.20	2.30	0.1806	28.22	9.0090
4.5%	12	1.50	5.19	203.80	2.33	0.1829	27.84	9.1710
4.5%	13	1.60	5.30	199.50	2.36	0.1851	30.21	8.9775
4.5%	14	1.60	4.21	202.50	2.38	0.1870	29.87	9.1125
4.5%	15	1.70	4.11	201.90	2.44	0.1916	31.74	9.0855
4.5%	16	1.70	3.43	199.60	2.42	0.1901	32.00	8.9820
4.5%	17	1.80	4.35	200.60	2.49	0.1957	33.60	9.0270
4.5%	18	1.80	4.50	201.60	2.50	0.1963	33.49	9.0720
4.5%	19	1.90	2.49	193.80	2.50	0.1963	36.07	8.7210
4.5%	20	1.90	2.78	198.30	2.54	0.1992	35.51	8.9235
5.0%	1	1.00	12.46	201.60	2.00	0.1569	16.79	10.0800
5.0%	2	1.00	13.11	201.90	2.00	0.1571	16.76	10.0950
5.0%	3	1.10	10.59	204.80	2.09	0.1638	19.04	10.2400
5.0%	4	1.10	10.22	200.90	2.05	0.1614	19.38	10.0450
5.0%	5	1.20	8.97	200.30	2.11	0.1659	21.82	10.0150
5.0%	6	1.20	10.23	202.30	2.13	0.1672	21.63	10.1150
5.0%	7	1.30	7.02	198.70	2.16	0.1699	24.24	9.9350
5.0%	8	1.30	8.72	201.10	2.18	0.1714	24.00	10.0550

Batch	No.	Gap size [mm]	Upper force [kN]	Mass [mg]	Thickness [mm]	Volume [cm³]	Porosity [%]	UV Content
5.0%	9	1.40	6.67	201.70	2.25	0.1767	26.06	10.0850
5.0%	10	1.40	6.50	200.00	2.24	0.1756	26.23	10.0000
5.0%	11	1.50	5.65	200.30	2.30	0.1807	28.21	10.0150
5.0%	12	1.50	6.52	202.00	2.31	0.1818	28.03	10.1000
5.0%	13	1.60	5.22	199.40	2.36	0.1851	30.22	9.9700
5.0%	14	1.60	5.48	194.60	2.32	0.1821	30.77	9.7300
5.0%	15	1.70	3.93	195.00	2.38	0.1872	32.55	9.7500
5.0%	16	1.70	3.62	194.30	2.38	0.1868	32.63	9.7150
5.0%	17	1.80	3.37	199.70	2.48	0.1951	33.71	9.9850
5.0%	18	1.80	3.85	198.00	2.47	0.1940	33.91	9.9000
5.0%	19	1.90	3.92	207.20	2.61	0.2047	34.46	10.3600
5.0%	20	1.90	2.82	206.90	2.60	0.2046	34.49	10.3450

Appendix V.2: Variable porosity and thickness folic acid tablets external prediction batch

#	mass [mg]	thickness [mm]	porosity	UV content [mg]
1	204.5	1.99	18.67%	5.1125
2	206.7	2.00	19.42%	5.1675
3	200.2	2.00	20.18%	5.0050
4	199.8	2.00	21.43%	4.9950
5	204.0	2.07	22.69%	5.1000
6	205.7	2.08	23.33%	5.1425
7	200.8	2.10	23.98%	5.0200
8	200.0	2.11	25.51%	5.0000
9	202.2	2.20	27.04%	5.0550
10	205.7	2.20	27.88%	5.1425
11	196.0	2.22	28.71%	4.9000
12	203.7	2.28	29.96%	5.0925
13	199.2	2.31	31.21%	4.9800
14	199.0	2.30	32.16%	4.9750
15	194.5	2.37	33.10%	4.8625
16	200.9	2.39	34.27%	5.0225
17	198.7	2.45	35.43%	4.9675
18	202.2	2.47	36.23%	5.0550
19	198.9	2.53	37.03%	4.9725
20	194.7	2.55	37.50%	4.8675

17. Appendix VI

Appendix VI.1: Printed paper filters (exact experimental size)
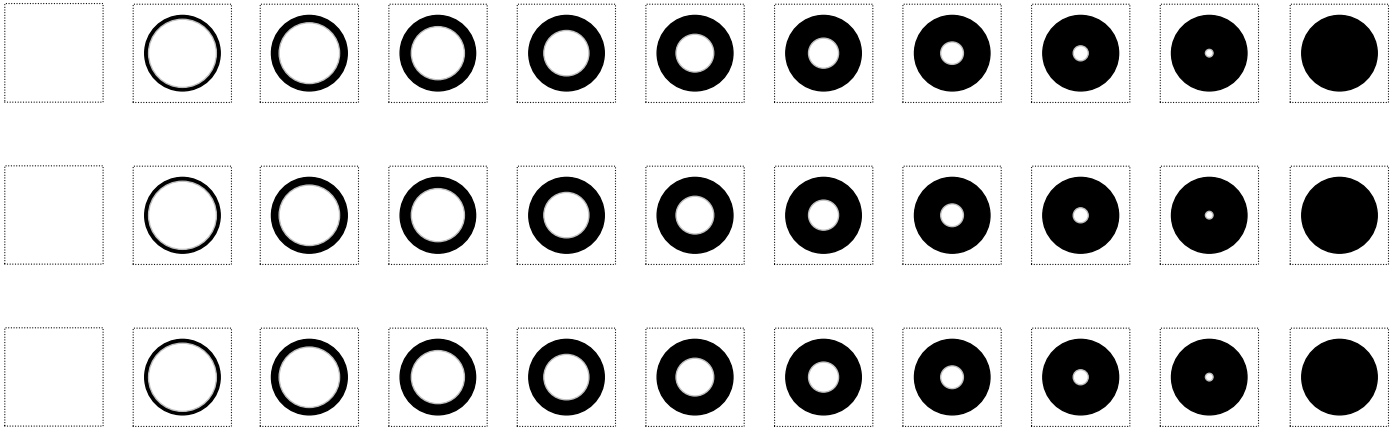
Appendix VI.2: Tableting data of DT sampling span tablets

#	Gap size [mm]	Upper force [kN]	Weight [mg]	Thickness [mm]	Volume [cm³]	Porosity [%]
1	1.00	12.40	199.77	1.95	**0.1532**	15.52
2	1.10	11.82	202.65	2.01	**0.1579**	16.86
3	1.20	9.24	204.73	2.11	**0.1657**	19.99
4	1.30	8.79	202.64	2.16	**0.1696**	22.64
5	1.40	6.11	204.55	2.26	**0.1775**	25.36

Appendix VI.3: DT data at 8880 cm^{-1} for 5 tablets and all filters. A, B and C represent 3 measurements for the same filter type, (Fx).

	Transmittance (non-pretreated)				
	15.52%	16.86%	19.99%	22.64%	25.36%
F0					
A	0.000594	0.000465	0.00039	0.000289	0.000251
B	0.0005987	0.0004728	0.000397	0.000296	0.000255
C	0.0005893	0.0004572	0.000383	0.000282	0.000247
F1					
A	0.000605	0.000429	0.000369	0.000287	0.000242
B	0.0006097	0.0004368	0.000376	0.000294	0.000246
C	0.0006003	0.0004212	0.000362	0.00028	0.000238
F2					
A	0.000582	0.000432	0.000364	0.000275	0.000228
B	0.0005867	0.0004398	0.000371	0.000282	0.000232
C	0.0005773	0.0004242	0.000357	0.000268	0.000224
F3					
A	0.00057	0.000449	0.000374	0.000291	0.00024
B	0.0005747	0.0004568	0.000381	0.000298	0.000244
C	0.0005653	0.0004412	0.000367	0.000284	0.000236
F4					
A	0.000528	0.000425	0.00037	0.000274	0.000229
B	0.0005327	0.0004328	0.000377	0.000281	0.000233
C	0.0005233	0.0004172	0.000363	0.000267	0.000225
F5					
A	0.000498	0.000387	0.000337	0.000236	0.000212
B	0.0005027	0.0003948	0.000344	0.000243	0.000216
C	0.0004933	0.0003792	0.00033	0.000229	0.000208
F6					
A	0.000385	0.000311	0.000263	0.000178	0.000162
B	0.0003897	0.0003188	0.00027	0.000185	0.000166
C	0.0003803	0.0003032	0.000256	0.000171	0.000158
F7					
A	0.000326	0.000261	0.00017	0.00016	0.000143
B	0.0003307	0.0002688	0.000177	0.000167	0.000147
C	0.0003213	0.0002532	0.000163	0.000153	0.000139
F8					
A	0.000199	0.000166	0.000104	0.000088	0.000085
B	0.0002037	0.0001738	0.000111	9.47E-05	8.93E-05
C	0.0001943	0.0001582	9.73E-05	8.13E-05	8.07E-05
F9					
A	0.000116	0.000083	0.000077	0.00006	0.000047
B	0.0001207	0.0000908	8.37E-05	6.67E-05	5.13E-05
C	0.0001113	0.0000752	7.03E-05	5.33E-05	4.27E-05
F10					

A	0.00007	0.00005	0.000044	0.000034	0.00003
B	0.0000747	0.0000578	5.07E-05	4.07E-05	3.43E-05
C	0.0000653	0.0000422	3.73E-05	2.73E-05	2.57E-05

18. Appendix VII

Appendix VII.1: Incremental thickness tableting data (Zwick)

Nominal thickness [mm]	Powder mass [mg]	Calculated force [N]	Achieved force [N]
0.5	42.12	4018	4058
1.0	84.23	3788	3791
1.5	126.35	3659	3641
2.0	168.47	3571	3550
2.5	210.58	3504	3494
3.0	252.70	3450	3456
3.5	294.82	3405	3413
4.0	336.94	3366	3373
4.5	379.05	3332	3370
5.0	421.17	3303	3372
5.5	463.29	3276	3370
6.0	505.40	3252	3385
6.5	547.52	3230	3369
7.0	589.64	3209	3383
7.5	631.75	3190	3370
8.0	673.87	3173	3404
8.5	715.59	3157	3417
9.0	758.11	3141	3424
9.5	800.22	3127	3439
10.0	842.34	3113	3460

Appendix VII.2: Excel macro VBA code

```
Sub Macro2()
'
' Macro2 Macro
'
' Keyboard Shortcut: Ctrl+w
'

    For i = 1 To 1501

    ActiveCell.Offset(0, -2).Range("A1:B1").Select
    Application.CutCopyMode = False
    Selection.Copy
    Sheets("graph").Select
    Range("B2").Select
    Selection.PasteSpecial Paste:=xlPasteValues, Operation:=xlNone, SkipBlanks _
        :=False, Transpose:=False
    Application.Calculate
    Sheets("conclusion").Select
    Range("L29:Q29").Select
    Application.CutCopyMode = False
    Selection.Copy
    Sheets("macro2").Select
    ActiveCell.Offset(0, 2).Range("A1").Select
    Selection.PasteSpecial Paste:=xlPasteValues, Operation:=xlNone, SkipBlanks _
        :=False, Transpose:=False
    ActiveCell.Offset(1, 0).Range("A1").Select

    Next
End Sub
```

Curriculum Vitae

PERSONAL DETAILS

Name	Muhanned Saeed
DoB	14.09.1976
Home address	Bürklistrasse 10
	4313 Möhlin
Nationality	British
E-Mail	m.saeed@unibas.ch

EDUCATION

2006 – 2010
University of Basel
PhD in Pharmaceutical Technology *magna cum laude*

2002 – 2006
University of Portsmouth
MPharm *First-degree Honours*

1988 – 1994
Secondary education

EMPLOYMENT

Aug 2011 – current
Production process scientist
Novartis Pharma – Stein – PU Solids

2010 – 2011
Post-doctoral fellow
Novartis Pharma / University of Basel

2006 – 2009
Teaching assistant
University of Basel

2006
Pre-registration pharmacist
Lloyds pharmacy – Chobham – UK

1999 – 2004
Software design and implementation
ATA Software Tech – London – UK

PUBLICATIONS

- M. Saeed, L. Probst, G. Betz. Assessment of diffuse transmission mode in near-infrared quantification – part II: comparison of information depth with diffuse reflection. Journal of Pharmaceutical Sciences. Volume 100, Issue 3, pages 1130–1141, March 2011
- Saeed et al. Assessment of diffuse transmission mode in near-infrared quantification - part I: The press effect on low-dose pharmaceutical tablets. Journal of Pharmaceutical Sciences. 2009, 98 (12), 4877-4886.

REFEREES

Dr Hedinn Valthorsson
QbD Leader PharmOps CH
Novartis Pharma Stein AG
E-Mail: **hedinn.valthorsson@novartis.com**
TEL: +41 62 8686198

Dr Lorenz Liesum
Novartis Pharma AG
Global Pharma Engineering
Senior PAT Expert
CHBS, WRO-1241.1.02
CH-4056 Basel
Switzerland
Phone: +41 61 3240299
Fax: +41 61 3243843
Cell: +41798618525
Email : **lorenz.liesum@novartis.com**